Bioactive Metabolites From Natural Sources For The Pharmaceutical, Nutraceutical And Cosmeceutical Industry

Antonella Delicato

Dottorato in Biotecnologie – XXXV ciclo

Università di Napoli Federico II

Dottorato in Biotecnologie – XXXV ciclo

Università di Napoli Federico II

BIOACTIVE METABOLITES FROM NATURAL SOURCES FOR THE PHARMACEUTICAL, NUTRACEUTICAL AND COSMECEUTICAL INDUSTRY

Antonella Delicato

Dottorando:	Antonella Delicato
Relatore:	Prof.ssa Viola Calabrò
Correlatore:	PhD Marco Masi
Coordinatore:	Prof. Marco Moracci
Settore Scientifico Disciplinare	Genetica BIO-18

INDEX

Riassunto

Uno degli obiettivi delle moderne biotecnologie è la continua ricerca e lo sviluppo di prodotti innovativi derivati da fonti naturali, con potenziali applicazioni in diversi settori industriali, come quello cosmeceutico, farmaceutico e nutraceutico. Gli organismi viventi terrestri e marini, come piante, alghe e funghi, sono un'ottima fonte di composti naturali strutturalmente diversi che sono significativi per le loro attività biologiche e potenziali applicazioni biotecnologiche. Le piante sono state ben documentate per i loro usi nella medicina tradizionale contro lesioni e malattie infettive. Si sono evolute e adattate nel corso di milioni di anni per resistere all'attacco di patogeni e agli stress ambientali quali condizioni climatiche, carenza di nutrienti, producendo metaboliti secondari bioattivi che le rendono competitive nel loro ambiente. Pertanto, è importante considerare che un particolare insieme di metaboliti prodotti da una pianta dipende fortemente dal luogo in cui cresce e più specificamente da una varietà di fattori ambientali quali luce, temperatura, acqua del suolo, fertilità del suolo e salinità.

I Metaboliti Secondari delle Piante (PSM) sono molecole organiche a basso peso molecolare originate dai metaboliti primari. Questi ultimi sono necessari per alcuni processi vitali, come la fotosintesi, la traslocazione nel floema e la respirazione. I prodotti derivati dai metaboliti primari, non direttamente coinvolti nella crescita e nello sviluppo sono considerati PSM. In generale, i PSM sono il prodotto quattro reazioni biosintetiche e sono ritenuti interessanti per la loro diversità strutturale e le loro numerose attività biologiche. Tra i metaboliti secondari vengono prodotti feromoni, molecole che solubilizzano e trasportano nutrienti, repellenti, veleni, tossine, che vengono utilizzate contro prede e predatori. Per molti metaboliti secondari, la funzione rimane sconosciuta. Alcuni metaboliti bioattivi possono inoltre essere sottoposti a derivatizzazioni chimiche per migliorarne le proprietà biologiche, sia in termini di biodisponibilità che di grado di attività. Si ritiene che i PSM conferiscano un vantaggio selettivo all'organismo che li produce o che, in analogia al sistema immunitario e grazie alla loro molteplicità di strutture, possano combattere una moltitudine di fattori deleteri per la pianta.

I metaboliti secondari sono utilizzati principalmente come prodotti farmaceutici, erbicidi, insetticidi, additivi alimentari e ingredienti cosmetici. Inoltre, grazie alle loro specificità di azione i PSM sono importanti per lo sviluppo di nuovi farmaci, diretti contro i bersagli

molecolari che stanno via via emergendo grazie al progetto Genoma Umano.
Il mio progetto di dottorato ha avuto come obiettivo l'isolamento e la caratterizzazione di metaboliti bioattivi da specie vegetali ampiamente utilizzate nella medicina tradizionale per lo sviluppo di nuovi composti per l'industria farmaceutica, nutraceutica o agricola.
Durante la prima parte della mia formazione di Dottorato, ho studiato *Crinum biflorum Rottb.* (syn*. Crinum distichum*), pianta appartenente alla famiglia delle Amaryllidaceae e raccolta in Senegal, e sulla quale sono stati effettuati pochissimi studi dal punto di vista chimico e delle possibili applicazioni pratiche. Le Amaryllidaceae sono diffuse principalmente nelle regioni tropicali e subtropicali del mondo, come il Sud America andino, il bacino del Mediterraneo e l'Africa meridionale**.** *Crinum biflorum Rottb*. si trova nelle savane del Senegal, della Nigeria e fino in Sudan in luoghi generalmente inondati dall'acqua a cadenza periodica. Le Amaryllidaceae sono una famiglia di piante ampiamente studiata essenzialmente per i suoi alcaloidi che sono noti per avere un ampio spettro di attività biologiche. Tra gli alcaloidi più studiati ed utilizzati di questa famiglia di piante ci sono: la **galantamina**, la quale è già commercializzata per la cura dell'Alzheimer, come potente e selettivo inibitore dell'enzima acetilcolinesterasi, e per questo di grande importanza per il settore farmacologico; la **licorina**, invece, ha una forte attività antivirale e ha dimostrato di avere una notevole attività antitumorale *in vitro* contro diversi tipi di tumori solidi come i suoi analoghi narciclasina, e pancratistatina. Oltre agli alcaloidi, le piante di Amaryllidaceae producono anche metaboliti meno studiati appartenenti ad altre classi di composti naturali come flavonoidi, lignani, cromoni, terpenoidi e ceramidi. Ad oggi circa 223 composti, essenzialmente flavani e fitosteroli, sono stati isolati da Amaryllidacaee, tutti con interessanti attività biologiche. In particolare, i flavonoidi sono una nota classe di composti naturali che hanno un'azione protettiva contro lo stress ossidativo, le malattie cardiache e alcuni tumori, e sono considerati salutari per l'uomo e il bestiame.
Crinum è un noto sottogruppo di Amaryllidaceae da tempo studiato ed è molto ricco di alcaloidi. Gli alcaloidi isolati da *Crinum*, inclusa la cherillina, hanno mostrato un'interessante attività inibitoria sulla replicazione virale. Esistono molti esempi di metaboliti bioattivi isolati da altre specie del genere *Crinum*, con proprietà citotossiche, neuroprotettive, antiangiogeniche e antibiotiche.
Durante il mio primo anno di dottorato, mi sono occupata dell'isolamento e caratterizzazione chimica e biologica di metaboliti da *Crinum*. Ho svolto questa parte del mio progetto di dottorato presso il

Dipartimento di Scienze Chimiche dell'Università degli Studi di Napoli Federico II. Nel laboratorio di chimica organica ho messo a punto i protocolli per la purificazione dei metaboliti da estratti crudi in modo da ottimizzare la resa in metaboliti puri. Inaspettatamente, non sono stati rilevati alcaloidi nell'estratto organico acido dai bulbi di *C. biflorum*, né utilizzando il metodo tradizionale di estrazione Soxhlet con etanolo, né il metodo di estrazione ottimizzato. Tuttavia, l'estratto organico ottenuto con il metodo Soxhlet ha mostrato la presenza di omoisoflavonoidi. Dalla specie *C. biflorum*, ho isolato e caratterizzato per la prima volta quattro **omoisoflavonoidi e un' alchilammide** in questa pianta di Amaryllidaceae raccolta in Senegal: sono stati caratterizzati come 5,6,7-trimetossi-3-(4-idrossibenzil)croman-4-one (1), come 3-idrossi-5,6,7-trimetossi-3-(4-idrossibenzil)croman-4-one (2), come 3-idrossi-5,6,7-trimetossi-3-(4-metossibenzile) croman-4-one (3) e come 5,6,7-trimetossi-3-(4-metossibenzil)croman-4-one (4), e l' alchilammide come (E)-N-(4-idrossifenil)-3-(4-idrossifenil)acrilammide (5), comunemente chiamata Np-cumaroiltiramina.

La seconda fase dello studio ha riguardato la caratterizzazione biologica dei metaboliti purificati. Presso il Dipartimento di Biologia dell'Università degli Studi di Napoli Federico II, ho svolto dei saggi *in vitro* per determinare le potenziali attività dei metaboliti ed i meccanismi molecolari in cui sono coinvolti.

I **flavonoidi 1, 3 e 4** hanno mostrato una significativa e promettente citotossicità selettiva contro le linee cellulari tumorali umane HeLa e A431. La **N-p-coumaroiltiramina** (5) era selettivamente tossica per le cellule tumorali A431 e HeLa, mentre proteggeva le cellule HaCaT immortalizzate dallo stress ossidativo indotto dal perossido di idrogeno. I composti 1-4 hanno anche attività inibitoria sull'enzima acetilcolinesterasi, con il metabolita 3 che mostrava la più forte attività alle più basse concentrazioni saggiate rivelandosi quindi più promettente. Sono state confermate l'attività antiamilasica e la forte attività antiglucosidasica del composto 5. I risultati ottenuti ampliano la libreria di composti isolati da *C. biflorum* e mostrano per la prima volta che questa specie di Amaryllidaceae produce composti di interesse nutraceutico e farmacologico con potenziali applicazioni come integratori alimentari con importanti proprietà antidiabetiche, antitumorali e di supporto per la cura delle malattie neurodegenerative. Test preclinici e saggi *in vivo* potranno fornire le necessarie conoscenze sulla biodisponibilità e l'efficacia terapeutica di questi metaboliti necessarie per una loro applicazione quali agenti per la cura di infezioni e malattie neurodegenerative.

La seconda pianta su cui ho lavorato durante il mio progetto di dottorato è *Cistanche phelypaea* appartenente alla famiglia delle Orobancaceae. Il genere *Cistanche* comprende più di 20 specie oloparassite, prive di clorofilla e foglie funzionali. Parassitano le radici di arbusti perenni alofiti tipicamente su deserti, terre aride o dune costiere. Oltre al loro interesse evolutivo o botanico, le specie *Cistanche* hanno suscitato interesse erboristico, essendo state utilizzate come cibo salutare o decotto nella medicina tradizionale cinese per più di 2000 anni. Inoltre c'è una reale prospettiva di estendere la coltivazione di *Cistanche* per rispondere alla richiesta del territorio di estendere le piantagioni di arbusti resistenti alla siccità che fungano da stabilizzanti, le cosidette "foreste rifugio", come possibile soluzione alla desertificazione globale. Sono state fatte previsioni sul potenziale adattamento di diverse specie di *Cistanche* a nuove regioni con compatibilità climatica ed il territorio che sembra adeguato alla coltivazione di *C. phelypaea* in Europa *sono le* aree aride del sud-est della Spagna.
Altre specie di *Cistanche* come *C. deserticola* e *C. tubulosa sono state oggetto di molti studi sia per quanto concerne la loro* composizione in metaboliti sia per le loro possibili applicazioni nel settore nutraceutico e farmacologico. La specie *C. phelypaea* è stata poco studiata. La prima indagine chimica su *C. phelypaea* è stata effettuata nel 1993 ed i suoi componenti principali sono i glicosidi feniletanoidi. Essi sono stati isolati dal suo estratto grezzo in acetato di etile. Alcuni recenti studi dimostrano che i glicosidi feniletanoidi possono inibire alcuni importanti enzimi quali l'acetilcolinesterasi, la tirosinasi e la butirrilcolinesterasi e sono stati utilizzati contro il diabete mellito di tipo 2 e l'iperpigmentazione cutanea. In letteratura è noto che i composti isolati da questa pianta hanno attività inibitoria su due enzimi coinvolti nel peculiare metabolismo glicolitico o lipidico delle cellule tumorali, rispettivamente la lattato deidrogenasi umana (LDH) e la monoacilglicerolo lipasi (MAGL). È stato segnalato che l'acetoside, che è il principale componente bioattivo di *Cistanche*, ha eccellenti attività antiossidanti, antinfiammatorie, neuroprotettive e anti-osteoporotiche.
La pianta *C. phelypaea* utilizzata nei miei esperimenti è stata coltivata e raccolta in Spagna. Mi sono stati forniti i bulbi essiccati, che ho sottoposto ad estrazione mediante Soxhlet. Dall'estratto organico ho potuto isolare ed identificare sei diversi metaboliti appartenenti a due differenti classi di composti: **acetoside, 2'-O- acetilacetoside, tubuloside** come glicosidi feniletanoidi, e **bartioside, 6-deoxycatalpol, gluroside** come glicosidi iridoidi. Data la notevole abbondanza di acetoside nell'estratto di *C. phelypaea*, mi sono concentrata sullo studio delle proprietà di questo composto.

Le strutture dei glicosidi feniletanoidi contengono gruppi idrossilici fenolici, che sono responsabili dell'attività antiossidante di *Cistanche*, e come ho dimostrato la differenza nella struttura chimica, come la presenza di gruppi sostituenti, può influenzare significativamente l' attività antiossidante dei singoli composti. Nei cheratinociti umani, l'attività di scavenging dei ROS dell'acetoside era del tutto paragonabile a quella del Trolox, il derivato idrosolubile della vitamina E. Sorprendentemente, nelle cellule progenitrici mesenchimali umane il Trolox era inefficace, mentre l'acetoside era ancora in grado di contrastare efficacemente la produzione di ROS, suggerendo una potenziale applicazione di questo metabolita come additivo nel mezzo di coltura cellulare hESC. Inoltre l'acetoside sembrava preservare il potenziale proliferativo dei cheratinociti basali umani e dei progenitori mesenchimali necessari per la morfogenesi e il rinnovamento dei tessuti. L'uso delle cellule staminali nell'ingegneria tissutale richiede la loro differenziazione controllata; Le hMSC hanno un grande potere terapeutico potenziale, tuttavia, la loro utilità è limitata dalla senescenza cellulare secondaria all'aumento dei livelli di ossigeno reattivo, specialmente durante la loro propagazione in coltura. Per la prima volta ho testato il potenziale terapeutico di questo composto su cellule staminali pluripotenti considerando la sua possibile applicazione nella medicina rigenerativa e nella riparazione tissutale. Dunque ho potuto dimostrare che, oltre al suo forte potenziale antiossidante, l'acetoside può sostenere la pluripotenza dei progenitori delle cellule staminali mesenchimali necessarie per la morfogenesi e il rinnovamento dei tessuti.

Parte della mia attività di dottorato è stata dedicata allo sfruttamento sostenibile dell'estratto di vinaccia per produrre particelle edibili cariche di composti antiossidanti e pro-rigenerativi in una prospettiva di economia circolare. L'economia circolare implica la creazione di un ecosistema a circuito chiuso per il consumo e l'uso effettivo delle risorse attraverso l'adozione di paradigmi di riduzione, riuso e riciclo. Secondo questo paradigma, la riduzione della produzione di rifiuti attraverso il loro riciclaggio e riutilizzo, nonché la gestione sostenibile e l'uso efficiente delle risorse naturali sono le principali sfide per la moderna economia circolare. È necessaria una transizione verso un ciclo economico riparatore e rigenerativo basato su pratiche più sostenibili e impatti ambientali ridotti della produzione e del consumo.

La vinaccia è uno dei sottoprodotti più abbondanti dell'agroindustria soprattutto in Italia, uno dei più importanti produttori di vino al mondo. Circa il 75% delle uve prodotte viene utilizzato per la produzione di vino, di cui il 20-30% sono prodotti di scarto. Questi scarti sono anche

chiamati vinacce e sono costituiti da bucce, polpa residua, semi e gambi e rappresentano sottoprodotti che determinano lo smaltimento dei rifiuti, o sono utilizzati per produrre grappa, o come fertilizzante, o mangime per animali. Lo smaltimento di tali rifiuti crea problemi ambientali come l'inquinamento delle acque sotterranee e superficiali, l'attrazione di vettori patogeni e il consumo di ossigeno nel suolo e nelle acque sotterranee che possono avere un impatto sulla fauna selvatica. Le vinacce contengono quantità significative di sostanze che possono essere considerate benefiche per la salute. I più abbondanti nella vinaccia sono le fibre alimentari che sono presenti in livelli elevati (fino all'85% a seconda della varietà di uva) e i composti polifenolici che rimangono principalmente (circa il 70%) nella vinaccia dopo il processo di vinificazione. Il fatto che la vinaccia abbia un grande potenziale biotecnologico ha dato origine a numerosi studi che si sono occupati della possibilità di utilizzarla come ingrediente di fortificazione alimentare, in un'ottica di economia circolare. Inoltre, la composizione della vinaccia come prodotto di scarto dipende fortemente dal tipo di rifiuto, dal vitigno, dall'ambiente di impianto, dal metodo di lavorazione e da molti altri fattori. Durante la lavorazione dell'uva, i polifenoli rimangono principalmente nelle vinacce a causa della loro incompleta estrazione. I principali rappresentanti dei composti polifenolici in questo sottoprodotto sono gli antociani (solo nelle vinacce di uve rosse), le catechine, i glicosidi flavonolici, gli acidi fenolici e gli alcoli. Insieme alle fibre alimentari, i composti fenolici sono i composti più preziosi della vinaccia con proprietà benefiche per la salute, come il mantenimento della salute intestinale e la prevenzione delle malattie croniche e del cancro e hanno un effetto sinergico nella regolazione del metabolismo e nella prevenzione e cura di malattie, come obesità, insulino-resistenza, aterosclerosi, osteoporosi.
Nell'ambito della valorizzazione del nostro territorio, nell’ultima parte del mio Dottorato ho collaborato con l'azienda vinicola Mastroberardino, una delle più grandi realtà vitivinicole della Campania e d'Italia, al fine di riutilizzare gli estratti di vinaccia, come potenziale alimento funzionale, riproponendolo nel mercato. L'azienda mi ha fornito le vinacce derivanti dalla loro produzione di vino rosso. Ho ottimizzato dapprima il processo estrattivo dalla vinaccia, la quale è stata sottoposta prima a liofilizzazione e successivamente a macerazione nel solvente organico. L'etanolo è stato selezionato come mezzo di estrazione in base alla sua completa biocompatibilità e potere solubilizzante dei polifenoli. Nel caratterizzare l'estratto di vinaccia utilizzato nei miei studi, i principali costituenti tra i polifenoli sono risultati essere la (+)-catechina e il suo epimero, (-)-epi-catechina. Tuttavia,

l'incorporazione di fenoli nei prodotti alimentari è limitata dalla loro suscettibilità alla degradazione e all'epimerizzazione, a condizioni estreme di pH e temperatura. Altri fattori rilevanti che devono essere presi in considerazione sono la loro limitata solubilità in acqua e la consegna non mirata. Sulla base della recente letteratura, diverse tecnologie incapsulamento sono utilizzate per proteggere la bioattività dei composti incapsulati, controllarne il rilascio all'esterno, ridurne la tossicità e promuovere il rilascio mirato dopo l'assorbimento dal tratto gastrointestinale. È già stato dimostrato che l'applicazione di fenoli incapsulati invece di molecole libere migliora la capacità antiossidante degli alimenti arricchiti di fenoli.
Ho collaborato con l'IPCB (Istituto Polimeri Compositi e Biomateriali CNR) alla messa a punto di un metodo di incapsulamento a base di una matrice polimerica, quale la pectina, e reticolanti ionici bivalenti, Fe^{2+} o Ca^{2+}, per migliorarne la funzionalità e le proprietà organolettiche e per favorire l'apporto di due micronutrienti cationici essenziali. I biopolimeri naturali come quelli costituiti dalla pectina, che è anche un componente naturale della vinaccia, sono particolarmente interessanti a questo scopo per le loro buone proprietà di biocompatibilità, sicurezza e rilascio controllato. Ho quindi testato diverse miscele di metaboliti antiossidanti incorporati in beads edibili di pectina. Ho valutato l'efficienza di caricamento delle beads, il rilascio dei composti bioattivi e la loro attività antiossidante in un ambiente che imita il tratto gastrointestinale. Le beads sono state sottoposte a diverse analisi strutturali e funzionali, per poi essere caricate con l'estratto grezzo della vinaccia. Successivamente sono state poste in soluzioni a pH=2 e pH=7,4, per mimare il rilascio dei composti bioattivi nel tratto gastrointestinale. Alcune tra le formulazioni di beads testate, sembravano essere altamente biocompatibili e in grado di ridurre il livello di ROS nelle cellule HaCaT (cheratinociti immortalizzati umani), indotto dal trattamento con perossido di idrogeno. Ho dimostrato che i rilasciati dalle beads coniugate con Fe^{2+} non mostravano un effetto antiossidante dose-dipendente. Quelli rilasciati dalle sfere reticolate con Ca^{2+} sembravano funzionare in modo più efficiente e in modo dose-dipendente, sia a pH=2 che a pH=7,4. Tuttavia, l'effetto antiossidante era inferiore rispetto a quello dell' estratto grezzo. Le nostre formulazioni con Ca^{2+} sembrano essere promettenti e pronte per i test *in vivo*, perché possono rilasciare efficacemente le molecole antiossidanti lungo il tratto gastrointestinale, preservandone l'integrità strutturale e funzionale. Dai profili NMR, le sfere reticolate con Fe^{2+} al contrario di quelle reticolate con Ca^{2+} , non sembrano restituire abbastanza metaboliti per ottenere l'effetto antiossidante desiderato.

Questo è in accordo con la loro scarsa efficienza di rilascio. Tuttavia, il ferro nelle formulazioni è ancora poco studiato, probabilmente a causa dei problemi di precipitazione dello ione ferrico intorno a pH=7. Attualmente è in corso la preparazione di altre formulazioni, per migliorarne le caratteristiche in termini di efficienza di caricamento e rilascio, e la conservazione dell'attività di scavenging di ROS. Una volta stabilita la migliore formulazione, la sua biodisponibilità sarà testata *in vivo* utilizzando modelli animali.

Durante il mio Dottorato, ho avuto l'opportunità di entrare a far parte del team del Prof. Nicholas Foulkes presso l' Institut für Technologie (KIT) di Karlsruhe, in Germania. Uno dei principali interessi scientifici del laboratorio del Prof. Foulkes è il meccanismo molecolare attraverso il quale nei vertebrati l'orologio circadiano controlla i principali processi cellulari fisiologici regolati dall'orologio circadiano, come la progressione del ciclo cellulare e la riparazione del danno al DNA nei vertebrati. L'interruzione dell'orologio circadiano, è stata collegata alla deregolazione della crescita cellulare e ad una maggiore incidenza del cancro. Questo è uno degli aspetti che rendono il suo studio così importante. Storicamente, *zebrafish* (*Danio rerio*) che rappresenta uno degli organismi modello più importanti per lo studio dello sviluppo embrionale nei vertebrati, è emerso anche come modello molto interessante per lo studio del sistema di temporizzazione circadiano. Oltre a fornire una potente raccolta di strumenti genetici per studiare i meccanismi dell'orologio *in vivo*, i pesci possiedono orologi periferici direttamente sensibili alla luce, anche nelle linee cellulari derivate dai pesci. Pertanto, questo ha reso il pesce zebra particolarmente utile per studiare i percorsi che trasmettono informazioni sulla luce all'orologio circadiano. Il gruppo guidato da Nicholas S. Foulkes, ha precedentemente esplorato come luce, temperatura, ROS o UV regolano l'espressione dei geni orologio per1b21, cry1a22 e per223 così come i geni di riparazione del DNA che in *zebrafish* sono anche attivati trascrizionalmente dalla luce visibile. Hanno identificato un elemento potenziatore reattivo alla luce, ROS e UV, l'elemento D-box17, che opera da solo o in combinazione con altri enhancer come i siti E-box o E2F.

Ho avuto l'opportunità di trascorrere sei mesi presso l' Institut für Technologie (KIT) di Karlsruhe, per apprendere la tecnologia NanoBit, una nuova tecnologia per studiare le interazioni proteina-proteina in tempo reale seguendo la cinetica di associazione proteica. Durante il mio periodo all'estero ho prodotto una serie di cloni di espressione nel sistema NanoBit, clonando la piccola subunità SmBit e la subunità maggiore LgBit di NanoLuc alle estremità C-ter e N-ter dei fattori di

trascrizione CRY5 e TEF2. Tali fattori possono legarsi agli enhancer D-box per regolare la trascrizione in risposta all'esposizione alla luce solare. Una volta ottenuti, i cloni, ho trasfettato le varie combinazioni C-ter e N-ter in linee cellulari di *zebrafish*, PAC2 (fibroblasti embrionali), per seguire la cinetica di interazione *in vivo* delle due proteine attraverso la luce emessa da SmBit e LgBit ricostituiti nel reporter NanoLuc. Ciò che ho potuto osservare è stata una debole interazione in alcune di queste combinazioni di cloni. Lo studio è in corso di approfondimenti, per confermare l'eventuale interazione dei due fattori trascrizionali all'enhancer D-box, chiarendo alcuni meccanismi molecolari che sono alla base dell'orologio circadiano.

Abstract

One goal of modern biotechnology is the continuous research and development of innovative products derived from natural sources with potential applications in diverse industrial sectors, such as the cosmeceutical, pharmaceutical and nutraceutical industries. Historically, natural metabolites have been used in folk medicine for the treatment of several diseases and injuries since ancient times until the renewed interest of the current scientific community.
Living terrestrial and marine organisms, such as plants, algae and fungi, are an excellent source of structurally different natural compounds which are significant for their biological activities and potential therapeutic applications as well as for agricultural applications such as pesticides and insecticides. In addition to their great structural diversity, secondary metabolites from natural sources can be subjected to chemical modifications to improve their biological properties both in terms of bioavailability and degree of activity. Some bioactive compounds can help to maintain cellular homeostasis while fighting degenerative factors. This is the reason why these compounds continued to be considered interesting drug candidates. Plants have been well-documented for their traditional medicinal uses against illness and infectious diseases. Plants have evolved and adapted over millions of years to withstand bacteria, insects, fungi, and aging producing unique and structurally diverse bioactive secondary metabolites. These include pheromones that act as social signaling molecules among individuals of the same species, communication molecules that attract and activate symbiotic organisms, agents that solubilize and carry nutrients, and competitive weapons (repellents, poisons, toxins, etc.) that are used against competitors, preys, and predators. For many other secondary metabolites, the function remains unknown. One hypothesis is that they give a competitive advantage to the organism that produces them or in analogy to the immune system they can fight a multitude of deleterious factors thanks to their different chemical structures and properties.
In my thesis, I chose to deal mainly with two plant species, *Crinum biflorum Rottb*. (sin. *Crinum distichum*) and *Cistanche phelypaea* belonging to the Amaryllidaceae and Orobanchaceae families, respectively. Both species grow in a tropical or desert climate. *C. biflorum* is widely used in traditional African medicine, although very few studies have been carried out from a chemical point of view and possible practical applications. I have isolated four homoisoflavanoids

and an alkylamide, never reported before in this species. Remarkably, some of these flavonoids have shown promising anticancer properties being cytotoxic at low micromolar concentrations to Hela and A 431 human cancer cell lines. The N-p-coumaroyltyramine (alkylamide) was cytotoxic in A431 and Hela cancer cells but not in not transformed HaCaT cells. Il also showed acetylcholinesterase inhibitory activity and interesting antiamylase and anti-glucosidase activity. The obtained results indicate that *C. biflorum* produces compounds of nutraceutical and pharmacological interest with potential applications as food supplements having important anti-diabetic properties and supplements in the therapy against cancer and neurodegenerative diseases.

C. phelypaea belongs to the genus *Cistanche* including more than 20 species typically growing in deserts or coastal dunes. They are considered parasitic plants of shrub roots. *Cistanche* species have long been a source of traditional herbal medicine or food, *C. deserticola* and *C. tubulosa* are the most used in China. I have isolated and identified some of the most abundant phenylethanoid glycosides and iridoids, obtained from the hydroalcoholic extract of *C. phelypaea* collected in Spain. Besides their antioxidant property, I have explored the potential of novel bioactivities never investigated so far in Cistanche metabolites such as the effect on keratinocytes and pluripotent stem cells proliferation and differentiation in light of their potential application in regenerative medicine and the cosmeceutical industry. In particular, I have explored the effect of acetoside which is the most abundant metabolite in *C. phelypaea* extract. I have shown that acetoside, in addition to its strong antioxidant potential, can sustain the proliferative potential of human basal keratinocytes and the pluripotent status of mesenchymal progenitors needed for tissue morphogenesis and renewal. Although obtained *in vitro* my results strongly suggest that acetoside may be of practical relevance for the application of human stem cell culture protocols in tissue engineering and regeneration.

Finally, in the last period of my PhD project, I focused on the sustainable exploitation of pomace extract to produce edible particles based on pectin and divalent metal ions, loaded with antioxidant compounds in a circular economy perspective. After the optimization of the grape pomace extraction process and its characterization, the mixture of polyphenolic compounds was loaded into edible particles for nutraceutical applications. The release capacity of the polyphenols encapsulated in the beads and the conservation of their antioxidant activity in the gastrointestinal environment were tested *in vitro*.

Finally, in the last period of my PhD project, I focused on the sustainable exploitation of pomace extract in a circular economy perspective. After the optimization of the grape pomace extraction process and its chemical and biological characterization, the mixture of polyphenolic compounds was exploited to produce edible particles based on pectin and divalent metal ions, for nutraceutical applications. The release efficiency of the encapsulated polyphenols, and the preservation of their antioxidant activity in the gastrointestinal environment, were tested *in vitro*.

Aim

My PhD project aimed to isolate and characterize bioactive metabolites from plant species widely used in traditional medicine as potential sources of bioactive metabolites for the development of novel compounds for pharmaceutical, nutraceutical, or agricultural industries. My research activity was based on a multidisciplinary approach and included organic chemistry analyses, molecular biology techniques and nanoparticle formulations. My work has gone through four different phases:

(1) **Isolation and chemical characterization of bioactive compounds**. I carried out this part of my PhD project at the Department of Chemical Sciences of the University of Naples Federico II. In the laboratory of organic chemistry, I've set the protocols for the extraction and purification of metabolites from the selected plants to obtain the maximum yield of purified products to carry out their chemical characterization.

(2) **Biological characterization of purified metabolites**. At the Department of Biology of the University of Naples Federico II, I carried out *in vitro* assays to determine the antioxidant and cytotoxic activity of purified metabolites. To speculate on the potential molecular mechanism or signaling pathways involving the purified metabolites of interest, I performed gene expression analyses in control and metabolite-treated cells as well as immunoblots and immunofluorescence analyses to monitor the expression level of the well-known cell cycle, differentiation, apoptosis and DNA damage markers including keratins, aquaporin 3, filaggrin, p63, cyclins, p21WAF, CK1 and involucrin. Finally, I've tested the effect of isolated metabolites on keratinocyte differentiation and mesenchymal cell stemness potential. Both properties are of great relevance for

evaluating the possible applications of total plant extracts or isolated metabolites in the cosmeceutical industry.

3) **Sustainable exploitation of grape pomace extract within the circular economy**. From the point of view of the circular economy, I took part in another project, aimed at enhancing a waste product of the agri-food industry, grape pomace. I took care of optimizing the extraction of known antioxidant components, such as catechins, epicatechins, gallic acid, and flavonoids, with a green extraction, thus limiting the consumption of solvents. The goal was to reintegrate a waste product into a product suitable for the industry such as a nutraceutical. In collaboration with the ICBP-CNR Pozzuoli, Naples, particles formulations loaded with pomace extract have been formulated for intestinal delivery, as a promising technological and green solution for exploiting agri-food waste and by-products and developing products with high added value for human health. Mixtures of antioxidant metabolites incorporated into pectin edible formulations were tested, evaluating the loading efficiency of the crude extract and the release in an environment mimicking the gastrointestinal tract. Then, the released fraction was tested to evaluate the preservation of the antioxidant activity. The particles were highly biocompatible and able to counteract oxidative damage induced in HaCaT cells using hydrogen peroxide.

(4) **Foreign experience**. During my PhD, I spent six months abroad at the Institut für Technologie of Karlsruhe (KIT) in Germany to learn the NanoBit technology, a new technology for studying real-time protein-protein interactions by following the kinetic of protein association. The goal was to understand the function of the bzip PAR and Nfil3 transcription factors family in *zebrafish* (*Danio rerio*). Such factors can bind to D-box enhancers to regulate transcription in response to sunlight exposure. The study of PAR and Nfil3-activated genes can help in understanding the regulation of the circadian clock and DNA repair mechanisms. I produced several expression plasmid clones, cloning the NanoLuc's small SmBit subunit and NanoLuc LgBit subunit at the C-ter and N-ter ends of CRY5 and TEF2 transcription factors. Once obtained, the clones expressing the various C-ter and N-ter combinations of CRY and TEF2 transcription factors were transfected into the *zebrafish*'s PAC2 cells (embryonic fibroblasts), to follow the interaction kinetics of the two proteins through light emitted from the reconstituted SmBit and LgBit in the NanoLuc reporter.

CHAPTER I

1. Introduction

1.1. Plant secondary metabolites

Plant secondary metabolites (PSMs) are small organic molecules originating from primary metabolites following exposure of plant cells to elicitors or precursors. Nearly 200,000 PSMs have been isolated and characterized which is a small number relative to the 391,000 described plant species (Divekar, P. A. *et al.,* 2022).; essentially they have molecular masses of less than 3000 da. The chemical nature and composition of metabolites in plants vary between species. There is no clear differentiation between primary and secondary metabolites and this is quite confusing to define, as most of the metabolites in plant natural products are secondary metabolites. The primaries provide the necessary supplies for processes, such as photosynthesis, translocation and respiration. Products derived from primary metabolites, not directly involved in growth and development are considered PSMs. In general, PSMs arise from primary metabolites via four biosynthetic pathways and are interesting due to their structural diversity and potency as candidate drugs and/or antioxidants.
PSMs are also a useful range of natural substances produced by plants as a defense system against pathogenic attacks and environmental stresses, that make them competitive in their environment. The secondary metabolites produced by plants can vary according to the general climatic conditions, the lack of nutrients or the attack of pathogenic agents. Therefore, it is important to consider that a particular set of metabolites produced by a plant is highly dependent on where it grows and more specifically on a variety of environmental factors such as light, temperature, soil water, soil fertility and salinity. They induce flowering, fruit set and abscission, maintain perennial growth or signal deciduous behavior. They act as antimicrobials and play the role of attractants or, conversely, repellents. Several medicinal herbs already rely on secondary plant metabolites for their actions. However, given the broad range of PSMs, the search for new by-products in plants with the hope of discovering new products or new approaches for treating disease is an ongoing process involving academic and pharmaceutical institutions.

1.2. Relevance of secondary metabolites in industry

It has been broadly documented that plants are rich sources of a variety of secondary metabolites that can be used for human benefit. These metabolic derivatives have a highly specific mechanism of activity and for this reason are potentially important in drug development, especially nowadays, when in-depth knowledge is emerging through the human genome sequencing of multiple new molecular targets that have been tested for their potential use as drug targets. Secondary metabolites are mainly used as pharmaceuticals, herbicides, insecticides, food additives and cosmetics ingredients. However, the specific functions and range of possible applications of the vast majority of them are still largely undefined. Several natural products are included in cosmetic preparations, due to their low toxicity to mammalian cells. Their uses in skin care include dryness, eczema, acne, scavenging of free radicals, anti-inflammatory effects, anti-aging and protection from UV.

Secondary metabolites can help to fight free radicals produced in excess which can eventually cause oxidative damage and disease. Nowadays it has been widely recognized that lowering oxidative stress can provide clinical benefits for a variety of pathological conditions. A nutraceutical antioxidant treatment is therefore considered a valid therapy to attenuate the oxidative lesions in inflammatory and degenerative disordersUses for plant secondary metabolites as therapeutic agents include: antimalarials, anti-inflammatory agents (both topical and internal), antioxidants, antiaging, anti-cancer as well as antibiotics/antimicrobials or antiviral drugs. The antimicrobial activity of natural metabolites in mammalian systems is not surprising given that, as previously mentioned, one of the major roles of PSMs in their native plant species is combating microbial/pathogen infection.

In particular, the anticancer activity of natural compounds has always been a research focus. Natural products are viewed as more biologically friendly and less toxic to normal cells. Food and Drug Administration data showed that 40% of the approved molecules are natural compounds or inspired by them, from which, 74% are used in anticancer therapy (Divekar, P. A. *et al*., 2022). A classical example is represented by the well-known Vincristine and Paclitaxel metabolites. Plant secondary/specialized metabolites have been demonstrated to exhibit several anti-cancer effects, such as the ability to either kill or arrest the proliferation of cancer cells, fight metastases or cancer cell multi-drug resistance. However, PSMs with anti-cancer activity include flavonoids, quinones, alkaloids, terpenoids and many other structurally diverse compounds. Secondary metabolites having particular beneficial properties for human health can be adequately formulated as

nutraceuticals, dietary supplements or functional food. In the food industry, PSMs are also widely used, as molecules that provide flavor, aroma, and/or color to many beverages or other food products. Coffee is a high-value food product where almost all of the flavor and sensory characteristics are provided by PSMs. Finally, given the important role of PSMs in regulating plant growth, development, and responses to environmental stimuli natural compounds have been employed in the agricultural industry to regulate crop production or as insecticides, herbicides, and/or herbivore-repellents.
In summary, natural products have long been considered a unique source of useful compounds and a profitable starting point in modern biotechnologies due to their unique chemical diversity, which is uncommon in synthetic compound libraries. However, by the end of the 20th century, research efforts aiming to identify natural products as a pool for drug discovery had declined. The research efforts of many pharmaceutical companies were more focused on new technologies such as combinatorial chemistry, metagenomics, and high-throughput screening to identify new drug candidates. However, these new methodologies did not deliver the expected results and, recently, natural products were reevaluated as one of the best sources of drugs and drug leads and a focus of modern biotechnologies.

1.3. *Crinum biflorum Rottb.*

During the first part of my PhD training, I studied ***Crinum biflorum Rottb.*** (syn. *Crinum distichum*), a plant belonging to the Amaryllidaceae family and collected in Senegal. Amaryllidaceae are principally diffused in tropical and subtropical regions of the world, such as Andean South America, the Mediterranean basin and Southern Africa (Nair, J.J. 2013) and include about 1600 species classified into about 75 genera (Christenhusz, M.J, 2016). *C. biflorum* is in locations seasonally flooded in savannahs from Senegal to Nigeria and up to Sudan (Burkill, H.M. *et al.,* 1985).
Amaryllidaceae is a plant family extensively studied essentially for its alkaloids and related isocarbostiryls which are known to have a broad spectrum of biological activities (Hoshino, O, 1998; Jin, Z. 2019). *Crinum* is a well-known long-studied subgroup of Amaryllidaceae and is very rich in crinine-type alkaloids, one of the 12 ring types in which they are. The alkaloids of Amaryllidaceae have grouped: Galanthamine, among them, has already spawned an Alzheimer's prescription drug as a potent and selective inhibitor of the enzyme

acetylcholinesterase (Lopez, S., *et al.*, 2002) that why it is of great importance for the pharmacology industry (Cimmino *et al.,* 2017). Lycorine, instead, has a strong antiviral activity and was shown to have remarkable *in vitro* anticancer activity against different types of solid tumors as its related isocarbostyryl analogs narciclasine and pancratistatine. Alkaloids isolated from *Crinum*, including cherylline, showed interesting inhibitory activity on viral replication. In addition to alkaloids, Amaryllidaceae plants also produce less investigated metabolites belonging to other classes of natural compounds such as flavonoids, lignans, chromones, terpenoids and ceramides. To date about 223 compounds, essentially flavan and phytosterols, have been isolated from Amayllidoideae, all with interesting biological activities (Ibrakav, A.S *et al*., 2020). In particular, flavonoids are a well-known class of natural compounds that have a protective action against oxidative stress, heart disease and some cancers, and are considered healthy for humans and livestock (Dewick, P.M, 2009; Osbourn, A.E. *et al.,* 2009). There are many examples of bioactive metabolites isolated from other species of the genus Crinum, with cytotoxic, neuroprotective, antiangiogenic and antibiotic properties (Likhitwitayawuid, K. *et al*., 1993; Nam, N.H. *et al*., 2009; Jin, A., *et al*.,2014; Nkanwen, E.R.S. *et al*., 2009).
During my PhD I tried to isolate and characterize compounds with interesting biological activities from *C. biflorum* bulbs collected in Senegal. I have isolated four homoisoflavonoids and an alkylamide. The obtained results expand the library of compounds isolated from *C. biflorum* and show for the first time that this species of Amaryllidaceae produces compounds of therapeutic interest against diabetes, cancer, and Alzheimer's disease.

1.4. *Cistanche phelypaea*

The second plant I worked on during my PhD project is ***Cistanche phelypaea*** belonging to the Orobancaceae family. The genus *Cistanche* includes more than 20 species that are holoparasites, lacking chlorophyll and functional leaves. They parasitize the roots of halophytic perennial shrubs typically on deserts, arid lands, or coastal dunes (Xu *et al.,* 2009). They are commonly known as "Deserthyacinths". Besides their evolutionary or botanist interest, *Cistanche* species raised herbalist interest, having been used in traditional Chinese medicine or food for more than 2000 years. However, its use in traditional medicine is not restricted to China, as it

has also been used in North African Sahara (Bougandoura *et al.,* 2016; Lakhdari *et al*., 2016; Volpato, Saleh, & Di Nardo, 2015). The used product is known as "*Herba cistanche*" and is traded as dried stems of a mix of *Cistanche* species that are either wild-harvested or cultivated by growing the host shrubs (Thorogood *et al.,* 2021). *C. deserticola* and *C. tubulosa* are "cultivated" in China with a harvest of about 6000 tons (Song, Zeng, Jiang, & Tu, 2021). There is a prospect for extending *Cistanche* cultivation, as in addition to the demand for *Herba cistanche*, there is a demand for the plantation of drought-tolerant shrubs to serve as stabilizing "shelter forests" as a possible solution to global desertification. Predictions have been made on the potential adaptation of several *Cistanche* species to new target regions based on climate (Wang, Zhang, Du, Pei, & Huang, 2019). In this line, prospects for the cultivation of *C. phelypaea* are currently being explored in dry areas of South-Eastern Spain. Nutraceutical and pharmacological composition and applications of *C. deserticola* and *C. tubulosa* are rather well studied, as they are widely used in China (Wang, Zhang, Du, Pei, & Huang, 2019), while the species *C. phelypaea* appears to be less investigated. The first chemical investigation on *C. phelypaea* was carried out in 1993 and the main components, identified as phenylethanoid glycosides, were isolated from its ethyl acetate extract (Melek *et al.,* 1993). Subsequently, a previously undescribed iridoid, named phelypaeside, was isolated from the dried aerial parts of the same plant grown in Qatar (Deyama *et al*., 1995). Additional chemical and biological investigations on *C. phelypaea* compounds and other species above mentioned were performed and the results are reviewed in a recent manuscript by Trampetti et al. (Trampetti *et al*., 2019). However, the biological activities of *C. phelypaea* are poorly investigated. Some recent studies show that the metabolites isolated from *C. phelypaea* have an inhibitory capacity of some important enzymes such as acetylcholinesterase, tyrosinase and butyrylcholinesterase and have been used against type 2 diabetes mellitus and skin hyperpigmentation. Another work shows that the compounds isolated from this plant were assayed for their inhibitory activity on two enzymes involved in the peculiar glycolytic or lipidic metabolism of cancer cells, human lactate dehydrogenase (LDH) and monoacylglycerol lipase (MAGL), respectively (Beladjila K.A. *et al*., 2018). Acetoside has been reported to be the main bioactive component in *Cistanche*; it has excellent antioxidant (Li *et al.,* 2018), anti-inflammatory (Qiao, Tang, Wu, Tang, & Liu, 2019), neuro-protective (Gu, Yang, & Huang, 2016) and anti-osteoporotic activities (Yang *et al*., 2019). The traditional uses of *Cistanche* species now cover

a wide range of applications as healthy food additives in Japan and Southeast Asia (Morikawa et al., 2019), for the treatment of renal deficiency and erectile dysfunction (Li, Jiang, & Liu, 2017) or female infertility and constipation in the elderly (Zhang, Wang, Zhang, Chen, & Liang, 2005). Concerning *Cistanche*, I've been able to isolate and identify some phenylethanoids and iridoid glycosides from hydroalcoholic extracts of *C. phelypaea* collected in Spain. Given the significant abundance of acetoside in *C. phelypaea* extract, my work aimed to broaden knowledge about the properties of this compound. For the first time, I tested the therapeutical potential of this compound on pluripotent stem cells considering its possible application in regenerative medicine and tissue repair. During my PhD training I was able to provide evidence that, in addition to its strong antioxidant potential, acetoside can sustain the pluripotency of mesenchymal stem cell progenitors necessary for the morphogenesis and renewal of tissues.

1.5. Grape pomace in circular economy

Finally, part of my project was focused on the sustainable exploitation of grape pomace extract to produce nanoparticles loaded with antioxidant and pro-regenerative compounds within a circular economy perspective.
The circular economy implies the creation of a closed-loop ecosystem for the effective consumption and use of resources through the adoption of reduction, reuse and recycling paradigms. According to this paradigm, the reduction of waste generation through its recycling and reuse, as well as the sustainable management and efficient use of natural resources are the main challenges for the modern circular economy. A transition to a restorative and regenerative economic cycle based on more sustainable practices and reduced environmental impacts of production and consumption is needed.
Grape pomace is one of the most abundant by-products of the agro-industry especially in Italy, one of the most important wine producers in the world. They are the most produced crops worldwide with a production estimation of more than 79 million tons in 2018, according to the Food and Agriculture Organization (FAO—United Nations) (FAOSTAT, 2018). Grape consumption was found to be beneficial for human health due to the high content of bioactive substances (Sousa, E.C. *et al.,* 2014). About 75% of the grapes produced are used for wine production, of which 20-30% are waste products (García-Lomillo, J. *et*

al., 2017; Bender, A.B. *et al*., 2017). These wastes are also called marc and consist of skins, remaining pulp, seeds and stems (Balbinoti, T.C.V. *et al.*, 2020). These by-products represent waste disposal or are used to produce wine alcohol, serve as fertiliser or as animal feed (García-Lomillo, J. *et al.,* 2017). The disposal of such waste creates environmental problems such as groundwater pollution and surface water pollution, the attraction of pathogenic vectors and oxygen consumption in soil and groundwater that can have an impact on wildlife (Dwyer, K. *et al.,* 2014). Part of this waste material is currently delivered to the distillery (by law) where it undergoes a distillation process that does not substantially change its chemical composition and does not solve the problem of environmental disposal. Large quantities of marc disposed of in landfills during the harvest season can harm biodegradation due to low pH and the presence of antibacterial substances, such as polyphenols (Bustamante, M.A. *et al*., 2008). Although the marc is rich in protein, it has been reported that most animals cannot digest it and use it as an energy source (Eleonora, N. *et al*., 2014). The use of marc as composting material is not economically viable due to the lack of certain essential nutrients (Dwyer, K. *et al.*, 2014). On the other hand, marc contains significant amounts of substances that can be considered beneficial for health (Bender, A.B.B. *et al*., 2020; Bennato, F. *et al*., 2020). The most abundant in grape marc are dietary fibers which are present in high levels (up to 85% depending on the variety of grape) and polyphenolic compounds which mainly (about 70%) remain in the marc after the vinification process (Acun, S. *et al*., 2014; Beres, C. *et al.,* 2017). The fact that pomace has great biotechnological potential has given rise to numerous studies which have dealt with the possibility of using it as a food fortification ingredient, within a circular economy perspective (Ianni, A. *et al*., 2019). During the last part of my PhD project, I worked to reuse grape marc-extracts, as a potential functional food, reiterating it in the market.

The composition of the grape pomace as a waste product is highly dependent on the type of waste, grape variety, planting environment, processing method, and many other factors (Garrido, M.D. *et al*., 2011). For instance, while red wine production includes the fermentation of the whole grape mass, rose and white wines are made by juice fermentation. The most important constituents of grape pomace are fibers, polyphenolic compounds, colorants, and minerals. Polyphenolic compounds, colorants, and anthocyanins are the main carriers of the grape pomace's antioxidant potential. The oily part of the grape pomace is rich in unsaturated fatty acids, colorants, and minerals. Immediately

after production, grape pomace contains large quantities of water, which affects its chemical stability and favors microbial spoilage. Consequently, it is very important to dry grape pomace and slow down those processes (García-Lomillo, J. *et al*., 2017). Dietary fibers were found as predominant compounds in red grape pomaces, though in white grape pomaces dietary fiber content is significantly reduced. Soluble sugars are the largest constituent in white grape pomace (Deng, Q.; Penner *et al.,* 2011). The main part of dietary fibers comprises insoluble fibers like cellulose and hemi-celluloses. Insoluble fibers are characterized by high porosity and low density, improving the efficiency of the digestive tract (Bender, A.B. *et al.,* 2014). Some fiber compounds in grape pomace make chemical bonds with phenolic substances and, thus, create antioxidant dietary fibers, giving the pomace stronger radical scavenging potential. This gives them a higher nutritive value in comparison to dietary fiber present in cereals. Studies confirmed the greater effect of these complex compounds with dietary fibers on human health (Mildner-Szkudlarz, S. *et al.,* 2013). Since fibers from grape skin consist of lignin, cellulose, and hemicellulose, these compounds represent the source of supporting materials (Beres, C. *et al.,* 2017). During grape processing, polyphenols mainly remain in the grape pomace due to their incomplete extraction. The main representatives of polyphenolic compounds in this byproduct are anthocyanins (only in red grape pomaces), catechins, flavonol glycosides, phenolic acids, and alcohols (Kammerer, D. *et al.,* 2004). Together with dietary fibers, phenolic compounds are the most valuable compounds of grape pomace with health beneficial properties, such as the maintenance of intestinal health and the prevention of chronic diseases and cancer and have a synergistic effect in the regulation of metabolism and the prevention and treatment of diseases, such as obesity, insulin resistance, atherosclerosis, osteoporosis (Bender, A.B.B. *et al*., 2020).

In the context of the enhancement of our territory, I have collaborated with Mastroberardino winery, one of the biggest winemakers in the Campania region and Italy. The company provided me with the marc derived from their red wine production. For the edible administration of these extracts/compounds, several formulations and delivery technologies already exist. For instance, recently chitosan and its derivatives have been used as a food excipient in encapsulation technology (T. Coviello *et al*., 2007; V.R. Sinha *et al*., 2001). These matrices are used to protect the bioactivity of encapsulated compounds, control their release outside, reduce their toxicity and promote targeted delivery after absorption from the gastrointestinal tract. This is partly

due to his mucoadhesive capacity, permeation-enhancing effect through biological surfaces, ease of chemical modification and biocompatibility (Liu L. *et al.,* 2003).
During my PhD, I collaborated with the IPCB (Istituto Polimeri Compositi e Biomateriali CNR) on the setting of a pectin-based encapsulation method using ionic crosslinkers Fe^{2+} or Ca^{2+}. Natural biopolymers as those made by pectin, which is also a natural component of the pomace, are particularly interesting for this purpose because of their good biocompatibility, safety, and controlled release properties (Coviello T. *et al*., 2007). Pectins are linear chains made of methoxy-esterified α, d-1, and 4-galacturonic acid units. Pectin with a low degree of esterification (< 50%) is useful for ionotropic gelation (V.R. Sinha *et al*., 2001). As pectins belong to dietary fiber, they are not hydrolyzed in the upper part of the gastrointestinal tract. For this reason, pectin matrices have been widely used to deliver drugs to the colon (Munjeri O., *et al*., 1997; Assifaoui A. *et al.*, 2011). Calcium and zinc have been majorly employed as divalent cations for ionotropic gelation, while the use of iron in that function has been rarely addressed (Ghibaudo F. *et al.,* 2017). Most of the dietary iron is absorbed in the duodenum, however, the colon mucosa also expresses the iron absorption proteins, thus enabling the absorption of 30% of the iron present in the gastrointestinal tract (MCKIE A. *et al.,* 2001). Non-digestible carbohydrates (e.g., pectins, inulins), resist digestion in the small intestine but are fermented in the colon to short-chain fatty acids, with a variety of health benefits, including the enhancement of iron absorption (Yeung, C.K. *et al.,* 2005). In my PhD project, I tested several mixtures of antioxidant metabolites incorporated in pectin-based formulations. I have evaluated the beads' loading efficiency, the release of the bioactive compounds, and their antioxidant activity in an environment mimicking the gastrointestinal tract. The beads appeared to be highly biocompatible and able to decrease the level of ROS in HaCaT cells following hydrogen peroxide treatment. These results are promising and lay the basis for *in vivo* experiments.

1.6. Extraction, purification and chemical characterization of secondary metabolites

C. biflorum bulbs were harvested in Senegal and taxonomically identified. While *C. phelypaea* was harvested at the Finca Torrecillas farm, Corvera, Murcia, Spain. I decided to start from a completely

dehydrated material. The weight of the starting material allowed us to precisely calculate the yield of the extraction procedure.
The bulbs of both *C. biflorum* and *C. phelypaea* plants were dried in the shade, and subsequently finely reduced to powder for the solid-liquid extraction procedure. Solid–liquid extraction is a widely used analytical technique for sample preparation of solids by the partition of analytes between the two involved phases, the matrix and the extractant. The process is regulated by three essential mechanisms: the extractant penetration in the solid matrix, the diffusivity of analytes to the outer space, and the solubility of the analytes in the extractant. Current solid-liquid extraction techniques are essentially based on diffusion and osmosis. To reduce the extraction time and increase the yield, the current trend is to the application of high temperature with high pressure and assistance with auxiliary energies, particularly, microwaves and ultrasound, or to repeat the contact of the extracting solvent with the matrix several times. Indeed, if a solid matrix containing extractable material is immersed in a liquid, the latter begins to enrich itself with compounds having similar chemical properties. This extraction procedure, also named maceration, is the simplest and cheapest one, therefore it is very common. Furthermore, since the extraction takes place at room temperature, there is no alteration of the thermolabile compounds; on the other hand, such a procedure is time-consuming because the extraction takes place mainly for diffusive effects, so much so that, from time to time, it is necessary to shake the system to favor the diffusion of the extracted compounds and avoid localized oversaturation near the surface of the solid to be extracted, which would lead to a slowdown in the global extraction process. Unfortunately, maceration is not always applicable due to the long contact times between the solid and the liquid: vegetables, for example, cannot be placed to macerate in water due to the onset of putrefaction phenomena. For applications, such as the production of essential oils and, in general, compounds with high vapor pressure, steam distillation can be used. This solid-liquid extraction technique requires the transport of volatile compounds by a stream of vapor. In any case, since the extraction system is subjected to certain heating, the thermolabile compounds undergo transformations and consequently are not recovered intact. Today, the research has been directed toward the use of supercritical fluids (SFE, Supercritical Fluid Extraction) . The carbon dioxide in the supercritical phase assumes the characteristics of a non-polar solvent and is comparable to n-hexane; with this method, it is therefore possible to extract non-polar compounds from solid matrices. The advantage of the SFE is that at the end of the extraction the solvent

(carbon dioxide) is removed in the form of gas, making it possible to recover the concentrated extracted compounds. This technique has industrial applications such as the extraction of oil from seeds, caffeine from coffee, nicotine from tobacco, fat from seed oil, etc. However, it is very expensive and not universally applicable.
To prepare the extract I used the Soxhlet process which can be consistently developed from small volumes to industrial scale. During Soxhlet extraction, the sample is finely powdered and placed into a porous bag made of filter paper. It is then placed into the Soxhlet extractor which is an apparatus containing different chambers with a heat source below it. An extractant will drip into the main chamber causing the liquid level of the main chamber to rise. Once the main chamber of the Soxhlet apparatus rises high enough, it will reach a siphon tube that will drip down into a flask at the bottom. This process is repeated continuously for an exhaustive extraction of active compounds from the plant matrix, with high efficiency and employing a low amount of solvent.
The SOXHLET equipment was created for the extraction of lipids from solid materials; the method replaces filtration in cases where the solute to be separated has a reduced solubility for the solvent and the impurities are insoluble in the solvent (if the solubility of the solute in the solvent is high enough, filtration is used). The advantage of solvent extraction in Soxhlet is that the extraction material is continuously in contact with the pure solvent, and this makes the continuous process much more efficient. Less solvent is used because it is continuously recirculated. Furthermore, during the whole operation, there is no dispersion of volatile solvents into the environment. The equipment is used for quantitative analysis in the determination of yield (yield% = extracted mass * 100 / raw mass). Another advantage is that different types of solvents can be used depending on the chemical nature of the compounds to be extracted. Unfortunately, it cannot be used for thermolabile molecules that degrade under the effect of heat. First, I used ethanol, to primarily extract the polar or mid-polar fraction of the plant. The obtained mixture of compounds was then purified for qualitative and quantitative evaluations using bioassay-guided chromatography techniques (TLC, LC, HPLC) according to their chemical and physical properties. Subsequently, using advanced spectroscopic techniques (IR, UV, EI-, ESI-MS, 1D e 2D 1H- and 13C-NMR) it was possible to determine their chemical structure. In some cases, it was possible to obtain crystals of particularly pure metabolites, by slow solvent evaporation. The three-dimensional, crystallographic structure was obtained by X-ray analysis.

CHAPTER II

2. Crinum biflorum Rottb.

2.1. Omoisoflavanoids and alkylamides isolated from *Crinum biflorum Rottb.* collected in Senegal

The raw extract of *C. biflorum* bulbs was fractionated on chromatographic columns, according to the experimental scheme shown in figure 1. Through these procedures, I could isolate and characterize four homoisoflavonoids and one alkylamide, as 5,6,7-trimethoxy-3-(4-hydroxybenzyl)chroman-4-one (1), as 3-hydroxy-5,6,7-trimethoxy-3-(4-hydroxybenzyl)chroman-4-one (2), as 3-hydroxy-5,6,7-trimethoxy-3-(4-methoxybenzyl)chroman-4-one (3) and as 5,6,7-trimethoxy-3-(4-methoxybenzyl)chroman-4-one (4), and the alkylamide as (E)-N-(4-hydroxyphenethyl)-3-(4-hydroxyphenyl)acrylamide (5), commonly named Np- coumaroyltyramine. Metabolites 2 and 3 were previously identified as urgeanin A and B, respectively; they have been isolated from this species for the first time (figure 2). The isolated compounds have been identified comparing their ^{1}H NMR and ESI MS spectra with the data reported in the literature. Furthermore, the specific optical rotation and the electronic circular dichroism (ECD) of the compounds of the isolated compounds supported their identification (figure 3).

To investigate the possible applications of *Crinum*-derived metabolites, I tested their biological activity by *in vitro* assays on human cells. These studies allowed me to observe the effects of isolated metabolites on pathways controlling cell proliferation and survival and derive some possible structure-activity relationships.

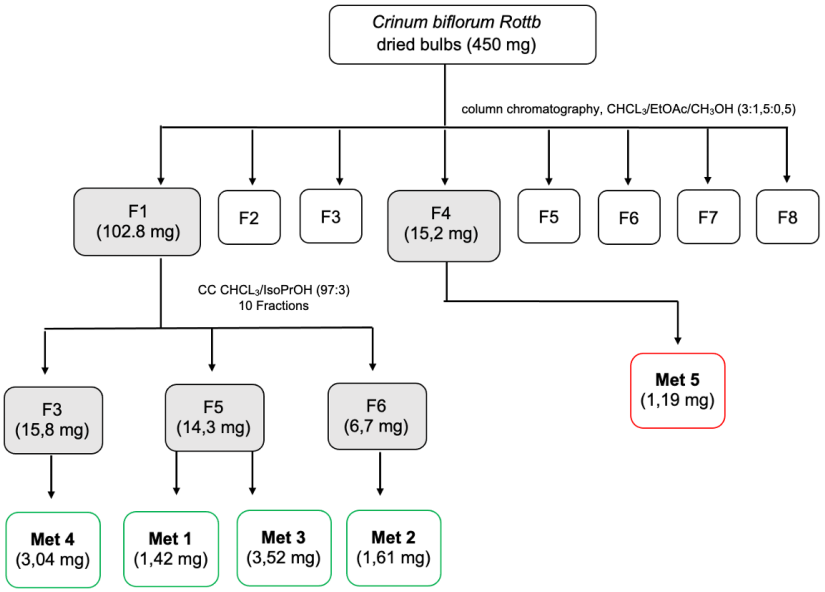

Figure 1. Schematic representation of the extraction and purification process of pure metabolites, starting from the dried bulbs of *C. biflorum*.

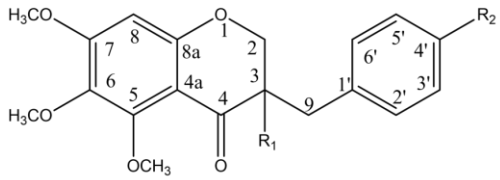

1, R_1=βH, R_2=OH
2, R_1=βOH, R_2=OH
3, R_1=βOH, R_2=OCH_3
4, R_1=αH, R_2=OCH_3

1, 3-(4-hydrobenzyl)-5,6,7-trimethoxychroman -4-one
2, 3-hydroxy-5,6,7-trimethoxy-3-(4-hydroxybenzyl)chroman-4-one = urgineanin B
3, 3-hydroxy-5,6,7-trimethoxy-3-(4-methoxybenzyl)chroman-4-one= urgineanin A
4, 5,6,7-Trimethoxy-3-(4-methoxy-benzyl)-chroman-4-one

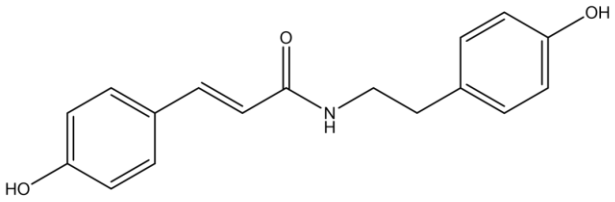

5, (*E*)-*N*-(4-hydroxyphenethyl)-3-(4-hydroxyphenyl)acrylamide

Figure 2. Structure of homoisoflavanoids (1 - 4) and alkylamide (5) isolated from *C. biflorum* bulbs.

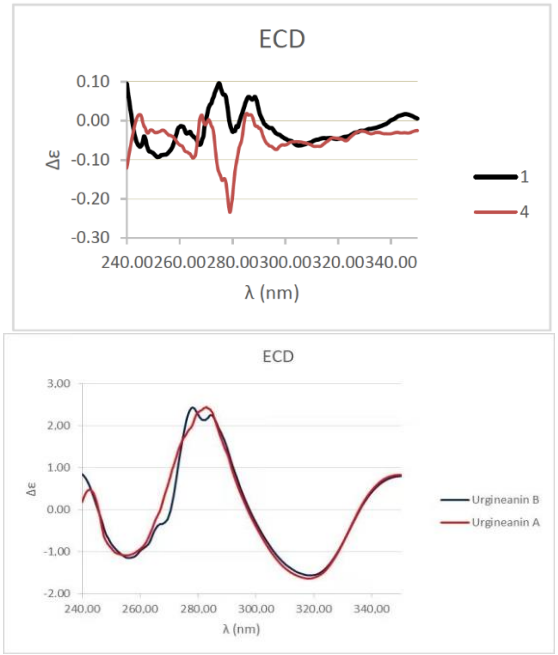

Figure 3. Experimental ECD spectra of homoisoflavanoids (1) (black solid line), and 4 (red line) on left; and of homoisoflavanoids (2) (black solid line), and 3 (red line) on right.

2.2. Biological properties of omoisoflavonoids and alkylammide

Flavonoids consist of a large group of polyphenolic compounds having a benzo-*γ*-pyrone structure and are ubiquitously present in plants. They are synthesized by the phenylpropanoid pathway. Flavonoids are hydroxylated phenolic substances responsible for a variety of pharmacological activities (Mahomoodally, M.F. *et al.,* 2005; Pandey, A.K., 2007); their activities are structure dependent. The chemical nature of flavonoids depends on their structural class, degree of hydroxylation, other substitutions and conjugations, and degree of polymerization (Kelly, E.H. et al., 2002). Flavonoids are synthesized by plants in response to microbial infection (Dixon, R.A. *et al.,* 1985). Several studies have suggested the protective effects of flavonoids against infectious diseases, bacterial and viral, as well as degenerative

diseases such as cancers, and cardiovascular and other age-related diseases. Flavonoids are known to promote human health and can induce protective enzyme systems in human cells. The best-described property of almost every group of flavonoids is their capacity to act as antioxidants. The flavonoid heterocycle contributes to antioxidant activity by permitting conjugation between the aromatic rings and the presence of a free 3-OH. Removal of a 3-OH annuls coplanarity and conjugation compromises scavenging ability. Generally, the O-methylation of hydroxyl groups of flavonoids decreases their radical scavenging capacity. Some flavonoids such as hesperidin, apigenin, luteolin, and quercetin are reported to possess anti-inflammatory and analgesic effects. Flavonoids may affect specifically the function of enzyme systems critically involved in the generation of inflammatory processes, especially tyrosine and serine-threonine protein kinases.

Fruits and vegetables containing flavonoids have been reported as cancer chemopreventive agents (Mishra, A. *et al*., 2013). Downregulation of mutant p53 protein, induction of cell cycle arrest and inhibition of Ras proteins expression are among the molecular mechanisms more frequently associated with the action of flavonoids

Alkylamides are structurally diverse with a wide range of pharmacological effects (Boonen, *et al*. 2012). Several studies on the chemical compositions and pharmacological activities of plants have established the contributions of alkylamides in pharmaceuticals, cosmetology, and the food industry (Taiwo O. E. *et al.,* 2020).

Alkylamide obtained from plants are usually lipophilic substances with some growth regulatory functions, like N-acylethanolamines (NAEs) (Hajdu *et al.,* 2014) and dependent on the cytokinin-signaling pathway (López-Bucio *et al*., 2007). Additional pharmacological activities include immunomodulatory, anti-inflammatory, analgesic, antiviral, and antifungal. For example, the antioxidant activity of the alkylamide fraction of *Echinacea* species was shown by measuring its inhibition activity of *in vitro* Cu (II)-catalyzed oxidation of human low-density lipoprotein (LDL).

To test the potential use of Np-cumaroyltyramine alkylamide as an adjuvant in anticancer treatment, I performed *in vitro* MTT cell viability assays using tumor and immortalized cell lines as control.

Similarly, I evaluated the *in vitro* cytotoxicity of omoisoflavonoids (1–4) from *C. biflorum* towards HaCaT, A431 and HeLa human cells. To this aim, low-density cells were treated with increasing concentrations of each metabolite, from 0.5 to 10 μM in DMSO, for 24 and 48 h of incubation. The results of these experiments are shown in figure 4. All metabolites isolated were toxic to tumor cell lines in a dose- and time-

dependent manner with HeLa cells being more sensitive than A431. Remarkably, all metabolites appeared to be less toxic on immortalized HaCaT keratinocytes at the concentration range tested and 24 hours of incubation although a significant reduction in HaCaT cell viability was caused by metabolites 3 and 4 when assayed at 48 h incubation time. The N-p-cumaroyltyramine (5) at the lower concentrations tested, 0.5 and 1 μM, increased the viability of HaCaT cells while it was ineffective at higher concentrations. At 10 μM it was cytotoxic in both A431 and HeLa cancer cells (figure 4).

- HaCaT cells: 96-well, sixfold, $1^* 10^4$

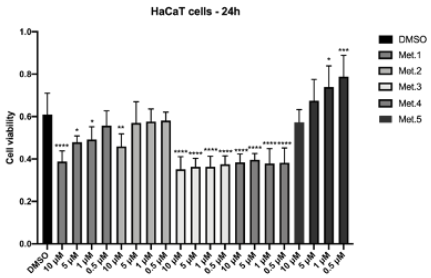

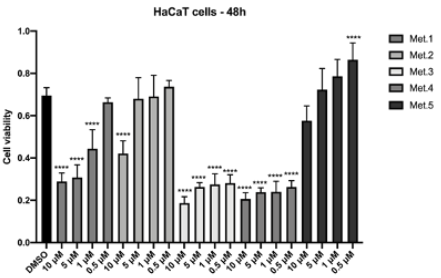

- A431 cells: 96-well, sixfold, $8^* 10^3$

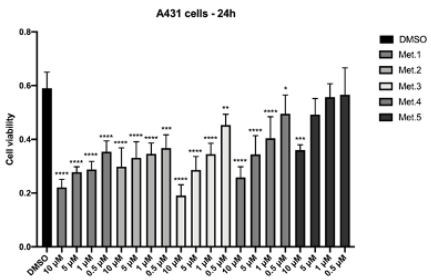

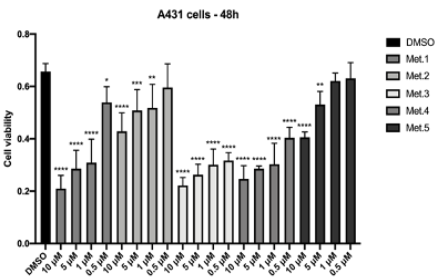

- Hela cells: 96-well, sixfold, $8^* 10^3$

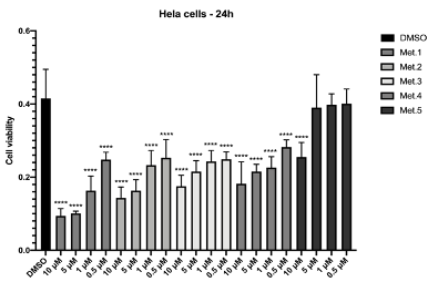

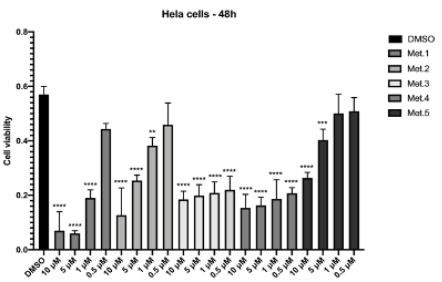

Figure 4. MTT viability assays with homoisoflavanoids 1–4 and N-p-coumaroyltyramine (5) from *C. biflorum* on HaCaT, A431 and Hela human cell lines. Statistical analyses were performed using one-way ANOVA and Dunnett's multiple comparisons test. Levels of significance between points of expression are indicated (**** $p < 0.001$, *** $p < 0.01$, ** $p < 0.02$, * $p < 0.05$).

To get insights into the mechanism of cytotoxicity of these metabolites, I investigated their ability to induce genomic damage. DNA damage changes the spatial configuration of the helix. Normally, cells respond to this alteration in two ways depending on the extent of the damage itself: by implementing repair processes or by dying by apoptosis or other cell death program paradigms.

The γ-H2AX foci assay indirectly supplies evidence of the DNA double-strand breaks (DSB) occurrence and/or DNA replication stress (Sangermano *et al.*, 2019). The γ-H2AX assay exploits the phosphorylation of the histone variant H2AX (resulting in γ-H2AX) in response to the induction of DNA DSB (Nakamura A. J. *et al*., 2008; Rogakou, E.P. *et al.,* 1998; Rogakou, E. P. *et al.,* 1999; Sedelnikova, O. A. *et al.,* 2003). The phosphorylation is initiated at a site of DSB but extends to the adjacent chromatin area (Collins, P. L. *et al*., 2020). After induction of a DNA double-strand break, H2AX histone becomes rapidly phosphorylated to serine 139 (Rogakou, E.P. *et al.,* 1998). This phosphorylation event is dynamic, complex and depends on the interactions between MDC1, H2AX and ATM and more kinase to persist (Dickey, J.S. *et al.,* 2009). This amplified response is easily detected using specific antibodies versus γ-H2AX, which manifests discrete nuclear foci.

To detect metabolite-induced DNA damage I performed immunofluorescence using antibodies versus γ-H2AX following the treatment of HaCaT, HeLa and A431 cells with 10 μM metabolites 3 or 4. as they showed the greatest cytotoxicity. Upon 24 h of treatment, I revealed a remarkable increase of nuclear γ-H2AX foci in all tested cell lines, Interestingly, the HaCaT cells displayed significantly fewer foci of DNA damage than tumor cells indicating that immortalised cells were more resistant to the cytotoxic effect of metabolites (figure 5).

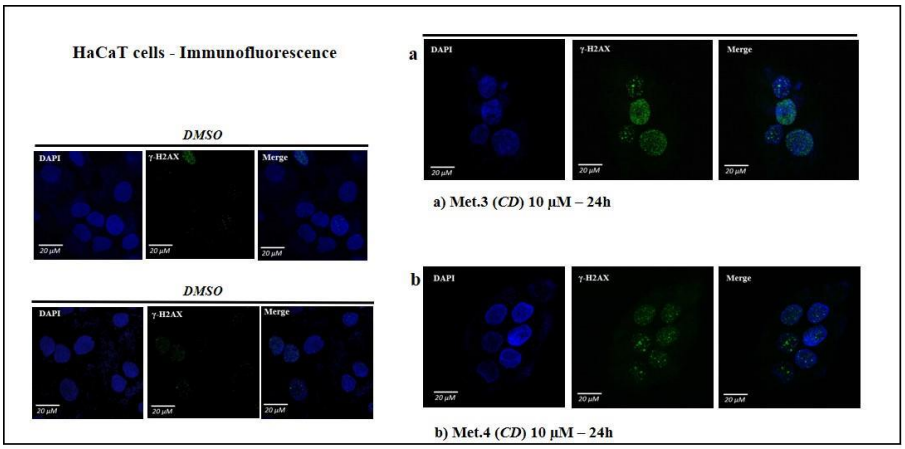
HaCaT cells - Immunofluorescence
DMSO
DAPI
γ-H2AX
Merge
20 μM
DMSO
DAPI
γ-H2AX
Merge
20 μM
a
DAPI
γ-H2AX
Merge
20 μM
a) Met.3 (CD) 10 μM – 24h
b
DAPI
γ-H2AX
Merge
20 μM
b) Met.4 (CD) 10 μM – 24h

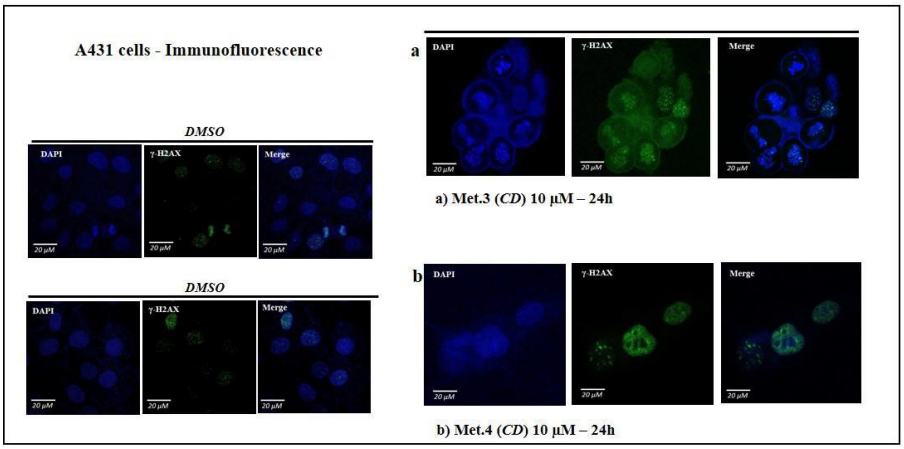
A431 cells - Immunofluorescence
DMSO
DAPI
γ-H2AX
Merge
20 μM
DMSO
DAPI
γ-H2AX
Merge
20 μM
a
DAPI
γ-H2AX
Merge
20 μM
a) Met.3 (CD) 10 μM – 24h
b
DAPI
γ-H2AX
Merge
20 μM
b) Met.4 (CD) 10 μM – 24h

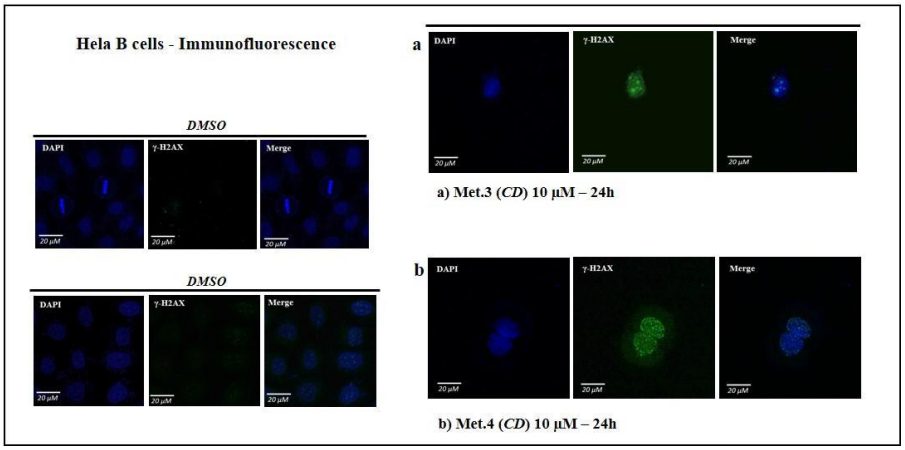
Hela B cells - Immunofluorescence
DMSO
DAPI
γ-H2AX
Merge
20 μM
DMSO
DAPI
γ-H2AX
Merge
20 μM
a
DAPI
γ-H2AX
Merge
20 μM
a) Met.3 (CD) 10 μM – 24h
b
DAPI
γ-H2AX
Merge
20 μM
b) Met.4 (CD) 10 μM – 24h

Quantification of γ-H2AX mean fluorescence

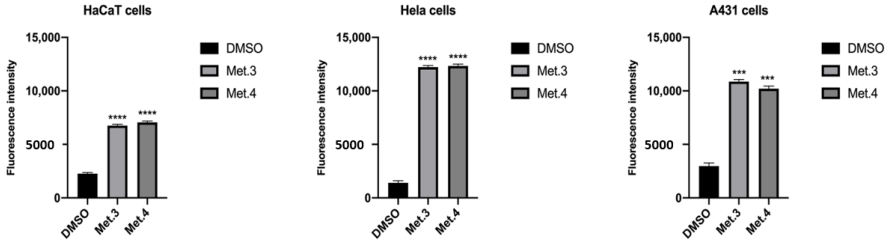

Figure 5. Immunofluorescence microscopy showing γ-H2AX foci formation (green) in nuclei of HaCaT, A431 cells or HeLa cells treated with DMSO alone or 10 μM 3 or 4 for 24 h. Nuclei were stained with DAPI (blue). Note the abnormal morphology of nuclei induced by 3 and 4 in A431 cells compared to HaCaT cells. Images from 3 fields per each experimental point were collected to obtain data for up to 150 cells. Quantitation of γ-H2AX foci fluorescence was performed by Image J software and shown as mean ± SD in graph bars of panels (under). Statistical analyses were performed using one-way ANOVA and Dunnett's multiple comparisons test. Levels of significance between points of expression are indicated (**** $p < 0.001$, *** $p < 0.01$).

The occurrence of DNA damage following treatment with secondary metabolites could be associated with the hyper-production of reactive oxygen species. The cell possesses a powerful antioxidant defense system to fight an increase in ROS production. However, if ROS generation exceeds their natural antioxidant defenses, the cells undergo oxidative stress. This condition appears to be related to aging and the onset of human degenerative diseases including cancer, atherosclerosis and neurodegenerative and cardiovascular diseases. Therefore, it is important to determine and quantitate whether a certain compound can induce the production of reactive oxygen. The DCFDA assay is a rapid and reproducible fluorometric assay, which allows evaluating the intracellular production of peroxides, using the 2'-7'-dichlorofluorescine diacetate (DCFH-DA), a molecule able to cross freely the cell membranes. The DCFH-DA is enzymatically hydrolyzed by intracellular esterase to non-fluorescent dichlorofluorescein (DCFH), thus losing the ability to back diffuse across the membrane. In the presence of ROS, DCFH is oxidized to DCF highly fluorescent, detectable, and quantifiable by flow cytometry or spectrofluorimetry; the antioxidant capacity can therefore be related to the fluorescence of the probe (Wang *et al.,* 1999). The cells are pretreated with the different metabolites, then with DCFH-DA: this allows us to evaluate the effect of secondary metabolites on intracellular redox status.

As shown in figure 6.A, following 24 treatments with metabolites 3 and 4 we didn't observe an increase in ROS production thus indicating that a molecular mechanism other than ROS generation was responsible for the observed DNA damage (figure 6.A). Then, I tested the induction of apoptosis which represents an important therapeutic goal of anticancer compounds. PARP1 cleavage immunodetection is a typical molecular feature of apoptosis. Poly (ADP-ribose) polymerase-1 (PARP-1), a 115 kDa protein, plays the active role of a "nick sensor" during DNA repair and apoptosis when it synthesizes ADP-ribose from NAD+ in the presence of DNA strand breaks. In addition, PARP-1 becomes a target of apoptotic caspases, which give rise to two proteolytic fragments of 89 and 24 kDa. Analysis of the presence of the 89 kDa proteolytic fragment revealed that proteolysis of PARP-1 by caspases is associated with the synthesis of poly (ADP-ribose). It is a very early response to the apoptotic stimulus (Soldani C. *et al*., 2001).
Therefore, I performed immunoblots of extracts from cells treated with metabolites 3 or 4 for 48 hrs. As shown in figure 6.B, the cleaved PARP-1 signal (89 kDa) was evident in all tested cell lines while the level of the cell cycle inhibitor p21WAF was significantly reduced thus indicating that the decrease in cell viability was due to apoptotic cell death rather than cell proliferation arrest (figure 6.B).

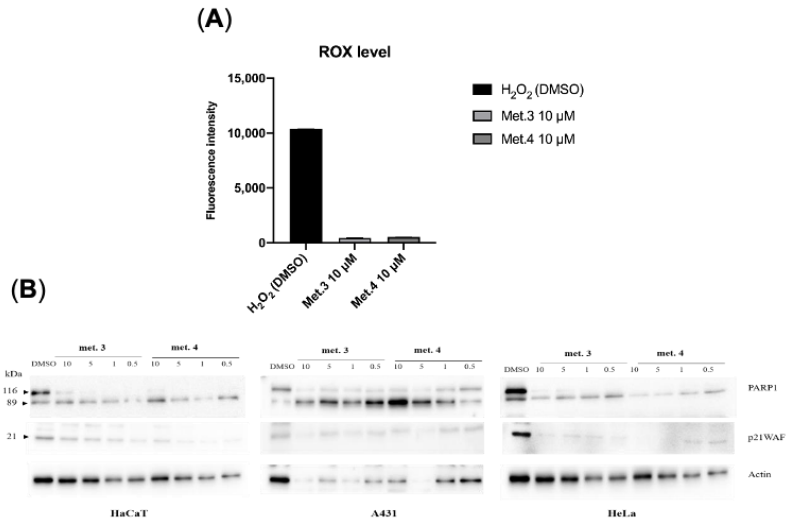

Figure 6. **(A)** DCFDA on HaCaT cells pre-treated for 4 h with 10 μM 3 and 4 from *C. biflorum*. H_2O_2 (1 mM; 3%) was added to the medium for 45' and used as a positive control. The fluorescence intensity of DCFDA was read after 45' of incubation. **(B)** Representative immunoblot analysis showing the effect of 3 and 4 on PARP1 activation and p21WAF protein levels. Full-length and cleaved PARP1 bands were revealed by immunoblot with specific antibodies. The blots were then re-probed with an actin antibody to check for protein loading.

As described before, low concentration of N-p-coumaroyltyramine (met. 5) up to 10 μM, caused a slight increase of viability in HaCaT cells. Moreover, given the chemical structure of the metabolite, made up of a conjugated structure of double bonds, we tested its ability to scavenge ROS. The ability to inhibit the production of ROS can be verified by measuring the ROS level in cells treated or not with the metabolite after cell exposure to oxidizing agents such as hydrogen peroxide.
Therefore, HaCaT immortalized cells were pretreated for 4 hrs with metabolite 5, at the concentrations of 10 and 100 μM, and then subjected to oxidative stress by H_2O_2 addition. As shown in figure 7, fluorescence intensity of DCF in sample treated with met 5 was comparable to those of samples treated with 10 μM Trolox, the water-soluble derivative of vitamin E used as a positive control. thus suggesting that met 5 is a promising antioxidant agent.

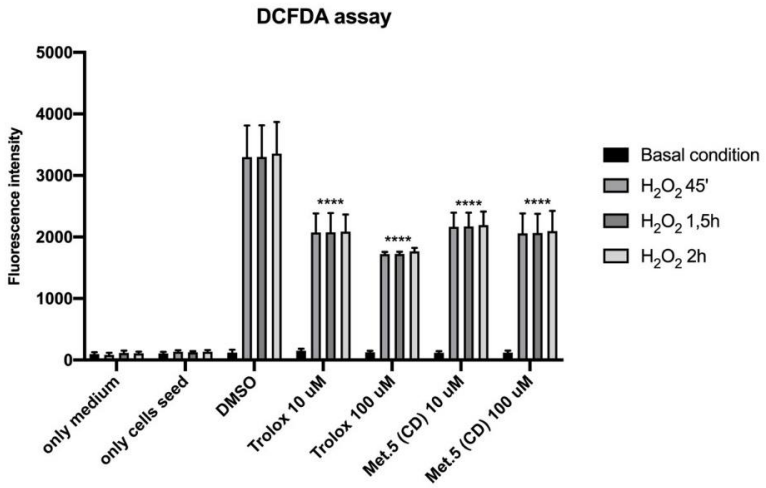

Figure 7. DCFDA assay. HaCaT cells were seeded and pre-treated for 4 h with 10 and 100 μM N-p coumaroyltyramine (5) from *C. biflorum*. H_2O_2 (1 mM; 3%) was added to the medium for 45', 1.5 and 2 h. The fluorescence intensity of DCFDA was read after 450 of incubation. Trolox was used as a positive control. Levels of significance between points of expression are indicated (**** $p < 0.001$).

During my PhD, I purified a higher amount of metabolites from Crinum to send them to the Department of Chemistry, Biochemistry and Physics, at the University of Quebec, Canada to evaluate additional biological activities. I had the opportunity to collaborate with the group

of Prof. Isabel Desgagnè Penix, who investigated the antiviral, anti-acetylcholinesterase and anti-diabetic properties of our isolated metabolites. Increasing concentrations of the metabolites from 12.5 to 100 μM were tested to evaluate the antiviral activity towards cells infected using VSV-G pseudotyped HIV-1 particles. Metabolites 1, 2, and 5 showed weak antiviral activity at 50 μM, while metabolites 3 and 4 significantly enhanced the death of infected cells at all concentrations tested. Cytotoxicity was evaluated by propidium iodide staining of TPH-1 after an incubation time of 72 hours. These experiments were performed using a single-cycle infection system when the intrinsic metabolite cytotoxicity was negligible. In conclusion, it can therefore be said that the metabolites present in *Crinum* also have significant antiviral activity, especially metabolites 3 and 4 (figure 8).

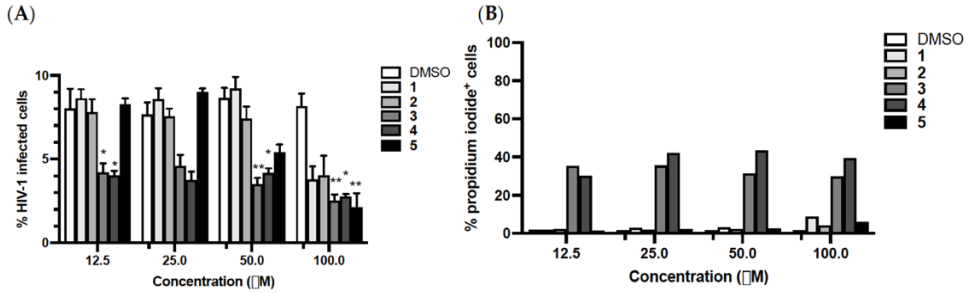

Figure 8. Antiviral activity of compounds 1–5. **(A)** THP-1 cells were treated with four concentrations (12.5, 25, 50 and 100 μM) of each compound in triplicates and infected with VSV-G pseudo typed HIV-1GFP at MOI = 1. Infection levels were assessed by flow cytometry 72 h post-infection. Bars show means with standard deviation. Kruskal–Wallis and uncorrected Dunn's tests were performed to assess statistically significant differences between groups. * $p < 0.05$; ** $p < 0.01$. **(B)** Cell death (% propidium iodide+ cells) was measured by flow cytometry following PI staining 72 h post-treatment of THP-1 with 1, 2, 3, 4 and 5. Matched concentrations of DMSO were used as a negative control.

The increasing interest in flavonoids is due to their wide range of pharmacological activities. Indeed, they can bind to biological polymers including enzymes, transporters, hormones and DNA. They can chelate transition metal ions such as Fe^{2+}, Cu^{2+} and Zn^{2+}, catalyze electron transport and debug free radicals.

Metabolite 5, N-p-coumaroyltyramine, which showed no cytotoxic activity was tested for possible anti-acetylcholinesterase properties. Acetylcholinesterase inhibitors (AChEI) are the best available pharmacotherapy for the treatment of Alzheimer Disease (AD)

symptoms, increasing the neurotransmitter acetylcholine levels at cerebral cortex synapses. Many natural products have been reported as acetylcholinesterase inhibitors, mainly alkaloids. Therefore, current efforts to identify new AChEI are mostly focused on alkaloids, however, today there is increasing interest also on non-alkaloid compounds. (Uriarte-Pueyo *et al*., 2011). The mechanism by which medicinal plants can induce therapeutic effects in AD patients may be diverse and include the production of anti-amyloid, anti-apoptotic, antioxidant and anti-inflammatory activities, as well as targeting cholinergic deficiencies (Howes and Houghton 2003; Hajiaghaee and Akhondzadeh 2012; Syad & Devi, 2014). Acetylcholinesterase (AChE) is an enzyme belonging to the hydrolase class and to the cholinesterase family which catalyzes the following reaction: acetylcholine + H_2O → choline + acetate. The enzyme is normally present in the mammalian organism localized in the post-synaptic membrane of the cholinergic junctions. Its function is to hydrolyze acetylcholine by splitting it into choline and acetic acid. The activity of this enzyme can be modified both by drugs, in the treatment of diseases such as Alzheimer's, and by natural toxins, such as the well-known alkaloid galantamine. These metabolites block the enzyme that degrades acetylcholine (acetylcholinesterase), a neurotransmitter important for promoting communication between neurons. The final effect that derives from the blockade of acetylcholinesterase is the increase of acetylcholine levels in the synaptic space, the junctions between neurons.
Metabolite 5 was shown to be ineffective in inhibiting the acetylcholinesterase enzyme. Metabolites 1, 2 and 4 reduced the AchE enzyme activity up to 20%, in a dose-dependent way, while metabolite 3 reduced the activity up to 30% at the lower concentrations thus being the most effective (figure 9).

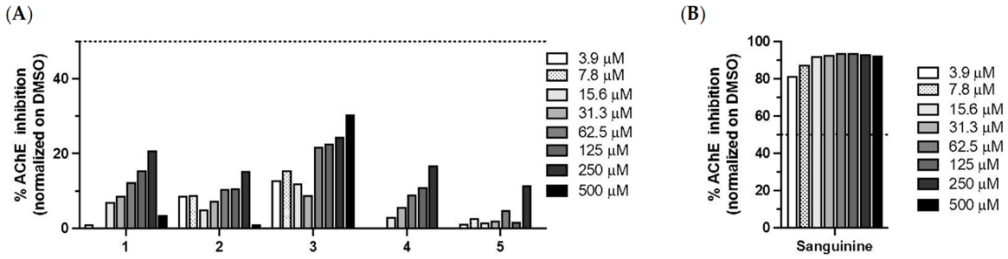

Figure 9. **(A)** Anti-AChE activity. AChE-catalyzed reaction was assessed in presence of each compound at concentrations ranging from 3.9–500 mM and matched concentrations of DMSO after a 10 min incubation. The percentage of anti-AChE inhibition was calculated according to

the following formula: 100 - [((E - S)/E) x 100], where E is the activity of the enzyme with matched concentrations of DMSO and S is the activity of the enzyme with the test sample. Compound 5 weakly inhibited AChE-catalyzed reaction at high concentrations. Compounds 1, 2 and 4 displayed increasing inhibition from 15.6 μM to 250 μM up to 20%. Compound 3 was the most potent inhibitor of AChE, blocking 15–30% of enzyme activity as concentrations increased from 3.9 to 500 μM. **(B)** Sanguinine (isolated from C. jagus) was used as a positive control.

Many flavonoids extracted from plants inhibit α-amylase and α-glucosidase activities *in vitro* and improve postprandial glycemia in diabetic animal models (Gong L. *et al*., 2020). Inhibition of the α-amylase enzyme has been positively associated with the antioxidant activity of the natural extract (Patrick L. *et al*., 2006). The consumption of foods rich in hydrolysing enzyme inhibitors is recommended for the nutraceutical therapy of diabetes. α-amylase initiates the process of carbohydrate digestion by hydrolysis of 1,4-glycosidic bonds of polysaccharides (starch, glycogen) to disaccharides, and α-glucosidase catalyzes disaccharides to monosaccharides, which leads to hyperglycemia. Taking a wheat amylase inhibitor, for 9 weeks after meals, was reported to reduce postprandial amylase levels, delay carbohydrate digestion and absorption, and lower blood glucose levels without affecting the growth of the pancreas (Bernfeld, 1955). The strategy of reducing carbohydrate digestibility by controlling the activity of two hydrolyzing enzymes (α-amylase and α-glucosidase) to control postprandial hyperglycemia is considered a viable prophylactic treatment of type 2 diabetes mellitus (T2DM). We have shown that a strong inhibitor of the anti-amylase and anti-glucosidase activity is N-p-coumaroyltyramine. Metabolites 1, 2 and 3 also showed inhibitory activity, but at high concentrations, so they are less efficient (figure 10).

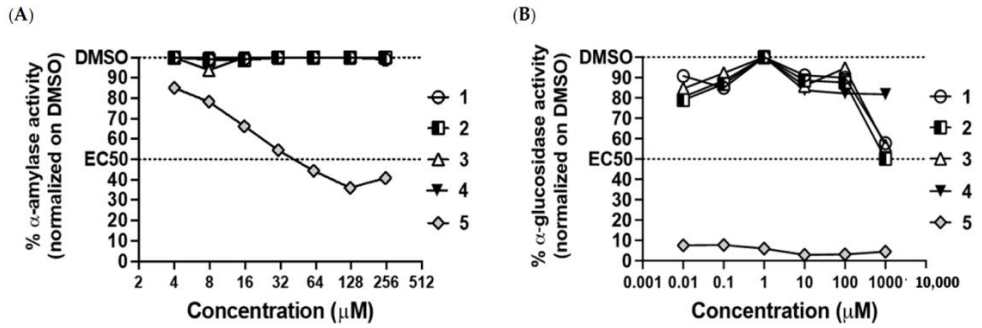

Figure 10. **(A)** Anti-α-amylase activity. Kinetics of α-amylase reaction was measured in presence of each compound at concentrations ranging from 3.9—250 µM, and matched concentrations of DMSO solvent over a 26 min period. Areas under the curves (AUC) of OD (410 nm) vs. time were calculated according to Zhang et al. (2014) and used to determine enzyme activity defined as the ratio of the AUC for each compound at each concentration normalized on the AUC in presence of DMSO matched concentration. Compound 5 strongly inhibited α-amylase catalyzed reaction with an IC50of 40 µM. **(B)** Anti-α-glucosidase activity. Kinetics of α-glucosidase reaction were measured in presence of each compound at concentrations ranging from 0.01–1000 µM, and matched concentrations of DMSO solvent over a 40 min period. Areas under the curves (AUC) of OD (410 nm) vs. time were calculated and used to determine enzyme activity defined as the ratio of the AUC for each compound at each concentration normalized on the AUC in presence of DMSO matched concentration. Compound 5 nearly completely inhibited α-glucosidase catalyzed reaction with at all concentration tested. Compounds 1, 2 and 3 inhibited 50% of the reaction at 1 mM. For all assays, enzyme, no compound, and inhibitor controls were included.

2.3. Conclusions

Prevention and cure of diseases using phytochemicals such as flavonoids and alkylamides are well known. A variety of these natural compounds possess their physical, chemical, and physiological properties. Structure-function relationship is the epitome of major biological activities. The medicinal efficacy of many flavonoids as antibacterial, hepatoprotective, anti-inflammatory, anticancer, and antiviral agents or of alkylamides as anti-diabete, and antioxidant agents is well established. These substances are more commonly used in developing countries. The therapeutic use of new compounds must always be validated using specific biochemical tests.

Very few studies have been performed on *C. biflorum* (syn. *C. distichum*) from a chemical and applicative point of view. Unexpectedly, no alkaloids were detected in the acid organic extract from bulbs of *C. biflorum*, neither using the traditional ethanol extraction method with Soxhlet nor the optimized extraction method (Evidente *et al*., 1984). However, the organic extract obtained with the Soxhlet method showed the presence of homoisoflavonoids. From *C. biflorum*, I have isolated and characterized four homoisoflavonoids and one alkylamide for the first time in this Amaryllidaceae plant collected in Senegal. Flavonoids 1, 3 and 4 have shown significant selective cytotoxicity against human cancer cell lines HeLa and A431. The N-p-coumaroyltyramine (met 5) was selectively toxic to A431 and HeLa cancer cells, while it protected immortalized HaCaT cells against oxidative stress induced by hydrogen peroxide. Compounds 1–4 also inhibited acetylcholinesterase activity, with compound 3 being the most potent. The anti-amylase and the strong anti-glucosidase activity of compound 5 were confirmed. *In vivo*

preclinical tests are now required to provide newer insights on these promising compounds, They will certainly lead to a new era of flavonoid and alkylamines based pharmaceutical agents for the treatment of many infectious and degenerative diseases. Finally, this study extends the chemical library of compounds that can be potential candidates as adjuvants in cancer chemotherapy.

biomolecules

MDPI

Article

Isolation and Biological Characterization of Homoisoflavanoids and the Alkylamide *N-p*-Coumaroyltyramine from *Crinum biflorum* Rottb., an Amaryllidaceae Species Collected in Senegal

Marco Masi [1,*], Manoj Koirala [2], Antonella Delicato [3], Roberta Di Lecce [1], Natacha Merindol [2], Seydou Ka [2,4], Matar Seck [4], Angela Tuzi [1], Isabel Desgagne-Penix [2], Viola Calabrò [3,*] and Antonio Evidente [1]

[1] Dipartimento di Scienze Chimiche, Universita' di Napoli Federico II, Complesso Universitario Monte Sant'Angelo, Via Cintia 4, 80126 Napoli, Italy; roberta.dilecce@unina.it (R.D.L.); tuzi@unina.it (A.T.); evidente@unina.it (A.E.)

[2] Département de Chimie, Biochimie et Physique, Université du Québec à Trois-Rivières, 3351, Boul. des Forges, C.P. 500, Trois-Rivières, Québec, G8Z 4M3, Canada; manoj.koirala@uqtr.ca (M.K.); natacha.merindol@uqtr.ca (N.M.); seydou.ka@uqtr.ca (S.K.); isabel.desgagne-penix@uqtr.ca (I.D.-P.)

[3] Dipartimento di Biologia, Universita' di Napoli Federico II, Complesso Universitario Monte Sant'Angelo, Via Cintia 4, 80126 Napoli, Italy; antonella.delicato@unina.it

[4] Laboratoire de Chimie Organique et Chimie Thérapeutique, Faculté de Médecine, de Pharmacie et d'Odontologie de Dakar, Dakar, Senegal; matarsec@yahoo.fr

* Correspondence: marco.masi@unina.it (M.M.); vcalabro@unina.it (V.C.)

Citation: Masi, M.; Koirala, M.; Delicato, A.; Di Lecce, R.; Merindol, N.; Ka, S.; Seck, M.; Tuzi, A.; Desgagne-Penix, I.; Calabrò, V.; Evidente, A. Isolation and Biological Characterization of Homoisoflavanoids and the Alkylamide *N-p*-Coumaroyltyramine from *Crinum biflorum* Rottb., an Amaryllidaceae Species Collected in Senegal. *Biomolecules* **2021**, *11*, 1298. https://doi.org/10.3390/biom11091298

Academic Editors: Anna Sparatore and Vito Verardo

Received: 22 July 2021
Accepted: 27 August 2021
Published: 31 August 2021

Abstract: *Crinum biflorum* Rottb. (syn. *Crinum distichum*) is an Amaryllidaceae plant used in African traditional medicine but very few studies have been performed on this species from a chemical and applicative point of view. Bulbs of *C. biflorum*, collected in Senegal, were extracted with ethanol by Soxhlet and the corresponding organic extract was purified using chromatographic methods. The pure compounds were chemically characterized by spectroscopic techniques (1D and 2D ^{1}H and ^{13}C NMR, HR MS and ECD) and X-ray analysis. Four homoisoflavonoids (**1–4**) and one alkylamide (**5**) were isolated and characterized as 5,6,7-trimethoxy-3-(4-hydroxybenzyl)chroman-4-one (**1**), as 3-hydroxy-5,6,7-trimethoxy-3-(4-hydroxybenzyl)chroman-4-one (**2**), as 3-hydroxy-5,6,7-trimethoxy-3-(4-methoxybenzyl)chroman-4-one (**3**) and as 5,6,7-trimethoxy-3-(4-methoxybenzyl)chroman-4-one (**4**), and the alkylamide as (*E*)-*N*-(4-hydroxyphenethyl)-3-(4-hydroxyphenyl)acrylamide (**5**), commonly named *N-p*-coumaroyltyramine. The relative configuration of compound **1** was verified thanks to the X-ray analysis which also allowed us to confirm its racemic nature. The absolute configurations of compounds **2** and **3** were assigned by comparing their ECD spectra with those previously reported for urgineanins A and B. Flavanoids **1**, **3** and **4** showed promising anticancer properties being cytotoxic at low micromolar concentrations towards HeLa and A431 human cancer cell lines. The *N-p*-coumaroyltyramine (**5**) was selectively toxic to A431 and HeLa cancer cells while it protected immortalized HaCaT cells against oxidative stress induced by hydrogen peroxide. Compounds **1–4** also inhibited acetylcholinesterase activity with compound **3** being the most potent. The anti-amylase and the strong anti-glucosidase activity of compound **5** were confirmed. Our results show that *C. biflorum* produces compounds of therapeutic interest with anti-diabetic, anti-tumoral and anti-acetylcholinesterase properties.

Keywords: *Crinum biflorum*; homoisoflavanoids; alkylamides; cytotoxicity; antioxidant; antidiabetic and anti-acetylcholinesterase activities

1. Introduction

Plants and microorganisms are well-known sources of bioactive metabolites which have only been partly investigated [1]. Among the plants' kingdom, the Amaryllidaceae is a plant family extensively studied essentially for its alkaloids and related isocarbostiryls content which show a broad spectrum of biological activities [2–5]. These plants are principally diffused in tropical and subtropical regions of the world, as Andean South America, the Mediterranean basin and Southern Africa [6], and include ca 1600 species classified into about 75 genera [7]. Hundreds of Amaryllidaceae alkaloids with different structures and biological activities were isolated and reported in several reviews. A Special Issue of the journal *Molecules* was edited by Bastida J. and Berkov S. in 2020 on different aspects of Amaryllidaceae alkaloids including biodiversity, chemoecology, pharmacology, in vitro production, structural characterization, mass spectrometry and molecular modeling [8]. Advances on the chemical and biological characterization of the alkaloids and analogs isolated in the last decade from this plant family were reviewed by Masi et al. (2020) [9] and embedded in this Special Issue [8].

Crinum is a well-known subgroup of Amaryllidaceae studied for a long time and shown to be very rich in crinine-type alkaloids [10], one of the 12 ring-type in which are grouped the Amaryllidaceae alkaloids [11]. Three undescribed alkaloids, gigantelline, gigantellinine and gigancrinine with anti-acetylcholinesterase activity, were recently isolated from *Crinum jagus,* together with the already known lycorine-, cherylline-, galanthamine- and crinine-type alkaloids [12]. We also showed that *C. jagus* crude alkaloid extract inhibited Dengue virus (DENV) infection [13]. Among the alkaloids isolated from this plant, cherylline inhibited efficiently of both DENV (EC_{50} = 8.8 μM) and Zika virus (ZIKV) replication (EC_{50} = 20.3 μM), whereas it was ineffective on human immunodeficiency virus type 1 (HIV-1) infection. Thus, cherylline could be optimized for new therapeutic approaches against flaviviruses [13].

Amaryllidaceae plants, and in particular the subfamily Amaryllidoideae, also produce metabolites belonging to other classes of natural compounds such as flavonoids, lignans, chromones, terpenoids and ceramides. However, metabolites different from alkaloids are less studied. Still, up to now about 223 compounds, essentially flavan and phytosterols, were isolated from Amayllidoideae, all with interesting biological activities and taxonomical importance [14]. In particular, flavonoids are a well-known class of natural compounds possessing protective action against oxidative stress, heart disease and some cancers, and are considered healthy for humans and livestock [15,16].

Examples of non-alkaloids bioactive metabolites used in folk medicine include 2(*S*)-4′-hydroxy-7-methoxyflavan with cytotoxic activity [17] and vanillin [18] from *Crinum bulbispermum*, while amabiloside and its 4-glucoside was isolated from *Crinum amabile* [19]. *Crinum latifolium*, a rare species growing in Vietnam, produced a coumarin derivative as 4-[(senecioyloxy)methyl)]-6,7-dimethoxycoumarin showing strong antiangiogenic activity [20]. *Crinum aurea* produced (7*S*)-7-(4-hydroxyphenyl)-7-hydroxypropyl)-2′-methylbenzene-3′,6′-diol exhibiting neuroprotection against H_2O_2/$CoCl_2$-induced neuronal cell death in dopaminergic neuroblastoma SH-SY5Y cells [21]. *Crinum asiaticum* L. var. *sinicum* produced several benzoic and cinnamic acid derivatives [22]. *Crinum purpurascens* produced β-sitosterol showing a weak antibiotic activity [23] while *Crinum ensifolium* produced parthenicin, a sesquiterpene exhibiting strong cytotoxic activity [24]. *Crinum angustum* produced aliphatic hydroxylketones [25] while *Crinum yemense* produced 6-hydroxy-2*H*-pyran-3-carbahaldehyde showing strong inhibition of tyrosinase enzyme [26]. Acetovanillone and 4-hydroxyacetophenone, also known, respectively, as apocynin and piceol, were recently isolated from *Crinum buphonoides*, while only the former was isolated from *Crinum graminicola* [27].

Crinum biflorum Rottb. (syn. *Crinum distichum*) is found in seasonally flooded places in savannas from Senegal to Nigeria and extending to Sudan [28] but few studies have been carried out on its constituents and their biological properties [29].

Thus, the present study aimed to identify compounds with interesting biological activities from bulbs of *C. biflorum* collected in Senegal. Four homoisoflavonoids and one alkylamide were isolated. The chemical and biological properties were characterized to envisage their potential nutraceutical and pharmacological applications. This study expands the library of compounds isolated from *C. biflorum* and shows for the first time that this Amaryllidaceae species produces compounds of therapeutic interest against diabetes, cancer and Alzheimer's disease.

2. Materials and Methods

2.1. General Experimental Procedures

A JASCO P-1010 digital polarimeter (Jasco, Tokyo, Japan) was used to measure the optical rotations in CH_3OH. Electronic circular dichroism (ECD) spectra were recorded on a JASCO J-815 spectrometer (Jasco, Tokyo, Japan) in CH_3OH. 400 Anova Advance (Bruker, Karlsruhe, Germany) and Inova 500 MHz (Varian, Palo Alto, CA, USA) instruments were used to record ^1H and ^{13}C NMR spectra in $CDCl_3$ or CD_3OD at 400/100 or 500/125 MHz, respectively. The same solvents were used as internal standards. Correlation spectroscopy with a 45° mixing pulse (COSY-45), Nuclear Overhauser effect spectroscopy (NOESY), heteronuclear single quantum correlation (HSQC) and heteronuclear multiple bond correlation (HMBC) experiments were performed using Bruker or Varian microprograms. Electrospray ionization (ESI) mass spectra and liquid chromatography/mass spectrometry (LC/MS) analyses were carried out using the LC/MS time-of-flight (TOF) system Agilent 6230B, high-performance liquid chromatography (HPLC) 1260 Infinity. A Phenomenex LUNA [C_{18} (2) 5 um 150 × 4.6 mm column] was utilized to perform the HPLC separations. Analytical and preparative thin-layer chromatography (TLC) were performed on silica gel (Kieselgel 60, F_{254}, 0.25 and 0.5 mm, respectively, Merck) plates. The spots were visualized by exposure to ultraviolet (UV) radiation (254) or iodine vapors. Column chromatography (CC) was performed using silica gel (Kieselgel 60, 0.063–0.200 mm, Merck). Sigma-Aldrich Co. (St. Louis, MO, USA) supplied all the reagents and the solvents.

2.2. Plant Material

Bulbs of *C. biflorum* were collected in Senegal, in Kaffrine department, in December 2018. A senior scientist from the Herbarium of IFAN of University Cheikh Anta Diop of Dakar taxonomically identified the plant materials.

2.3. Extraction and Purification of Compounds **1**–**5**

Fresh bulbs of *C. biflorum* were dried at room temperature and then finely powdered. The resultant powder (545 g) was extracted with ethanol by Soxhlet obtaining a semisolid brown extract (450 mg). The latter was fractionated by CC eluted with $CHCl_3$/EtOAc/CH_3OH (3:1.5:0.5 *v*/*v*/*v*), affording eight groups of homogeneous fractions (F1-F8). The residue (102.8 mg) of fraction F1 was further purified by CC eluted with $CHCl_3$/*iso*PrOH (97:3 *v*/*v*) yielding ten groups of homogeneous fractions (F1.1-F1.10). The residue (15.8 mg) of F1.3 was purified by preparative TLC eluting with CH_2Cl_2/MeOH (97:3 *v*/*v*) yielding compound **4** (3.04 mg). The residue (14.3 mg) of F1.5 was purified by preparative TLC eluting with *n*-hexane/EtOAc (6:4 *v*/*v*) yielding compound **1** (1.42 mg) and compound **3** (3.52 mg). Compound **1** was crystallized from a $CHCl_3$-*iso*PrOH 9:1 *v*/*v* solution. The residue (6.7 mg) of F1.6 was purified by TLC eluted with $CHCl_3$/*iso*PrOH (9:1 *v*/*v*) yielding compound **2** (1.61 mg). The residue (15.2 mg) of F4 was further purified by preparative TLC eluting with $CHCl_3$/*iso*PrOH (95:5 *v*/*v*) yielding compound **5** (1.19 mg).

2.4. Spectroscopic Data of Compounds **1**–**5**

5,6,7-trimethoxy-3-(4-hydroxybenzyl)chroman-4-one (**1**). $[\alpha]^{25}_D$: 0 (*c* 0.3 CH_3OH); ^1H NMR data are very similar to those reported by Sylao et al. 1999 [30]; ESIMS (+) *m*/*z*: 727 $[2M + K]^+$, 719 $[2M + Na]^+$, 383 $[M + K]^+$, 367 $[M + Na]^+$, 345 $[M + H]^+$.

3-hydroxy-5,6,7-trimethoxy-3-(4-hydroxybenzyl)chroman-4-one (**2**). ECD (*c* 0.010 mM, CH_3OH) Δε 255 (−1.1), 280 (+2.5), 317 (−1.6); lit. [31]: ECD (*c* 0.031 mM, CH_3OH) Δε 281 (+10.4), 316 (−7.3); ^1H NMR data are very similar to those reported for urgineanin B [31]; ESIMS (+) *m*/*z*: 383 $[M + Na]^+$, 361 $[M + H]^+$.

3-hydroxy-5,6,7-trimethoxy-3-(4-methoxybenzyl)chroman-4-one (**3**). ECD (*c* 0.010 mM, CH_3OH) Δε 255 (−1.1), 281 (+2.5), 317 (−1.6); lit. [31]: ECD (c 0.031 mM, CH_3OH) Δε 280 (+10.8), 315 (−7.2); ^1H NMR data are very similar to those reported for ungirneanin A [31]; ESIMS (+) *m*/*z*: 397 $[M + Na]^+$, 375 $[M + H]^+$.

5,6,7-trimethoxy-3-(4-methoxybenzyl)chroman-4-one (**4**). $[\alpha]^{25}_D$: 0 (*c* 0.2 CH_3OH); ^1H NMR data are very similar to those reported by Sidwell and Tamm (1970) [32]; ESIMS (+) *m*/*z*: 381 $[M + Na]^+$, 359 $[M + H]^+$.

(*E*)-*N*-(4-hydroxyphenethyl)-3-(4-hydroxyphenyl)acrylamide (*N*-*p*-coumaroyltyramine) (**5**). ^1H and ^{13}C NMR data are very similar to those reported by Bhatti et al. (1992) [33]; ESIMS (+) *m*/*z*: 306 $[M + Na]^+$; ESIMS (−) *m*/*z*: 282 $[M - H]^-$.

2.5. Crystal Structure Determination of Compound **1**

Single crystals of **1** suitable for X-ray structure analysis were obtained by slow evaporation of a $CHCl_3$-*iso*PrOH 9:1 *v*/*v* solution. One selected crystal was mounted at ambient temperature on a Bruker–Nonius KappaCCD diffractometer (Bruker-Nonius, Delft, The Netherlands) (graphite monochromated MoKα radiation, λ = 0.710 73 Å, CCD rotation images, thick slices and φ and ω scan to fill the asymmetric unit). A semi-empirical absorption correction (multiscan, SADABS) was applied. The structure was solved by direct methods using the SIR97 program [34] and anisotropically refined by the full-matrix least-squares method on F^2 against all independently measured reflections using the SHELXL-2018/3 program [35] with the aid of program WinGX [36]. Water solvent crystallization molecules are present in the structure. The hydroxy and water H atoms were located in different Fourier maps and freely refined with Uiso(H) equal to 1.2 Ueq of the carrier atom. All of the other hydrogen atoms were introduced in calculated positions and refined according to the riding model with C–H distances in the range of 0.93–0.96 Å and with Uiso(H) equal to 1.2 Ueq or 1.5 Ueq (Cmethyl) of the carrier atom. One stereogenic center is present in the compound that crystallizes in the centrosymmetric P-1 space group as a racemate. The E-statistics indicate that the structure is centrosymmetric. Two independent X-ray structure analyses performed on different crystals confirmed the result. Unitary cell parameters were checked on several crystals. Figures were generated using ORTEP-3 [36] and Mercury-CSD-3.9. [37]. Crystallographic data of 1: empirical formula: $C_{19}H_{20}O_6 \cdot H_2O$; formula weight: 362.36 g mol^{-1}; triclinic, P-1; a: 8.368(2) Å; b: 10.183(2) Å; c: 12.0420(6) Å; α: 104.470(8)°; β: 108.252(13)°; γ: 100.010(19)°; V: 907.4(3) $Å^3$; Z: 2, Dx: 1.326 Mg/m3. All homoisoflavanoid crystallographic data for (**1**) were deposited in the Cambridge Crystallographic Data Centre with deposition number CCDC 2092030. These data can be obtained free of charge from www.ccdc.cam.ac.uk/data_request/cif.

2.6. Cell Culture and Reagents

HaCaT, spontaneously immortalized keratinocytes from adult skin, were purchased from Service Cell Line (GmBH, Eppelheim, CLS, Germany) and cultured as described [38,39]. HeLa cervical cancer cells (CCL-2) and A431 (ATCC-CRL1555) human epidermoid carcinoma cells were from American Type Culture Collection (ATCC, Manassas, VA, USA). According to the p53 compendium database (http://p53.fr/tp53-database/the-tp53-cell-line-compendium, 05/05/2021), HaCaT cells contain mutant p53 (H179Y/R282W), HeLa have p53 impaired function by viral infection while A431 cells contain only one p53 mutated allele (R273H). All mentioned cell lines were cultured in Dulbecco's Modified Eagle's Medium (DMEM, Sigma Chemical Co, St. Louis, MO, USA) supplemented with 10% fetal bovine serum (FBS, Hyclone Laboratories, Inc. Logan, UT, USA) at 37 °C in a

humified atmosphere of 5% CO_2. All cell lines were routinely tested for mycoplasma contamination and were not infected.

2.7. MTT Assay

Cell viability was assessed by 3-(4,5-dimethylthiazol-2-yl)-2,5-diphenyltetrazolium bromide (MTT) assay following the published procedure [40]. Briefly, cells were seeded at $10^5/cm^2$ density in 96-well plates. Twenty-four hours later, the medium was changed and supplemented with the specified concentrations of metabolite (from 0.5 to 10 mM in DMSO) for 24 and 48 h. MTT solution 1:10 (stock solution 5 mg/mL) was added to each well and the absorbance was measured in dual-wavelength mode (570 nm and 630 nm). The percentage of cell viability was calculated as follows: mean (A570-A630) and compared to cells supplemented with DMSO alone. Values shown in the plot are mean ± SD of sixfold determinations. Mean and the standard deviation was calculated on biological triplicates using GraphPad Prism8 software (GraphPad, San Diego, CA).

2.8. Detection of DNA Damage

Cells were seeded in 35 mm dishes on micro cover glasses (BDH) and treated with the metabolite at a concentration of 10 μM. At 48 h after treatment, cells were washed with cold phosphate-buffered saline (PBS) and fixed with 4% paraformaldehyde Sigma-Aldrich (Merck Life Science, Milan, Italy) for 15 min at RT. Cells were permeabilized with ice-cold 0.5% Triton X-100 for 5 min and then washed with PBS. Cells were then incubated with phospho-histone H2A.X (Ser139) antibody (from Cell Signaling Technologies 9542, Boston, MA, USA) for 1 h, followed by DAPI (Sigma-Aldrich) for 3 min and washed with PBS/0.05% Tween. Coverslip was mounted with Ibidi mounting medium (Ibidi GmbH, Martinsried, Germany). Images were taken with a Zeiss confocal laser-scanning microscope Axio Observer (Zeiss, Ostfilden, Germany) (scale bar, 20 μm). A 40× objective was used and image analysis was performed using Fiji ImageJ open source software project (https://imagej.net/imaging/). All the images were taken with the same setting [39].

2.9. Western Blot Analysis

Western blot was performed as previously reported [39,41]. Briefly, 30 μg of whole-cell extracts were separated by sodium dodecyl sulfate polyacrylamide gel electrophoresis (SDS-PAGE), subjected to Western blot and incubated overnight at 4 °C with antibodies. Antibodies against p21WAF, Poly [ADP-ribose] polymerase 1 (PARP1) and actin were from Cell Signaling Technologies 9542, Boston, MA, USA. Each experiment was run in triplicate. Signal intensities of Western blot bands were quantified by Quantity One analysis software (Version Number 2, Biorad Laboratories, London, UK) and analyzed by GraphPad Prism 8.0.2 software (GraphPad, San Diego, CA).

2.10. DCFDA Assay

N-p-coumaroyltyramine antioxidant activity was measured using 2′−7′dichlorofluorescein diacetate (DCFDA), a non-fluorescent compound permeable to the cell membrane, which can be oxidized by reactive oxygen species (ROS) giving a fluorescent compound. Cells were seeded at 2.5×10^4 in 96 well and pre-treated with *N-p*-coumaroyltyramine (10 and 100 mM). The medium was removed after 4 h and 1 mM (3%) H_2O_2 was added for 45 min, 1.5 and 2.0 h. Cells were washed with PBS and a fresh medium with DCFDA (30 mM) was added for 45 min, then DCFDA was removed by washing in PBS and the cells were harvested. The measurement of ROS was obtained using the Sinergy H4 microplate reader (Gen5 2.07, Thermofisher, Waltham MA, USA. The fluorescence emitted from the cells treated with DCFDA was compared to the untreated cells. Trolox was used as a positive control. Values shown in the plot are mean ± SD of sixfold determinations. The mean and the standard deviation were calculated on biological triplicates using GraphPad Prism 8.0.2 software (GraphPad, San Diego, CA).

2.11. 2Pseudotyped HIV-1$_{GFP}$ Infectivity Assay

The anti-HIV-1 activity of compounds **1–5** was evaluated using VSV-G pseudotyped NL43$_{GFP}$ infection of human monocytic THP-1 cells. THP-1 and NL4–3$_{GFP}$ were generously provided by Lionel Berthoux and Amita Singh and are described in Ka et al. (2021) [13]. THP-1 cells were seeded at 2.0 x 10^4 cells per well in 96 well-plates. The next day, cells were treated with 4 concentrations of each compound (12.5, 25, 50 and 100 mM) and then infected with HIV$_{GFP}$ at a MOI of 1. After 72 h, cells were stained with propidium iodide (PI, 0.5 mg/mL) and both PI$^+$ and HIV-1$_{GFP^+}$ infected cells frequencies were assessed on a FC500 MPL cytometer (Beckman Coulter, Inc., Mississauga, ON, Canada) and analyzed using FlowJo software (FlowJo LLC, BD Biosciences, Ashland, OR, USA). Matched concentrations of dimethyl sulfoxide (DMSO) were used as negative controls. All infection assays were performed in triplicate.

2.12. α-Glucosidase and α-Amylase Inhibitor Assay

α-glucosidase and α-amylase inhibitor screening kits (colorimetric) were purchased from Biovision (Milpitas, CA, USA). In total, 10 mM of stock solution of all the tested compounds were dissolved in DMSO and serially diluted in the assay buffer of each kit. Experiments were performed according to the manufacturer's protocol. Briefly, for the α-glucosidase assay, 10 µL of serially diluted compounds at the corresponding concentration (10 nm—1 mM) were added into designated wells of clear 96 well-plates. Subsequently, 10 µL of the α-glycosidase enzyme was added to each well and volume was adjusted to 80 µL and plates were incubated for 15-min at room temperature in dark condition. Then, 20 µL of α-glycosidase substrate mixture was added in all wells and kinetic of reaction was measured at OD: 410 nm for 60 min at 2 min intervals by using a multiplate reader, Biotek instrument, Inc., Canada. Enzyme control (no inhibitor), background control (no enzyme), solvent control (DMSO) and inhibitor control (acarbose) were included in the plates. For the α-amylase assay, 50 µL of serially diluted compounds (3.25 µM to 500 µM) were added into a clear 96-well plate with 50 µL of assay buffer and 50 µL of α-amylase enzymes. The plate was incubated at room temperature in the dark for 10 min. Then 50 µL of the α-amylase substrate was added in all wells. The kinetic of reaction was measured at OD:410 nm for 26 min at intervals of 2 min by using a multiplate reader. Control α-amylase inhibitor was provided by the manufacturer, enzyme control, background control and solvent control were all included. Enzyme inhibition was calculated according to Zhang et al. (2014) [42]. In summary, ODs were plotted according to the time for each sample. Areas under the curve (AUC) were calculated, and enzyme inhibition was measured as $100-(AUC_{compound}/AUC_{enzyme}) \times 100$ for each dilution of each compound.

2.13. Anti-Acetylcholinesterase Assays

In vitro acetylcholinesterase (AChE) activity was assessed exactly as in Ka et al. (2020) [12] following Ellman's colorimetric protocol [43] with the Acetylcholinesterase Assay Kit (Abcam Inc., Boston, MA, USA). Briefly, 50 µL serial dilutions (3.9–500 µM) of compounds **1–5** were prepared in Tris-HCl pH = 7.9 buffer into designated wells of a clear 96 well-plate. A total of 5 µL of DTNB was added in each well, then 50 µL of diluted acetycholinesterase was added. The plate was incubated for 10 min in the dark. Matched concentrations of DMSO were used as a negative control. Kinetic of reaction was measured in a multiple plate reader at 410 nm in kinetic mode for 40 min at room temperature. The percentage of anti-AChE inhibition was calculated according to the following formula: $100 - [((E - S)/E) \times 100]$, where E is the activity of the enzyme with matched concentrations of DMSO and S is the activity of the enzyme with the test sample.

2.14. Statistical Analysis

Statistical analyses were carried out using the GraphPad Prism version 8.1.2 (https://www.graphpad.com/scientific-software/prism/). Data were represented as the mean ± standard deviation and analyzed for statistical significance using ordinary one-way analysis of variance (ANOVA) and multiple comparisons. For all tests, $p < 0.05$ was considered to indicate a statistically significant difference.

3. Results

3.1. Identification of Metabolites Isolated from C. biflorum

The purification of the crude organic extract from bulbs of *C. biflorum* allowed us to isolate four homoisoflavanoids ((**1**)–(**4**), Figure 1) identified using spectroscopic (essentially 1D and 2D ^{1}H and ^{13}C NMR and HR MS) methods as 5,6,7-trimethoxy-3-(4-hydroxybenzyl)chroman-4-one (**1**), as 3-hydroxy-5,6,7-trimethoxy-3-(4-hydroxybenzyl)chroman-4-one (**2**), as 3-hydroxy-5,6,7-trimethoxy-3-(4-methoxybenzyl)chroman-4-one (**3**) and as 5,6,7-trimethoxy-3-(4-methoxybenzyl)chroman-4-one (**4**).

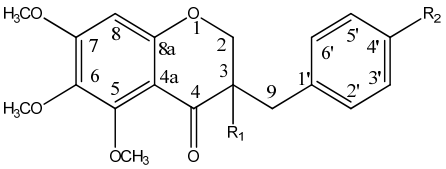

1, R_1=βH, R_2=OH
2, R_1=βOH, R_2=OH
3, R_1=βOH, R_2=OCH_3
4, R_1=αH, R_2=OCH_3

1, 5,6,7-trimethoxy-3-(4-hydroxybenzyl)chroman-4-one
2, 3-hydroxy-5,6,7-trimethoxy-3-(4-hydroxybenzyl)chroman-4-one = urgineanin B
3, 3-hydroxy-5,6,7-trimethoxy-3-(4-methoxybenzyl)chroman-4-one = urgineanin A
4, 5,6,7-trimethoxy-3-(4-methoxybenzyl)chroman-4-one

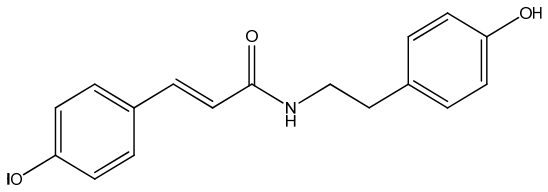

5, (*E*)-*N*-(4-hydroxyphenethyl)-3-(4-hydroxyphenyl)acrylamide

Figure 1. Structure of homoisoflavanoids (**1**)–(**4**) and alkylamide (**5**) isolated from *C. biflorum* bulbs.

The identification of **1** was performed comparing its ^{1}H NMR spectrum with that reported in the literature when it was isolated for the first time from *Scilla nervosa*, subsp. *rigidifolia* collected in Botswana where it is used in Zulu folk medicine to treat rheumatic fever and as a purge for children [30]. ESI MS spectrum showed the potassium $[2M + K]^+$ and sodium $[2M + Na]^+$ dimeric, the potassium $[M + K]^+$ and sodium $[M + Na]^+$ and the protonated $[M + H]^+$ adduct ions at *m*/*z*: 727, 711, 383, 367 and 345.

The structure of the homoisoflavanoid (**1**) was confirmed by X-ray analysis of a single crystal obtained by slow evaporation of a $CHCl_3$-isoPrOH 9:1 *v*/*v* solution. Compound **1** crystallizes in the P-1 space group with one molecule of **1** and one H_2O solvent molecule contained in the independent unit. All bond lengths and angles are in a normal range. The molecule consists of a substituted cromanone system. The six-membered croman-4-one ring assumes an envelope conformation with C2 atom at the flap. The 4-hydroxybenzyl substituent at C3 is in the equatorial position and places nearly parallel to the benzene

ring of the chromanone system (Figure 2A,B). The crystal packing is stabilized by strong OH…O hydrogen bonds involving **1** and solvent water molecules (Figure 3A,B).

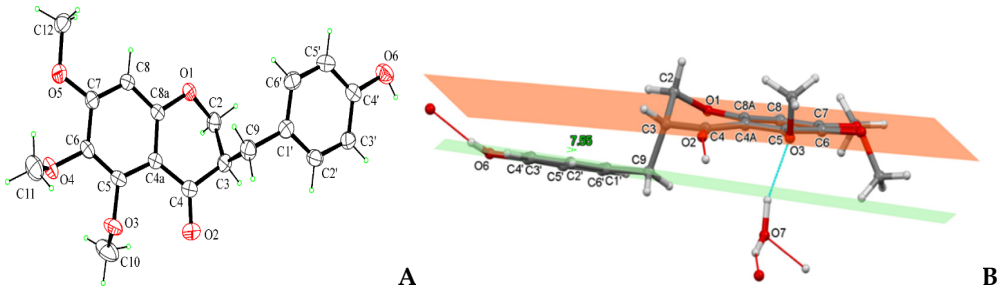

Figure 2. (**A**) ORTEP view of the homoisoflavanoid (**1**) molecular structure, with ellipsoids drawn at the 30% probability level. (**B**) Independent unit of compound 1 in a perspective view showing a quite parallelism between hydroxybenzene plane (green) and benzene ring of chromanone system (orange) (angle of 7.55° between the two planes). Ball-and-stick style. Hydrogen bonds drawn as cyan and red dashed lines.

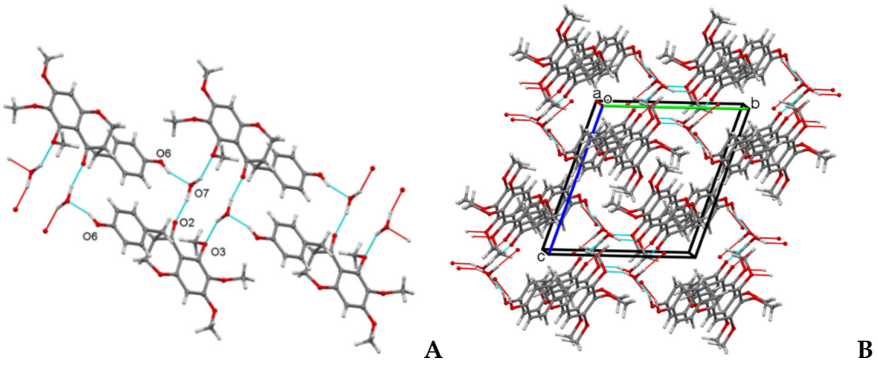

Figure 3. (**A**) Details of hydrogen bonding pattern in compound **1**. (**B**) Perspective view of the crystal packing of compound **1** with hydrogen bond pattern drawn as cyan and red lines. Ball-and-stick style.

The homoisoflavonoid (**1**) molecule contains one stereogenic center at C3 atom and crystallizes in the centrosymmetric P-1 space group as a racemate. The racemic nature of crystals was confirmed by performing two independent X-ray structure analyses on different crystals (Figure 2B). This result can be ascribed to easy inversion at the chirality center, because of the presence at C-3 of a proton which could exchange by keto-enol tautomerism. The ECD spectrum of **1** (Figure 4, black line) cannot be interpreted due to the presence of a racemic mixture. These results were confirmed by the optical inactivity found by measuring the specific optical rotation of compound **1**.

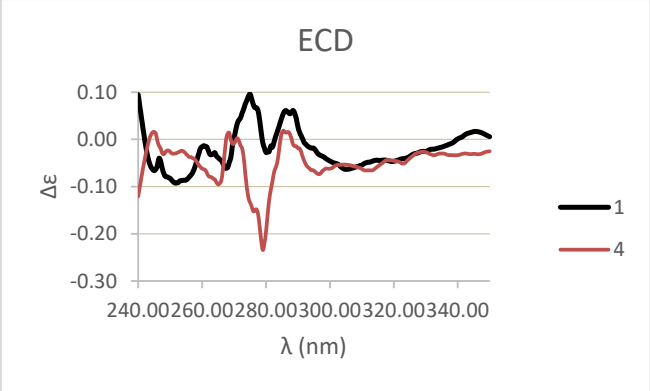

Figure 4. Experimental ECD spectra of homoisoflavanoids (**1**) (black solid line), and **4** (red line).

Homoisoflavanoides **2** and **3** were identified by comparing their physic (ECD) and spectroscopic data (^{1}H NMR) with those reported in the literature for urgineanins B and A, isolated from *Urginea depressa*. This is an Asparagaceae collected in South Africa and used for its antiproliferative activity against the A2780 ovarian cancer cell line [31]. The ESI MS spectra of both **2** and **3** confirmed their identification showing the sodiated and protonated adduct ions $[M + Na]^+$ and $[M + H]^+$, respectively, at *m*/*z* 383 and 361 and 397 and 375. The absolute configuration of homoisoflavanoids **2** and **3** was the same of urgineanins B and A as appeared by comparison of their ECD spectra (Figure 5, black line for **2** and red line for **3**) with those already reported in the literature by Dai et al. (2013) [31] which assigned a *R* configuration at C-3 of the two homoisoflavanoids by comparison of their experimental ECD spectra with those reported in literature for caesalpiniaphenol A [31].

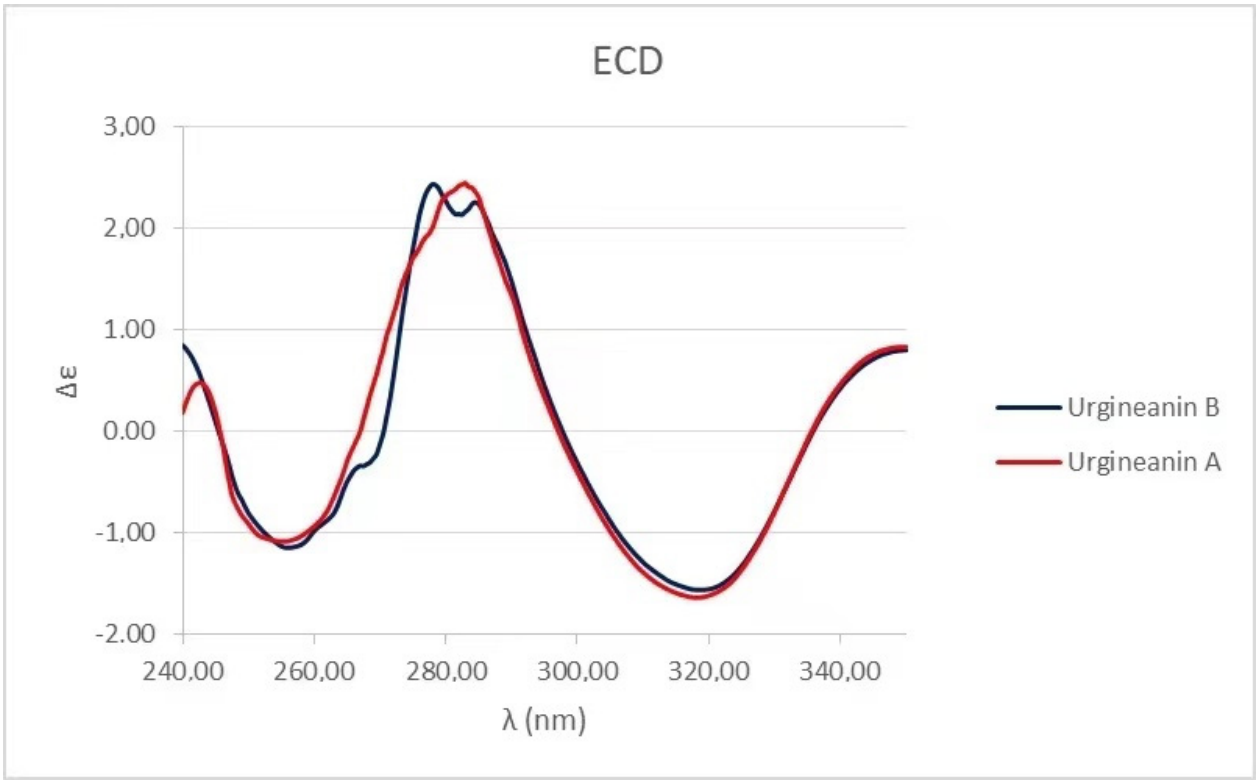

Figure 5. ECD spectra of homoisoflavanoids (**2**) (black solid line), and **3** (red line).

The fourth homoisoflavanoid (**4**) was identified as the 5,6,7-trimethoxy-3-(4-methoxybenzyl)chroman-4-one by comparing its physic and spectroscopic data with those reported for the trimethyl derivative of 3,9-dihydroautumnalin obtained together to other homoisoflavanoids from *Eucomis autumnalis* (Liliaceae) [32]. The same derivative was also obtained from 3,9-dihydroeucomnsalin, which resulted to be identical to 3,9-dihydroautumnalin, which was isolated from the bulbs of *Muscari comsum* (commonly named lampascioni) collected in Basilicata region, Italy, where they are used in traditional cuisine as bitter plants [44]. The identification of compound **4** was also supported by ESI MS data which showed the sodiated $[M + Na]^+$ and protonated $[M + H]^+$ adduct ions at *m*/*z* 381 and 359. The ECD spectrum of **4** (Figure 4, red line) cannot be interpreted, as in the case of compound **1**, due to the presence of a racemic mixture, as confirmed by the optical inactivity found by measuring the specific optical rotation of **4**.

From the ethanolic extract of the *C. biflorum* bulbs and alkylamide was also isolated and identified compound **5**, or (*E*)-*N*-(4-hydroxyphenethyl)-3-(4-hydroxyphenyl)acrylamide (**5**, Figure 1). Compound **5** was identified by comparison of its spectroscopic data with those reported in the literature when isolated from the first time from crude Chinese drug "Xiebai", the tuber of *Allium bakeri* Reg. (Liliaceae) and used for inhibition on human platelet aggregation [45]. A similar comparison was done with the data reported when **5** was isolated together with some alkaloids from *Fumaria indica*, collected in Multan City (Punjab, Pakistan) and inappropriately indicated as an alkaloid instead of amide [33]. The identification of compound **5** was also supported by ESI MS data which showed the sodiated $[M + Na]^+$ adduct ion at *m*/*z* 306. When the same spectrum was recorded in negative modality, the pseudomolecular ion $[M - H]^-$ at *m*/*z* 282 was observed.

3.2. In Vitro Cytotoxicity

Considering that the anti-tumor activities of homoisoflavonoids (**1**–**4**) from *C. biflorum* have not yet been addressed, we evaluated the in vitro cytotoxicity of isolated homoisoflavonoids towards HaCaT, A431 and HeLa human cell lines using the MTT viability assay. The *N*-*p*-coumaroyltyramine (**5**) alkylamide was also included in these experiments. Cells were plated and supplemented with each metabolite, at low micromolar concentrations ranging from 0.5 to 10 μM in DMSO, and incubated at 37 °C for 24 and 48 h. As shown in Figure 6, all tested metabolites were toxic for cancer cell lines, in a dose and time-dependent way, with HeLa cells being more sensitive than A431. Remarkably, 48 h treatment with 5 μM metabolite **1** reduced HeLa cells viability to less than 20% of the untreated control. All metabolites were less active on HaCaT immortalized keratinocytes at 24 h of incubation over the range of concentration tested although a significant reduction of HaCaT cell viability was caused by metabolites **3** and **4** when the incubation was extended for 48 h. Table 1 lists the IC_{50} values obtained with the test compounds are means of triplicates at 24 h. The *N*-*p*-coumaroyltyramine (**5**) was also found to be toxic on A431 and HeLa cancer cells while at the lower concentration tested, 0.5 and 1 μM, it was shown to significantly increase HaCaT cell viability (Figure 6). Detection of nuclear γ-H2A.X foci provides indirect evidence of the occurrence of DNA double-strand breaks (DSB) and/or DNA replication stress [40]. Upon induction of a DNA double-strand break, the H2A.X histone becomes rapidly phosphorylated at serine 139 to form γH2AX [46]. This phosphorylation event is dynamic, complex and depends on interactions between MDC1, H2AX and ATM and other kinases to persist [47]. This amplified response is easily detected using specific antibodies against γ-H2AX, manifesting discrete nuclear foci.

- HaCaT cells: 96-well, sixfold, 1* 10^4

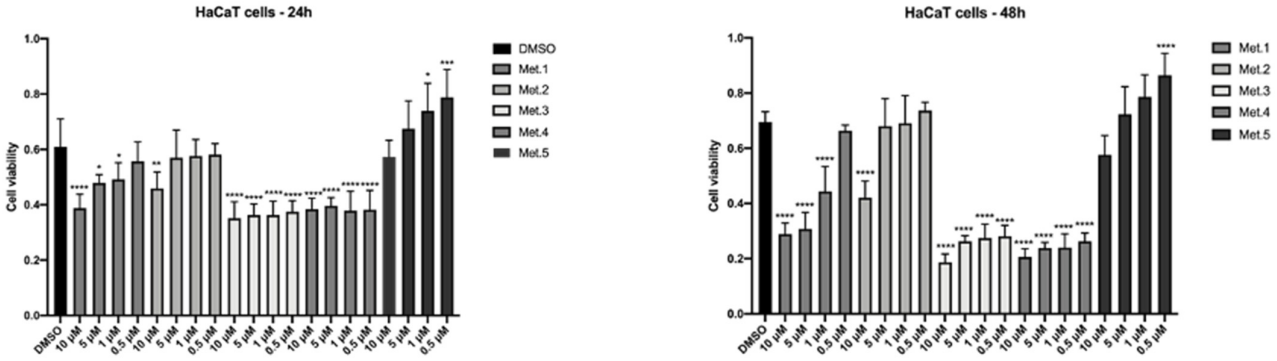

- A431 cells: 96-well, sixfold, 8* 10^3

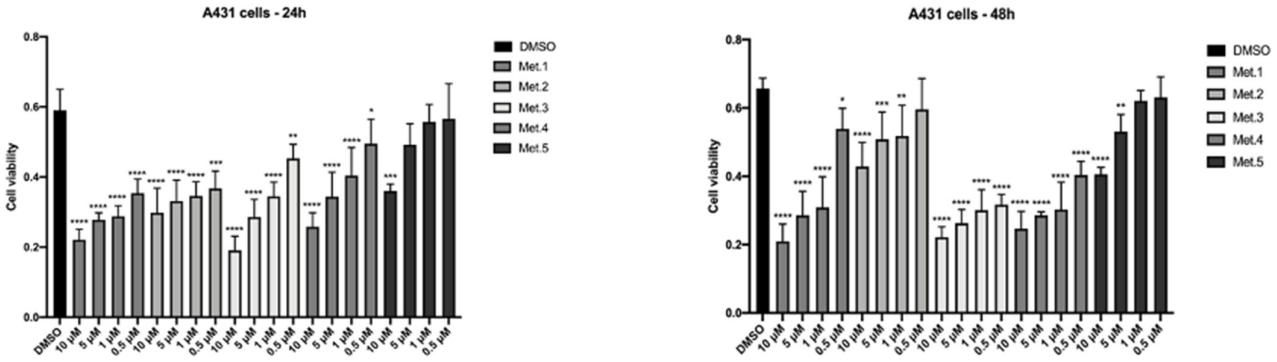

- Hela cells: 96-well, sixfold, 8* 10^3

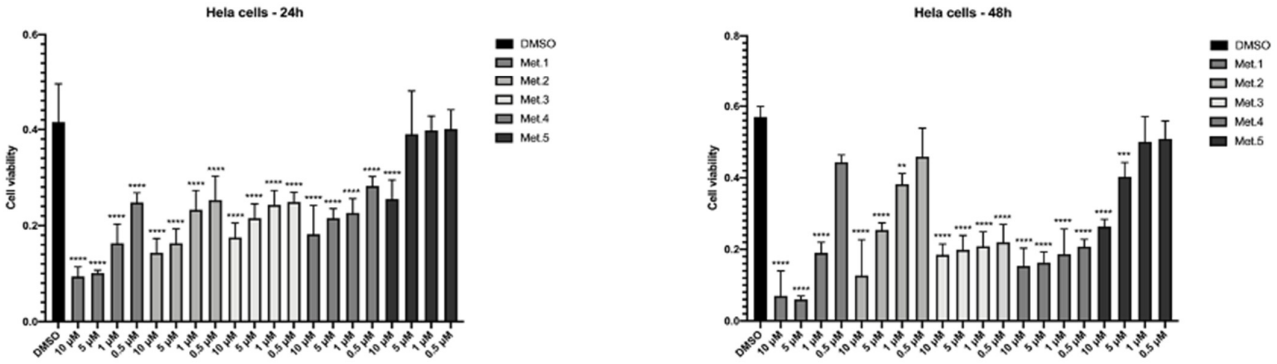

Figure 6. MTT viability assays with homoisoflavanoids **1**–**4** and *N*-*p*-coumaroyltyramine (**5**) from *C. biflorum* on HaCaT, A431 and Hela human cell lines. Statistical analyses were performed using one-way ANOVA and Dunnett's multiple comparisons test. Levels of significance between points of expression are indicated (****$p < 0.001$, ***$p < 0.01$, **$p < 0.02$, *$p < 0.05$).

Table 1. Cytotoxic activities of metabolites **1–5**. Compounds IC_{50} (μM) [1].

Compound	HaCaT	A431	HeLa
1	>10	6.0	1.0
2	>10	>10	4.0
3	>10	4.0	4.5
4	>10	6.5	5.5
5	Not detected	>10	7.5

[1] IC_{50} was calculated after 24 h of incubation.

The formation of γ-H2AX foci by immunofluorescence using the antibody against the histone H2A.X phosphorylated in Serine 139 was monitored considering that the homoisoflavonoids isolated from *C. biflorum* reduced cell viability. HaCaT, HeLa and A431 cells were treated with 10 μM metabolites **3** and **4** for 24 h to detect DNA damage foci. As shown in Figure 7 a remarkable increase of nuclear γH2AX foci was observed in all tested cell lines.

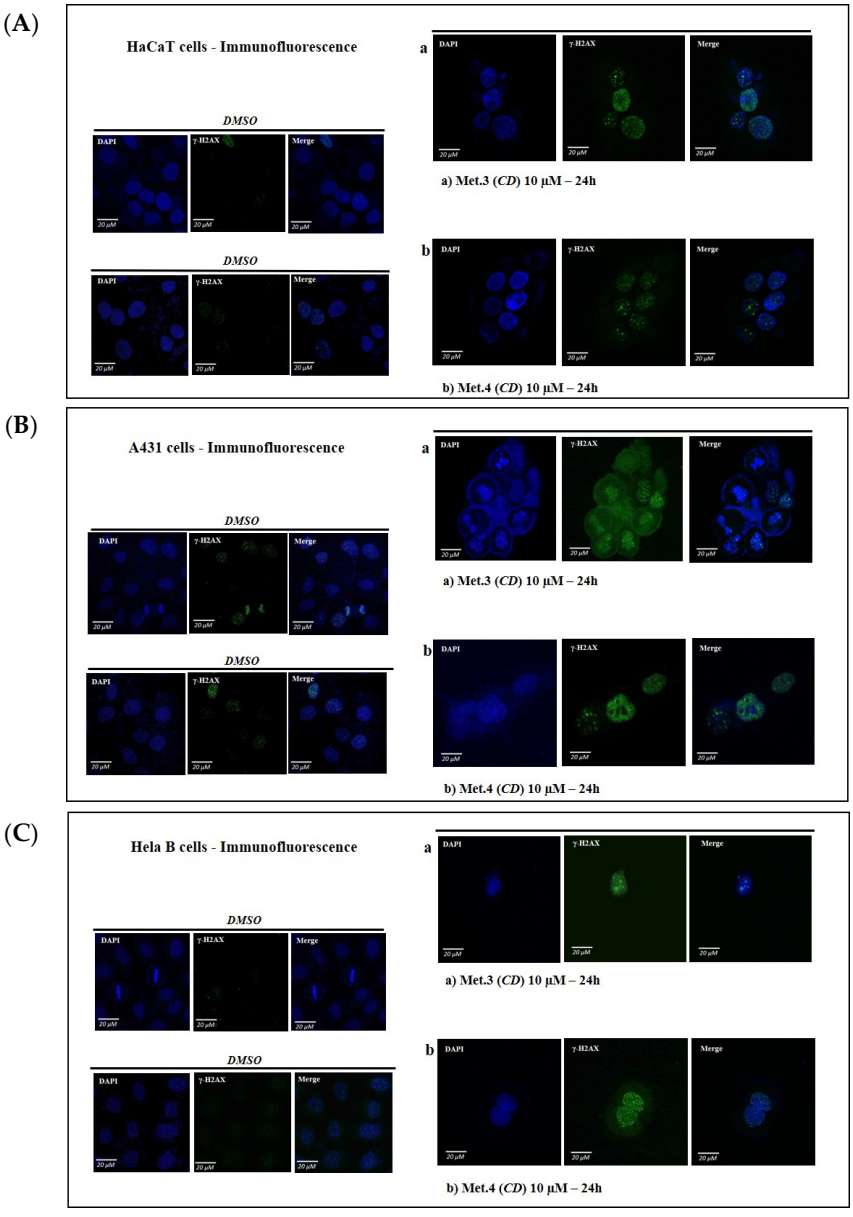

(**D**). **Quantification of γ-H2AX mean fluorescence**

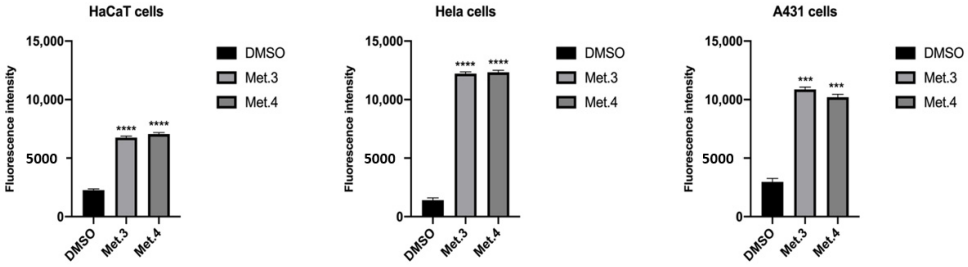

Figure 7. Immunofluorescence microscopy showing γ-H2AX foci formation (green) in nuclei of HaCaT (panel (**A**)), A431 cells (panel (**B**)) or HeLa cells (panel (**C**)) treated with DMSO alone or 10 μM **3** or **4** for 24 h. Nuclei were stained with DAPI (blue). Note the abnormal morphology of nuclei induced by **3** and **4** in A431 cells compared to HaCaT cells. Images from 3 fields per each experimental point were collected to obtain data for up to 150 cells. Quantitation of γ-H2AX foci fluorescence was performed by Image J software shown as mean ± SD in graph bars of panels (**D**). Statistical analyses were performed using one-way ANOVA and Dunnett's multiple comparisons test. Levels of significance between points of expression are indicated (****$p < 0.001$, ***$p < 0.01$).

Determination of reactive oxygen species (ROS) induced by H_2O_2 in HaCaT cells treated with 10 and 100 μM *N-p*-coumaroyltyramine alkylamide revealed that **5** has antioxidant activity comparable to Trolox, the water-soluble derivative of vitamin E used as a positive control (Figure 8). Remarkably, treatment of HaCaT cells with 10 μM metabolite **3** or **4** did not increase the production of reactive oxygen species (ROS) implying that ROS generation was not responsible for the observed DNA damage (Figure 9A,B).

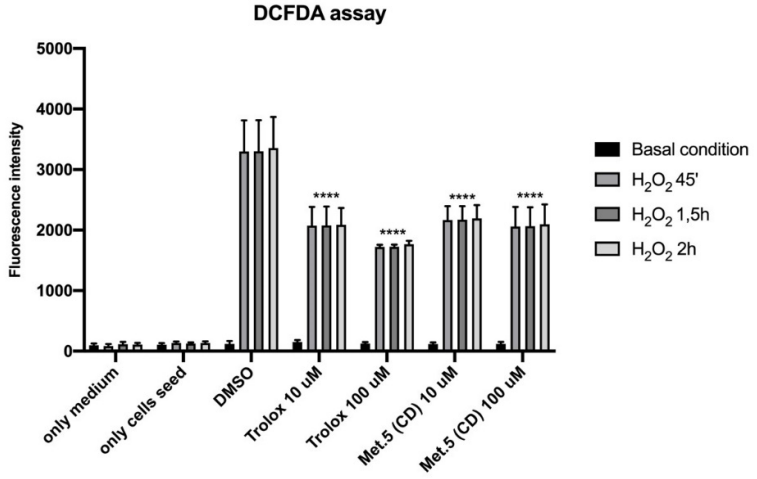

Figure 8. DCFDA assay. HaCaT cells were seeded and pre-treated for 4 h with 10 and 100 μM *N-p*-coumaroyltyramine (**5**) from *C. biflorum*. H_2O_2 (1 mM; 3%) was added to the medium for 45′, 1.5 and 2 h. The fluorescence intensity of DCFDA was read after 45′ of incubation. Trolox was used as a positive control. Levels of significance between points of expression are indicated (****$p < 0.001$).

(**A**)

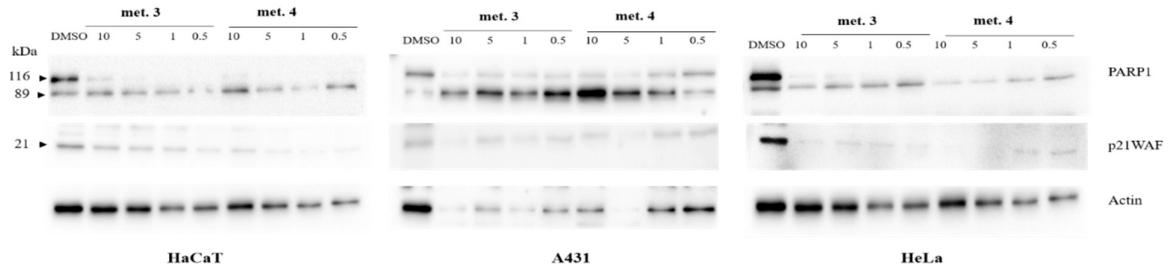

(**B**)

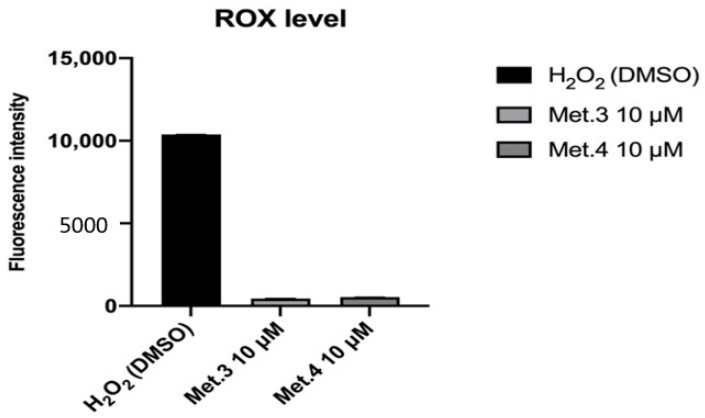

Figure 9. (**A**) Representative immunoblot analysis showing the effect of **3** and **4** on PARP1 activation and p21WAF protein levels. Full length and cleaved PARP1 bands were revealed by immunoblot with specific antibodies. The blots were then re-probed with actin antibody to check for protein loading. (**B**) DCFDA on HaCaT cells pre-treated for 4 h with 10 µM **3** and **4** from *C. biflorum*. H_2O_2 (1 mM; 3%) was added to the medium for 45′ and used as a positive control. Fluorescence intensity of DCFDA was read after 45′ of incubation.

3.3. Antidiabetic and Anti-Acetylcholinesterase Properties

Next, we assessed the anti-acetycholinesterase and antidiabetic (Figure 10A,B) properties of *C. biflorum*-isolated compounds. We confirmed that compound **5** was a strong inhibitor of α-amylase and α-glucosidase (Figure 10) [48]. Compound **1, 2, 3** also inhibited 50% of α-glucosidase at high concentration (1 mM) (Figure 10B). Altogether, the results support the antidiabetic properties of *C. biflorum*. Compounds **1–4** also showed anti-acetylcholinesterase activity. Interestingly, compound **5** weakly inhibited AChE catalyzed reaction at high concentrations, while **1**, **2** and **4** displayed increasing inhibition from 15.6 to 250 µM up to 20% (Figure 11). Compound **3** was the most potent inhibitor, blocking from 15 to 30% of enzyme activity as concentrations increased from 3.9 to 50 µM (Figure 11).

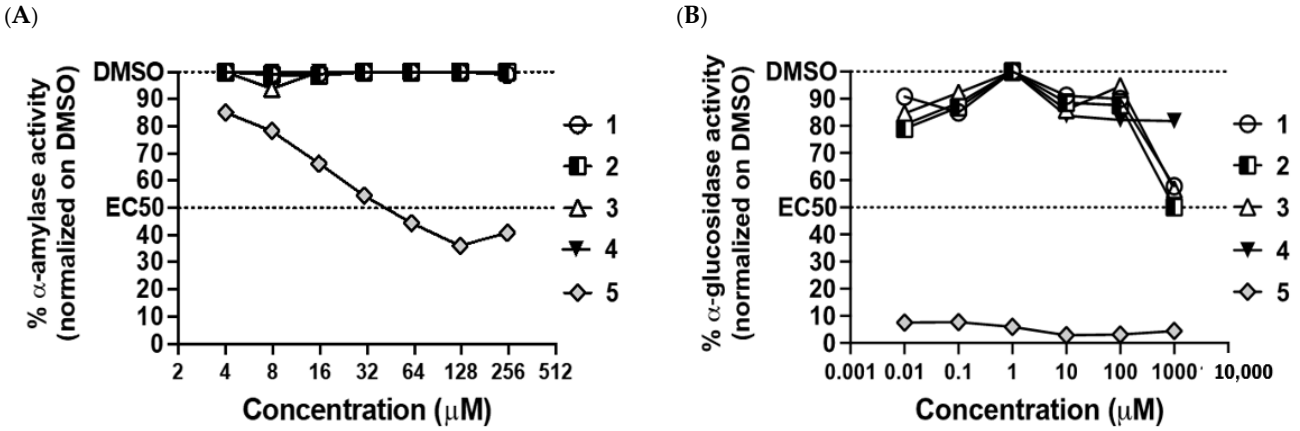

Figure 10. (**A**) Anti-α-amylase activity. Kinetics of α-amylase reaction was measured in presence of each compound at concentrations ranging from 3.9—250 μM, and matched concentrations of DMSO solvent over a 26 min period. Areas under the curves (AUC) of OD (410 nm) vs. time were calculated according to Zhang et al. (2014) [42] and used to determine enzyme activity defined as the ratio of the AUC for each compound at each concentration normalized on the AUC in presence of DMSO matched concentration. Compound **5** strongly inhibited α-amylase catalyzed reaction with an IC_{50} of 40 μM. (**B**) Anti-α-glucosidase activity. Kinetics of α-glucosidase reaction were measured in presence of each compound at concentrations ranging from 0.01–1000 μM, and matched concentrations of DMSO solvent over a 40 min period. Areas under the curves (AUC) of OD (410 nm) vs. time were calculated and used to determine enzyme activity defined as the ratio of the AUC for each compound at each concentration normalized on the AUC in presence of DMSO matched concentration. Compound **5** nearly completely inhibited α-glucosidase catalyzed reaction with at all concentration tested. Compounds **1, 2** and **3** inhibited 50% of the reaction at 1 mM. For all assays, enzyme, no compound and inhibitor controls were included.

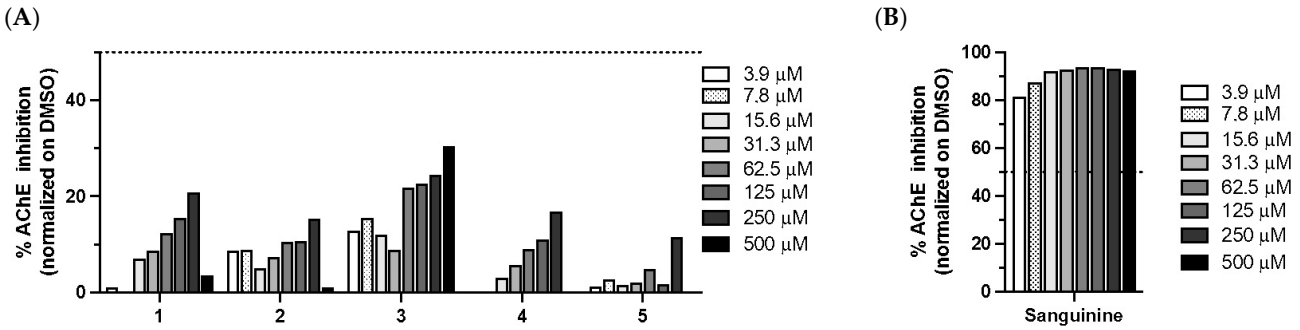

Figure 11. (**A**) Anti-AChE activity. AChE-catalyzed reaction was assessed in presence of each compound at concentrations ranging from 3.9–500 mM and matched concentrations of DMSO after a 10 min incubation. The percentage of anti-AChE inhibition was calculated according to the following formula: 100 − [((E − S)/E) × 100], where E is the activity of the enzyme with matched concentrations of DMSO and S is the activity of the enzyme with the test sample. Compound **5** weakly inhibited AChE catalyzed reaction at high concentrations. Compounds **1, 2** and **4** displayed increasing inhibition from 15.6 μM to 250 μM up to 20%. Compound **3** was the most potent inhibitor of AChE, blocking 15–30% of enzyme activity as concentrations increased from 3.9 to 500 μM. (**B**) Sanguinine (isolated from *C. jagus* [12]) was used as a positive control. For all assays, enzyme, no compounds and inhibition controls were included.

3.4. Antiviral Activity

Flavonoids and alkylamides have also been shown to exhibit antiviral activity [49]. Thus, we tested the anti-retroviral effect of compounds **1**–**5** using VSV-G pseudotyped HIV-1 particles. Interestingly, all compounds displayed anti-HIV-1 potential at 100 μM (Figure 12A). Infection dropped from a mean of 8.16%, when cells were treated with DMSO, to means of 3.78, 4.03, 2.51, 2.76 and 2.12 %, when compounds **1** to **5** were added, respectively. These differences were statistically significant for compounds **3**, **4** and **5**. At 50 μM, there was a 2.0, 2.4 and 1.6-fold decrease in infection when **3**, **4** and **5** were added to the cell media, respectively. At lower concentrations only **3** and **4** decreased infection levels. Cytotoxicity

was verified following propidium iodide staining of THP-1 cells after an incubation of 72 h with compounds (Figure 12B). Compounds **1**, **2** and **5** were weakly cytotoxic to THP-1 at 100 μM with 8.74, 4.15 and 5.97% of PI^+ cells, respectively. In total, 30–40% of cells treated with **3** and **4** were dead at all concentrations tested. Thus, although cytotoxicity could contribute to the observed antiviral activity, this experiment was performed using a single-cycle infection system, lessening the effect of cell loss on further cycles of viral replication. In conclusion, *C. biflorum* contains compounds with interesting anti-retroviral activity.

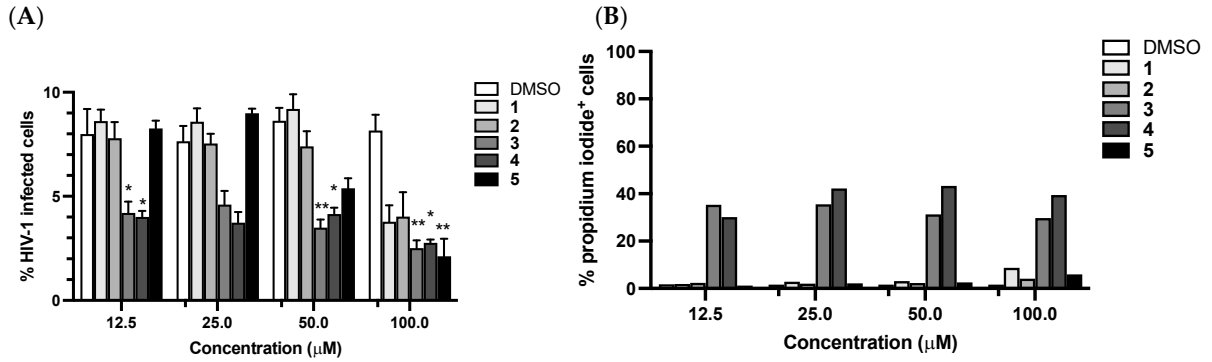

Figure 12. Antiviral activity of compounds **1**–**5.** (**A**) THP-1 cells were treated with four concentrations (12.5, 25, 50 and 100 μM) of each compound in triplicates and infected with VSV-G pseudotyped HIV-1GFP at MOI = 1. Infection levels were assessed by flow cytometry 72 h post-infection. Bars show means with standard deviation. Kruskal–Wallis and uncorrected Dunn's tests were performed to assess statistically significant differences between groups. * $p < 0.05$; ** $p < 0.01$. (**B**) Cell death (% propidium $iodide^+$ cells) was measured by flow cytometry following PI staining 72 h post-treatment of THP-1 with **1**, **2**, **3**, **4** and **5**. Matched concentrations of DMSO were used as a negative control.

4. Discussion

Very few studies have been performed on *C. biflorum* (syn. *C. distichum*) from a chemical and applicative point of view. A phytochemical investigation on this Amaryllidaceae species was carried out on the ethanol extract of the whole plant using HPLC analysis. A new natural flavan, (2*S*)-4′,7-dimethoxyflavan, was isolated together with the already known (2*S*)-4′-hydroxy-7-methoxyflavan, (2*R*)-4′-hydroxy-5,7-dimethoxyflavan, hippadine and hippacine. All the compounds, except the new flavan, showed moderate antibacterial activity [50]. Another study was carried out on the ethyl acetate extract from the whole plant of *C. biflorum* collected in Cameroon. Its phytochemical investigation allowed to isolate a new flavan-3-ol derivative, namely (2*R*,3*R*)-3-hydroxy-7-methoxy-3′,4′-methylenedioxyflavan, together with (2*S*)-7-hydroxy-3′,4′-methylenedioxyflavan, (2*R*,3*R*)-7-methoxy-flavan-3-ol, (2*S*)-7-hydroxy-3′,4′-dimethoxyflavan, 3′,7-dihydroxy-4′-methoxyflavan, 4′,7-dimethoxy-3′-hydroxyflavan, farrerol, β-sitosterol, β-sitosterol-3-*O*-β-D-glucopyranoside, oleanolic acid, kaempferol, pancratistatin, lupeol, aurantiamide acetate, narciprimine and 2,3-dihydroxypropyl palmitate [29]. Some of them were also isolated from Muscari species among a series of homoisoflavanones containing the 3-benzylchroman-4-one skeleton [51].

Compounds **2** and **3** were characterized as 3-hydroxy-5,6,7-trimethoxy-3-(4-hydroxybenzyl)chroman-4-one (**2**), as 3-hydroxy-5,6,7-trimethoxy-3-(4-methoxybenzyl)chroman-4-one (**3**) and resulted to be the previously isolated homoisoflavanoids named urgineanins B (**2**) and A (**3**) [31].

No alkaloids were detected in the acid organic extract from bulbs of *C. biflorum*, object of the present study, using either the optimized extraction method [52] or the traditional extraction with ethanol by Soxhlet. However, the organic extract obtained with the latter method showed the presence of four homoisoflavonoids and one alkylamide. The racemate nature of compound **1** was never reported before; only the absolute configuration of its *p*-bromobezoyl derivative was previously determined by X-ray [53]

when configurations were also confirmed by ECD comparing their ECD spectra with those previously reported. Urgineanin A was previously reported to have antiproliferative activity at submicromolar concentration against ovarian carcinoma, melanoma and non-small lung cancer cells [31].

Compound **4** is also a racemic mixture and therefore its ECD spectrum could not be interpreted (Figure 4). This result differed from that previously reported for **4** when synthesized from the (3*R*)-3,9-dihydroeucomnalin and wrongly reported as *R* enantiomer [44]. Compound **4,** as well as the starting homoisoflavonoid above described for compound **1**, are a racemic mixture for the presence at C-3 of a proton which could exchange by keto-enol tautomerism.

Racemic natural products are rare and could be obtained from nonenzymatic reactions [54]. However, a chiral tertiary asymmetric carbon in α position to a carbonyl group is easily subject to racemization, as in compounds **1** and **4** [55]. To the best of our knowledge no literatures are available in which compounds **1** and **4** are reported as racemates. However, Sylao et al. 1990 [30] isolated for the first time homoisoflavanoid **1** (named compound **12**) along with other compounds from *Scilla nervosa* subsp. *rigidifolia*. The previously undescribed homoisoflavanoinds were also fully characterized by spectroscopic data (UV, IR, ^{1}H and ^{13}C NMR and EIMS) but any experiments to determine the absolute configuration of the chiral compounds were neither carried out nor discussed. Among the homoisoflavanoids isolated as new compounds, only for some of them, including **12** (=**1**), was reported the optical specific activity. Based on our experience, these results did not surprise us as the speed of inversion of the configuration of carbon 3, due to the keto-enol tautomerism, could depend on the properties of the solution in which the measurement of the optical rotational power is measured and not from the plant source. Thus, it is possible to have also a scalemic mixture that has optical activity according to the percentage of the predominant enantiomer, as reported for some optical active homoisoflavanois by Sylao et al. 1999 [30]. Scalemic mixtures of two enantiomers are reported in the literature for some different secondary metabolites isolated from several sources as i.e.: phantasmidine, an alkaloid found to be a 4:1 scalemic mixture, enriched in the (2a*R*,4a*S*,9a*S*) enantiomer isolated from the poison frog *Epipedobates anthonyi* [56]; α-pinene, 1-octen-3-ol linalool found as a scalemic mixture of 34% (*R*)-(+) to 66% (*S*)-(−), 95% (*R*)-(−) to 5% (*S*)-(+), 96% (*R*)-(−) to 4% (*S*)-(+) when isolated from the edible wild mushroom *Tricholoma magnivelare* [57]; a furoic acid derivative, containing a chiral center in benzylic position, was found to be a scalemic mixture with an excess of the (*S*) enantiomer, when obtained from the endophytic fungus *Coniothyrium* sp. was isolated from leaves of *Quercus robur* [58]; six pairs of new 6-monosubstituted dihydrobenzophenanthridine alkaloids were separated as scalemic mixtures from the aerial part of *Chelidonium majus*, a plant belonging to the Papaveraceae family, which is widely used in Chinese folk medicine [59].

Compounds **5**, the alkylamide, was isolated for the first time, together with *N-trans*-feruloyl octopamine, *N-trans-p*-coumaroyl octopamine, vanillin, isoscopoletin, ethyl caffeate, ferulic acid and *p*-amminonenzaldehyde, from the eggplant roots [60]. Successively, **5** was also isolated together with close alkylamides from stem parts of *Annona montana* (Annonaceae) and showed significant inhibition of rabbit platelets aggregation induced by thrombin, arachidonic acid, collagen and PAF (platelet-activating factor) and selective cytotoxicity against the P-388 cell line [61,62]. Compound **5** was also found together with other close alkylamides and several phenolic compounds in the methanol extract of basil, lemon thyme, mint, oregano, rosemary, sage and thyme showing antioxidant and anti-inflammatory activities [63].

Alkylamides are a group of bioactive natural compounds widely distributed in plant families and characterized by broad structural variability and a plethora of important biological activities, such as immunomodulatory, antimicrobial, antiviral, larvicidal, insecticidal, diuretic, pungent, analgesic, cannabimimetic and antioxidant activities. Furthermore, they have reinforced the efficacy of antibiotics and inhibited prostaglandin

biosynthesis, RNA synthesis and arachidonic acid metabolism [64]. In addition, alkylamides accumulate in rice plants as a defense against the harmful *Cochliobolus miyabeanus* and *Xanthomonas oryzae* pathogens [65].

Flavonoids were also reported to have cytotoxic and anticancer activity, although this aspect was not deeply addressed [66,67]. We found that all tested metabolites were toxic for cancer cells, in a dose- and time-dependent way, although the degree of inhibition of cell viability was cell-type specific. Remarkably, homoisoflavanoids **1**, **3** and **4** were more effective on A431 and HeLa cells compared to immortalized but not transformed HaCaT, thus suggesting that cancer cells were more sensitive to homoisoflavanoid cytotoxicity. The increase of nuclear γH2AX foci upon treatment with metabolites **3** and **4** strongly suggests the occurrence of DNA damage by double-strand breaks (DSBs). However, both **3** and **4** did not increase the production of ROS indicating that a molecular mechanism different from ROS generation is responsible for the observed DNA damage induced by **3** and **4**. Additional experiments are needed to precisely define the molecular mechanism. Moreover, we also detected the signal of cleaved PARP-1 (89 kDa) by immunoblot while the level of the cell cycle inhibitor p21WAF, which causes cell growth arrest preventing the induction of apoptosis, was reduced, thus confirming that the decrease of cell viability was due to cell death rather than cell cycle arrest.

Isolated compounds displayed additional interesting biological properties. As previously described but isolated for the first time in a *Crinum* species, **5** is a strong anti-α-glucosidase and anti-α-amylase inhibitor. Recently, the efficacy of flavanoids for type 2 diabetes mellitus (T2DM) was shown in clinical therapies. T2DM is a metabolic disorder associated with the overproduction of free radicals and oxidative stress. Diabetes is increasing exponentially, and the World Health Organization estimates that by the year 2030, it could be the seventh cause of death worldwide [68,69]. The flavonoids appear to play a role in multiple processes involved in T2DM [70,71] such as the regulation of glucose metabolism, hepatic enzymes activities and a lipid profile [72]; thus, studies on nutritional flavonoids to manage diabetes and its complications are currently in progress [73].

Interestingly, the *N-p*-coumaroyltyramine alkylamide (**5**) was selectively cytotoxic against A431 and HeLa cancer cells while it protected immortalized HaCaT cells against oxidative stress induced by hydrogen peroxide. This result is highly relevant for a potential application of **5** in anticancer therapy. Furthermore, we observed the antidiabetic properties of **5** and the anti-acetylcholinesterase activity in compounds **1**–**4**. Homoisoflavanoids are also known for their anti-acetylcholinesterase properties, a key enzyme to Alzheimer's disease development [74]. We detected anti-acetylcholinesterase activity in compound **3**, a property that had not yet been reported for urgineanins A and B, to our knowledge. Finally, as we recently showed that *Crinum jagus* contained antiviral compounds, we measured the antiretroviral activity of isolated compounds. We report that all compounds possessed anti-retroviral potential, **3** and **4** being the most potent inhibitors.

5. Conclusions

Four homoisoflavanoids and one alkylamide were isolated and characterized from *C. biflorum*, an Amaryllidaceae plant used in African traditional medicine, collected in Senegal. Flavonoids **1**, **3** and **4** showed promising anticancer properties being cytotoxic at low micromolar concentrations towards HeLa and A431 human cancer cell lines. The *N-p*-coumaroyltyramine (**5**) was selectively toxic to A431 and HeLa cancer cells, while it protected immortalized HaCaT cells against oxidative stress induced by hydrogen peroxide. Compounds **1**–**4** also inhibited acetylcholinesterase activity, with compound **3** being the most potent. The anti-amylase and the strong anti-glucosidase activity of compound **5** were confirmed. This study extends the chemical library of compounds that can be a potential candidate for the treatment of cancer, viral infections, diabetes and Alzheimer's disease.

Author Contributions: Conceptualization, M.M., A.E., I.D.-P. and V.C.; M.M., M.K., A.D., R.D.L., N.M., S.K., A.T., M.S. formal analysis and investigation; writing—original draft preparation, M.M., A.E., I.D.-P. and V.C.; writing—review and editing, M.M., A.E., I.D.-P. and V.C. All authors have read and agreed to the published version of the manuscript.

Funding: This research was funded by the Canada Research Chair on plant specialized metabolism grant number 950-232164 to I.D-P.

Institutional Review Board Statement: Not applicable.

Informed Consent Statement: Not applicable.

Acknowledgments: A.E. is associated with the Instituto di Chimica Biomolecolare del CNR, Pozzuoli, Italy. HIV$_{GFP}$, THP-1 and NL4-3$_{GFP}$ were generously provided by Professor Lionel Berthoux at the Université du Québec à Trois-Rivières (Trois-Rivières, QC, Canada).

Conflicts of Interest: The authors declare no conflict of interest.

References

1. Newman, D.J.; Cragg, G.M. Natural products as sources of new drugs over the nearly four decades from 01/1981 to 09/2019. *J. Nat. Prod.* **2020**, *83*, 770–803.
2. Hoshino, O. The amaryllidaceae alkaloids. *Alkaloids* **1998**, *51*, 323–376.
3. Evidente, A.; Kornienko, A. Anticancer evaluation of structurally diverse Amaryllidaceae alkaloids and their synthetic derivatives. *Phytochem. Rev.* **2009**, *8*, 449–459.
4. Nair, J.J.; van Staden, J. Pharmacological and toxicological insight to the South Africa Amaryllidaceae. *Food Chem. Toxicol.* **2013**, *62*, 262–275.
5. Jin, Z.; Yao, G. Amaryllidaceae and Sceletium alkaloids. *Nat. Prod. Rep.* **2019**, *36*, 1462–1488.
6. Nair, J.J.; Bastida, J.; Codina, C.; Viladomat, F.; van Staden, J. Alkaloids of the South African Amaryllidaceae: A review. *Nat. Prod. Commun.* **2013**, *8*, 1335–1350.
7. Christenhusz, M.J.; Byng, J.W. The number of known plants species in the world and its annual increase. *Phytotaxa* **2016**, *26*, 201–217.
8. Bastida, J.; Berkov, S. Amaryllidaceae Alkaloids. *Molecules* **2020**.
9. Masi, M.; Di Lecce, R.; Cimmino, A.; Evidente, A. Advances in the chemical and biological characterization of Amaryllidaceae alkaloids and natural analogues isolated in the last decade. *Molecules* **2020**, *25*, 5621.
10. Ghosal, S.; Saini, K.S.; Razdan, S. *Crinum* alkaloids: Their chemistry and biology. *Phytochemistry* **1985**, *24*, 2141–2156.
11. Kornienko, A.; Evidente, A. Chemistry, biology, and medicinal potential of narciclasine and its congeners. *Chem. Rev.* **2008**, *108*, 1982–2014.
12. Ka, S.; Masi, M.; Merindol, N.; Di Lecce, R.; Plourde, M.B.; Seck, M.; Marcin, G.; Pescitelli., G.; Desgagne-Penix, I.; Evidente, A. Gigantelline, gigantellinine and gigancrinine, cherylline-and crinine-type alkaloids isolated from *Crinum jagus* with anti-acetylcholinesterase activity. *Phytochemistry* **2020**, *175*, 112390.
13. Ka, S.; Merindol, N.; Sow, A.A.; Singh., A.; Landelouci, K.; Plourde, M.B.; Pepin, G.; Masi, M.; Di Lecce, R.; Evidente, A.; et al. Amaryllidaceae alkaloid cherylline inhibits the replication of dengue and Zika viruses. *Antimicrob. Agents Chemother.* **2021**, *65*, 9, doi:10.1128/AAC.00398-21.
14. Ibrakav, A.S.; Akinfewa, A.O.; Hussein, A.A. A comprehensive review on non alkaloids chemical constituents from Amaryllidaceae. *South Afr. J. Bot.* **2020**, In press.
15. Dewick, P.M. *Medicinal Natural Products: A Biosynthetic Approach*; John Wiley & Sons: Chichester, UK, 2009.
16. Osbourn, A.E.; Lanzotti, V. *Plant-Derived Natural Products Dordrecht*; Springer: Berlin, Germany, 2009; pp. 361–384.
17. Abd El-Hafiz, M.A. Aliphatic hydroxyketones from *Crinum augustum*. *Phytochemistry* **1991**, *30*, 3127–3129.
18. Watt, J.M.; Breyer-Brandwijk, M.G. The medicinal and poisonous plants of Southern and Eastern Africa. *Kew Bull.* **1964**, *17*, 463.
19. Likhitwitayawuid, K.; Ruangrungsi, N.; Cordell, G.A. Amabiloside, a new glycoside from *Crinum amabile*. *Nat. Prod. Lett.* **1993**, *3*, 1–4.
20. Nam, N.H.; Jae, Y.Y. NF-κB Inhibitory activities of the methanol extracts and some constituents therein of some Vietnamese medicinal plants. *Sci. Pharm.* **2009**, 77, 389–400.
21. Jin, A.; Li, X.; Zhu, Y.Y.; Yu, H.Y.; Pi, H.F.; Zhang, P.; Ruan, H.L. Four new compounds from the bulbs of *Lycoris aurea* with neuroprotective effects against $CoCl_2$ and H_2O_2-induced SH-SY5Y cell injuries. *Arch. Pharm. Res.* **2014**, *37*, 315–323.
22. Sun, Q.; Zhang, W.D.; Shen, Y.H.; Zhang, C.; Li, H.L. A new phenolic compound from *Crinum asiaticum* L. *Chin. Chem. Lett.* **2008**, *19*, 447–449.
23. Nkanwen, E.R.S.; Gatsing, D.; Ngamga, D.; Fodouop, S.P.C.; Tane, P. Antibacterial agents from the leaves of *Crinum purpurascens* herb (Amaryllidaceae). *Afric. Health Sci.* **2009**, *9*, 264–269.
24. Khoi, N.M.; Dat, N.T.; Na, M.K.; Thuong, P.T.; Min, B.S.; Bae, K.H. Cytotoxic activity of parthenin, a sesquiterpene isolated from a *Crinum ensifolium*. *Nat. Prod. Sci.* **2011**, *17*, 100–103.

25. Abd El Hafiz, M.A.; Ramadan, M.A.; Jung, M.L.; Beck, J.P.; Anton, R. Cytotoxic activity of Amaryllidaceae alkaloids from *Crinum augustum* and *Crinum bulbispermum*. *Planta Med.* **1991**, *57*, 437–439.
26. Abdel-Halim, O.B.; Marzouk, A.M.; Mothana, R.; Awadh, N. A new tyrosinase inhibitor from *Crinum yemense* as potential treatment for hyperpigmentation. *Die Pharm. Int. J. Pharm. Sci.* **2008**, *63*, 405–407.
27. Masi, M.; Mubaiwa, B.; Cimmino, A.; Van Otterlo, W.A.L.; Green, I.R.; Evidente, A. First isolation of acetovanillone and piceol from *Crinum buphanoides* and *Crinum graminicola* (I. Verd.) Amaryllidaceae. *South Afric. J. Bot.* **2018**, *114*, 37–39.
28. Burkill, H.M. *The Useful Plants of West Tropical Africa*; Royal Botanic Gardens: London, UK, 1985; Volume 1, pp. 163.
29. Kianfé, B.Y.; Teponno, R.B.; Kühlborn, J.; Tchuenguem, R.T.; Ponou, B.K.; Helaly, S.E.; Dzoyemd, J.P.; Opatz, T.; Tapondjou, L.A. Flavans and other chemical constituents of *Crinum biflorum* (Amaryllidaceae). *Biochem. Syst. Ecol.* **2019**, *87*, 103953.
30. Silayo, A.; Ngadjui, B.T.; Abegaz, B.M. Homoisoflavonoids and stilbenes from the bulbs of *Scilla nervosa* subsp. *rigidifolia*. *Phytochemistry* **1999**, *52*, 947–955.
31. Dai, Y.; Harinantenaina, L.; Brodie, P.J.; Goetz, M.; Shen, Y.; TenDyke, K.; Kingston, D.G. Antiproliferative homoisoflavonoids and bufatrienolides from *Urginea depressa*. *J. Nat. Prod.* **2013**, *76*, 865–872.
32. Sidwell, W.T.L.; Tamm, C. The homo-isoflavones II1). Isolation and structure of 4′-*O*-methyl-punctatin, autumnalin and 3,9-dihydro-autumnalin. *Tetrahedron Lett.* **1970**, *11*, 475–478.
33. Bhatti, M.K.; Akhtar, F.; Choudhary, M.I. Alkaloids of *Fumaria indica*. *Phytochemistry* **1992**, *31*, 2869–2872.
34. Altomare, A.; Burla, M.C.; Camalli, M.; Cacarano, G.L.; Giacovazzo, C.; Guagliardi, A.; Moliterni, A.G.G.; Polidori, G.; Spagna, R. SIR97: A new tool for crystal structure determination and refinement. *J. Appl. Crystallogr.* **1999**, *32*, 115–119.
35. Sheldrick, G.M. Crystal structure refinement with SHELXL. *Acta Crystallogr. Sect. C Struct. Chem.* **2015**, *71*, 3–8.
36. Farrugia, L.J. WinGX and ORTEP for Windows: An update. *J. Appl. Crystallogr.* **2012**, *45*, 849–854.
37. Macrae, C.F.; Bruno, I.J.; Chisholm, J.A.; Edgington, P.R.; McCabe, P.; Pidcock, E.; Rodriguez-Monge, L.; Taylor, R.; van de Streek, J.; Wood, P.A. Mercury CSD 2.0-new features for the visualization and investigation of crystal structures. *J. Appl. Crystallogr.* **2008**, *41*, 466–470.
38. Amoresano, A.; Di Costanzo, A.; Leo, G.; Di Cunto, F.; La Mantia, G.; Guerrini, L.; Calabrò, V. Identification of ΔNp63α protein interactions by mass spectrometry. *J. Proteome Res.* **2010**, *9*, 2042–2048.
39. Vivo, M.; Fontana, R.; Ranieri, M.; Capasso, G.; Angrisano, T.; Pollice, A.; Calabrò, V.; La Mantia, G. p14ARF interacts with the focal adhesion kinase and protects cells from anoikis. *Oncogene* **2017**, *36*, 4913–4928.
40. Sangermano, F.; Masi, M.; Vivo, M.; Ravindra, P.; Cimmino, A.; Pollice, A.; Evidente, A.; Calabrò, V. Higginsianins A and B, two fungal diterpenoid α-pyrones with cytotoxic activity against human cancer cells. *Toxicol. In Vitro* **2019**, *61*, 104614.
41. di Martino, O.; Troiano, A.; Guarino, A.M.; Pollice, A.; Vivo, M.; La Mantia, G.; Calabrò, V. DNp63a controls YB-1 protein stability: Evidence on YB-1 as a new player in keratinocyte differentiation. *Genes Cells* **2016**, *21*, 648–660.
42. Zhang, J.; Zhao, S.; Yin, P.; Yan, L.; Han, J.; Shi, L.; Zhou, X.; Liu, Y.; Ma, C. α-Glucosidase inhibitory activity of polyphenols from the burs of *Castanea mollissima* Blume. *Molecules* **2014**, *19*, 8373–8386.
43. Ellman, G.L.; Courtney, K.D.; Andres Featherstone, R.M. A new and rapid colorimetric determination of acetylcholinesterase activity. *Biochem. Pharmacol.* **1961**, *7*, 88–95.
44. Borgonovo, G.; Caimi, S.; Morini, G.; Scaglioni, L.; Bassoli, A. Taste–active compounds in a traditional Italian food:'Lampascioni'. *Chem. Biodiver.* **2008**, *5*, 1184–1194.
45. Okuyama, T.; Shibata, S.; Hoson, M.; Kawada, T.; Osada, H.; Noguchi, T. Effect of oriental plant drugs on platelet aggregation; III1. Effect of Chines drug "Xiebai" on human platelet aggregation. *Planta Med.* **1986**, *52*, 171–175.
46. Rogakou, E.P.; Pilch, D.R.; Orr, A.H.; Ivanova, V.S.; Bonner, W.M. DNA doublestranded breaks induce histone H2AX phosphorylation on serine 139. *J. Biol. Chem.* **1998**, *273*, 5858–5868.
47. Dickey, J.S.; Redon, C.E.; Nakamura, A.J.; Baird, B.J.; Sedelnikova, O.A.; Bonner, W.M. H2AX: Functional roles and potential applications. *Chromosoma* **2009**, *118*, 683–692.
48. Nishioka, T.J.; Watanabe, J.; Kawabata, J.R.; Niki, I. Isolation and activity of *N*-*p*-coumaroyltyramine, an α-glucosidase inhibitor in welsh onion (*Allium fistulosum*). *Biosci. Biotech. Biochem.* **1997**, *61*, 1138–1141.
49. Pasetto, S.; Pardi, V.; Murata, R.M. Anti-HIV-1 activity of flavonoid myricetin on HIV-1 infection in a dual-chamber in vitro model. *PLoS ONE* **2014**, *9*, e115323.
50. Koagne, R.R.; Annang, F.; de la Cruz, M.; Bitchagno, G.T.M.; Perez-Victoria, I.; Konga, I.S.; Vincente, F.; Reyes, F.; Tane, P. Antibacterial activity of flavans from *Crinum distichum*. *Nat. Prod. Commun.* **2018**, *13*, 1637–1638.
51. Barone, G.; Corsaro, M.M.; Lanzetta, R.; Parrilli, M. Homoisoflavanones from *Muscari neglectum*. *Phytochemistry* **1988**, *27*, 921–923.
52. Evidente, A.; Iasiello, I.; Randazzo, G. An improved method for the large-scale preparation of lycorine. *Chem. Ind.* **1984**, *9*, 348–349.
53. Giordano, F.; Lanzetta, R. Structure and absolute configuration of (–)-(3*R*)-5, 7-dimethoxy-3,9-dihydro-4'-eucomnalinyl *p*-bromobenzoate: An uncommon case. *Acta Crystallogr. Sect. C Struct. Chem.* **1989**, *45*, 1603–1606.
54. Zask, A.; Ellestad, G. Biomimetic syntheses of race-mic natural products. *Chirality* **2018**, *30*, 157–164.
55. Di Lecce, R.; Masi, M.; Linaldeddu, B.T.; Pescitelli, G.; Maddau, L.; Evidente, A. Bioactive secondary metabolites produced by the emerging pathogen *Diplodia olivarum*. *Phytopathol. Mediterr.* **2021**, *60*, 129–138.
56. Fitch, R.W.; Snider, B.B.; Zhou, Q.; Foxman, B.M.; Pandya, A.A.; Yakel, J.L.; Olson, T.T.; Al-Muhtasib, N.; Xiao, Y.; Welch, K.D.; et al. Absolute configuration and pharmacology of the poison frog alkaloid phantasmidine. *J. Nat. Prod.* **2018**, *81*, 1029–1035.

57. Murray, A.F.; Moore, A.J.; Munafo, J.P., Jr. Key odorants from the american matsutake, *Tricholoma magnivelare*. *J. Agric. Food Chem.* **2020**, *68*, 9768–9775.
58. Tran-Cong, N.M.; Mándi, A.; Király, S.B.; Kurtán, T.; Lin, W.; Liu, Z.; Proksch, P. Furoic acid derivatives from the endophytic fungus *Coniothyrium* sp. *Chirality* **2020**, *32*, 605–610.
59. Deng, A.J.; Zhang, H.J.; Li, Q.; Li, Z.H.; Zhang, Z.H.; Wu, L.Q.; Li, L.; Qin, H.L. Six scalemic mixtures of 6-monosubstituted dihydrobenzophenanthridine alkaloids from *Chelidonium majus* and optically active structures of enantiomers. *Phytochemistry* **2017**, *144*, 159–170.
60. Yoshihara, T.; Takamatsu, S.; Sakamura, S. Three new phenolic amides from the roots of eggplant (*Solanum melongena* L.*). Agric. Biol. Chem.* **1978**, *42*, 623–627.
61. Wu, Y.C.; Chang, G.Y.; Ko, F.N.; Teng, C.M. Bioactive constitutents from the stems of *Annona montana*. *Planta Med.* **1995**, *61*, 146–149.
62. Barbalho, S.M.; de Alvares Goulart, R.; Vasques Farinazzi-Machado, F.M.; da Silva Soares de Souza, M.; Cincotto dos Santos Bueno, P.; Landgraf Guiguer, E.; Araújo, A.C.; Groppo, M. *Annona* sp: Plants with multiple applications as alternative medicine-A review. *Curr. Bioact. Compd.* **2012**, *8*, 277–286.
63. Park, J.B. Identification and quantification of a major anti-oxidant and anti-inflammatory phenolic compound found in basil, lemon thyme, mint, oregano, rosemary, sage, and thyme. *Int. J. Food Sci. Nutr.* **2011**, *62*, 577–584.
64. Rios, M.Y. Natural alkamides: Pharmacology, chemistry, and distribution. In *Drug Discovery: Research in Pharmacognosy*; Books on Demand: *Norderstedt, Germany,* 2012; pp. 107–144.
65. Morimoto, N.; Ueno, K.; Teraishi, M.; Okumoto, Y.; Mori, N.; Ishihara, A. Induced phenylamide accumulation in response to pathogen infection and hormone treatment in rice (*Oryza sativa*). *Biosci. Biotech. Bioch.* **2018**, *82*, 407–416.
66. Castelli, M.V.; López, S.N. Homoisoflavonoids: Occurrence, biosynthesis, and biological activity. In *Studies in Natural Products Chemistry*; Elsevier: Amsterdam, The Netherlands, 2017; pp. 315–354.
67. Abegaz, B.M.; Kinfe, H.H. Naturally occurring homoisoflavonoids: Phytochemistry, biological activities, and synthesis (Part II). *Nat. Prod. Commun.* **2019**, 14, doi:10.1177/1934578x19845813.
68. Danaei, G.; Finucane, M.M.; Lu, Y.; Singh, G.M.; Cowan, M.J.; Paciorek, C.J. Global burden of metabolic risk factors of chronic diseases collaborating, G. National, regional, and global trends in fasting plasma glucose and diabetes prevalence since 1980: Systematic analysis of health examination surveys and epidemiological studies with 370 country-years and 2.7 million participants. *Lancet* **2011**, *378*, 3140.
69. World Health Organization. *Definition and Diagnosis of Diabetes Mellitus and Intermediate Hyperglycemia: Report of a WHO/IDF Consultation*; World Health Organization: Geneva, Switherland, 2006; pp. 1–50.
70. Mohan, S.; Nandhakumar, L. Role of various flavonoids: Hypotheses on novel approach to treat diabetes. *J. Med. Hypot. Ideas* **2014**, *8*, 1–6.
71. Testa, R.; Bonfigli, A.R.; Genovese, S.; De Nigris, V.; Ceriello, A. The possible role of flavonoids in the prevention of diabetic complications. *Nutrients* **2016**, *8*, 310.
72. AL-Ishaq, R.K.; Abotaleb, M.; Kubatka, P.; Kajo, K.; Büsselberg, D. Flavonoids and their anti-diabetic effects: Cellular mechanisms and effects to improve blood sugar levels. *Biomolecules* **2019**, *9*, 430.
73. Vinayagam, R.; Xu, B. Antidiabetic properties of dietary flavonoids: A cellular mechanism review. *Nutr. Metab.* **2015**, *12*, 60.
74. Li, Y.; Qiang, X.; Luo, L.; Yang, X.; Xiao, G.; Zheng, Y.; Cao, Z.; Sang, Z.; Su, F.; Deng, Y. Multitarget drug design strategy against Alzheimer's disease: Homoisoflavonoid Mannich base derivatives serve as acetylcholinesterase and monoamine oxidase B dual inhibitors with multifunctional properties. *Bioorg. Med. Chem.* **2017**, *25*, 714-726.

CHAPTER III

3. Cistanche phelypaea

3.1. Phenylethanoid glycosides and Iridoids isolated from the *Cistanche phelypaea* plant collected in Spain

The *Cistanche phelypaea* species is commonly found in the Iberian Peninsula, and in particular, the plant I studied was collected at the Finca Torrecillas farm, Corvera, Murcia, Spain; then it was sliced and dried in an open room in the shade for 15 days (figure 11).

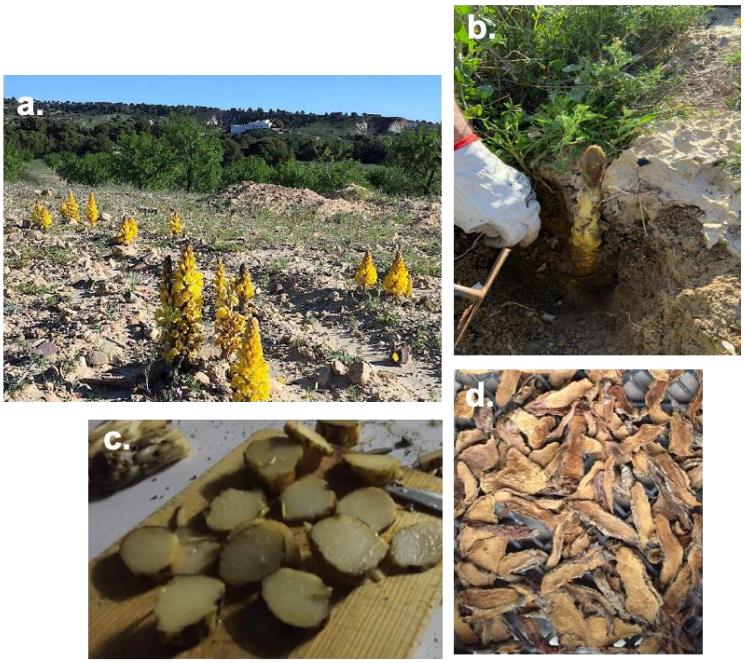

Figure 11. Collection procedure of *C. phelypaea*. **(a, b)** The date of harvest was winter 2020. Bulbs harvested when starting to crack the soil and show a few centimeters of the top above the soil surface. Done manually trying to obtain full pieces from the root. **(c, d)** After harvesting from the field, the bulbs of *C. phelypaea* were washed with water to remove the mood and then cut into slices. Finally set it in an open room in the shade for drying.

The dried bulbs were first ground and then extracted in ethanol with the Soxhlet apparatus to isolate the polar component, which is the most abundant in this species.
We obtained an oily organic extract, which has been dissolved in distilled water and re-extracted in EtOAc. As a preliminary step of the bio-guided purification procedure, I tested the possible cytotoxicity of the whole plant extract by the MTT viability assay on human immortalized keratinocytes (HaCaT cells). The EtOAc extract was tested at concentrations ranging from 0.001 to 1 mg/mL for 48 to 72 hours.
At concentrations lower than 0.01 mg/ml and 48 hours of treatment, *Cistanche* extracts induced a significant increase in cell viability (figure 12 A). The observed increase in cell viability was probably due to an improvement in cellular metabolism (figure 12 B). Given that, the cell proliferation rate was unaffected by the treatment. At a concentration higher than 0.1 mg/ml the cytotoxic effect became predominant (figure 12 A).

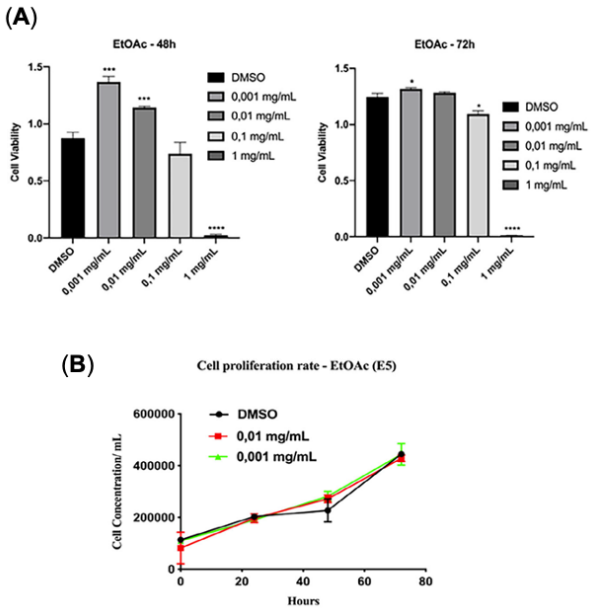

Figure 12. (A) MTT viability test. HaCaT cells were incubated with the indicated amount of EtOAc organic extract for 48 and 72 h. The values were the mean's six values for each experimental point of two independent biological replicates. Each means was compared using a Dunnett's multiple comparisons test of ANOVA one-way (p-value *< 0.01, ** < 0.05, ***p < 0.001; ****p < 0.0001). **(B)** Cell proliferation rate. HaCaT cells were plated and treated with EtOAc extract at the indicated concentrations. Following the treatment, they were counted with the Scepter cell counter, at times 0 and 24, 48, and 72 h, creating the proliferation curve. There

is no significant change in the proliferation rate of the treated cells, compared to the DMSO control.

The obtained result suggested that the *C. phelypaea* extract was a complex mixture of cytotoxic and stimulatory metabolites whose positive effect on cell metabolism predominates at low concentrations of the extract. Therefore, the crude extract was fractionated by chromatographic columns and the various fractions were chemically characterized. The isolated metabolites belonged to two different classes of compounds: **phenylethanoid glycosides** and **iridoids**. The purity of the isolated compounds was >98% as ascertained by ^{1}H NMR and HPLC analyses. There were 6 different metabolites identified and purified according to the fractionation scheme shown in figure 13: acetoside (1), 2'-O- acetylacetoside (2), tubuloside (3) as phenylethanoid glycosides, and bartioside (4); 6-deoxycatalpol (5), gluroside (6) as iridoids glycosides (figure 14). Their identification was confirmed by the ESIMS spectra and by comparing their specific optical rotation data with those reported in the literature. Furthermore, the acid hydrolysis of compounds 1–3 afforded D-glucose and D-xylose while that of compounds 4–6 only D-glucose by co-TLC with standard sugars samples and recording the specific optical rotation.

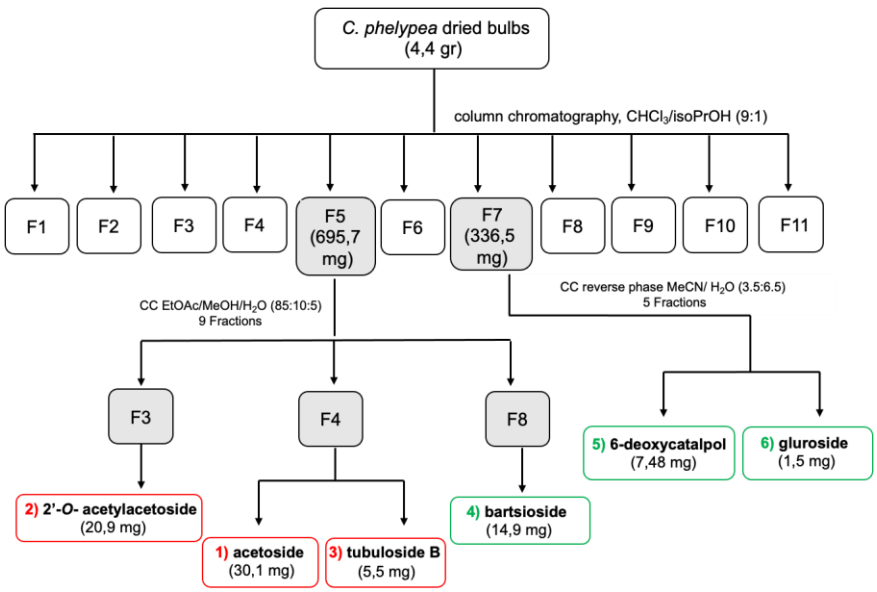

Figure 13. Schematic representation of the extraction and purification process of pure metabolites, starting from the dried bulbs of *C. phelypaea*.

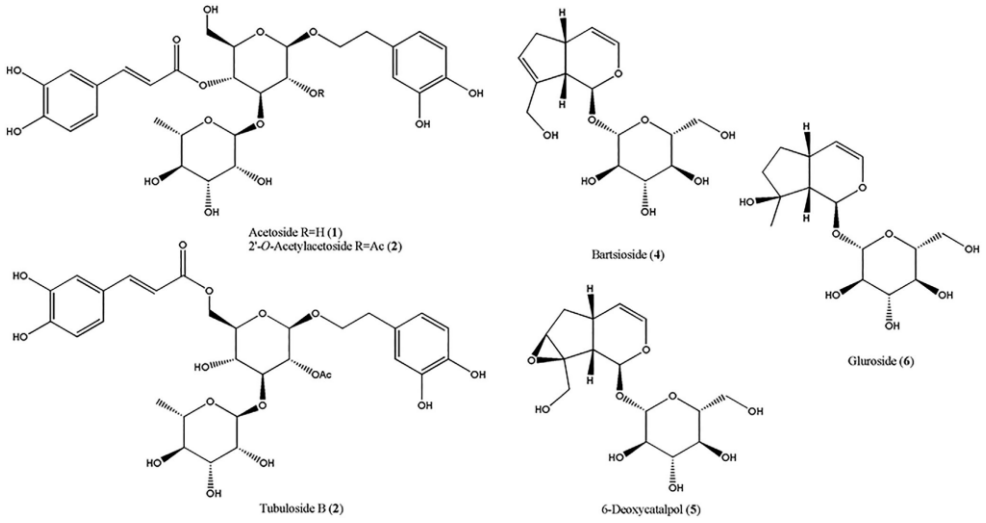

Figure 14. Structures of the phenylethanoid glycosides acetoside, 2'-O-acetylacetoside, and tubuloside B (1-3), and of the iridoid glycosides bartsioside, 6-deoxycatalpol, and gluroside (4-6), isolated from the EtOAc extract of *C. phelypaea.*

3.2. Analysis of *Cistanche phelypaea* metabolites

Phenylethanoid glycosides (PhG) are a valuable class of phytochemical compounds, with significant benefits for human health. PhG are generally water-soluble phenolic compounds found as the main component in many pharmacological products. PhGs have been isolated from roots, stems, barks, leaves, flowers, fruits, and seeds of medicinal plants, as well as from suspension cell cultures, callous tissue and adventitious root cultures. They are also found in various plant-based foods such as edible flowers and tea. However, their accumulations in each plant organ can vary. By June 2020, up to 572 PhGs were already known from the wild. These 572 PhGs are distributed in 21 orders and among 35 families of the plant kingdom.
In general, the basic structure of PhGs consists of a hydroxyphenylethyl unit such as an aglycone which is attached to a sugar moiety primarily

a β-D-glucopyranose via a glycosidic linkage at the C-1 site. In most cases, glucose is esterified with a cinnamic or hydroxycinnamic acid derivative such as caffeic, coumaric, or ferulic acid. Rhamnose, xylose, arabinose, allose, galactose and apiose, among others, can also be attached to the glucose residue. The diversity of sugar and hydroxyphenylethyl fractions makes the extraordinary variety of PhG. Generally, the number of sugars ranges from one to three. However, four and five sugars residues are also occasionally found (Fu G. *et al*., 2008). Many PhG and PhG-rich extracts have shown potent antioxidant activity. It was observed that PhGs with more sugars had weaker antioxidant activity. Indeed, more sugars mean a greater steric hindrance in the compounds and prevent them from approaching free radicals easily, eventually resulting in the weakest DPPH radical scavenging ability. The structure of PhGs can contain α and β conjugated unsaturated esters thus allowing easier electron delocalization to inhibit free radicals.

In some diseases such as cancer and aging, DNA damage induced by oxygen radicals has often been regarded as a causal event. In the literature, it is reported that PhGs may play a protective role in DNA damage (Shi, Y. *et al*., 1999; Delalande, O. *et al.,* 2002). Li *et al*. suggested that the PhGs acteoside and pedicularioside A can suppress the formation of the thymine lesions and are therefore potential radioprotectors and anticarcinogens (Smith T. A. *et al*., 2017). Given their antioxidant properties, many PhGs have also been evaluated for their neuroprotective, hepatoprotective, anti-inflammatory, and immunomodulatory activity. Another major asset of PhGs is their antiviral and antibacterial activity.

The second class of compounds isolated from *C. phelypaea* are the glycosylated iridoids. Iridoids, a large and still expanding class of cyclopentane pyran monoterpenes, are composed of two basic carbon structures, substituted iridoids and secoiridoids. Based on the structure, these compounds can be divided into four groups: iridoid glycosides, secoiridoid glycosides, non-glycosidic iridoids, and bis-iridoids. Iridoids have hemiacetalic hydroxyl groups and are active. Furthermore, they are mostly in the form of glycosides and are combined with glucose in the C-1 hydroxyl group (Xue, Z., & Yang, B., 2016; Xue, J. *et al.,* 2018). Their important effects on various diseases have proved their importance in pharmaceutical chemistry research. They are active molecules used in natural and traditional Chinese medicine. Modern pharmacological studies have shown that these compounds have anticancer, antidepressant, liver protective, neuroprotective and other health effects. The antitumor activity of the iridoid has been extensively

studied; ether terpenes have been found to inhibit DNA polymerase activity, suggesting that they can be used to inhibit DNA synthesis (Wang, C. *et al*., 2020). Some iridoids, such as gentiopicroside, can arrest ovarian cancer cells in the G2/M phase of the cell cycle and halt cancer cell invasion and migration. In other studies, gentiopicroside was shown to reduce the activity of metalloproteases 2 (MMP-2) and 9 (MMP-9) by inhibiting the adhesion of HepG2 tumor cells, and thus the metastasis and invasion of human hepatocellular carcinoma cells (Ahn, J. H. *et al*., 2018; Jiang, Y. *et al*., 2016).

Anti-inflammatory properties of the iridoids have also been reported. The bis-iridoid aglycones reduced TNF-α and LPS-induced NF-κB activation and reduced inflammatory factors that inhibit free radical production in human cells. In recent years, with continuous improvement in extraction methods and storage conditions, an increasing number of iridoids have been identified. However, they are subject to degradation under both physical and chemical stress conditions and have poor chemical stability, which produces limitations in the study of their monomers and hinders the study of their activities and functions. Furthermore, most of the studies on iridoids are still focused on determining their structures and analyzing their activities. Systematic research on their structure types and structure-activity relationships is lacking. Therefore, the analysis and comparative studies on the structure and function of iridoids should be further intensified, to better confirm the main active functional groups and effects of iridoids and provide effective data support for chemical modification and development of new drugs, which will constitute a new research center on natural products (Wu, L. *et al.,* 2020).

To test and compare the anti-free radical activity of all isolated *C. phelypaea*-derived metabolites I performed the ROS assay with 2'-7' dichlorofluorescein diacetate (DCFDA), as previously described, on human immortalized HaCaT keratinocytes, pre-treating them with 50 and 100 μM acetoside (1), 2'-O-acetylacetoside (2), tubuloside B (3), bartioside (4), 6-deoxycatalpol (5) and gluroside (6). The positive control used was Trolox, a water-soluble analog of vitamin E, while the negative control was treated with vehicle (DMSO 0.1%) used to dilute all compounds. As shown in figure 15, acetoside (1) was the strongest antioxidant metabolite almost comparable to the analog of vitamin E, and also at the lowest concentration tested (figure 15). The other tested metabolites can only moderately lower the production of ROS thus demonstrating how even small chemical differences, such as a single substituent group as in the case of 2'-O-acetylacetoside (2), can have a large effect on biological activity. Iridoid glycosides certainly have a

more moderate scavenging activity than PhGs. The latter have caffeic acid in their structure, which contributes considerably to their antioxidant activity, especially after being metabolized.

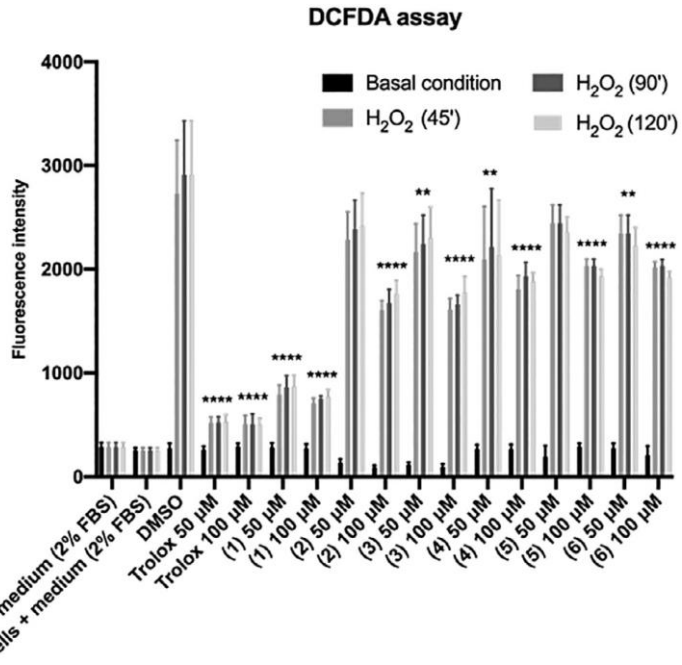

Figure 15. DCFDA assay. HaCaT cells were seeded and pretreated for 4 h with 50 and 100 µM 1-6 metabolites from *C. phelypaea*. H_2O_2 (1 mM; 3%) was added to the medium for 45',1.5, and 2h. The fluorescence intensity of DCFDA was read after 45' of incubation. Trolox was used as a positive control and DMSO, in which the metabolites are dissolved, as a negative control. The values are the mean's six values for each experimental point of two independent biological replicates. Statistical analysis was performed with two-way ANOVA, using Tukey's multiple comparison test. Levels of significance between points of expression are indicated (****p < 0.001, ***p < 0.01, **p < 0.05).

Given its remarkable antioxidant power, I focused my attention on acetoside exploring activities that had not yet been demonstrated. Moreover, acetoside was also the most abundant metabolite isolated from *Cistanche*. I first evaluated the cytotoxicity of acetoside over long incubation periods, but I found in the literature that the caffeoyl group of acetoside can interfere with the MTT test and give unreliable results due to the mitochondrial decoupling effects (Wang, Zhou, Xu, & Gao, 2015). Therefore, I evaluated the cytotoxicity of acetoside on human immortalized keratinocytes HaCaT e A431 human squamous cell carcinoma cells by trypan blue exclusion wise. The results obtained

revealed that at the concentrations tested acetoside was not toxic to human keratinocytes while causing cell death in tumor cells between 12 and 20% at the concentration of 100 μM (Table 1). Furthermore, I compared the cell proliferation rate of HaCaT and A431 cells in an acetonide-containing medium and we consistently found a time- and dose-dependent reduction in the rate of cell proliferation in both immortalized and transformed keratinocytes. It is interesting to note that the carcinoma-derived A431 cells were more sensitive than HaCaT to the cell growth inhibitory effect of acetoside (figure 16).

A431 Time of incubation	% viability	100		10
24 h	96	95	93	90
48 h	94	80	97	97
72 h	96	88	95	98
Hacat Time of incubation	**% viability**	**100**	**50**	**10**
24 h	96	86	98	94
48 h	97	97	97	94
72 h	95	93	98	90

Table 1. Percentage of viable cells. HaCaT and A431 cells were seeded and treated with acetoside (1) 10, 50, and 100 μM. Dead cells were counted with Trypan Blue after 24, 48, and 72 h from treatments, and the percentage of live cells was measured out of the total number of cells. Numbers are the average of triplicate data.

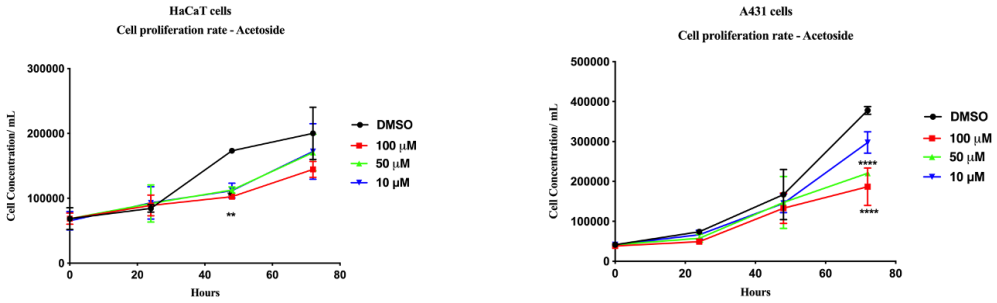

Figure 16. Cell proliferation rate. HaCaT and A431 cells were seeded and treated with acetoside (1) 10, 50, and 100 μM. Cells were counted with Scepter at T0, 24, 48, and 72 h of treatments. Results are the mean ± SEM of three independent biological experiments relative to the experimental control (DMSO). Statistical analysis was performed with one-way ANOVA,

using Dunnett's multiple comparison test. Levels of significance between points of expression are indicated (****p < 0.001, **p < 0.01).

3.3. Acetoside as an inhibitor of the human keratinocytes and pluripotent cells differentiation

Adult stem cells from bone marrow and other tissues can differentiate into many cell types, including osteocytes, chondrocytes, smooth muscle cells, hepatocytes, cardiomyocytes, neurons, and retinal cells and are considered promising resources for regenerative cell therapy (Mimeault M *et al.,* 2007). Yamanaka and colleagues have demonstrated that these induced pluripotent stem (iPS) cells could be generated from mouse and human embryonic fibroblasts through retrovirus-mediated transfection of four transcription factors, namely Oct3/4, Sox2, c-Myc and Klf-4, transcription factors whose expression can convert somatic cells from a terminally differentiated state to an embryonic one (Okita, K., & Yamanaka, S. 2011).
Some natural antioxidants such as Resveratrol (trans-3,5,4′-trihydroxystilbene), a natural polyphenol found largely in the skin of red grapes, walnuts, pomegranates, and red wine have anti-aging activities and cell life span extension in addition to other health benefits effects (Ozcan T. *et al.,* 2014). Recent studies have proved that resveratrol improves osteoblast differentiation (Ornstrup M. J. *et al*., 2016). In addition, two independent studies, published in 2010, reported that vitamin C could promote DNA demethylation in Embryonal Stem Cells (ESC) (Cimmino L. *et al*., 2018) and enhance somatic cell reprogramming in iPSCs (Brabson J. P. *et al*., 2021). Other antioxidants compounds have been shown to maintain stemness such as Vitamin C which is required to maintain ESC proliferation *in vitro* (Cimmino L. *et al*., 2018) and was originally added to the media of somatic cells to counteract ROS generated during reprogramming in an attempt to improve the efficiency or quality of generated iPSCs (Brabson, J. P. *et al.,* 2021). However, vitamin C has proved itself substantially more efficient at enhancing iPSC generation than other antioxidants.
Therefore, I explored the effect of acetoside on cell differentiation due to its strong antioxidant activity. HaCaT keratinocytes represent an immortalized cell type that proliferates indefinitely and being untransformed is still able to differentiate in culture under appropriate stimuli. The terminal differentiation of HaCaT immortalized keratinocytes is coupled to cell cycle withdrawal and this process has

been associated with a transient upregulation of p21WAF cell cycle inhibitor. After Ca^{2+} addition, HaCaT cells differentiate and express CK1 and CK10, the suprabasal skin prominent markers of differentiation. To test the differentiation potential of HaCaT cells in the presence of acetoside, I evaluated the expression of CK1 and CK10 as well as the expression of ΔNp63α, a known epithelial stem cell marker. As shown in figure 17, the addition of Ca^{2+} caused a reduction of ΔNp63α and a concomitant increase of p21WAF, CK1, and CK10. In keratinocytes treated with acetoside, on the other hand, we observed sustained induction of p21WAF without an increase in CK1 and CK10 expression. In particular, the level of ΔNp63α remained unchanged (figure 17).

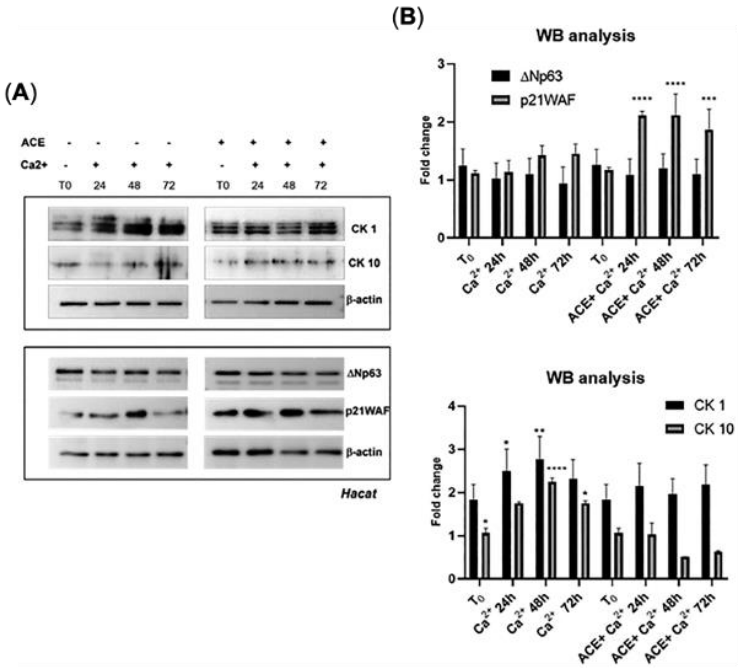

Figure 17. Representative western blot analysis of a total extract from HaCaT keratinocytes in response to Ca^{2+} addition in the presence or absence of acetoside. HaCaT cells were differentiated with 2 mM Ca^{2+} and compared with cells treated with Ca^{2+} plus 50 μM acetoside (ACE) for 48 and 72 h. **(A)** Immunoblot was probed with ΔNp63α, p21WAF, CK1 and CK10 antibodies. β-Actin was used as a loading control. **(B)** The signals of protein bands were quantified by ImageLab software version 4.1 (Bio-Rad) Statistical analyses were performed using 2-way ANOVA and Sidak's multiple comparisons or Dunnett's multiple comparisons test. Levels of significance between points of expression are indicated (***p < 0.001, **p < 0.01, *p < 0.05).

The obtained results suggest that acetoside can preserve the keratinocyte stemness required for epithelial morphogenesis and renewal. The data observed in keratinocytes prompted us to study the activity of acetoside on human mesenchymal pluripotent stem cells. Human mesenchymal stem cells (hMSCs) can differentiate into osteoblasts using *in vitro* differentiation protocol that aims to recapitulate the osteogenic development program. The hMSCs were induced to osteogenic differentiation replacing the basal medium with an osteogenic medium supplemented or not with acetoside at a concentration of 100 µM for 16 days. Transcriptional activation of genes such as COL1A1, RUNX2, OCN and ALPL indicates osteogenic differentiation. Therefore, I evaluated expression of these differentiation biomarkers at different times by quantitative Real-Time PCR. In untreated samples the expression of COL1A1, RUNX2, OCN and ALPL were significantly increased by day 7 while inhibition of their expression was observed in acetoside processed samples. These results suggest that acetoside can regulate the stem nature of the mesenchymal progenitors maintaining their undifferentiated state (figure 18).
Finally, I performed a DCFDA test to evaluate the antioxidant potential of acetoside in human mesenchymal stem cells (hMSC) compared to that of (+)-catechin and (±)-epi-catechin, two well-known antioxidants flavonoids. hMSC cells were pretreated with 10 and 100 µM of catechin, (±)-epi-catechin and acetoside from *C. phelypaea*. As shown in figure 19, acetoside has antioxidant activity comparable to catechins at the same concentration.

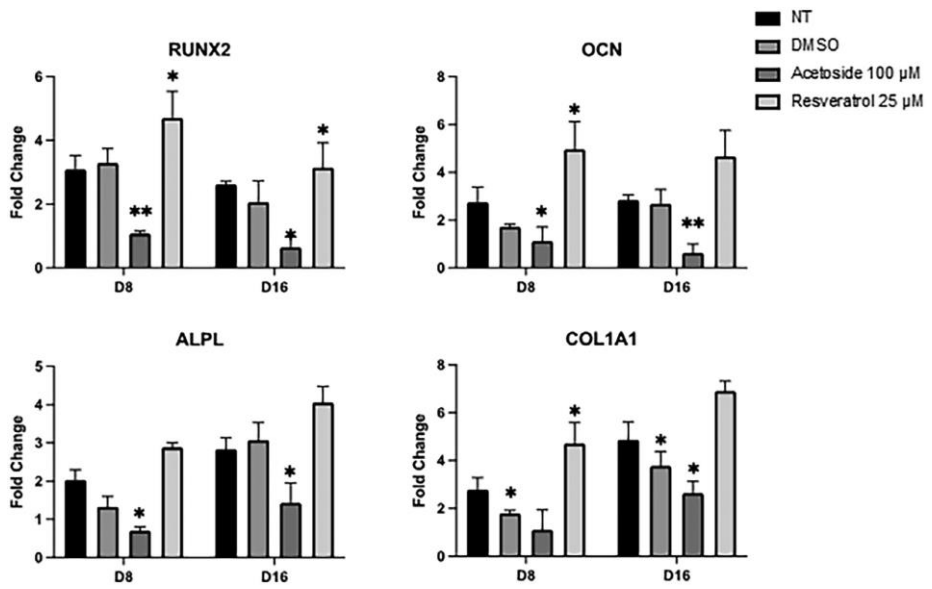

Figure 18. RT-qPCR analysis of the osteogenic markers (COL1A1, RUNX2, OCN and ALPL). The mRNA levels were normalized to Gapdh expression and reported as a fold change to the value in D0. Resveratrol was used as a positive control of differentiation. The values shown are mean ± SD, based on triplicate assays. Statistical analyses were performed using Student's t-test, where $p < 0.05$ was considered significant (*$p < 0.05$, **$p < 0.01$).

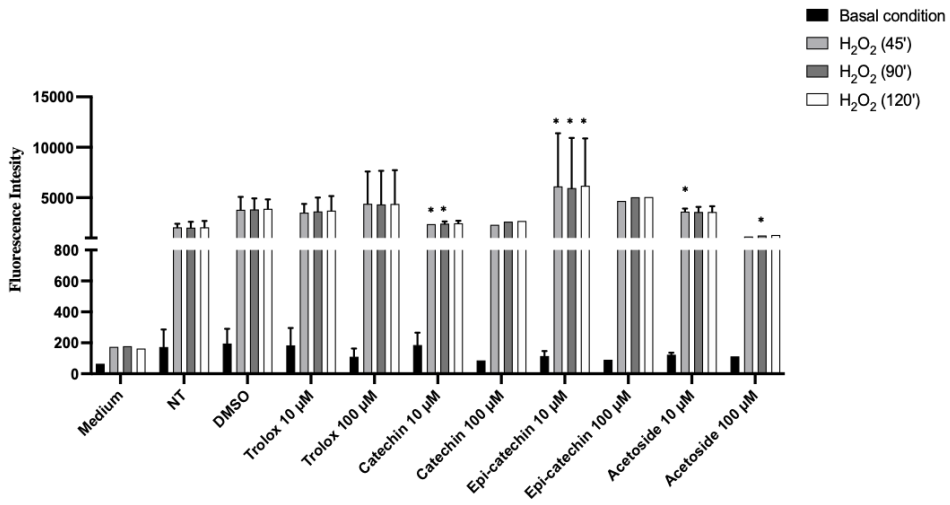

Figure 19. DCFDA assay. hMSC cells were seeded and pre-treated for 4 h with 10 and 100 µM of catechin, epicatechin, and acetoside. H_2O_2 (1 mM; 3%) was added to the medium for 45', 1,5, and 2h. The fluorescence intensity of DCFDA was read after 45' of incubation. Trolox

was used as a positive control and DMSO, in which the metabolites are dissolved, as a negative control. The values are the mean's six values for each experimental point of two independent biological replicates. Statistical analysis was performed with two-way ANOVA, using Tukey's multiple comparison test. Levels of significance between points of expression are indicated (***p < 0.001, **p < 0.01, *p < 0.05).

3.4. Conclusions

In conclusion, *C. phelypaea* is a rich source of metabolites with antioxidant activity that can be used as functional ingredients for food preservation and nutraceuticals. The fractionation procedure allowed us to isolate two classes of compounds abundant in this plant species: phenylethanoid glycosides and iridoid glycosides, with acetoside and 2'-O-acetylacetoside being the most abundant glycosides. The structures of phenylethanoid glycosides contain phenolic hydroxyl groups, which are responsible for the antioxidant activity of *Cistanche* (Zhang *et al.,* 2016), and as I demonstrated the difference in chemical structure, such as the presence of substituent groups, can significantly affect the antioxidant activity of the compound.

In human keratinocytes, the ROS scavenging activity of acetoside was fully comparable to that of Trolox, the water-soluble derivative of vitamin E. Remarkably, in human mesenchymal progenitor cells Trolox was ineffective while acetoside was still able to effectively counteract the production of ROS suggesting a potential application of this metabolite as an additive in hESC cell culture medium.

Skin keratinocytes have a high turnover rate. The basal proliferative compartment of stratified squamous epithelia consists of the stem and transient amplifying (TA) keratinocytes. Engagement of differentiation promotes the withdrawal of keratinocytes from the quiescent stem cell compartment and their transit to the tissue's upper layers and surface. TA keratinocytes transiently acquire an appreciable proliferative capacity and show markedly reduced ΔNp63α biomarker. These data indicate that co-treatment of human keratinocytes with Ca^{2+}, a trigger of keratinocyte differentiation, and acetoside induced a reversible cell cycle arrest. Indeed, in the presence of Ca^{2+} and acetoside, p21WAF expression was upregulated, while ΔNp63α, a pro-proliferative marker, was not reduced thus suggesting that acetoside preserves the regenerative potential of keratinocytes. Furthermore, in the presence of Ca^{2+} and acetoside, cytokeratins 1 and 10 did not increase thus indicating that keratinocyte differentiation was inhibited or slowed down. On the other hand, it is worth mentioning that acetoside also

suppresses the differentiation of macrophages into osteoclasts without affecting their viability (Lee, Lee, Yi, Kook, & Lee, 2013).
Furthermore, I found that acetoside inhibited osteoblastic differentiation of hMSCs that serve as the primary tool of tissue engineering. They are multipotent cells with a cell renewal capacity such that they can differentiate *in vitro* into a variety of cell types, adipocytes, chondrocytes and osteoblasts (Okolicsanyi *et al*., 2015). Furthermore, they persist in various tissues and are responsible for maintaining tissue homeostasis and repairing tissue damage by replenishing senescence and damaged cells. In general, stem cells are more sensitive than their progeny to the adverse effects of ROS even though low levels of ROS are required to maintain quiescence and self-renewal of pluripotent stem cells (Zhou, Shao, & Spitz, 2014). Excess ROS, however, can inhibit stem cell self-renewal not only by promoting cell differentiation but also by inducing senescence and/or apoptosis. When ROS production is induced, acetoside maintains the undifferentiated state of mesenchymal stem cells, osteoblasts, and osteoclast precursors.
In recent work, it was demonstrated that total extract from *C. deserticola* was able to mediate bone formation by upregulating BMP-2 (Bone Morphogenetic Factor 2) and OPG (Osteoprotegerin) and downregulating RANKL thus promoting osteoporotic bone reconstruction (Wang, Tu, Zeng & Jiang, 2021). Thus, phenylethanoids glycosides from *Cistanche* extract can regulate the balance between multipotent mesenchymal stem cells, bone-forming osteoblasts, and bone-resorbing osteoclasts. Therefore, they are promising therapeutic agents for bone homeostasis.
In conclusion, acetoside appears to preserve the proliferative potential of human basal keratinocytes and mesenchymal progenitors required for tissue morphogenesis and renewal. The use of stem cells in tissue engineering requires their controlled differentiation; hMSCs have great potential therapeutic power, however, their utility is limited by cellular senescence secondary to increased reactive oxygen levels, especially during their propagation in culture (Ogrodnik *et al.,* 2017). In this regard, acetoside may be of practical relevance for the clinical application of human stem cell cultures for regenerative medicine.
Almost 50 years have passed since the first PhGs were isolated and many experimental data have demonstrated the potent pharmacological activities of PhGs.
The therapeutic potential of PhGs should be further explored to elucidate their mechanism of action and structure-activity relationships. Preclinical trials in organoids and animal models will give more insights into the safety and efficiency of PhG.

Received: 14 February 2022 | Revised: 5 June 2022 | Accepted: 12 June 2022

DOI: 10.1002/ptr.7548

RESEARCH ARTICLE

WILEY

In vitro characterization of iridoid and phenylethanoid glycosides from *Cistanche phelypaea* for nutraceutical and pharmacological applications

Antonella Delicato[1] | Marco Masi[2] | Francisco de Lara[3] | Diego Rubiales[4] | Ida Paolillo[1] | Valeria Lucci[1] | Geppino Falco[1] | Viola Calabrò[1] | Antonio Evidente[2]

[1]Dipartimento di Biologia, Università di Napoli Federico II, Complesso Universitario Monte Sant'Angelo, Naples, Italy

[2]Dipartimento di Scienze Chimiche, Università di Napoli Federico II, Complesso Universitario Monte Sant'Angelo, Naples, Italy

[3]Farmstate Finca Torrecillas eco retreat, Murcia, Spain

[4]Institute for Sustainable Agriculture, CSIC, Córdoba, Spain

Correspondence
Viola Calabrò, Dipartimento di Biologia, Università di Napoli Federico II, Complesso Universitario Monte Sant'Angelo, Via Cintia 4, 80126 Naples, Italy.
Email: vcalabro@unina.it

Abstract

"Desert hyacinths" are a remarkable group of parasitic plants belonging to genus *Cistanche*, including more than 20 accepted species typically occurring in deserts or coastal dunes parasitizing roots of shrubs. Several *Cistanche* species have long been a source of traditional herbal medicine or food, being *C. deserticola* and *C. tubulosa* the most used in China. This manuscript reports the isolation and identification of some phenylethanoid and iridoid glycosides, obtained from the hydroalcoholic extract of *C. phelypaea* collected in Spain. The present study aims to characterize the antioxidant activity of C. *phelypaea* metabolites in the light of their application in nutraceutical and cosmeceutical industries and the effect of acetoside, the most abundant metabolite in *C. phelypaea* extract, on human keratinocyte and pluripotent stem cell proliferation and differentiation. Our study demonstrated that acetoside, besides its strong antioxidant potential, can preserve the proliferative potential of human basal keratinocytes and the stemness of mesenchymal progenitors necessary for tissue morphogenesis and renewal. Therefore, acetoside can be of practical relevance for the clinical application of human stem cell cultures in tissue engineering and regenerative medicine.

KEYWORDS
antioxidants, *Cistanche*, *Cistanche phelypaea*, iridoid glycosides, phenylethanoid glycosides, nutraceuticals

1 | INTRODUCTION

The genus *Cistanche* includes more than 20 species that are holoparasites, lacking chlorophyll and functional leaves. They parasitize the roots of halophytic perennial shrubs typically on deserts, arid lands, or coastal dunes (Xu et al., 2009). They are commonly known as "Desert hyacinths". Besides their evolutionary or botanist interest, *Cistanche* species raised herbalist interest, having used in traditional Chinese medicine or food for more than 2000 years. However, its use in traditional medicine is not restricted to China, as it has also been used in

Antonella Delicato and Marco Masi equally contributed to this work.

North African Sahara (Bougandoura et al., 2016; Lakhdari et al., 2016; Volpato, Saleh, & Di Nardo, 2015). The used product is known as "Herba cistanche" and is traded as dried stems of a mix of Cistanche species that are either wild-harvested or cultivated by growing the host shrubs (Thorogood et al., 2021). *C. deserticola* and *C. tubulosa* are "cultivated" in China with a harvest of about 6000 tons (Song, Zeng, Jiang, & Tu, 2021). There is prospect for extending *Cistanche* cultivation, as in addition to the demand of Herba cistanche, there is a demand for plantation of drought-tolerant shrubs to serve as stabilizing "shelter forests" as a possible solution to the global desertification. Suitable shrubs for this purpose, such as saxaul and tamarisk happen to be ideal hosts of *Cistanche*, offering opportunities to expand *Cistanche* co-cultivation (Salehi, Esmailzadeh, Kheyli, Malekshah, & Zaroudi, 2019) and relieving pressure on wild populations due to unsustainable harvesting. Predictions have been made on the potential adaptation of several *Cistanche* species to new target regions based on climate (Wang, Zhang, Du, Pei, & Huang, 2019). In this line, prospects for the cultivation of *C. phelypaea* are currently being explored in dry areas of South-Eastern Spain.

Composition and nutraceutical and pharmacological applications of *C. deserticola* and *C. tubulosa* are rather well studied, as they are widely used in China (Wang, Zhang, Du, Pei, & Huang, 2019), but this is less the case for *C. phelypaea*, a food resource for Saharan populations, having a more Mediterranean distribution (Gast, 2000). Acetoside was reported to be the main bioactive constituent in genus *Cistanche*; it possesses excellent biological activities including antioxidant (Li et al., 2018), antiinflammatory (Qiao, Tang, Wu, Tang, & Liu, 2019), neuro-protective (Gu, Yang, & Huang, 2016), and anti-osteoporotic activity (Yang et al., 2019).

The first chemical investigation on *C. phelypaea* was carried out in 1993. Acetoside, 2′-acetylacetoside, pheliposide, and tuboliside were isolated from its ethyl acetate extract as the main components (Melek, El-Shabrawy, El-Gindy, & Miyase, 1993). Subsequently, a new iridoid, named phelypaeside, was isolated from the dried aerial parts of the same plant grown in Qatar (Deyama, Yahikozawa, Al-Easa, & Rizk, 1995). Additional chemical investigations on *C. phelypaea* compounds and other species above mentioned were performed (Trampetti et al., 2019). Recently, in *C. phelypaea* water extract, antioxidant activity, in vitro inhibitory activity against acetyl- (AchE) and butyrylcholinesterase (BuChE) for Alzheimer's disease treatment, α-glucosidase, α-amylase for diabetes, and tyrosinase for skin hyperpigmentation disorders were reported (Trampetti et al., 2019).

The traditional uses of *Cistanche* species now cover a wide range of applications such as healthy food additives in Japan and Southeast Asia (Morikawa et al., 2019), for the treatment of kidney deficiency and erectile dysfunction (Li, Jiang, & Liu, 2017) or female infertility and constipation in elderly people (Zhang, Wang, Zhang, Chen, & Liang, 2005).

Here, we report the isolation and identification of some phenylethanoid and iridoid glycosides, obtained from the hydroalcoholic extract of *C. phelypaea* collected in Spain. The present study aims to expand the knowledge on acetoside, the most abundant phenylethanoid glycoside in *C. phelypaea* extract, focusing on human keratinocyte and pluripotent stem cells in the light of its application in cosmeceutical, nutraceutical, and pharmaceutical industries. Our study demonstrated that acetoside besides its strong antioxidant potential can preserve the stemness of human keratinocyte and mesenchymal progenitors necessary for tissue morphogenesis and renewal.

2 | MATERIALS AND METHODS

2.1 | General experimental procedures

Optical rotations were measured on a Jasco (Tokyo, Japan) P-1010 digital polarimeter; ^{1}H and ^{13}C nuclear magnetic resonance (NMR) spectra were recorded at 400/500 and 100/125 MHz on Bruker (Karlsruhe, Germany) or Varian (Palo Alto, CA, USA) spectrometers, respectively. Electrospray ionization (ESI) mass spectra and liquid chromatography (LC/MS) analyses were performed using the LC/MS TOF system AGILENT 6230B, HPLC 1260 Infinity. The HPLC separations were performed with a Phenomenex LUNA (C18 5u 150 × 4.6 mm). Analytical and preparative Thin-Layer Chromatography (TLC) was performed on silica gel plates (Kieselgel 60, F_{254}, 0.25 and 0.5 mm, respectively) or on reverse phase (Whatman, KC18, F_{254}, 0.20 mm) (Merck, Darmstadt, Germany) plates and the compounds were visualized by exposure to UV light and/or iodine vapors and/or by spraying first with 10% H_2SO_4 in MeOH, and then with 5% phosphomolybdic acid in EtOH, followed by heating at 110°C for 10 min. CC: silica gel (Merck, Kieselgel 60, 0.063–0.200 mm) and C_{18}-reverse-phase silica gel. D-glucose and D-xylose standards were supplied from Sigma-Aldrich (Milan, Italy). The purity of the isolated compounds was >98% as ascertained by ^{1}H NMR and HPLC analyses.

2.2 | Plant material

The *C. phelypaea* is common in the Iberian Peninsula (Pujadas-Salvá & López-Saéz, 2002), being particularly common in Murcia province (López-Espinosa, 2022). The specimens included in this study were collected at farmstate Finca Torrecillas, Corvera, Murcia, Spain in March 2020, identified by Dr J.A. López-Espinos (pers. comm.) and then sliced and dried in a shadow open room for 15 days. The plant voucher is deposited in the same farmstate.

2.3 | Extraction and purification of metabolites

400 g of dried *C. phelypaea* bulbs was milled with a blender and extracted with a Soxhlet apparatus using EtOH (1 × 500 ml, 12 h) obtaining 9.3 g of organic extract as an oily residue. This residue was dissolved in distilled H_2O (200 ml) and extracted with EtOAc (3 × 200 ml) obtaining 4.4 g of organic extract that was further fractionated by column chromatography on silica gel eluted with $CHCl_3$/*iso*PrOH (9:1, v/v) yielding 11 homogeneous fractions (F1-F11). The residue (695.7 mg) of F5 was further purified by CC on silica gel,

eluting with EtOAc/MeOH/H_2O (85:10:5, v/v/v), yielding nine homogeneous fractions (F5.1-F5.9). The residue of F5.3 (62.9 mg) was further purified by preparative TLC eluting with EtOAc/MeOH/H_2O (85:10:5, v/v/v) affording 2′-*O*-acetylacetoside (**2**, 20.9 mg) as an amorphous solid. The residue (172.1 mg) of F5.4 was purified by CC on reverse phase eluted with MeCN/H_2O (3.5:6.5, v/v) affording acetoside (**1**, 30.1 mg) and tubuloside B (**3**, 5.5 mg). The residue (18.3 mg) of F5.8 was further purified by TLC on reverse phase eluting with MeCN/ H_2O (3.5:6.5, v/v) yielding bartioside (**4**, 14.9 mg). The residue (336.5 mg) of F7 was purified by CC on reverse phase eluting with MeCN/ H_2O (3.5:6.5, v/v) affording five fractions (F7.1-F7.5) yielding 6-deoxycatalpol (**5**, 7.48 mg) and gluroside (**6**, 1.50 mg). The purification process has been repeated five times to accumulate the pure compounds for chemical and biological characterization.

Acetoside (**1**): amorphous solid, $[\alpha]^{25}_{D}$-67.4 (*c* 1.0, MeOH) (ref. Aligiannis et al., 2003 $[\alpha]^{25}_{D}$-69.6 (*c* 1.0, MeOH)); ^{1}H and ^{13}C NMR data are in agreement with those previously reported by Kobayashi et al., 1987 and Kim, Kim, Jung, Ham, & Whang, 2009; ESI MS (+): *m/z* 647 $[M + Na]^+$.

2′-O- Acetylacetoside (**2**) amorphous solid, $[\alpha]^{25}_{D}$-63.4 (*c* 0.3, MeOH) (ref. Li, Ishibashi, Satake, Oshima, & Ohizumi, 2003 $[\alpha]^{25}_{D}$-65.2 (*c* 0.1, MeOH)); ^{1}H and ^{13}C NMR data are in agreement with those previously reported by Kobayashi et al., 1987; Han et al., 2012; ESI MS (+): *m/z* 667 $[M + H]^+$.

Tubuloside (**3**) amorphous solid, $[\alpha]^{25}_{D}$-37.4 (*c* 0.5, MeOH) (ref. Kobayashi et al., 1987 $[\alpha]^{25}_{D}$-39.0 (*c* 1.0, MeOH)); ^{1}H and ^{13}C NMR data are in agreement with those previously reported by Kobayashi et al., 1987; ESI MS (+): *m/z* 667 $[M + H]^+$.

Bartioside (**4**) amorphous solid, $[\alpha]^{25}_{D}$-86.4 (*c* 0.5, MeOH) (ref. Venditti, Serrilli, & Bianco, 2013 $[\alpha]^{25}_{D}$-89.0 (*c* 0.3, MeOH)); ^{1}H and ^{13}C NMR data are in agreement with those previously reported by Kobayashi et al., 1987; Venditti, Serrilli, & Bianco, 2013; ESI MS (+): *m/z* 353 $[M + Na]^+$, 330 $[M + H]^+$.

6-Deoxycatalpol (**5**) amorphous solid, $[\alpha]^{25}_{D}$-50.0 (*c* 0.3, MeOH) (ref. Yoshizawa, Deyama, Takizawa, Usmanghani, & Ahmad, 1990 $[\alpha]^{25}_{D}$-50.1 (*c* 0.7, MeOH)); ^{1}H and ^{13}C NMR data are in agreement with those previously reported by Arslanian, Harris, & Stermitz, 1985; Kobayashi, Karasawa, Miyase, & Fukushima, 1985); ESI MS (+): *m/z* 347 $[M + H]^+$.

Gluroside (**6**) amorphous solid, $[\alpha]^{25}_{D}$-150.0 (*c* 0.1, MeOH) (ref. Sticher & Weisflog, 1975 $[\alpha]^{20}_{D}$-178.5 (*c* 0.7, MeOH)); ^{1}H and ^{13}C NMR data are in agreement with those previously reported by Sticher & Weisflog, 1975; Kobayashi, Karasawa, Miyase, & Fukushima, 1985); ESI MS (+): *m/z* 333 $[M + H]^+$.

2.4 | Acid Hydrolisis of compounds 1–6

The acid hydrolysis of compounds **1**–**6** was conducted as previously described (Cimmino et al., 2016). Briefly, the glycosides (5.0 mg) were separately dissolved in 0.1 M HCl solution and stirred at 80°C for 3 h. The reaction mixture was concentrated under a vacuum obtaining amorphous solids as residues. The sugar and aglycones yield is 50%. Pure sugars were identified by co-TLC eluting with *iso*PrOH/H_2O (8.2 v/v) with standards and recording their specific optical rotation.

2.5 | Cell culture and reagents

HaCaT, spontaneously immortalized keratinocytes from adult skin, were purchased from Service Cell Line (GmBH, Eppelheim, CLS, Germany) and cultured as described (Amoresano et al., 2010; Vivo et al., 2017). A431 (ATCC-CRL1555) human epidermoid carcinoma cells were from American Type Culture Collection (ATCC, Manassas, VA, USA). According to the p53 compendium database (http://p53.fr), HaCaT cells contain mutant p53 (H179Y/R282W), while A431 cells contain only one p53 mutated allele (R273H). All mentioned cell lines (10–14 passages) were cultured in Dulbecco's Modified Eagle's Medium (DMEM, Sigma Chemical Co, St. Louis, MO, USA) supplemented with 10% fetal bovine serum (FBS, Hyclone Laboratories, Inc. Logan, UT, USA) at 37°C in a humified atmosphere of 5% CO_2.

hTERT-immortalized adipose-derived mesenchymal stem cells (hMSCs) were purchased from American Type Culture Collection (ATCC SCRC-4000; Virginia, USA). Cells (3–4 passages) were cultured in DMEM high glucose supplemented with 10% South American Fetal Bovine Serum (FBS), 2 mM glutamine, 100 units/ml Penicillin/ Streptomycin (Gibco), and maintained in a humidified atmosphere of 5% CO_2 at 37°C. Media, sera, and antibiotics for cell culture were from Thermo Fisher Scientific (Waltham, MA, USA). All cell lines were routinely tested for mycoplasma contamination and were not infected.

2.6 | Differentiation protocol

For HaCaT differentiation, cells were seeded in an RMPI medium. The day after seeding, the medium wad changed in RMPI without FBS, and cells were treated with Ca^{2+} at 2 mM until the cells reach confluence.

For osteogenic differentiation, the previously stored cells were plated at 8×10^3 cells/cm^2 on 0.2 μg/cm^2 human collagen I coating (Corning) in a growth medium for 3 days at 37°C, 5% CO_2 in a humidified incubator, changing the medium after 2 days, before replacing the growth medium with osteogenic media (StemPro Osteogenesis Differentiation Kits_ThermoFisher Scientific) and maintaining for up to 18 days, with media changes every 2–3 days.

2.7 | Western blot analysis

Western blot was performed as previously reported (di Martino et al., 2016; Vivo et al., 2017). Briefly, 20 μg of whole-cell extracts were separated by sodium dodecyl sulfate-polyacrylamide gel electrophoresis (SDS-PAGE), subjected to western blot, and incubated overnight at 4°C with antibodies. Antibodies against p21WAF, Cytokeratin (VIK-10), Cytokeratin (K1207), and β-actin were from Cell

Signaling Technologies (Boston, MA, USA), and ΔNp63α from Abcam (Cambridge, UK). Each experiment was run in triplicate. Signal intensities of western blot bands were quantified by Quantity One analysis software (Version Number 2, Biorad Laboratories, London, UK) and analyzed by GraphPad Prism 8.0.2 software (GraphPad, San Diego, CA).

2.8 | DCFDA assay

Antioxidant activity of 1–6 metabolites was measured using 2′−7′ dichlorofluorescein diacetate (DCFDA), a non-fluorescent compound permeable to the cell membrane, which can be oxidized by reactive oxygen species (ROS) giving a fluorescent compound as previously described (Xiao, Powolny, & Singh, 2008). In brief, 3×10^5 cells were treated with 50 or 100 μM of purified metabolites as indicated. The medium was removed after 4 h and 1 mM (3%) H_2O_2 was added for 45 min, 1.5, and 2.0 h. Cells were washed with PBS and a fresh medium with DCFDA (30 mM) was added for 45 min, then DCFDA was removed by washing in PBS 1× and the cells were harvested. The measurement of ROS was obtained using the Sinergy H4 microplate reader Gen5 2.07 (Thermofisher, Waltham MA, USA). The fluorescence emitted from the cells treated with DCFDA was compared to the untreated cells. Trolox was used as a positive control. Values shown in the plot are mean ± SD of sixfold determinations. The mean and the standard deviation were calculated on biological triplicates using GraphPad Prism 8.0.2 software (GraphPad, San Diego, CA).

2.9 | Cell viability assay

Cell viability was evaluated by measuring the reduction of 3-(4,5-dimethylthiazol-2) 2,5- diphenyltetrazolium bromide (MTT) to formazan by the mitochondrial enzyme succinate dehydrogenase (Van Meerloo, Kaspers, & Cloos, 2011). Briefly, 10×10^3 cells were seeded on 96-well plates and exposed to different concentrations of total extract or metabolites for 48 and 72 h. MTT/PBS solution (0.5 mg/ml) was then added to the wells and incubated for 3 h at 37°C in a humidified atmosphere. The reaction was stopped by removal of the supernatant followed by dissolving the formazan product in acidic isopropanol and the optical density was measured with Sinergy H4 microplate reader Gen5 2.07 (Thermofisher, Waltham MA, USA) using a 570 nm filter. Under these experimental conditions, no undissolved formazan crystals were observed. Cell viability was assessed by comparing the optical density of the treated samples compared to the controls.

2.10 | Trypan blue assay

1 part of 0.4% trypan blue and 1 part of cell suspension were mixed. The mixture was allowed to incubate for ~3 min at room temperature. The mixture was loaded into a Bürker chamber and the dead cells and the total number of cells were counted to evaluate the percentage of viable cells (Warren, 2015).

2.11 | Cell proliferation analysis

A total of 6×10^4 HaCaT and A431 cells were seeded in a 12-well plate; cells were serum-starved for 24 h; after starvation, total extract or acetoside were added at different concentrations. Every 24 h cells were gently rinsed with 1× PBS, trypsinized, and counted. The count was confirmed by Scepter 2.0 analysis (Millipore, Burlington, MI, USA) as previously described (Fontana, 2018).

2.12 | RNA extraction, cDNA preparation, and qRT-PCR

Total RNA was extracted using TRIzol reagent (Invitrogen) and cDNA was synthesized using iScript cDNA Synthesis kit according to the manufacturer's instructions (Bio-Rad, Hercules, CA, USA). 1 μg of total RNA was used for each cDNA synthesis. Primer 3 software (http://primer3.ut.ee/) was used to design the oligo primers setting the annealing temperature to 59–61°C for all primer pairs. Oligo sequences are reported in Table. For gene expression analyses, 25 ng of cDNA was used for each PCR reaction with each primer pair (forward/reverse primers mix: 0.2 μM, in a final volume of 25 μl). Real time-qPCR analysis was performed using the iTaq™ Universal SYBR® Green Supermix (Bio-Rad, Hercules, CA, USA) in a 7500 Real-Time PCR System (Applied Biosystems, Foster City, CA, USA) under the following conditions: 2 min at 50°C, 10 min at 95°C, followed by 40 cycles of 15 s at 95°C, and 1 min at 60°C. The GAPDH probe served as a control to normalize the data. The gene expression experiments were performed in triplicate on three independent experiments and a melting analysis was performed at the end of the PCR run. To calculate the relative expression level, we used the 2−DDCT method.

Gene name	Forward primer 5′–3′	Reverse primer 5′–3′
ENG	AGCCCCACAAGTCTTGCAG	GCTAGTGGTATATGTCACCTCGC
COL1A1	CCCCTGGAAAGAATGGAGATG	TCCAAACCACTGAAACCTCTG
OCN	GGCGCTACCTGTATCAATGG	TCAGCCAACTCGTCACAGTC
ALPL	ACGTACAACACCAATGCCC	GGTCACAATGCCCACAGATT
RUNX2	CTGTGGTTACTGTCATGGCG	AGGTAGCTACTTGGGGAGGA
GAPDH	GGTATCGTGGAAGGACTCATGAC	ATGCCAGTGAGCTTCCCGTTCAG

PCR primers.

2.13 | Statistical analysis

Statistical analyses were carried out using the GraphPad Prism version 8.1.2 (https://www.graphpad.com/scientific-software/prism/). Data were represented as the mean standard deviation and analyzed for

statistical significance using ordinary one-way analysis of variance (ANOVA) and multiple comparisons. For all tests, $p < 0.05$ was considered to indicate a statistically significant difference.

3 | RESULTS

3.1 | In vitro cytotoxicity test of *C. phelypaea* EtOAc extract and isolation of metabolites

The whole EtOAc extract obtained from the *C. phelypaea* aerial parts was preliminarily tested for cytotoxicity on human Hacat keratinocytes by the MTT viability test. The MTT viability test measures the mitochondrial succinate dehydrogenase activity and its ability to convert MTT into blue/purplish formazan salts. The EtOAc extract was tested at concentrations between 0.001 and 1 mg/ml for 48 and 72 h. At concentrations up to 0.01 mg/ml and 48 h of treatment, the extract positively impacted cell viability (Figure 1a, left panel). However, the proliferation rate of cells was not significantly affected by the treatments thus indicating that the observed increase in cell viability *was likely due* to an improvement of cellular metabolism (Figure 1b). At higher concentrations, the cytotoxic effect became predominant (Figure 1a).

The low in vitro cytotoxicity of *C. phelypaea* extract prompted us to proceed with the isolation of pure metabolites. The EtOAc extract of *C. phelypaea* was chromatographed as detailed in the Experimental Section to afford six homogeneous compounds. By comparing their spectroscopic data (essentially ^{1}H and ^{13}C NMR) with those reported in the literature (Kim, Kim, Jung, Ham, & Whang, 2009; Kobayashi et al., 1987) they were identified as the phenylethanoid glycosides acetoside, 2′-*O*-acetylacetoside (Han et al., 2012; Kobayashi et al., 1987), and tubuloside B (Kobayashi et al., 1987) (**1**–**3**, Figure 2) and the iridoid glycosides bartsioside (Kobayashi, Karasawa, Miyase, & Fukushima, 1985; Venditti, Serrilli, & Bianco, 2013), 6-deoxycatalpol (Arslanian, Harris, & Stermitz, 1985; Kobayashi, Karasawa, Miyase, & Fukushima, 1985), and gluroside (Kobayashi, Karasawa, Miyase, & Fukushima, 1985; Sticher & Weisflog, 1975) (**4**–**6**, Figure 2). Their identification was confirmed by the ESIMS spectra and comparing their specific optical rotation data with those reported in the literature. Furthermore, the acid hydrolysis of compounds **1**–**3** afforded D-glucose and D-xylose while that of compounds **4**–**6** only D-glucose by co-TLC with standard sugars samples and recording the specific optical rotation. Compounds **1**–**3** belong to the phenylethanoid glycosides (PhGs) class of natural substances (Tian et al., 2021), while compounds **4**–**6** belong to the iridoid class (Wang et al., 2020) both known to possess significant bioactivities including antiviral, hepatoprotective, antibacterial, neuroprotective, antitumor, antiinflammatory, and antioxidant among others (Dewick, 2009; Tian et al., 2021; Wang et al., 2020). Their co-existence in *Cistanche* as well as in many other plants is well-known despite their different structures and biosynthetic pathways.

3.2 | Acetoside is the main antioxidant compound in *C. phelypaea*

We evaluated the in vitro antioxidant activities of glycosides and iridoids (**1**–**5**) isolated from *C. phelypaea* in human immortalized HaCaT keratinocytes using a 2′ − 7′ dichlorofluorescein diacetate (DCFDA) assay. HaCaT keratinocytes represent an immortalized cell type that proliferates indefinitely and being untransformed it is still able to differentiate in culture under appropriate stimuli.

Briefly, we compared Reactive Oxygen Species (ROS) induced by 1 mM H_2O_2 (1 mM, 3%) in cells pretreated for 4 h with 50 and 100 μM with the following metabolites: acetoside also known as verbascoside (**1**), 2′-*O*-acetylacetoside (**2**), tubuloside B (**3**), bartioside (**4**), 6-deoxycatalpol (**5**) and gluroside (**6**). A permeable vitamin E analog, TROLOX, was used as a positive control. The negative control was

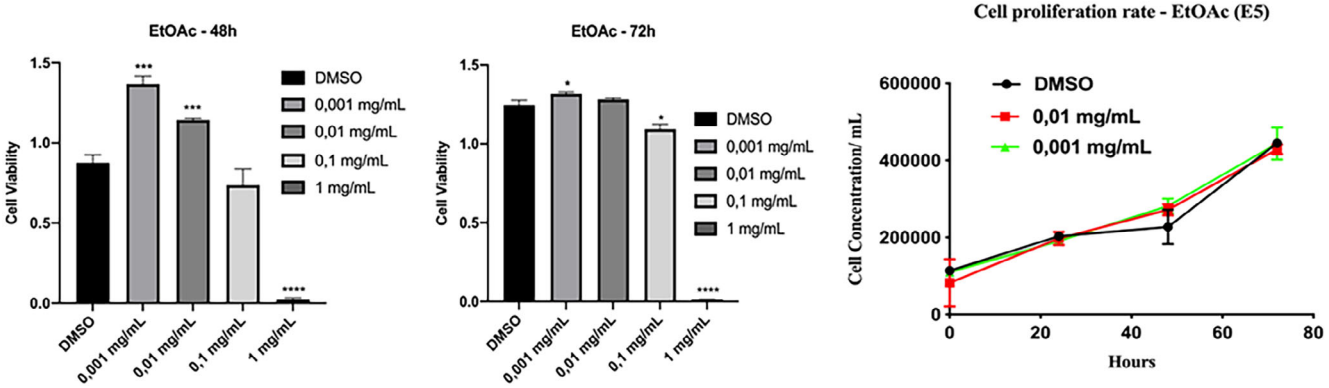

FIGURE 1 (a) MTT viability test. HaCaT cells were incubated with the indicated amount of EtOAc organic extract for 48 and 72 h. The values were the mean's six values for each experimental point of two independent biological replicates. Each mean was compared using a Dunnett's multiple comparisons test of ANOVA one-way (*p*-value *< 0.01, ** < 0.05, ***$p < 0.001$; ****$p < 0.0001$). (b) Cell proliferation rate. HaCaT cells were plated and treated with EtOAc extract at the indicated concentrations. Following the treatment, they were counted with the Scepter cell counter, at times 0 and 24, 48, and 72 h, creating the proliferation curve. There is no significant change in the proliferation rate of the treated cells, compared to the DMSO control

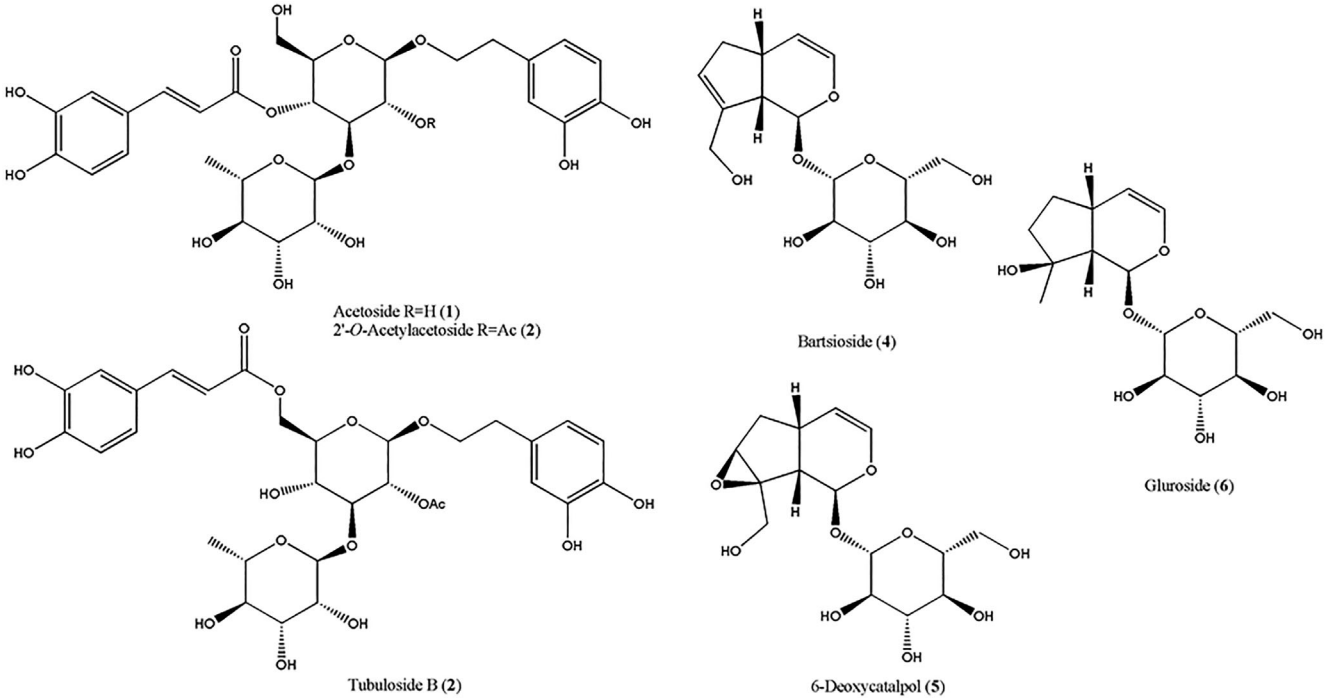

FIGURE 2 Structures of the phenylethanoid glycosides acetoside, 2′-*O*-acetylacetoside, and tubuloside B (**1**-**3**), and of the iridoid glycosides bartsioside, 6-deoxycatalpol, and gluroside (**4**-**6**), isolated from the EtOAc extract of *C. phelypaea*

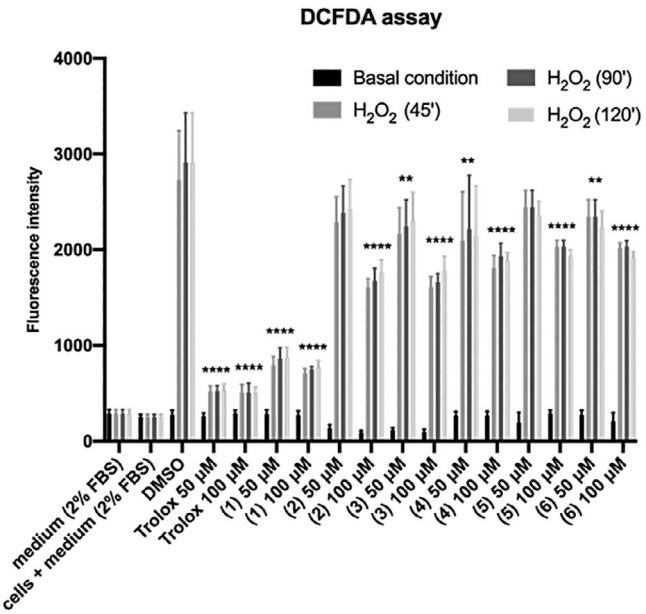

FIGURE 3 DCFDA assay. HaCaT cells were seeded and pre-treated for 4 h with 50 and 100 µM 1-6 metabolites from *C. phelypaea*. H2O2 (1 mM; 3%) was added to the medium for 45′, 1.5, and 2h. The fluorescence intensity of DCFDA was read after 45′ of incubation. Trolox was used as a positive control and DMSO, in which the metabolites are dissolved, as a negative control. The values are the mean's six values for each experimental point of two independent biological replicates. Statistical analysis was performed with two-way ANOVA, using Tukey's multiple comparison test. Levels of significance between points of expression are indicated (****$p < 0.001$, ***$p < 0.01$, **$p < 0.05$)

treated with the vehicle (DMSO 0.1%) used for diluting all compounds.

As shown in Figure 3, acetoside at a concentration of 50 and 100 µM dramatically reduced the level of ROS induced by H_2O_2 treatment. Pretreatment with 50 µM acetoside resulted in a 65% reduction of DCFDA fluorescence after 45′ of treatment with H_2O_2. No further effects were observed by extending the treatment beyond 45′ (Figure 3). This result was comparable to that obtained with an equal concentration of Trolox, the water-soluble derivative of vitamin E used as a positive control (Figure 3) thus indicating that acetoside has a strong radical scavenging activity. A reduction of intracellular ROS was also observed with all the other metabolites tested but it was moderate when compared to acetoside.

3.3 | Effect of *C. phelypaea* metabolites on cell proliferation and viability

The MTT assay is a widely used approach to measure the viability and proliferation of cells. However, the caffeoyl group of acetoside was shown to cause conflicting results in the MTT assay due to mitochondrial uncoupling effects (Wang, Zhou, Xu, & Gao, 2015). Therefore, we evaluated acetoside cytotoxicity on Hacat keratinocytes and human A431 squamous carcinoma cells by the Trypan blue exclusion assay. The obtained results revealed that at the concentrations tested acetoside was not toxic for human keratinocytes while causing minimal cell death in tumor cells (between 12 and 20%) at the concentration of 100 µM (Table 1).

TABLE 1 Percentage of viable cells. HaCaT and A431 cells were seeded and treated with acetoside (**1**) 10, 50, 100 μM. Dead cells were counted with Trypan Blue after 24, 48, 72 h from treatments, and the percentage of live cells was measured out of the total number of cells. Numbers are the average of triplicate data

A431 Time of incubation	% viability	100		10
24 h	96	95	93	90
48 h	94	80	97	97
72 h	96	88	95	98
Hacat Time of incubation	**% viability**	**100**	**50**	**10**
24 h	96	86	98	94
48 h	97	97	97	94
72 h	95	93	98	90

Moreover, we compared the cell proliferation rate of Hacat and A431 cells in acetoside containing medium and we consistently found a time and dose-dependent reduction in the rate of cell proliferation both in immortalized and transformed keratinocytes. Interestingly, carcinoma-derived cells were more sensitive than Hacat to the cell growth inhibitory effect of acetoside (Figure 4).

We also carried out the MTT assay on Hacat and A431 cells after treatment with increasing doses of iridoids glucosides **4**, **5,** and **6** from 10 to 100 μM to evaluate their cytotoxicity. Data shown in Figure 5 indicate that Hacat keratinocytes are slightly sensitive to the toxicity effects of bartioside (**4**), 6-deoxycatalpol (**5**), and gluroside (**6**) while cell viability of A431 cancer cells was significantly reduced (less than 60%) after 48 of incubation with 100 μM of **4**, **5,** and **6** (Figure 5, right panel). The observed reduction of cell viability was more pronounced at 48 of treatment thus revealing time-dependent toxicity of iridoids (Figure 5, compare left and right panel).

3.4 | Acetoside inhibits differentiation of human keratinocyte and pluripotent cells

The obtained results indicate that among the main compounds isolated from C. *phelypaea*, acetoside is the least toxic and the most effective against ROS production. Therefore, we explored the effect of acetoside on cell differentiation. Terminal differentiation of Hacat immortalized keratinocytes is coupled to cell cycle withdrawal, and this process has been associated with a transient up-regulation of the cell cycle inhibitor p21WAF. Upon Ca^{2+} stimulation, Hacat cells differentiate and express CK1 and CK10, the prominent suprabasal skin differentiation markers. To test the differentiation potential of HaCaT cells in presence of acetoside, we evaluated the expression of CK1 and CK10 as well as the expression of ΔNp63α, a well-known epithelial stem cell marker. As shown in Figure 6, the addition of Ca^{2+} caused a reduction of ΔNp63α and a concomitant increase of p21WAF, CK1, and CK10. In acetoside-treated keratinocytes, instead, we observed sustained p21WAF induction without an increase of CK1 and CK10 expression. Notably, the level of ΔNp63α remained unaffected (Figure 6) These observations suggest that acetoside can preserve keratinocyte stemness necessary for epithelial morphogenesis and renewal.

Data obtained on keratinocytes prompted us to investigate the activity of acetoside on pluripotent stem cells. Human mesenchymal stem cells (hMSC) can differentiate in osteoblasts using an in vitro differentiation protocol which is intended to recapitulate the osteogenic development in vivo. The hMSCs were induced to the osteogenic differentiation by replacing the basal medium with an osteogenic medium supplemented or not with acetoside at a concentration of 100 μM for 16 days. Activation of the transcription of genes (such as COL1A1, RUNX2, OCN, and ALPL) participating in osteogenic induction at different terms of differentiation was evaluated by real-time PCR. As expected, in untreated samples the expression of COL1A1, RUNX2, OCN, and ALPL was significantly increased starting from day 7 whereas inhibition of their expression was observed in acetoside treated samples. These results suggest that acetoside can regulate the stemness of mesenchymal progenitors by maintaining their undifferentiated state (Figure 7).

Finally, we performed a DCFDA assay to evaluate the antioxidant potential of acetoside in human mesenchymal stem cells (hMSC) with that of (+)-catechin and (−)-*epi*-catechin, two well-known antioxidant flavonoids. hMSC cells were seeded and pretreated for 4 h with 10 and 100 μM of catechin, (−)-*epi*-catechin, and acetoside from *C. phelypaea*. H_2O_2 (1 mM; 3%) was added to the medium for 45′, 1.5, and 2 h. As shown in Figure 8, acetoside has a strong antioxidant effect comparable to catechin at the same concentration.

4 | DISCUSSION

Like Herba *Cistanche*, *C. phelypaea* is rich in metabolites with antioxidant activity demonstrating the potential to be used as functional *ingredients* for foods and nutraceuticals. Our fractionation procedure allowed us to isolate the phenylethanoid glycosides acetoside, 2′-*O*-acetylacetoside, and tubuloside B, and the iridoid glycosides bartsioside, 6-deoxycatalpol, and gluroside. Acetoside and 2′-*O*-acetylacetoside were the most abundant glycosides we isolated from *C. phelypaea*. The structures of phenylethanoid glycosides were all rich in phenolic hydroxyl groups, which are responsible for the antioxidant activity of *Cistanche* (Zhang et al., 2016).

In human keratinocytes, acetoside had a strong radical scavenging activity that was quite comparable to that of the Trolox, the water-soluble derivative of vitamin E currently used as a control antioxidant standard. Surprisingly, in human mesenchymal progenitor cells, acetoside was still able to efficiently counteract ROS production while Trolox was ineffective.

Skin keratinocytes have a high rate of turnover. The basal proliferative compartment of stratified squamous epithelia consists of the stem and transient amplifying (TA) keratinocytes. Differentiation commitment promotes the withdrawal of keratinocytes from the quiescent stem cell compartment and their transit toward the surface of the tissue. TA keratinocytes transiently acquire appreciable proliferative capacity and

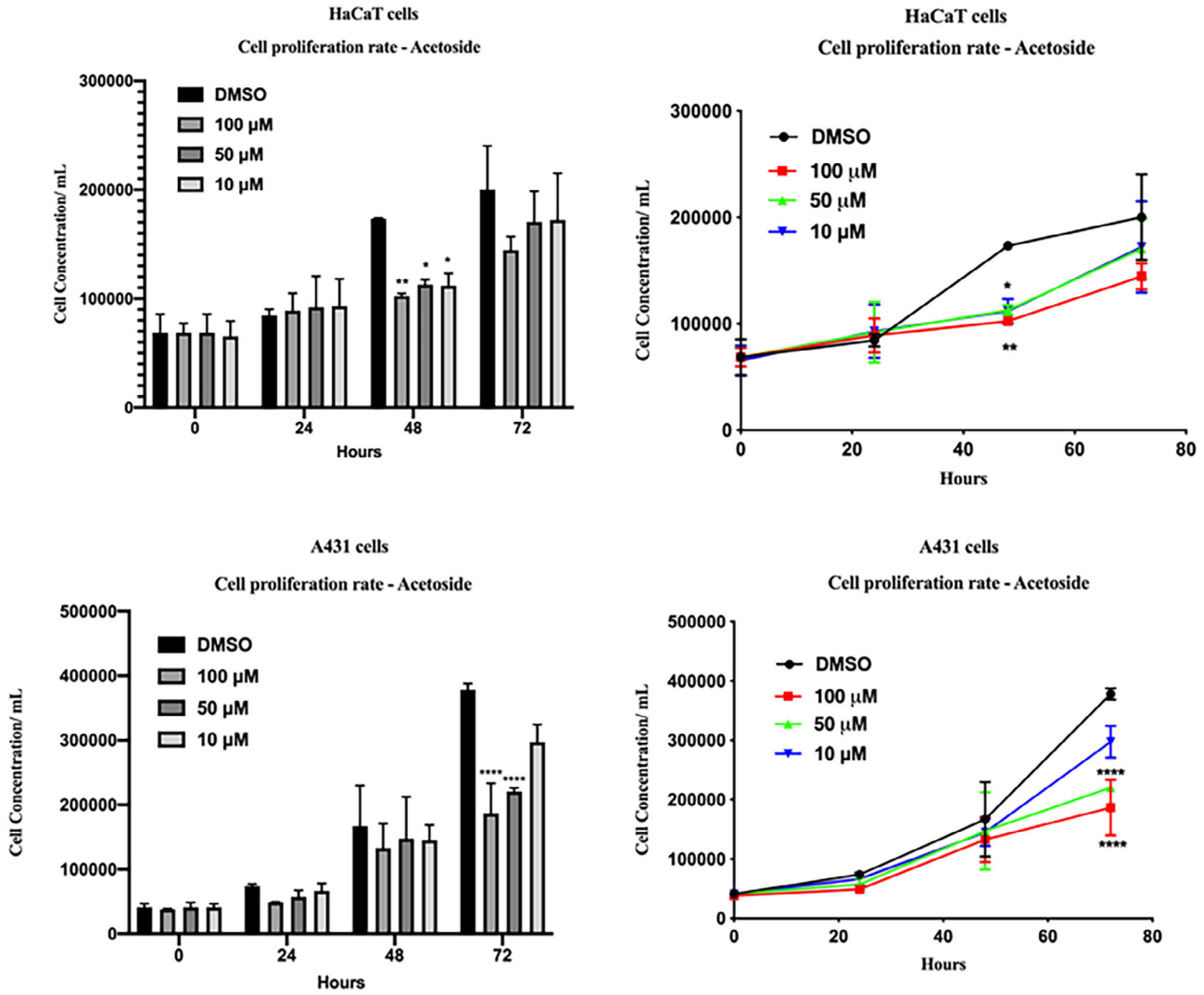

FIGURE 4 Cell proliferation rate. Hacat and A431 cells were seeded and treated with acetoside (1) 10, 50, 100 µM. Cells were counted with Scepter at T0, 24, 48, 72 h of treatments. Results are the mean ± SEM of three independent biological experiments relative to the experimental control (DMSO). Statistical analysis was performed with one-way ANOVA, using Dunnett's multiple comparison test. Levels of significance between points of expression are indicated (****$p < 0.001$, **$p < 0.01$)

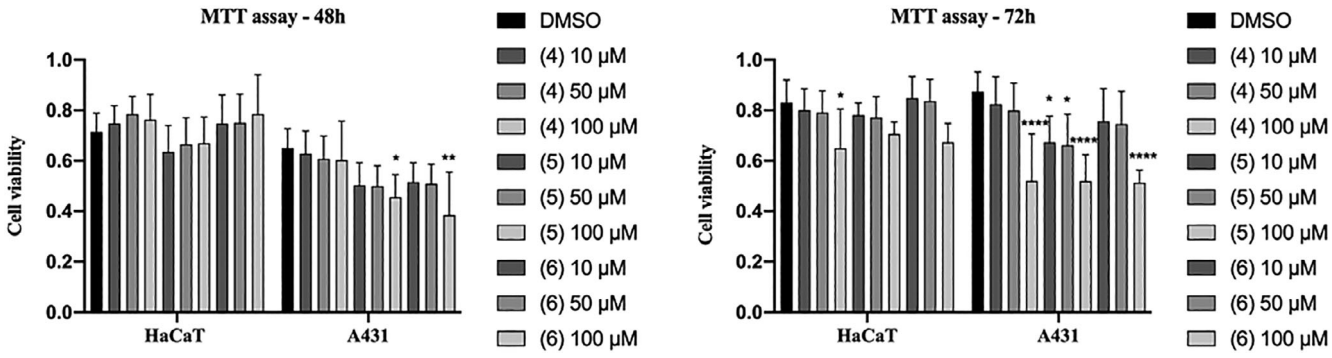

FIGURE 5 MTT viability test. Hacat and A431 cells were incubated with the indicated amounts of metabolites 4, 5, 6, for 24 and 48 h. The values were the mean's six values for each experimental point of two independent biological replicates. Each mean was compared using a Dunnett's multiple comparisons test of ANOVA one-way (p-value *< 0.01, ** < 0.05, ***$p < 0.001$; ****$p < 0.0001$)

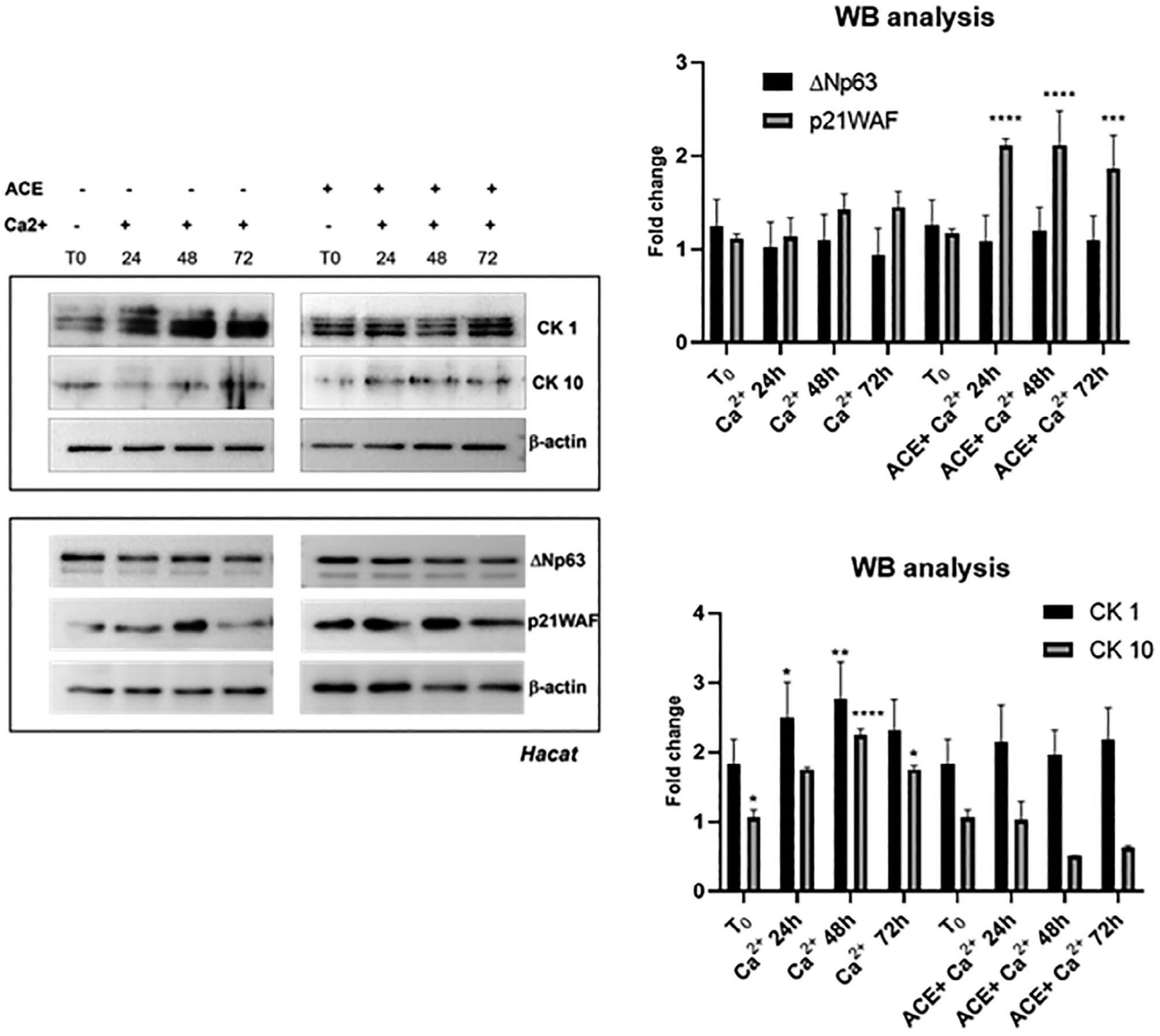

FIGURE 6 Representative western blot analysis of a total extract from Hacat keratinocytes in response to Ca^{2+} addition in the presence or absence of acetoside. Hacat cells were differentiated with 2 mM Ca^{2+} and compared with cells treated with Ca^{2+} plus 50 μM acetoside (ACE) for 48 and 72 h. (a) Immunoblot was probed with ΔNp63α, p21WAF, CK1 and CK10 antibodies. β-Actin was used as a loading control. (b) The signals of protein bands were quantified by ImageLab software version 4.1 (Bio-Rad) Statistical analyses were performed using 2-way ANOVA and Sidak's multiple comparisons or Dunnett's multiple comparisons test. Levels of significance between points of expression are indicated (***$p < 0.001$, **$p < 0.01$, *$p < 0.05$)

exhibit greatly reduced ΔNp63α. Our data indicate that the co-treatment of human keratinocytes with Ca^{2+}, a trigger of keratinocyte differentiation, and acetoside induced a reversible cell cycle arrest. Indeed, in presence of Ca^{2+} and acetoside the expression of p21WAF was upregulated while ΔNp63α, a pro-proliferative marker, was not reduced thus suggesting that acetoside preserves the regenerative potential of keratinocytes. Moreover, in presence of Ca^{2+} and acetoside, cytokeratins 1 and 10 did not increase thereby indicating that keratinocyte differentiation was inhibited or slowed down. On the other hand, it is worth mentioning that acetoside also suppresses macrophages differentiation in osteoclasts without affecting their viability (Lee, Lee, Yi, Kook, & Lee, 2013).

Finally, we found that acetoside inhibited osteoblastic differentiation of hMSCs. hMSCs serve as a primary instrument of tissue engineering. They are multipotent cells with a cell renewal capacity that can differentiate in vitro into a variety of cell types, adipocytes, chondrocytes, and osteoblasts (Okolicsanyi et al., 2015). In addition, they persist in various tissues and are responsible for maintaining tissue homeostasis and repairing tissue injury by replenishing senescent and damaged cells. In general, stem cells are more sensitive than their progeny to the adverse effects of ROS even though a low level of ROS was shown to be required to maintain quiescence and self-renewal of pluripotent stem cells (Zhou, Shao, & Spitz, 2014).

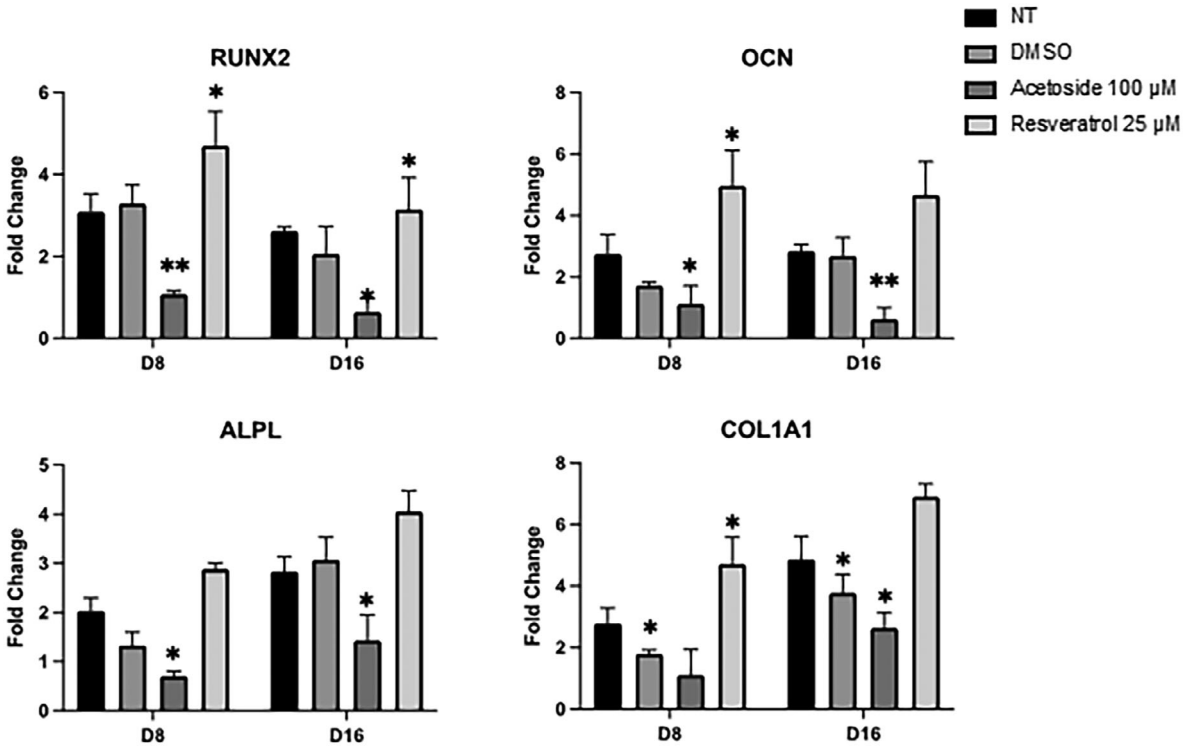

FIGURE 7 RT-qPCR analysis of the osteogenic markers (COL1A1, RUNX2, OCN and ALPL). The mRNA levels were normalized to Gapdh expression and reported as fold change to the value in D0. Resveratrol was used as a positive control of differentiation. The values shown are mean ± SD, based on triplicate assays. Statistical analyses were performed using Student's *t*-test, where $p < 0.05$ was considered significant ($^{*}p < 0.05$, $^{**}p < 0.01$)

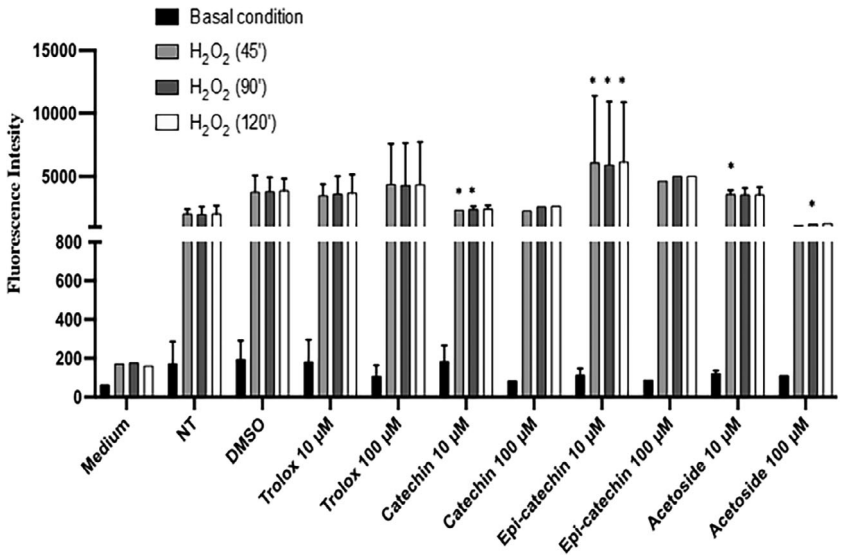

FIGURE 8 DCFDA assay. hMSC cells were seeded and pre-treated for 4 h with 10 and 100 µM of catechin, *epi*-catechin, and acetoside. H 2 O 2 (1 mM; 3%) was added to the medium for 45′, 90′, and 120′. The fluorescence intensity of DCFDA was read after 45′ of incubation. Trolox was used as a positive control and DMSO, in which the metabolites are dissolved, as a negative control. The values are the mean's six values for each experimental point of two independent biological replicates. Statistical analysis was performed with two-way ANOVA, using Tukey's multiple comparison test. Levels of significance between points of expression are indicated ($^{***}p < 0.001$, $^{**}p < 0.01$, $^{*}p < 0.05$)

Excess ROS, instead, can inhibit stem cell self-renewal not only by promoting stem cell differentiation but also via induction of senescence and/or apoptosis. Our data indicate that while controlling ROS production, acetoside preserves the undifferentiated status of mesenchymal stem cells, osteoblasts and osteoclasts precursors. Remarkably, in recent work, total glycosides, and polysaccharides from *C. deserticola* were found to mediate bone formation by upregulating BMP-2 (Bone Morphogenetic Factor 2) and OPG (Osteoprotegerin) and downregulating RANKL thus promoting the reconstruction of osteoporotic bone (Wang, Tu, Zeng, & Jiang, 2021). Therefore, *Cistanche* extract likely contains metabolites regulating the balance between multipotential mesenchymal stem cells, bone-forming osteoblasts, and bone-resorbing osteoclasts. Therefore, total glycosides and polysaccharides from *Cistanche* are

promising bone-protective therapeutic agents. Further studies will help to clarify the precise activity of each metabolite.

In conclusion, besides its strong antioxidant potential, acetoside appears to preserve the proliferative potential of human basal keratinocyte and mesenchymal progenitors which is necessary for tissue morphogenesis and renewal. The use of stem cells in tissue engineering demands their controlled differentiation; hMSCs have great therapeutic potential, however, their usefulness is limited by cellular senescence occurring secondary to increased levels of reactive oxygen species during their propagation in culture (Ogrodnik et al., 2017). To this respect, acetoside can be of practical relevance for the clinical application of human stem cell cultures for regenerative medicine.

ACKNOWLEDGMENTS

A. Evidente is associated to the Istituto di Chimica Biomolecolare del CNR, Italy. Open Access Funding provided by Universita degli Studi di Napoli Federico II within the CRUI-CARE Agreement.

CONFLICT OF INTEREST

The authors declare no conflict of interest.

DATA AVAILABILITY STATEMENT

The data supporting this study's findings are available from the corresponding author upon; reasonable request.

ORCID

Antonella Delicato https://orcid.org/0000-0002-8268-2038
Viola Calabrò https://orcid.org/0000-0002-6508-8889

REFERENCES

Aligiannis, N., Mitaku, S., Tsitsa-Tsardis, E., Harvala, C., Tsaknis, I., Lalas, S., & Haroutounian, S. (2003). Methanolic extract of *Verbascum macrurum* as a source of natural preservatives against oxidative rancidity. *Journal of Agricultural and Food Chemistry*, *51*, 7308–7312.

Amoresano, A., Di Costanzo, A., Leo, G., Di Cunto, F., La Mantia, G., Guerrini, L., & Calabro, V. (2010). Identification of ΔNp63α protein interactions by mass spectrometry. *Journal of Proteome Research*, *9*, 2042–2048.

Arslanian, R. L., Harris, G. H., & Stermitz, F. R. (1985). Some iridoid glucosides, including the new 6-deoxycatalpol, from Indian paintbrush species related to *Castilleja miniata*. *Journal of Natural Products*, *48*, 957–961.

Bougandoura, A., D'Abrosca, B., Ameddah, S., Scognamiglio, M., Mekkiou, R., Fiorentino, A., … Benayache, F. (2016). Chemical constituents and in vitro anti-inflammatory activity of *Cistanche violacea* Desf. (Orobanchaceae) extract. *Filoterapia*, *109*, 248–253.

Cimmino, A., Mathieu, V., Evidente, M., Ferderin, M., Banuls, L. M. Y., Masi, M., … Evidente, A. (2016). Glanduliferins a and B, two new glucosylated steroids from *Impatiens glandulifera*, with in vitro growth inhibitory activity in human cancer cells. *Fitoterapia*, *109*, 138–145.

Dewick, P. M. (2009). *Medicinal natural products* (3rd ed.). Chicester, UK: John Wiley and Sons Ltd.

Deyama, T., Yahikozawa, K., Al-Easa, H. S., & Rizk, A. M. (1995). Constituents of plants growing in Qatar: Part xxviii. *Constituents of Cistanche Phelypaea*. http://hdl.handle.net/10576/9781

di Martino, O., Troiano, A., Guarino, A. M., Pollice, A., Vivo, M., La Mantia, G., & Calabrò, V. (2016). ΔNp63α controls YB-1 protein stability: Evidence on YB-1 as a new player in keratinocyte differentiation. *Genes to Cells*, *21*, 648–660.

Gast, M. (2000). *Moissons du désert. Utilisation des ressources naturelles au Sahara central*. Paris: Ibis Press 160 p. voir la notice.

Gu, C., Yang, X., & Huang, L. (2016). Cistanches Herba: A neuropharmacology review. *Frontiers in Pharmacology*, *7*, 289.

Han, L., Ji, L., Boakye-Yiadom, M., Li, W., Song, X., & Gao, X. (2012). Preparative isolation and purification of four compounds from *Cistanches deserticola* YC Ma by high-speed counter-current chromatography. *Molecules*, *17*, 8276–8284.

Kim, K. H., Kim, S., Jung, M. Y., Ham, I. H., & Whang, W. K. (2009). Anti-inflammatory phenylpropanoid glycosides from *Clerodendron trichotomum* leaves. *Archives of Pharmacal Research*, *32*, 7–13.

Kobayashi, H., Karasawa, H., Miyase, T., & Fukushima, S. (1985). Studies on the constituents of Cistanchis herba. VI. Isolation and structure of a new iridoid glycoside, 6-deoxycatalpol. *Chemical and Pharmaceutical Bulletin*, *33*, 3645–3650.

Kobayashi, H., Oguchi, H., Takizawa, N., Miyase, T., Ueno, A., Usmanghani, K., & Ahmad, M. (1987). New Phenylethanoid glycosides from *Cistanche tubulosa* (SCHRENK) HOOK. F.I. *Chemical and Pharmaceutical Bulletin*, *35*, 3309–3314.

Lakhdari, W., Dehliz, A., Acheuk, F., Mlik, R., Hammi, H., Doumandji-Mitiche, B., & Chergui, S. (2016). Ethnobotanical study of some plants used in traditional medicine in the region of Oued Righ (Algerian Sahara). *Journal of Medicinal Plant Studies*, *4*, 204–211.

Lee, S. Y., Lee, K. S., Yi, S. H., Kook, S. H., & Lee, J. C. (2013). Acteoside suppresses RANKL-mediated osteoclastogenesis by inhibiting c-Fos induction and NF-κB pathway and attenuating ROS production. *PLoS One*, *8*, e80873.

Li, Y., Ishibashi, M., Satake, M., Oshima, Y., & Ohizumi, Y. (2003). A new iridoid glycoside with nerve growth factor-potentiating activity, gelsemiol 6′-*trans*-caffeoyl-1-glucoside, from *Verbena littoralis*. *Chemical and Pharmaceutical Bulletin*, *51*, 1103–1105.

Li, H., Jiang, H., & Liu, J. (2017). Traditional Chinese medical therapy for erectile dysfunction. *Translational Andrology and Urology*, *6*, 192–198.

Li, X., Xie, Y., Li, K., Wu, A., Xie, H., Guo, Q., … Chen, D. (2018). Antioxidation and Cytoprotection of Acteoside and its derivatives: Comparison and mechanistic chemistry. *Molecules*, *23*, 498.

López-Espinosa, J.A. 2022. *Cistanche Phelypaea*. https://www.regmurcia.com/servlet/s.SI?sit=a,0,c,365,m,1309&r=ReP-29346-DETALLE_REPORTAJES. Accessed March 22, 2022.

Melek, F. R., El-Shabrawy, O. A., El-Gindy, M., & Miyase, T. (1993). Pharmacological activity and composition of ethyl acetate extract of *Cistanche phelypaea*. *Fitoterapia*, *64*, 11.

Morikawa, T., Xie, H., Pan, Y., Ninomiya, K., Yuan, D., Jia, X., … Muraoka, O. (2019). A review of biologically active natural products from a desert plant *Cistanche tubulosa*. *Chemical and Pharmaceutical Bulletin*, *67*, 675–689.

Ogrodnik, M., Miwa, S., Tchkonia, T., Tiniakos, D., Wilson, C. L., Lahat, A., & Jurk, D. (2017). Cellular senescence drives age-dependent hepatic steatosis. *Nature Communications*, *8*, 1–12.

Okolicsanyi, R. K., Camilleri, E. T., Oikari, L. E., Yu, C., Cool, S. M., Van Wijnen, A. J., & Haupt, L. M. (2015). Human mesenchymal stem cells retain multilineage differentiation capacity including neural marker expression after extended in vitro expansion. *PLoS One*, *10*, e0137255.

Pujadas-Salvá, A.J., & López-Saéz, J.A. (2002). Cistanche. In: López-Sáez, J. A, Catalán, P. & Sáez, Ll. (Eds.), *Plantas parásitas de la Península Ibérica e Islas Baleares* (pp. 440–451). Madrid, Spain: Editorial Mundi-Prensa.

Qiao, Z., Tang, J., Wu, W., Tang, J., & Liu, M. (2019). Acteoside inhibits inflammatory response via JAK/STAT signaling pathway in osteoarthritic rats. *BMC Complementary and Alternative Medicine*, *19*, 264.

Salehi, M., Esmailzadeh, S. H., Kheyli, S. A. G., Malekshah, A. F., & Zaroudi, M. (2019). *Cistanche tubulosa* could be considered as medicinal plant in halophytes farming. In R. Tucker (Ed.), *Halophytes* (pp. 193–233). New York, NY: Nova Science Publishers, Inc.

Song, Y., Zeng, K., Jiang, Y., & Tu, P. (2021). Cistanches Herba, from an endangered species to a big brand of Chinese medicine. *Medicinal Research Reviews*, *41*, 1539–1577.

Sticher, O., & Weisflog, A. (1975). Detection and isolation of the iridoid glucoside of *Galeopsis tetrahit* L.(Labiatae) as well as elucidation of the structure of gluroside. *Pharmaceutica Acta Helvetiae*, *50*, 394–403.

Thorogood, C. J., Leon, C. J., Lei, D., Adughayman, M., Huan, L.-F., & Hawkins, J. A. (2021). Desert hyacinths: An obscure solution to a global problem. *Plants, People, Planet*, *3*, 302–307.

Tian, X. Y., Li, M. X., Lin, T., Qiu, Y., Zhu, Y. T., Li, X. L., & Chen, L. P. (2021). A review on the structure and pharmacological activity of phenylethanoid glycosides. *European Journal of Medicinal Chemistry*, 209, 112563.

Trampetti, F., Pereira, C., Rodrigues, M. J., Celaj, O., D'Abrosca, B., Zengin, G., … Custódio, L. (2019). Exploring the halophyte *Cistanche phelypaea* (L.) Cout as a source of health-promoting products: In vitro antioxidant and enzyme inhibitory properties, metabolomic profile and computational studies. *Journal of Pharmaceutical and Biomedical Analysis*, *165*, 119–128.

Van Meerloo, J., Kaspers, G. J. L., & Cloos, J. (2011). Cell sensitivity assays: The MTT assay. *Methods in Molecular Biology*, *731*, 237–245.

Venditti, A., Serrilli, A. M., & Bianco, A. (2013). Iridoids from *Bellardia trixago* (L.) all. *Natural Product Research*, *27*, 1413–1416.

Vivo, M., Fontana, R., Ranieri, M., Capasso, G., Angrisano, T., Pollice, A., … La Mantia, G. (2017). p14ARF interacts with the focal adhesion kinase and protects cells from anoikis. *Oncogene*, *36*, 4913–4928.

Volpato, G., Saleh, S. M. L., & Di Nardo, A. (2015). Ethnoveterinary of Sahrawi pastoralists of Western Sahara: Camel diseases and remedies. *Journal of Ethnobiology and Ethnomedicine*, *11*, 54.

Wang, C., Gong, X., Bo, A., Zhang, L., Zhang, M., Zang, E., & Li, M. (2020). Iridoids: Research advances in their phytochemistry, biological activities, and pharmacokinetics. *Molecules*, *25*, 287.

Wang, F., Tu, P., Zeng, K., & Jiang, Y. (2021). Total glycosides and polysaccharides of *Cistanche deserticola* prevent osteoporosis by activating Wnt/β-catenin signaling pathway in SAMP6 mice. *Journal of Ethnopharmacology*, *271*, 113899.

Wang, Y. E., Zhang, L. I., Du, Z., Pei, J., & Huang, L. (2019). Chemical diversity and prediction of potential cultivation areas of *Cistanche* herbs. *Scientific Reports*, *9*, 19737.

Wang, Y. J., Zhou, S. M., Xu, G., & Gao, Y. Q. (2015). Interference of phenylethanoid glycosides from *Cistanche tubulosa* with the MTT assay. *Molecules*, *20*, 8060–8071.

Warren, S. (2015). Trypan blue exclusion test of cell viability. *Current Protocol Immunology*, *111*, A3.B.1–A3B.3.

Xiao, D., Powolny, A. A., & Singh, S. V. (2008). Benzyl isothiocyanate targets mitochondrial respiratory chain to trigger reactive oxygen species-dependent apoptosis in human breast cancer cells. *Journal of Biological Chemistry*, *283*, 30151–30163.

Xu, R., Chen, J., Chen, S. L., Liu, T. N., Zhu, W. C., & Xu, J. (2009). *Cistanche deserticola* Ma cultivated as a new crop in China. *Genetic Resources and Crop Evolution*, *56*, 137–142.

Yang, L., Zhang, B., Liu, J., Dong, Y., Li, Y., Li, N., … Ma, X. (2019). Protective effect of Acteoside on Ovariectomy-induced bone loss in mice. *International Journal of Molecular Sciences*, *20*(12), 2974.

Yoshizawa, F., Deyama, T., Takizawa, N., Usmanghani, K., & Ahmad, M. (1990). The constituents of *Cistanche tubulosa* (SCHRENK) HOOK. f. II.: Isolation and structures of a new phenylethanoid glycoside and a new neolignan glycoside. *Chemical and Pharmaceutical Bulletin*, *38*, 1927–1930.

Zhang, W., Huang, J., Wang, W., Li, Q., Chen, Y., Feng, W., Zheng, D., Zhao, T., Mao, G., Yang, L., Wu, X. (2016) Extraction, purification, characterization and antioxidant activities of polysaccharides from *Cistanche tubulosa*. *International Journal of Biological Macromolecules*, *93*, 448–458.

Zhang, C. Z., Wang, S. X., Zhang, Y., Chen, J. P., & Liang, X. M. (2005). In vitro estrogenic activities of Chinese medicinal plants traditionally used for the management of menopausal symptoms. *Journal of Ethnopharmacology*, *98*, 295–300.

Zhou, D., Shao, L., & Spitz, D. R. (2014). Chapter one – Reactive oxigen species in normal and tumor stem cells. *Advances in Cancer Reseach*, *122*, 1–67.

How to cite this article: Delicato, A., Masi, M., de Lara, F., Rubiales, D., Paolillo, I., Lucci, V., Falco, G., Calabrò, V., & Evidente, A. (2022). In vitro characterization of iridoid and phenylethanoid glycosides from *Cistanche phelypaea* for nutraceutical and pharmacological applications. *Phytotherapy Research*, 1–12. https://doi.org/10.1002/ptr.7548

CHAPTER IV

4. Grape pomace

4.1. Waste is a waste only if wasted: optimization of extraction and *in vitro* screening of grape pomace

The grape pomace was supplied to us by the Mastroberardino Winery, Italy, a leader in the production of wine in Campania territory, Southern Italy. During grape processing, grape polyphenols mainly remain in the pomace due to their incomplete extraction. The main representatives of polyphenolic compounds in this byproduct are anthocyanins (only in red grape pomaces), catechins, flavonol glycosides, phenolic acids, and alcohols (Kammerer, D. *et al.,* 2004). Together with dietary fibers, phenolic compounds are the most valuable compounds of grape pomace with health-beneficial properties in the regulation of metabolism and prevention of chronic diseases such as obesity, diabetes, atherosclerosis, osteoporosis and cancer (Bender, A.B.B. *et al*., 2020).

4.2. Grape pomace extraction procedure

The first phase of the extraction process was **lyophilization**, to eliminate the water present in the pomace samples, which could compromise the stability of phenolic compounds. The next stage was the **maceration** of the solid phase in pure ethanol. Maceration was carried out at room temperature to preserve the high content of pomace polyphenolic compounds which are thermolabile. Given that this extraction procedure relies mainly on diffusion of the compounds from the solid to the liquid phase, it was necessary to shake the system to avoid localized oversaturation close to the surface of the solid to be extracted, which would lead to a slowdown of the global diffusion process. After the elimination of the solid phase the ethanolic phase was removed by **evaporation** under reduced pressure (figure 20).

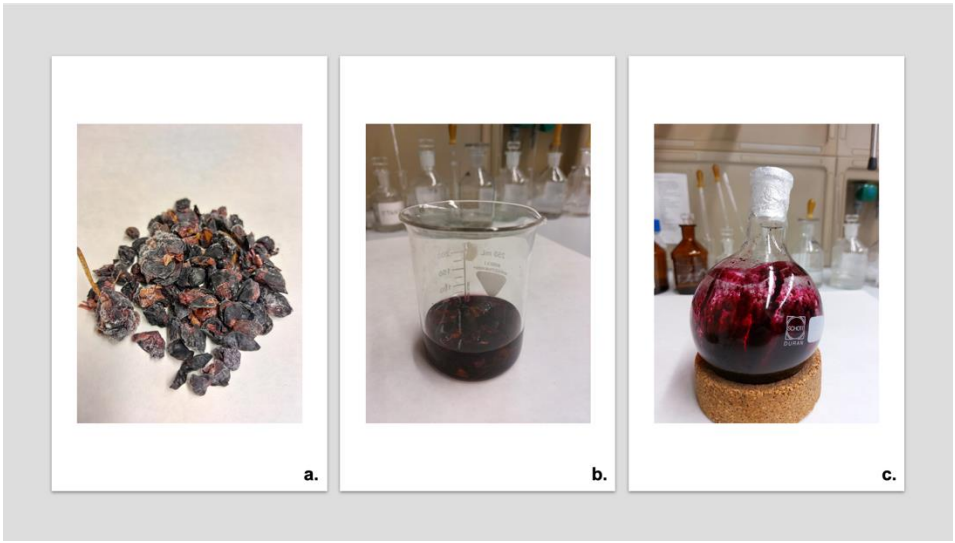

Figure 20. Process of extraction of the pomace. **(a)** freeze-dried pomace; **(b)** maceration in ethanol; **(c)** organic extract obtained after filtration and solvent recovery.

The chemical profile of the pomace extract was analyzed by Thin Layer Chromatography TLC. The most abundant metabolites among the flavonoids class were represented by (+)-catechin and its epimer, (-)-epi-catechin, which were purified from the apolar fraction. Their identification was confirmed by comparing their ^{1}H-NMR spectra and specific optical rotation power with the data reported in the literature. As previously mentioned, we can expect that the composition of the pomace extract could change depending on the climatic and environmental growth conditions of the plants.

4.3. Cytotoxicity assay

The effect of the grape pomace extract on cell viability was tested by the MTT assay on immortalized HaCaT keratinocytes using a range of concentrations of the extract from 1 to 1000 μg/ml and DMSO (0,5%) as a negative control. The well-known cytotoxic alkaloid, lycorine, effective against several immortalized and tumor cell lines, was used as a positive toxicity control.
As shown in figure 21, up to 100 μg/mL and 72 hrs of incubation the extract was not toxic. The lower cell viability observed at 100 μg/mL and 48 hrs of incubation was likely due to a transient cell cycle or metabolic

arrest, indeed cells completely recovered their viability at 72h. Instead, at the concentration of 1000 µg/mL, the extract was cytotoxic both at 48 and 72h, and its toxicity was completely comparable to that of lycorine (figure 21).

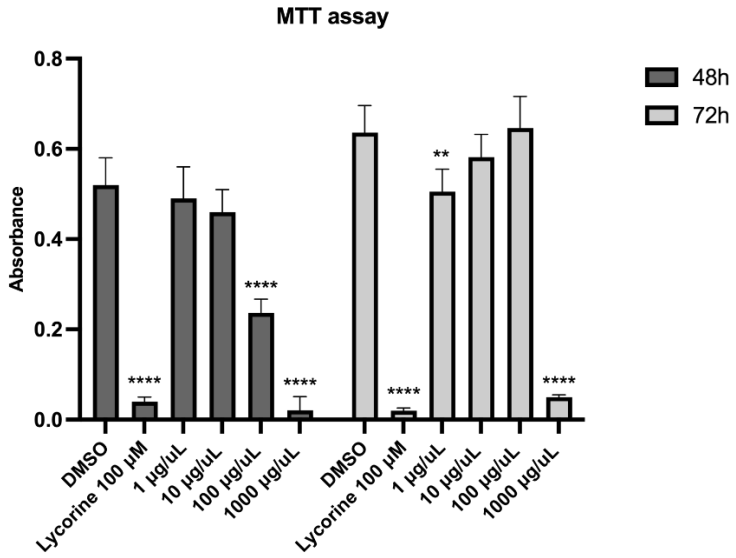

Figure 21. MTT viability assays with concentrations ranging from 1 µg/mL to 1000 µg/mL of grape pomace total extract in EtOH on HaCaT cell line at 48 and 72h of incubation. DMSO was used as negative control and Lycorine as a positive toxicity control. Statistical analyses were performed using one-way ANOVA and Dunnett's multiple comparisons tests. Levels of significance between points of expression are indicated (**** $p < 0.001$, *** $p < 0.01$, ** $p < 0.02$).

4.4. Antioxidant assay

The antioxidant power of the total extract obtained from grape pomace was evaluated by the DCFDA assay on human immortalized HaCaT keratinocytes. Cells were pretreated for 4h with different concentrations of the grape pomace extract dissolved in DMSO, ranging from 1 to 100 µg /mL range that resulted well tollereted by cells. Then I performed the DCFDA assay as described in the Materials and Methods section, using the antioxidant standard Trolox, the water-soluble analog of vitamin E, as an antioxidant positive control and the DMSO vehicle, as a negative control. The percentage of DMSO (0.5%) was kept constant at each

experimental point. As shown in figure 22, the grape pomace extract has a significant dose-dependent antioxidant effect. At the concentration of 100 μg/ml the grape pomace extract was well tolerated by cells and the ROS activity was reduced by 50% (figure 22). In summary, the extraction protocol we used was an effective procedure that could preserve the strong antioxidant power of grape pomace polyphenols and a method applicable on a large scale and with the least expenditure possible of organic solvent.

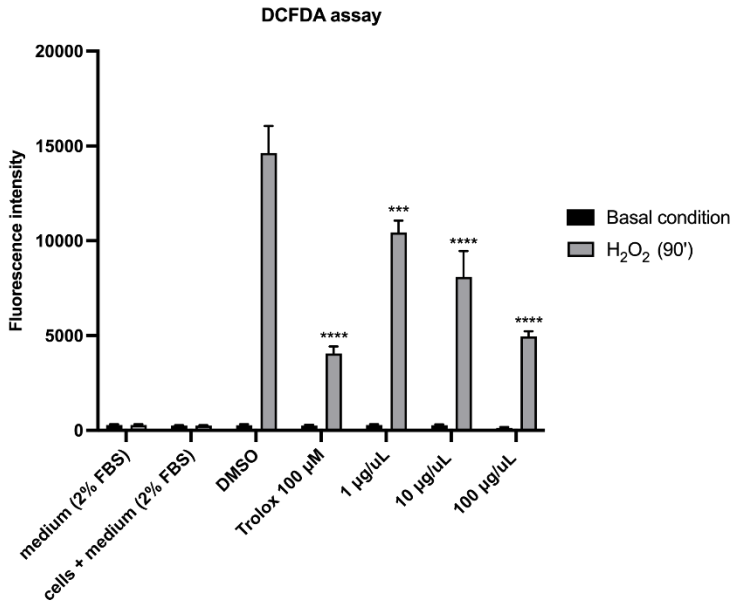

Figure 22. DCFDA assay. HaCaT cells were seeded and pretreated for 4 h with concentrations ranging from 1 μg/mL to 100 μg/mL of grape pomace total extract in EtOH. H_2O_2 (1 mM; 3%) was added to the medium for 1.5 h. The fluorescence intensity of DCFDA was read after 45' of incubation. Trolox was used as a positive control and DMSO, in which the metabolites were dissolved, as a negative control. The values are the mean's six values for each experimental point of three independent biological replicates. Statistical analysis was performed with two-way ANOVA, using Tukey's multiple comparison test. Levels of significance between points of expression are indicated (****$p < 0.001$, ***$p < 0.01$).

4.5. Encapsulation of the extract in edible pectin beads

Formulations of grape pomace extract were carried out at the CNR-IPCB (National Research Council-Institute for Polymers, Composites and Biomaterials), Pozzuoli, Italy.

Pectin is a heteropolysaccharide in which the principal component is galacturonic acid: a sugar acid derived from galactose. The abundance of this component defines a parameter called methoxylation degree (MD) as the percentage of carbonyl groups esterified with methanol. Pectin with high MD (>50%) have the capability to form gels with simple carbohydrates in presence of acid, on the other hand pectin with low MD(<50%) can reticulate in presence of bivalent metal ions. The latter pectin was used for formulation of beads loaded with grape pomace extract.
Briefly, pectin (Low MD) was dissolved in MilliQ water (4%wt/v.) with different percentages by mass of extract (50-75%). Once homogeneity was reached, this solution was added dropwise to a solution containing a bivalent ionic crosslinker solution (Fe^{+2} or Ca^{+2} ;250 or 500 mM) which allows the entrapment of the extract compounds into the polysaccharide matrix as show in figure 23 (a-d). The beads obtained were then freeze-dried and characterized. The freeze-drying process resulted in an acceptable volumetric loss, of the order of about 1/5 with respect to the initial mass, consequently it did not cause problems for the bead structure. Loading efficiency of grape pomace extract was determined by UV-Vis reading absorbance at 560nm, values are reported in table 2.
Characterization of thermal properties was carried out using TGA (Thermo-Gravimetric Analysis) in order to evaluate the state of the polymeric material, the stability of the active compounds and confirm loading efficiency.

Sample	% Loading efficiency
Fe^{+2} (250 mM)	96
Ca^{+2} (250 mM)	64
Ca^{+2} (500 mM)	94

Table 2. Percentage of loading efficiency with different metals (Ca^{2+} or Fe^{2+}) and concentrations.

Furthermore, the dispersion of the extract in polymer matrix was evaluated using a Scanning Electron Microscope (SEM) showing good dispersion and phase continuity confirming the affinity between components (figure 23.e).

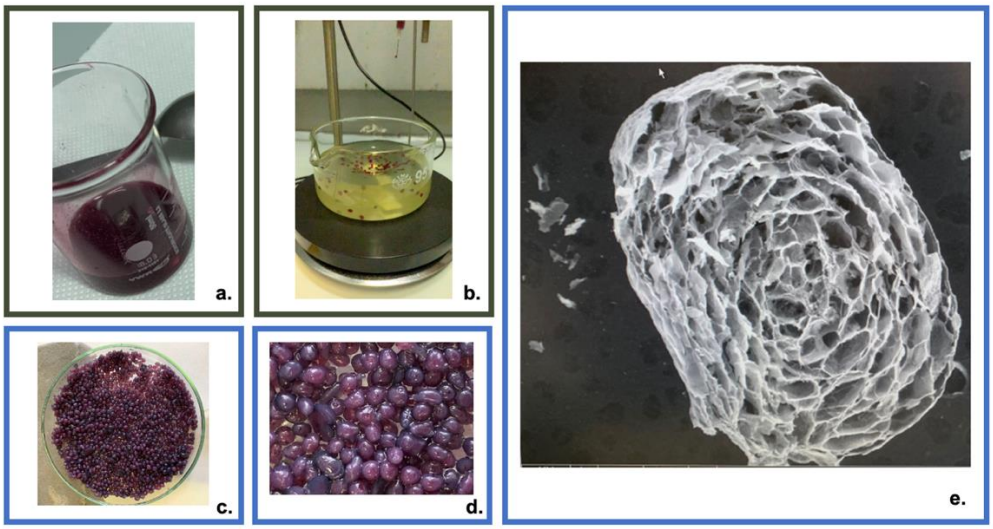

Figure 23. Steps of grape pomace-loaded beads preparation. **(a)** pectin and grape pomace mix. **(b)** Addition of crosslinking ions. **(c)** Freeze-dried beads. **(e)** SEM acquisition showing the dispersion of the grape pomace extract in the polymeric matrix.

From the analysis emerged that the iron-crosslinked beads appeared to have a more rigid network and a perfectly spheroidal shape. The formulation which envisaged the use of calcium ions, instead, appeared to have a looser network and irregular morphology.
Finally, the beads purpose i.e., the release of the active compounds in the intestinal tract overcoming the gastric tract. A resistance test to the gastric environment was conducted by placing the beads in acid environment (pH=2) from 2h up to 5h under magnetical stirring. At the end of this test, the beads resulted in unaltered morphology as show in figure 24.

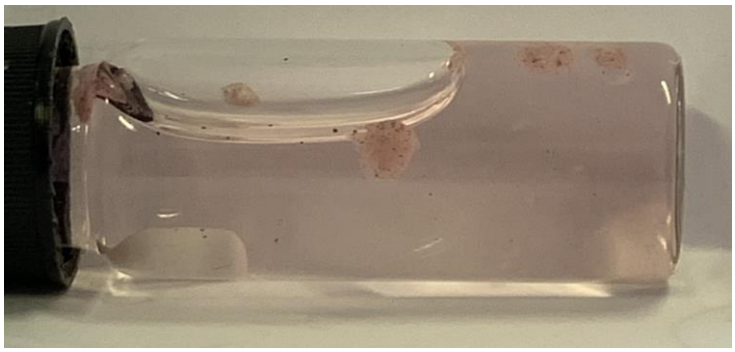

Figure 24. Beads appearance after 5h in pH=2 solution. The morphology is unalterated after the passage in an acid environment.

Then, the **extract-loaded beads** were then placed in a solution at pH=2.0 for 2h to mimic the gastric environment, while a solution at pH=7.4 for 3 h was used to mimic the intestinal tract (as required by Pharmacopoeia). Moreover, the release of the compounds from the beads was evaluated after a first step in the acid solution and then at pH=7,4. The compounds released from the beads were freeze-dried to eliminate the water present and finally weighed to determine the yield of the released. The different experimental points are listed in the table below (table 3) along with the estimated loading and release efficiency. The Fe^{2+} cross-linked beads had a lower release efficiency than the Ca^{2+} crosslinked beads.

Sample	Ca/Fe	pH	%Release efficiency
1	Fe	7.4	1.3
2	Ca	7.4	49
3	Fe	7.4	6.3
4	Ca	2	53.8
5	Ca	from 2 to 7.4	1.5
6	Fe	from 2 to 7.4	2.6
7	Fe	from 2 to 7.4	1.6
8	Fe	2	12.5
9	Fe	from 2 to 7.4	1.2
10	Fe	2	10.5
11	Fe	2	8

Table 3. The samples were loaded by placing them in direct contact with beads crosslinked with Fe^{2+} and Ca^{2+} ions. The beads were immersed in solutions at different pH, and their loading and release efficiency was calculated.

The samples were all subjected to ^{1}H-NMR compared with the spectrum of the original total extract (figure 25).

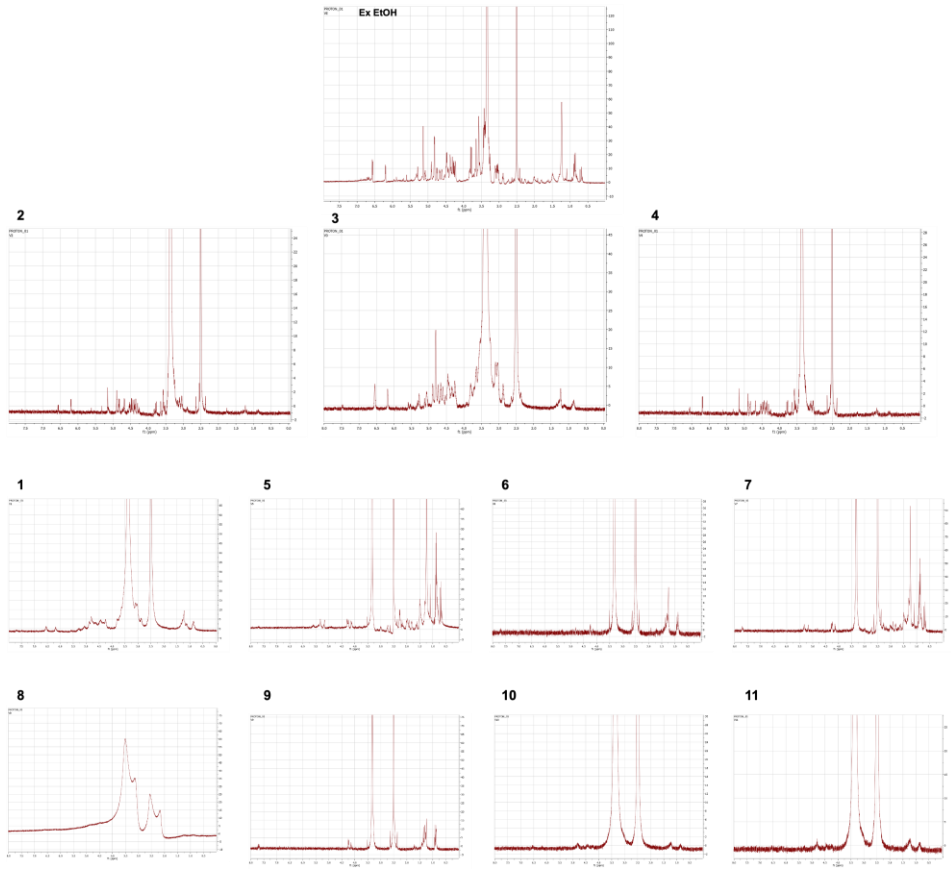

Figure 25. Comparison of ^{1}H NMR spectra. ^{1}H NMR spectra of the ethanolic grape pomace extract (on the top) and of the compounds in DMSO released from the beads in the different experimental conditions listed in Table XXXX. Spectra were recorded at 500 MHz. The samples showing a representative spectrum of the crude ethanolic extract are samples n° 2, 3, and 4.

The obtained spectra indicate that the beads cross-linked with Ca^{2+} can release all their content, both at pH=2 and pH=7.4 in about 3 h, the time of digestion along the human gastrointestinal tract. While the iron-reticulated pearls can release only 8-9% of the compounds contained in the total extract loaded.

The samples released by the beads were dissolved in DMSO and tested, using the ROS assay, to determine if they have preserved at least in part the antioxidant power and if the pH of the medium for the release of compounds could have in some way altered their activity. Therefore, I performed the DCFDA assay, as previously described on HaCaT cells pretreated for 4h with the released compounds at concentrations from 1 to 100 µg/mL (figure 26). I decided to exclude the

highest concentration of 1000 µg/mL because of a possible cytotoxic effect.

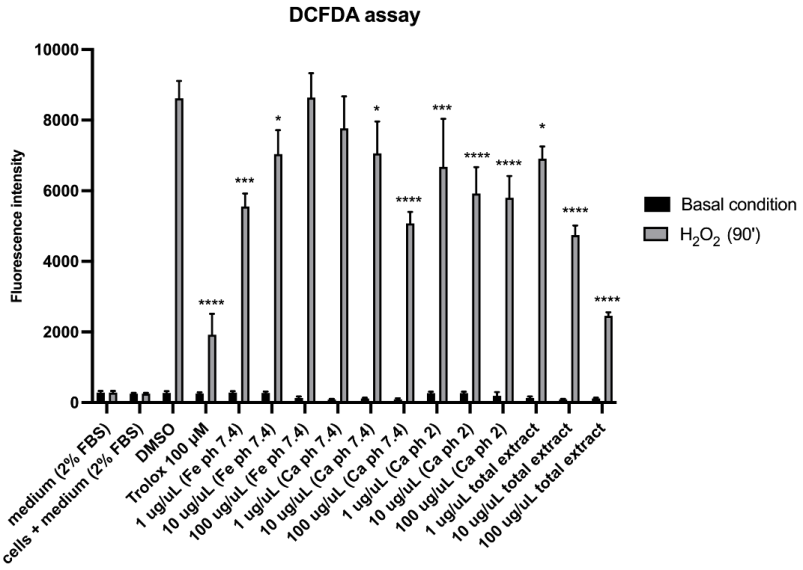

Figure 26. DCFDA assay. HaCaT cells were seeded and pretreated for 4 h with concentrations ranging from 1 µg/mL to 100 µg/mL of compounds released from the beads crosslinked with Fe^{2+} and placed in a solution at pH 7.4, and beads crosslinked with Ca^{2+} and placed in a solution at pH 2 and pH 7.4. H_2O_2 (1 mM; 3%) was added to the medium for 1,5 h. The fluorescence intensity of DCFDA was read after 45' of incubation. Trolox was used as a positive control and DMSO, in which the metabolites are dissolved, as a negative control. The same concentrations of the total crude extract were also used as a positive control. The values are the mean's six values for each experimental point of three independent biological replicates. Statistical analysis was performed with two-way ANOVA, using Tukey's multiple comparison test. Levels of significance between points of expression are indicated (****$p < 0.001$, ***$p < 0.01$, *$p < 0.05$).

Interestingly, I observed that compounds released from particles conjugated with Fe^{2+} did not show any antioxidant effect. This was in agreement with the results of the ^{1}H-NMR spectra. Those released from Ca^{2+} crosslinked beads appeared to function efficiently and in a dose-dependent manner, both at pH=2 and pH=7.4. However, the antioxidant effect was lower compared to that of the whole extract. This point should be improved and deserves further investigations.

4.6. Conclusions

During this part of my PhD training I prepared phyto complex from the grape pomace of the Mastroberardino company, in the Campania region, Italy. The ethanol was selected as extraction medium based on its complete biocompatibility and solubilizing power.
Then, I contributed to characterize a mixture of antioxidant compounds from grape pomace waste for developing a possible formulation in edible beads for the nutraceutical industry with potential benefit for human health. I loaded the compounds and crosslinked them with two different ions, Fe^{2+} or Ca^{2+}, to improve their functionality and organoleptic properties and to favor the supply of two essential cationic micronutrients.
Moreover, I tested the structure of the beads, the functional loading and delivery of the formulated system mimicking the gastrointestinal tract environment. The compounds released by the beads have been tested and found to be compatible with mammalian cells and effective in counteracting the intracellular free radicals generated by H_2O_2 treatment. In characterizing the grape pomace extract, I found that the major constituents among metabolites were (+)-catechin and its epimer, (-)-epi-catechin, two isomeric flavonoids. Catechin has been reported to be more reactive and stable than epicatechin. The hydroxyl group position on the ring C of the catechol structure represents a factor that influences this relative stability (Eugène, E. A. *et al*., 2022). The reduction in antioxidant activity of the released from the beads, compared to the starting raw extract could be attributable to the loss of epi-catechin activity, which becomes highly unstable when passing through environments at different pH levels.
Polyphenolic secondary metabolites as flavonoids have a variety of well-known healthy-promoting properties and therefore are valuable options to exploit in the design of innovative products food formulations with health benefits. Furthermore, if it is possible to design novel formulations using flavonoids and edible polysaccharides polymers that also derive from waste products of the agri-food industry, everything falls within the perspective of the circular economy.
However, the incorporation of phenols in prescription food products is limited by their susceptibility to degradation and epimerization, extreme pH and temperature conditions. Other relevant factors that must be taken into account are their limited water solubility, and untargeted delivery. Based on the recent literature, different encapsulation technology as delivery strategies can improve the stability, functionality and bioavailability of phenols in edible formulations. It has been already

shown that applying encapsulated phenols instead of free molecules improves the antioxidant capacity of enriched phenols foodstuffs (Pateiro, M. *et al.,* 2021). Nevertheless, further research needs to be done to compare the effects of encapsulation techniques using different coating materials on phenolic compounds to determine the best carrier system for encapsulation of phenols in any type of food product formulations in terms of functionality, bioavailability and organoleptic properties. Our formulations with Ca^{2+} appear to be promising and almost ready for *in vivo* testing, because they can efficiently release the antioxidant molecules along the gastrointestinal tract, preserving their structural and functional integrity. The beads cross-linked with Fe^{2+} having a poor release efficiency, do not seem to give back enough compounds to get the desired antioxidant effect. However, iron in formulations is still poorly investigated, probably due to the problems of precipitation of the ferric ion around pH=7 (Hove, M. *et al*., 2007). The preparation of other formulations of these beads is currently underway, to improve their characteristics in terms of loading and release efficiency, and the preservation of the ROS scavenging activity. Once the best prescription will be established, its bioavailability will be tested *in vivo* using animal models.

CHAPTER V

5. Other collaborations

During my PhD I had the opportunity to take part in other side projects of my laboratory team as a collaborative effort. One of them was focused on the characterization of secondary metabolites isolated from the infesting fungi of forest plants. The results from these studies have been published in the manuscript:

5.1. Anti-Biofilm Activity of the Fungal Phytotoxin Sphaeropsidin A Against Clinical Isolates of Antibiotic-Resistant Bacteria.

Roscetto E, Masi M, Esposito M, Di Lecce R, **Delicato A**, Maddau L, Calabrò V, Evidente A, Catania MR. *Toxins (Basel).* 2020 Jul 8;12(7):444. doi: 10.3390/toxins12070444.

Antibiotic resistance has a major impact on people, animals and the environment. Indeed, if a microorganism acquires the ability to resist the action of an antibiotic, the infectious disease caused by it may be more difficult to cure: the longer course increases the risk of complications, up to outcomes that can be disabling or lead to the death of the patient. Antibiotic resistance, therefore, has important consequences on people's quality of life and also a significant economic impact on the individual and the community. The excessive or inappropriate use of antibiotics in human medicine but also zootechnics and agriculture induces the development of new resistances not only directly in the microorganisms, but also entails a risk for the possible release into the environment of residues of these medicines that contaminate water, soil and vegetation. These residues continue to be active in the environment, inducing selective pressure against the bacteria that live there. Bacteria in nature can be present both in free form (planktonic form) and organized in structures called biofilms which are aggregates of microorganisms that manifest themselves in a polymeric matrix capable of holding them together and anchoring them firmly to a surface. This matrix is made up of sugars, DNA and proteins. The formation of the biofilm helps the bacterial community to protect itself from environmental stresses (such as temperature variations and dehydration), favors the retention of nutrients and creates real communication between the bacteria (through the quorum-sensing process). Approximately 60% of microbial infections are associated with the formation of biofilms as the bacterial cells organized in this structure can better resist disinfectants and antibiotics and attacks by

the host's immune system. Many gods currently available drugs hardly penetrate the biofilm, and the bacteria in the biofilm are 10-1000 times more resistant than the planktonic counterpart. Therefore, it is necessary to promote coordinated interventions to reduce the development and spread of antibiotic resistance. Among these, the discovery of new natural molecules with antimicrobial properties is of great interest. Among terrestrial ecosystems, forests represent a huge reservoir of pathogens and endophytic fungi, studied for several years to evaluate their biosynthesis capacity for phytotoxic metabolites and explore the myriad biological activities including antibacterial properties. Therefore, in this work, 20 secondary metabolites produced by pathogenic fungi of forest plants and belonging to different classes of naturally occurring compounds, such as butenolides, cyclohexenoxides, diterpenes, isobenzofuranones, isocoumarins, macrolides, etc., were evaluated for the first time against clinical isolates of antibiotic-resistant Gram-negative and Gram-positive bacteria. In particular, among all tested metabolites, three of them, namely **epi-epoformin**, **sphaeropsidone** and **sphaeropsidin A**, proved to be effective against all strains tested. The most powerful metabolite among them was sphaeropsidin A, which was effective even at very low concentrations against all reference and clinical test strains with minimum inhibitory concentration (MIC) values between 6.25 µg/mL and 12.5 µg/mL. Moreover, sphaeropsidin A at sub-inhibitory concentrations decreased the biofilm formation of methicillin-resistant S. aureus (MRSA) and P. aeruginosa. Moreover, mixtures of sphaeropsidin A and epi-epoformin showed antimicrobial synergistic effects with a concomitant reduction of cytotoxicity against immortalized human keratinocytes, showing promising antimicrobial properties. Sphaeropsidin A activity appears notable for its ability to inhibit biofilm formation, preventing a growth mode that results in particular resistance to antibiotic treatment. The obtained results are preliminary for further experiments aimed at the development of biocompatible formulations of epi-epoformin and sphaeropsidin A, suitable for preventing the development of serious infections.

5.2. Functions and regulations of oncoprotein Y Box binding protein 1

During my PhD I was involved in a project focused on the functional characterization of Y Box binding protein 1, an oncoprotein that was

identified in the laboratory of Prof. Viola Calabrò as a physical interactor of the p63 protein, a transcription factor belonging to the p53 tumor suppressor family. I have studied different aspects of this multifunctional protein, as a sensor of oxidative stress, as a prooncogenic factor in the molecular pathways of cancers, as a factor involved in DNA repair. The results of my experimental activity on this topic were published in the following manuscripts:

YB-1 recruitment to stress granules in *zebrafish* cells reveals a differential adaptive response to stress.
Guarino AM, Mauro GD, Ruggiero G, Geyer N, **Delicato A**, Foulkes NS, Vallone D, Calabrò V.Sci Rep. 2019 Jun 21;9(1):9059. doi: 10.1038/s41598-019-45468-6

Y box binding protein 1 (YB-1) oncoprotein at the hub of DNA proliferation, damage and cancer progression.
Sangermano F, **Delicato A**, Calabrò V.Biochimie. 2020 Dec;179:205-216. doi: 10.1016/j.biochi.2020.10.004. Epub 2020 Oct 12.

YB-1 Oncoprotein Controls PI3K/Akt Pathway by Reducing Pten Protein Level.
Delicato A, Montuori E, Angrisano T, Pollice A, Calabrò V.Genes (Basel). 2021 Sep 29;12(10):1551. doi: 10.3390/genes12101551.

5.1.1. YB-1 recruitment to stress granules in *zebrafish* cells reveals a differential adaptive response to stress

Y-box binding protein 1 (YB-1, YBX1) is a member of the DNA- and RNA-binding protein family with an evolutionarily ancient and conserved cold shock domain. Except for the CDS which retains a β-barrel structure, the C and N-ter ends of the protein are unfolded, and thanks to the dynamism of its three-dimensional structure able to modify by adapting to the different cellular partners, YB-1 performs different functions depending on the specifications conditions and the cellular district in which it is located. YB-1 participates in a wide variety of DNA/RNA-dependent events, including DNA repair, pre-mRNA transcription and splicing, mRNA packaging, and regulation of mRNA stability and translation. At the cellular level, the multiple activities of YB-1 are manifested as its involvement in cellular proliferation and differentiation, stress response, and malignant cellular transformation.

YB-1, under physiological conditions, is partly localized in particles ribonucleoproteins (mRNPs), polysomes or in P-bodies and regulates the translation of 5'-cap dependent and independent mRNAs. The importance of YB-1 function in the response to oxidative stress is clear in the literature. More specifically, under normal conditions YB-1 co-localizes with Processing Bodies (PBs) while, during oxidative stress, it interacts with G3BP1 (the canonical marker of SGs) and leads to the formation of SGs as part of a survival program, sequestering messenger RNAs and preventing the cell from wasting energy and optimizing the cellular response to the particular type of stress. These represent cytoplasmic foci where untranslated mRNAs are sorted or processed for reinitiation, degradation, or packaging into mRNPs.
The survival of cells exposed to adverse environmental conditions leads to various alterations of cellular function, including major changes in the transcriptome and a radical reprogramming of protein translation. In mammals, this process has been extensively studied, while stress responses in non-mammalian vertebrates remain poorly understood. One of the key cellular responses to many different types of stressors is the transient generation of stress granules (SG). Using the evolutionarily conserved Y-box binding protein 1 (YB-1) and G3BP1 as markers, we investigated stress granule formation in *zebrafish* (*Danio rerio*) in response to several environmental stressors. *zebrafish* is a freshwater fish of the cyprinid family and represents one of the most popular and versatile genetic models for studies of human diseases. We demonstrated that following heat shock, zebrafish cells, like mammalian cells, form stress granules that contain both YB-1 and G3BP1 proteins. Furthermore, zfYB-1 knockdown impairs G3BP1 recruitment to SG, under heat shock conditions with a consequent reduction in cell viability. My observations highlight the essential role played by YB-1 in SG assembly and cell survival. Interestingly, I've observed for the first time that *zebrafish* embryonic fibroblasts do not assemble YB-1-positive stress granules upon oxidative stress induced by treatment with arsenite, copper, or hydrogen peroxide. This is in contrast with the situation in human cells where SG formation is strongly induced by exposure to oxidative stressors. Thus, our results indicate fundamental differences in the mechanisms by which mammalian and *zebrafish* cells respond to oxidative stress.

5.1.2. Y box binding protein 1 (YB-1) oncoprotein at the hub of DNA proliferation, damage and cancer progression

A deep search in the YB-1 literature gave me the possibility to write a review focused on the role of YB-1 in cancer progression and chemoresistance.
YB-1 is a hallmark of cancer, overexpressed in a wide variety of cancers, sometimes aggressive or for which there is no effective cure. As mentioned above, YB-1 performs different functions depending on the cellular compartment where the protein is located. Indeed, the subcellular localization of YB-1 is finely regulated. The cytoplasmic form is predominant under physiological conditions with an apparent molecular weight of 45/50 kDa. However, increased expression of YB-1, mostly nuclear, appears to be a central driver of cancer development and chemoresistance and it correlates with a worse prognosis. YB-1 was first described as a transcriptional activator of genes involved in cell survival and chemotherapy resistance. Surprisingly, YB-1 is increasingly emerging as a multifaceted player in the detection and repair of DNA lesions and the maintenance of genome integrity.
In particular, under stress conditions, YB-1 plays its pro-survival role by first participating in the stress granules organization where it temporarily controls protein synthesis, then it takes part in DNA damage repair when significant genotoxic damage has occurred. In this way, it can preserve cancer cells from chemotherapy-induced death. Thus, strategies aimed at counteracting YB-1 activities on DNA damage repair could significantly increase the success of anticancer therapies.
In our review manuscript, I have collected and summarized published data on YB1 proposed role in major cancer types such as breast, colorectal, epidermoid carcinoma, neuroblastoma and so on. In particular, I reported the experimental evidence on YB-1 involvement in DNA damage repair mechanisms.
I am currently investigating the role of YB-1 in the recognition of damaged DNA by investigating the existence of YB-1 protein complexes at the damaged site using the **DiVA** (**Inducible Double strand breaks via Asisi system**) cell system. This system relies on the use of the restriction enzyme AsiSI to generate unambiguously positioned sequence-specific DSBs. Moreover, I'm also taking advantage of **Homology**-directed repair (**HDR**) Hela **DR-GFP** cells through which I'm monitoring the repair efficiency of wild-type or mutant YB-1 overexpressed protein.

5.1.3. YB-1 Oncoprotein Controls PI3K/Akt Pathway by Reducing Pten Protein Level

When stress stimuli or mitogenic signals arrive in the cell, YB-1 undergoes activation by PI3K and RSK signaling and moves into the nucleus serving as a prosurvival factor. In this way, it can also regulate many cell signaling pathways in different types of malignancies. In cancer, activation of the PI3K/Akt pathway is common. The PI3K/Akt signaling induces phosphorylation on several target genes, which in turn activate genes involved in cancer proliferation and progression. Activated Akt enhances the pro-proliferative and pro-survival activities of YB-1 by inducing phosphorylation of YB1 at S102 thereby promoting its nuclear translocation. The gene that inhibits the activation of the PI3K/Akt pathway is the well-known tumor suppressor PTEN, which is often mutated in cancer. We demonstrated that YB-1 controls PTEN protein levels by acting at the transcriptional level. Our data show for the first time a direct functional link between PTEN and YB-1 that has never been reported. Functionally, YB-1 overexpression can downregulate PTEN expression by indirectly inducing the activation of the PI3K/Akt pathway in precancerous cells. The level of PTEN appears to be tightly controlled at both the transcriptional and post-transcriptional levels. Although the precise mechanism by which YB-1 controls PTEN mRNA level remains to be determined, our data suggest the existence of a positive feedback loop between YB-1 and Akt, which reinforce each other, probably at an early stage of cancer progression thus conferring a selective advantage over precancerous cells.

5.3. Abroad experience. Cellular processes regulated by the circadian clock

During my PhD training, I had the opportunity to join the team of Prof. Nicholas Foulkes at the KIT Institute of Karlsruhe, Germany. One of the main scientific interest of Prof. Foulkes's laboratory is the molecular mechanism through which in vertebrates the circadian clock control major physiological cellular processes such as the cell cycle progression and DNA damage repair. The timing of cell proliferation is a key factor contributing to the regulation of normal growth. Disruption of the circadian clock, in turn, has been linked to cell growth deregulation and increased incidence of cancer. Historically *zebrafish* represents one of the most important model organisms for studying embryonic development in vertebrates, it has also emerged as a very

attractive model for studying the circadian timing system. As well as providing a powerful collection of genetic tools for studying clock mechanisms *in vivo*, fish possess directly light-entrainable peripheral clocks, even in fish-derived cell lines. Therefore, this has made the *zebrafish* particularly useful for studying the pathways conveying light information to the circadian clock. Data from the literature demonstrated that exposure of *zebrafish* larvae or adults to light-dark cycles causes a range of different cell types to enter S-phase predominantly at the end of the light period. This is an evolutionary mechanism to prevent light from causing damage to DNA (Dekens, M. P. S. *et al*., 2003; Idda, M. L. *et al*., 2012).The group led by Nicholas S. Foulkes, previously explored how light, temperature, ROS or UV regulate the expression of the clock genes per1b21, cry1a22 and per223 as well as DNA repair genes which in *zebrafish* are also transcriptionally activated by visible light. They have identified an enhancer element reactive to light, ROS and UV, the D-box17 element, which operates alone or in combination with other enhancers such as the E-box or E2F sites (Vallone, D. *et al.,* 2004; Mracek, P. *et al*. 2012; Vatine, G. *et al*., 2009; Zhao, H. *et al.,* 2018).

During my period at the Institut für Technologie (KIT) in Karlsruhe, I learned the NanoBit technology, a new technology, to study protein-protein interactions in real-time by following the kinetics of protein-protein association. The main objective of my work was to understand the functional relationships between the PAR factor, belonging to the bzip transcription factor family, and Nfil3. Such factors may bind to D-box enhancers to regulate transcription in response to exposure to sunlight. New knowledge about PAR and Nfil3-regulated genes can help to understand the functional relationships between DNA repair mechanisms and the circadian clock. During my period abroad I've produced many of expression clones in the NanoBit system, by cloning the small SmBit subunit of NanoLuc and the LgBit subunit of NanoLuc to the C-ter and N-ter ends of the transcription factors CRY5 and TEF2. I've obtained 8 clones for each gene, the various C-ter and N-ter combinations were transfected into *zebrafish* cell lines, PAC2 (embryonic fibroblasts), to follow the *in vivo* interaction kinetics of the two proteins through the light emitted by the reconstituted SmBit and LgBit in the NanoLuc reporter. The results observed in *zebrafish* embryonic fibroblasts led to two conclusions: the first being that some of the C-/N-ter clone combinations tested, showed a weak interaction between the two proteins; the second is that by recloning the transcription factors with SmBit or LgBit in plasmids under the control of more efficient promoter for expression in *zebrafish*, it will be possible

to confirm the interaction of the two factors on the enhancer domains of the D-box, and to clarify the molecular mechanisms that control the response to light in relation to the circadian rhythm.

toxins

MDPI

Article

Anti-Biofilm Activity of the Fungal Phytotoxin Sphaeropsidin A against Clinical Isolates of Antibiotic-Resistant Bacteria

Emanuela Roscetto [1,*], Marco Masi [2,*], Matilde Esposito [1], Roberta Di Lecce [2], Antonella Delicato [3], Lucia Maddau [4], Viola Calabrò [3], Antonio Evidente [2] and Maria Rosaria Catania [1]

1 Dipartimento di Medicina Molecolare e Biotecnologie Mediche, Università di Napoli Federico II, Via Pansini 5, 80131 Naples, Italy; matilde.esposito87@gmail.com (M.E.); mariarosaria.catania@unina.it (M.R.C.)
2 Dipartimento di Scienze Chimiche, Università di Napoli Federico II, Complesso Universitario Monte S. Angelo, Via Cintia 4, 80126 Napoli, Italy; roberta.dilecce@unina.it (R.D.L.); evidente@unina.it (A.E.)
3 Dipartimento di Biologia, Università di Napoli Federico II, Complesso Universitario Monte S. Angelo, Via Cintia 4, 80126 Napoli, Italy; antonella.delicato@unina.it (A.D.); vcalabro@unina.it (V.C.)
4 Dipartimento di Agraria, Sezione di Patologia Vegetale ed Entomologia, Università degli Studi di Sassari, Viale Italia 39, 07100 Sassari, Italy; lmaddau@uniss.it
* Correspondence: emanuela.roscetto@unina.it (E.R.); marco.masi@unina.it (M.M.); Tel.: +39-081674238 (M.M.)

Received: 27 May 2020; Accepted: 6 July 2020; Published: 8 July 2020

Abstract: Many pathogens involved in human infection have rapidly increased their antibiotic resistance, reducing the effectiveness of therapies in recent decades. Most of them can form biofilms and effective drugs are not available to treat these formations. Natural products could represent an efficient solution in discovering and developing new drugs to overcome antimicrobial resistance and treat biofilm-related infections. In this study, 20 secondary metabolites produced by pathogenic fungi of forest plants and belonging to diverse classes of naturally occurring compounds were evaluated for the first time against clinical isolates of antibiotic-resistant Gram-negative and Gram-positive bacteria. *epi*-Epoformin, sphaeropsidone, and sphaeropsidin A showed antimicrobial activity on all test strains. In particular, sphaeropsidin A was effective at low concentrations with Minimum Inhibitory Concentration (MIC) values ranging from 6.25 µg/mL to 12.5 µg/mL against all reference and clinical test strains. Furthermore, sphaeropsidin A at sub-inhibitory concentrations decreased methicillin-resistant *S. aureus* (MRSA) and *P. aeruginosa* biofilm formation, as quantified by crystal violet staining. Interestingly, mixtures of sphaeropsidin A and *epi*-epoformin have shown antimicrobial synergistic effects with a concomitant reduction of cytotoxicity against human immortalized keratinocytes. Our data show that sphaeropsidin A and *epi*-epoformin possess promising antimicrobial properties.

Keywords: fungal secondary metabolites; toxins; biological activity; biofilm; antibiotic-resistance; sphaeropsidin A; *epi*-epoformin

Key Contribution: Twenty secondary metabolites produced by pathogenic fungi of forest plants were evaluated for the first time against clinical isolates of antibiotic-resistant Gram-negative and Gram-positive bacteria. Among them, the phytotoxic compounds *epi*-epoformin, sphaeropsidone, and sphaeropsidin A showed antimicrobial activity on all test strains.

1. Introduction

In the last century, the use of antibiotics has played a fundamental role in extending the average human life. They allow us to treat trivial or serious infections and to carry out complex medical and

surgical procedures that would otherwise result in very high mortality. However, the excessive or inappropriate use of antibiotics, in human medicine but also zootechnics and agriculture, results in bacterial strains possessing increased antibiotic resistance and isolation frequency.

The ability to transfer resistance determinants horizontally makes the bacterium frequently acquire resistance to multiple classes of drugs and consequently infection treatment becomes complicated. Indeed, multidrug-resistant bacteria are currently considered a global health challenge.

On the other hand, the development of new drugs is very slow due to lack of investment. The alarming epidemiological data prompted the WHO to predict that after 2050 deaths from previously treatable infections will be 10 million per year if no action is taken [1]. Increased antibiotic resistance has reduced the effectiveness of therapies by promoting the persistence of infections. The chronicity of many infections is also promoted by the ability of multiple pathogens to form biofilms on biotic or abiotic surfaces [2–4]. A biofilm is a mono- or polymicrobial community of cells embedded in an exopolysaccharide matrix. Within the biofilm, bacteria may be less susceptible to both the effectors of the immune response and antimicrobial drugs, so persistence of the infection is favored. The WHO has estimated that about 80% of chronic infections are related to the formation of biofilms. Many of the drugs currently available hardly penetrate the biofilm and the bacteria in the biofilm are 10–1000 times more resistant than the planktonic counterpart [5].

In this scenario, alternative strategies to conventional antimicrobial therapies are necessary and urgent. Among them, photodynamic therapy (PDT), first considered for the treatment of specific types of cancer [6], has been paid increasing attention as an innovative treatment to eradicate localized infections, supported by antibiotic-resistant biofilm-producing bacteria. [7,8]. Various studies report strategies to prevent biofilm formation on medical devices such as catheters, sutures, stents and bone cement [9–12]. Several researchers are involved in the design and evaluation of specific molecules with potential therapeutic use in chronic and biofilm-related infections [13,14]. In particular, antimicrobial peptides (AMPs), a small bioactive protein consisting of 12–50 amino acids, seem to have emerged as promising active agents against bacteria, viruses, fungi, and also as potential chemotherapeutic agents [15–18].

Plants and microorganisms have always been an invaluable source of secondary metabolites (SM) that could represent an efficient solution to this problem. SM are usually low molecular weight organic compounds produced by various organisms through the action of different enzymes. These specialized metabolites are often not essential for the growth, development, or reproduction of those organisms producing them, but they could be very important for functions such as protection, competition, and species interactions. Most of the SM isolated from microorganisms and plants have been shown to possess a broad spectrum of biological activities including antimicrobial properties. Furthermore, SM belong to diverse structural classes of naturally occurring compounds and have different mechanisms of action, a potential for the development of new drugs to overcome antimicrobial resistance and to treat biofilm-related infections [19–23].

Among the terrestrial ecosystems, forests represent an enormous reservoir of pathogenic and endophytic fungi, which have been studied for several years to evaluate their ability to biosynthesize phytotoxic metabolites. However, several SM produced by these organisms also possess other biological activities (including antibacterial properties) and most of them have shown potential applications in other fields such as medicine and agriculture [24].

Thus, in our continuing effort to find new natural antibacterial metabolites, 20 secondary metabolites produced by pathogenic fungi of forest plants and belonging to different classes of naturally occurring compounds, such as butenolides, cyclohexen oxides, diterpenes, isobenzofuranones, isocoumarins, macrolides, etc., were evaluated for the first time against reference and clinical strains of antibiotic-resistant staphylococci and *P. aeruginosa*.

2. Results and Discussion

The secondary metabolites assayed in this study (**1**–**20**, Figure 1) were isolated as phytotoxins produced by different fungal genera responsible for forest plant diseases such as *Diplodia*, *Seiridium*, *Biscogniauxia*, *Sardiniella* and *Hymenoscyphus* (Table 1) and are potentially involved in plant pathogenesis [25–36].

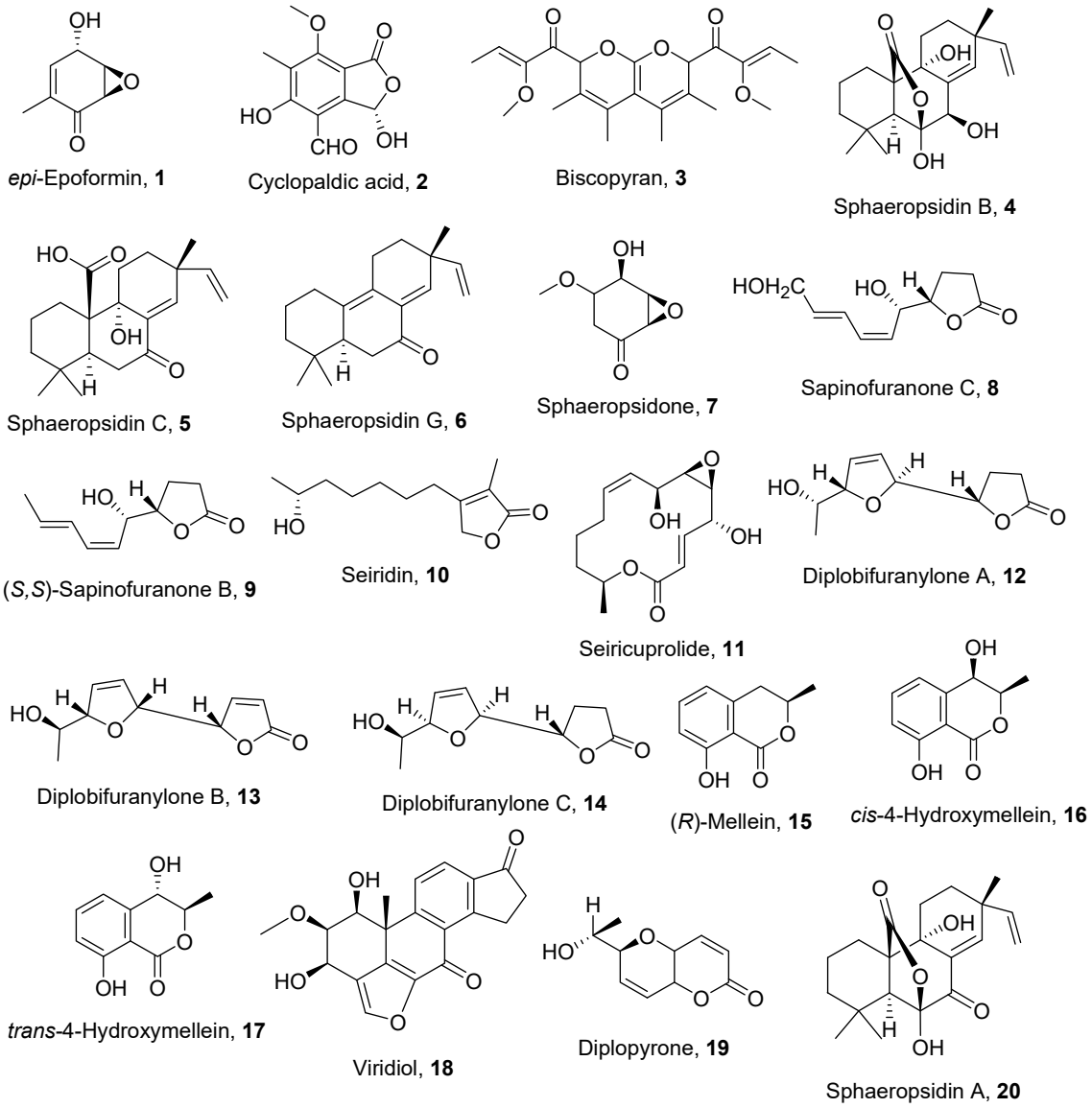

Figure 1. The structures of compounds **1**–**20**.

However, most of these compounds also showed other interesting biological activities as reported in detail in a recent review [24]. In particular, some of them have already been reported for their antifungal activity, such as cyclopaldic acid, *epi*-epoformin, sphaerosidins A–C, sphaeropsidone and (*R*)-mellein [24–26,30,37,38]. In addition, **1** and **2** were able to inhibit the development of two major rust fungi in agrarian crops *P. triticina* and *U. pisi* [39,40]. Compounds **2**, **10** and **20** had larvicidal and biting deterrent activity against *Aedes aegypti* (Diptera: Culicidae), the arboviruses vector responsible for dengue fever [41]. Compound **7** induced haustorium development in radicles of the parasitic weeds *Striga* and *Orobanche* [42]. Compound **20** exhibited in vitro antibacterial activity towards *Xanthomonas oryzae* pv. *oryzae*, the causal agent of rice bacterial blight [43] and showed promising anticancer activity against

drug-resistant melanoma cells [44,45]. Given that the absolute configuration (AC) is strictly linked to biological activity [46,47], the AC of **12**–**14**, **19** and **20** was determined using different methods [48–50].

Table 1. Fungal metabolites used in this study.

Number	Name	Chemical Family	Fungal Source	Ref.
1	*epi*-Epoformin	Cyclohexene oxide	*Diplodia quercivora*	[25]
2	Cyclopaldic acid	Isobenzofuranone	*Seiridium cupressi*	[26]
3	Biscopyran	Pyranopyran	*Biscogniauxia mediterranea*	[27]
4	Sphaeropsidin B	Diterpenoid	*Diplodia cupressi*	[28]
5	Sphaeropsidin C	Diterpenoid	*D. cupressi*	[28]
6	Sphaeropsidin G	Diterpenoid	*Diplodia corticola*	[29]
7	Sphaeropsidone	Cyclohexene oxide	*D. cupressi*	[30]
8	Sapinofuranone C	Furanone	*D. corticola*	[31]
9	(*S*,*S*)-Sapinofuranone B	Furanone	*D. corticola*	[31]
10	Seiridin	Butenolide	*S. cupressi*	[32]
11	Seiricuprolide	Macrolide	*S. cupressi*	[33]
12	Diplobifuranylone A	Furanone	*D. corticola*	[31]
13	Diplobifuranylone B	Furanone	*D. corticola*	[31]
14	Diplobifuranylone C	Furanone	*D. corticola*	[31]
15	(*R*)-Mellein	3,4-Dihydroisocoumarin	*Sardiniella urbana*	[34]
16	*cis*-4-Hydroxymellein	3,4-Dihydroisocoumarin	*S. urbana*	[34]
17	*trans*-4-Hydroxymellein	3,4-Dihydroisocoumarin	*S. urbana*	[34]
18	Viridiol	Furanosteroid	*Hymenoscyphus fraxineus*	[35]
19	Diplopyrone	Pyranopyrone	*D. corticola*	[36]
20	Sphaeropsidin A	Diterpenoid	*D. corticola*	[31]

Compounds **1**–**20** were tested at a single concentration of 100 µg/mL against reference and clinical strains of antibiotic-resistant Gram positive and Gram negative bacteria. *epi*-Epoformin (**1**), sphaeropsidone (**7**), and sphaeropsidin A (**20**) showed antimicrobial activity on all test strains; the growth inhibition rates were higher than 90% for Gram-positive bacteria and ranged from 50 to 100% for Gram-negative bacteria (Table 2). Dimethylsulphoxide (DMSO), used to dissolve the tested compounds, was simultaneously assayed at increasing concentrations (ranging from 0.1% to the maximum concentration used of 1%) to evaluate a possible effect on bacterial growth. The results showed no inhibition of the test strains in the presence of any of the DMSO concentrations used (data not shown). Therefore, the Minimum Inhibitory Concentration (MIC) and Minimum Bactericidal Concentration (MBC) values of substances **1**, **7**, **20** were determined (Table 3).

Sphaeropsidin A (**20**) was effective at low concentrations with MIC values ranging from 6.25 µg/mL to 12.5 µg/mL against all reference and clinical strains of both Gram-negative and Gram-positive bacteria. This result appears to be relevant because multi-drug resistant clinical strains were used as test strains. MBCs of compound **20** ranged from 25 to 100 µg/mL against Gram-positive bacteria, while MBC values were higher than 200 µg/mL for *P. aeruginosa* strains. MIC values of compound **1** were 100 µg/mL against all tested Gram-positive bacteria, with MBCs of 100 µg/mL, suggesting a bactericidal action. MIC values of 50 µg/mL were obtained for compound **1** against *P. aeruginosa* strains, while MBC values were higher than 200 µg/mL. For compound **7**, a MIC at concentrations below 100 µg/mL was not found for any of the test strains; the MBC values were all above 200 µg/mL.

In order to obtain increased antimicrobial activity using lower concentrations of the more active compounds, we evaluated the potential synergistic effect of sphaeropsidin A (**20**) in combination with *epi*-epoformin (**1**) or sphaeropsidone (**7**).

Table 2. Antibacterial activity, expressed as the percentage of growth inhibition, of **1**–**20** at the 100 μg/mL concentration against Gram-positive and Gram-negative test strains [1,2].

Compound	Bacterial Strain					
	S. aureus ATCC 43300	*MRSA*1118-116	*S. haemolyticus* ATCC 29970	*S. haemolyticus* VR 1219-118	*P. aeruginosa* PAO1	*P. aeruginosa* 0418-925
1	≥90	≥90	≥90	≥90	≥90	≥90
2	≥90	≥90	≥90	≥90	-	≥90
3	-	-	-	-	50	60
4	≥90	≥90	≥90	≥90	-	60
5	-	-	-	-	60	60
6	≥90	≥90	≥90	≥90	-	-
7	≥90	≥90	≥90	≥90	50	≥90
8	-	-	-	-	60	60
9	-	-	-	-	60	60
10	-	-	-	-	50	60
11	-	-	-	-	60	50
12	-	-	-	-	50	50
13	-	-	-	-	50	60
14	-	-	-	-	50	60
15	-	-	-	-	60	60
16	-	-	-	-	60	70
17	-	-	-	-	60	60
18	≥90	≥90	≥90	≥90	-	-
19	-	-	-	-	-	-
20	≥90	≥90	≥90	≥90	≥90	≥90
AK	nt	nt	nt	nt	>90	>90
TE	>90	>90	>90	>90	nt	nt

[1] For inhibition values below 50%, no data have been reported (-). AK = Amikacin; TE = Teicoplanin; nt = not tested.
[2] Amikacin (32 μg/mL) and teicoplanin (4 μg/mL) were used as positive controls.

Table 3. MIC (μg/mL) and MBC (μg/mL) of compounds **1**, **7**, **20** against Gram-positive and Gram-negative test strains [1].

Bacterial Strain	Compound 1		Compound 7		Compound 20		Amikacin		Teicoplanin	
	MIC	MBC	MIC	MBC	MIC	MBC	MIC	MBC	MIC	MBC
S. aureus ATCC 43300	100	100	100	>200	12.5	100	nt	nt	1	4
MRSA 1118-116	100	100	100	>200	6.25	25	nt	nt	0.5	4
S. haemolyticus ATCC 29970	100	100	100	>200	12.5	50	nt	nt	2	>4
S. haemolyticus VR 1219-118	100	100	100	>200	12.5	50	nt	nt	2	>4
P. aeruginosa PAO1	50	>200	>100	>200	12.5	>200	4	32	nt	nt
P. aeruginosa 0418-925	50	>200	100	>200	12.5	>200	16	>32	nt	nt

[1] Amikacin and teicoplanin were used as positive controls; nt = not tested.

Compound **7** showed no synergistic effect in combination with sphaeropsidin A (Fractional Inhibitory Concentration (FIC) index = 2, data not shown). For the combination of *epi*-epoformin with sphaeropsidin A, we obtained the highest synergistic interaction against Gram-positive bacteria at a concentration of 6.25 μg/mL sphaeropsidin A (1/2 MIC) and 3.12 μg/mL *epi*-epoformin (1/32 MIC). The highest synergistic interaction against Gram-negative bacteria was obtained at 3.12 μg/mL *epi*-epoformin (1/16 MIC) and 3.12 μg/mL sphaeropsidin A (1/4 MIC) (Figure 2).

The FIC index showed a synergistic effect of *epi*-epoformin and sphaeropsidin A against Gram-negative strains (FIC index < 0.5), and an additive effect against Gram-positive strains (0.5 ≤ FIC index ≤ 1.0).

The cytotoxic activity of metabolites **1**, **7**, and **20** was evaluated on human spontaneously immortalized HaCat keratinocytes. HaCat cells were treated at a concentration ranging from 3.12 μg/mL to 100 μg/mL of metabolites **1**, **7**, and **20** for 24 h and then subjected to the 3-(4,5-dimethylthiazol-2-yl)-2,5-diphenyl tetrazolium bromide (MTT) assay. At a concentration of 100 μg/mL, all tested metabolites dramatically reduced HaCat cell viability. At 12.5 and 6.25 μg/mL, sphaeropsidin A reduced cell viability to 38% and 43%, respectively. However, when HaCat cells were treated with a mixture of 3.12 μg/mL of sphaeropsidin A and 3.12 μg/mL of *epi*-epoformin, cell viability was around 60%. This combination was substantially less cytotoxic than 6.25 μg/mL of each compound alone (Figure 3). This result is encouraging given that the

combination of these two metabolites, at 3.12 µg/mL each, was shown to synergize against Gram-negative strains. A mixture of 6.25 µg/mL of sphaeropsidin A and 3.12 µg/mL of *epi*-epoformin showed an additive effect against Gram-positive bacteria. This combination reduced HaCat cell viability to 54% and was slightly less cytotoxic than 9.37 µg/mL of each compound alone (Figure 3).

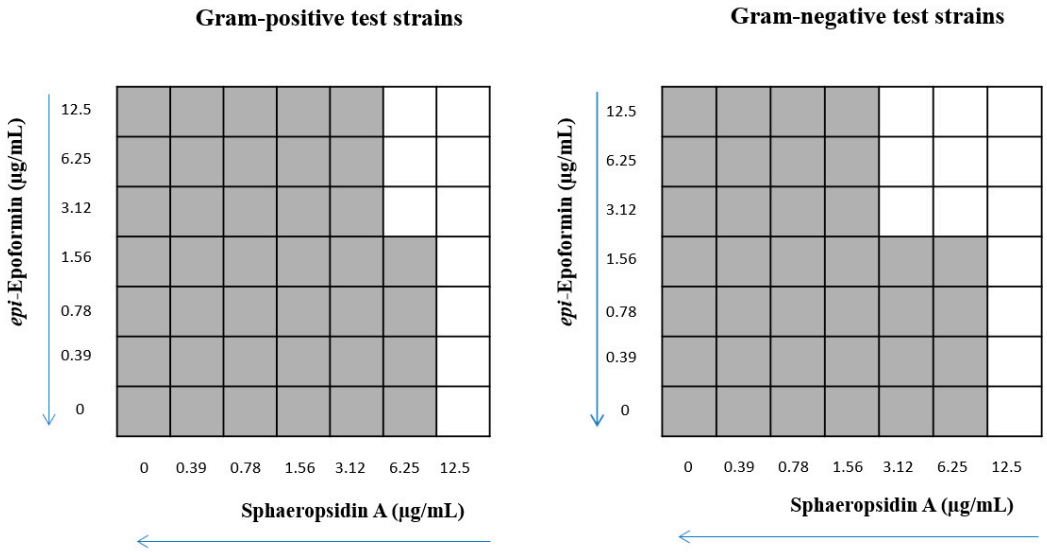

Figure 2. Multi-wells model of checkerboard assay to test the interaction between *epi*-epoformin and sphaeropsidin A. Turbidity was reported in grey and no bacterial growth in white.

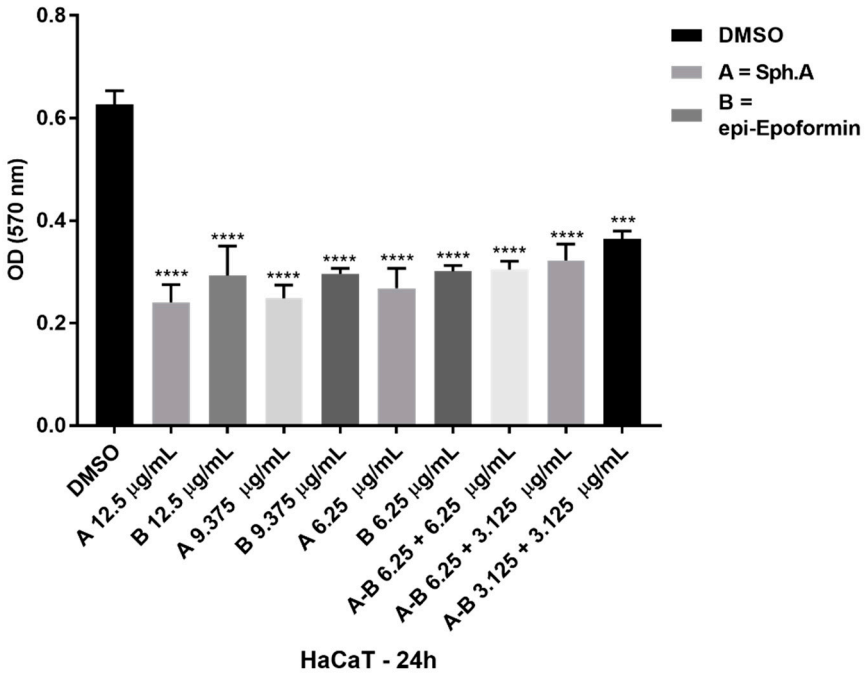

Figure 3. MTT viability test. Hacat cells were incubated with the indicated amount of spheropsidin A (compound A) and *epi*-epoformin (compound B) alone or in combination (AB) for 24 h. The MTT viability test was performed as described in Material. The values were the mean's three values for each experimental point of two biological replicates. Each pair of means were compared using a Tukey's multiple comparisons test *p*-value < 0.05, *** $p < 0.001$; **** $p < 0.0001$)

The persistence of infections is also frequently favored by the ability of bacteria to grow in the form of biofilm, within which the microorganism is protected from the host's response as well as from

many antimicrobial agents. Sphaeropsidin A (**20**) was also tested for its potential ability to inhibit biofilm formation, starting from sub-MIC concentrations that had shown no influence on the planktonic growth of the test strains (data not shown). In comparison with the untreated control, compound **20** was able to reduce the adhesion of *P. aeruginosa* clinical and reference strains by 62% and 50%, respectively, at a concentration of 3.12 μg/mL, corresponding to 1/4 MIC. The biofilm formation of MRSA clinical and reference strains was inhibited by 53% and 60% at the concentration of 1.56 μg/mL and 3. 12 μg/mL, respectively, corresponding to 1/4 MIC of compound **20** (Figure 4).

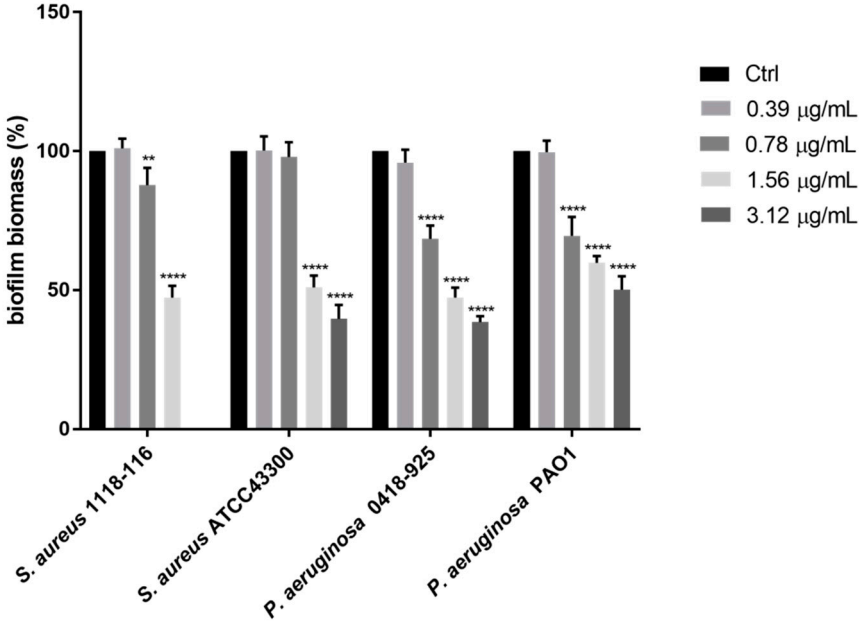

Figure 4. In vitro biofilm formation of test strains following overnight treatment with compound **20** at serial dilutions of sub-MIC concentrations. Biofilm formation was determined by cristal violet assay. Values are presented as mean percentage ± SD. ** p-value = 0.009, **** p-value < 0.001.

The formation of biofilm by *S. haemolyticus* strains did not appear to be inhibited by sphaeropsidin A. This latter, tested in synergy with *epi*-epoformin in combinations lower than the synergistic concentrations inhibiting planktonic growth, did not influence the anti-biofilm effect showed by sphaeropsidin A alone (data not shown).

S. aureus, as commensal of the skin, and *P. aeruginosa*, as an environmental saprophyte, are the most frequent opportunistic pathogens causing infections of surgical and traumatic wounds and burns [51–54]. The isolation of antibiotic resistant strains is continuously increasing [55–57]. Moreover, their attachment to host tissues, as well as to medical implants and the production of biofilm, play an important role in the persistence of these infections [58,59]. The establishment of a mature biofilm, which is significantly less sensitive to antimicrobial agents than genetically identical non-adherent planktonic cells, considerably delays the healing process [4,60,61]. A biofilm-focused therapeutic approach, that reduces the ability of these pathogens to form biofilms, would decrease the antibiotic recalcitrance of these infections, thus allowing treatment with the antibiotics in use, and faster and more effective healing. Therefore, our data seems to be interesting since sphaeropsidin A appears capable of reducing biofilm formation by all the test strains. To our knowledge, this is the first report on the anti-biofilm activity of sphaeropsidin A. This compound was able to inhibit the biofilm of clinical MRSA at a concentration of 1.56 μg/mL; this result encourages further studies on a greater number of clinical strains and on other bacterial species. In addition, *epi*-epoformin and sphaeropsidin A synergized against Gram-negative and showed an additive effect against Gram-positive bacteria. However, the clinical value of a drug is strictly dependent on the evaluation of its cytotoxicity for the host cells, but sphaeropsidin A and *epi*-epoformin did not show sufficient selectivity between

bacteria and eukaryotic cells. Nevertheless, in our opinion, the screening performed represents a promising basis to identify scaffolds with antimicrobial potential. *epi*-Epoformin, spheropsidone and sphaeropsidin A (**1**, **7** and **20**) contain structural features known to be responsible for such activity in naturally occurring compounds [62]. The functionalities are the epoxy group in **1** and **7** and the α, β-unsaturated ketone group in **1** and **20**, which could react with a nucleophilic group of the receptor (such as -NH_2 or -SH, etc.). In fact, the epoxide, through a bimolecular nucleophilic substitution (SN_2), and the α, β-unsaturated carbonyl group, through a Michael addition, could yield conjugates with a stable covalent bond, which could also be shown using spectroscopic techniques such as MS-TOF [63]. The knowledge of the action mechanism of these compounds could suggest chemical modifications of their structure to synthesize derivatives with acceptable biocompatibility and improved antimicrobial properties against multi-resistant and biofilm-producing bacteria.

3. Conclusions

Our results represent preliminary data on the antimicrobial activity of fungal secondary metabolites evaluated for the first time against clinical isolates of *P. aeruginosa* and *S. aureus*, considered as common opportunistic pathogens inducing severe human infections. Sphaeropsidin A activity appears noteworthy for its ability to inhibit biofilm formation, preventing a growth mode that results in particular resistance to antibiotic treatment. The results obtained are preliminary to further experiments aimed at developing biocompatible formulations of *epi*-epoformin and sphaeropsidin A, suitable for wound treatment to prevent the development of serious infections.

4. Materials and Methods

4.1. General Experimental Procedures

The secondary metabolites used in this study (**1**–**20**, Figure 1) have been isolated from pathogenic fungifollowing procedures previously reported and listed in Table 1. All the data regarding their source, their chemical family and literature are reported in Table 1. The purity of each compound was >98%, as ascertained by TLC, ESI-MS and NMR using well-established methods. Analytical and preparative thin-layer chromatography (TLC) was performed on silica gel (Kieselgel 60, F_{254}, 0.25 and 0.5 mm respectively) plates (Merck, Darmstadt, Germany); the spots were visualized by exposure to UV light or by spraying with 10% H_2SO_4 in CH_3OH and then 5% phosphomolybdic acid in EtOH, followed by heating at 110 °C for 10 min. ESI-MS spectra were recorded on Agilent Technologies 6120 quadrupole LC/MS instrument (Agilent instruments, Milan, Italy); ^{1}H NMR spectra were recorded at 400 MHz, on Bruker spectrometer (Bruker BioSpin GmbH., Karlsruhe, Germany), using the same solvent as an internal standard.

4.2. Microbial Strains and Culture Conditions

Bacterial strains used in this study were methicillin-resistant *Staphylococcus aureus* ATCC 43300, *Staphylococcus haemolyticus* ATCC 29970 and *Pseudomonas aeruginosa* PAO1 as reference strains, and three multi-drug resistant clinical isolates: methicillin-resistant *S. aureus* (MRSA) 1118-116, methicillin and vancomycin-resistant *S. haemolythicus* (VRSH) 1219-118, and extended-spectrum beta-lactamase (ESBL) producing *P. aeruginosa* 0418-925. The strains were obtained from a collection previously established at the Department of Molecular Medicine and Medical Biotechnologies (University of Naples Federico II). No ethical approval was required for the study because there was no access to patients' data. All strains were stored as 15% (v/v) glycerol stocks at −80 °C. Before each experiment, cells were sub-cultured from the stocks onto TSA plates at 37 °C for 24 h. Identification was performed by biochemical characterization using the Vitek2 (Biomerieux, Mercy-l'Etoile, France) and Phoenix (Becton Dickinson, Sparks, MD, USA) systems and confirmed by MS MALDI-TOF (Bruker Daltonics, Bremen, Germany). Susceptibility to antibiotics was assessed using automatic (Vitek2; Phoenix) and Kirby Bauer disk diffusion (Thermo Fisher Scientific, Basingstoke, UK) antibiotic sensitivity testing.

4.3. Antimicrobial Assays

The initial screening of 20 fungal metabolites was performed by standard broth micro-dilution assay in 96-wells polystyrene plates using Mueller-Hinton Broth 2 (MHB2) to test a single high concentration against all test strains. Briefly, 2 × stock solutions of all compounds were made by dissolving them in 2% DMSO. For each strain, the cell suspension was prepared at 0.5 McFarland standard (corresponding to approximately 10^8 CFU/mL) and subsequently adjusted to approximately 5×10^6 CFU/mL^{-1}. One hundred µL aliquots (5×10^5 CFU) of these bacterial suspensions were treated with 100 µL of 100 µg/mL solution of the compound under investigation; wells with only MHB2 were used as negative control and wells with no compounds as positive growth control. The effect of serial dilutions of DMSO starting from 1% on the growth of test strains was separately tested. Plates were incubated at 37 °C for 19 h under shaking (300 rpm). Then the medium turbidity was measured by a microtiter plate reader at 595 nm (Bio-rad Laboratories s.r.l.). Antimicrobial activity was expressed as a percentage of microbial growth inhibition. Each compound was tested in triplicate and each experiment was performed twice. Minimal inhibitory concentration (MIC) and Minimal Bactericidal Concentration (MBC) of selected compounds were determined by the broth micro-dilution assay. The starting inoculum was 5×10^6 CFU mL^{-1}, and the concentrations of the metabolites ranged from 200 to 0.78 µg/mL (twofold dilutions). As positive controls, conventional antimicrobials, selected depending on antibiotic-susceptibility profiles of the test strains, were included: amikacin (ranged from 32 to 2 µg/mL) was used for Gram-negative strains and teicoplanin (ranged from 0.5 to 4 µg/mL) for Gram-positive strains. Medium turbidity was measured by a microtiter plate reader at 595 nm. The MIC was defined as the lowest concentration of compound that caused ≥90% inhibition of bacterial growth. The MBCs were determined by transferring 200 µL of each sample, previously treated with compound concentrations equal to or higher than the MIC, onto TSA plates and incubating the plates at 37 °C for 24/48 h. The lowest compound concentration that yields no microbial growth on agar plates will be defined as the MBC. Each compound was tested in triplicate; each experiment was performed twice.

4.4. Synergy Assays

The interactions between selected metabolites were evaluated by the checkerboard method in 96-well microtiter plates [64]. The compounds to be tested in combination were serially diluted, one along with the x-axis and the other along with the y-axis. The final compounds' concentrations (after two-fold dilutions) varied from 0.19 µg/mL up to the 12.5 µg/mL for each one. The checkerboard plates were inoculated with test strains at a concentration of 5×10^6 CFU/mL and incubated at 37 °C for 19 h, then the microbial growth was visually assessed, and the turbidity measured by the microplate reader at 595 nm. To evaluate the effect of the combination treatment, the fractional inhibitory concentration (FIC) index for each combination was calculated as follows: FIC index = FIC of compound A + FIC of compound B, where FIC of compound A (or compound B) will be defined as the ratio of MIC of compound A (or compound B) in combination and MIC of compound A (or of compound B) alone. The FIC index values are interpreted as follows: ≤0.5, synergistic; >0.5 to ≤1.0, additive; >1.0 to ≤2.0, indifferent; and >2.0, antagonistic effects [64].

4.5. Biofilm Formation Inhibition Assay

The total biomass of the biofilm was analyzed using the Crystal Violet (CV) staining method in flat-bottomed 96-well microplates as described by Stepanović et al. [65]. For each strain, a cell suspension in MHB2 supplemented with 10% (w/v) glucose was prepared for turbidity of 0.5 McFarland. This suspension was further diluted at 1:100 and 100 µL of the suspension (1×10^6 CFU/mL) were incubated with 100 µL of MHB2 containing the selected compound at serial dilutions of sub-MIC concentrations. The negative control was prepared by inoculating 200 µL of a microbial suspension inactivated by boiling. The positive controls were compound-free wells. To assess biofilm formation,

the culture broth was gently aspirated, and each well was washed twice with PBS to remove exclusively non-adherent cells and dried at 60 °C for 45 min. The biofilm was stained by incubation for 30 min with 100 µL of a 0.1% (w/v) crystal violet solution. Any excess of crystal violet was removed by washing with PBS before adding 200 µL of absolute ethanol to release the dye from the biofilm. The absorbance was measured at 595 nm by a microplate reader and was related to the amount of biofilm produced. The percentage of biofilm mass reduction was calculated using the formula: [(Ac-At)/Ac] × 100, where Ac is the OD595 for control wells and At is the OD595 in the presence of the tested compound.

4.6. Cytotoxicity Test

HaCaT (human spontaneously immortalized keratinocytes from adult skin) were purchased from Cell Line Service (CLS, Hattersheim am Main, Germany). Cells were cultured in DMEM High Glucose (Gibco BRL Thermo Fisher, Milan, Italy) supplemented with 10% Fetal Bovine Serum (Gibco BRL, Thermo Fisher, Milan, Italy), 1% L-Glutamine (Gibco BRL) and 1% Pen-Strep solution (Gibco BRL) in a humidified incubator at 37 °C and 5% CO_2. Cells were routinely checked for mycoplasma contamination, using a mycoplasma detection kit (ABM, Vancouver, Canada). Cytotoxicity was determined by the MTT 3-(4,5-dimethylthiazol-2-yl)-2,5-diphenyl tetrazolium bromide assay (Sigma-Aldrich, St Louis, MO, USA). HaCaT were seeded in 24-well plates at 3.0×10^4 per well and treated with sphaeropsidin A, sphaeropsidone, and *epi*-epoformin at concentrations between 3.125 µg/mL and 100 µg/mL for 24 h. The assay was performed according to the manufacturer's instructions. The optical absorbance was determined at 570 nm and 630 nm using an iMark microplate reader (Bio-Rad, Milan, Italy). Each value shown in the plot is mean ± SD of triplicate determinations. Asterisks represent significant results (*** $p > 0.001$; **** $p < 0.0001$).

4.7. Statistical Analysis

Statistical analyses were carried out using the GraphPad Prism 8 software (San Diego, CA). Data were represented as the mean ± standard deviation and analyzed for statistical significance using ordinary one-way or two-way analysis of variance (ANOVA) and multiple comparisons. For all tests, $p < 0.005$ was considered to indicate a statistically significant difference.

Author Contributions: All the authors contributed to the design of the study, the analysis of the data and writing of the manuscript. provided the fungal cultures and their organic extracts, L.M.; purified the metabolites used in this study R.D.L.; conducted the experiments, E.R., M.E., M.M. and A.D.; writing—original draft preparation, M.M. and E.R.; writing—review and editing, V.C., A.E. and M.R.C.; funding acquisition, M.M. All authors have read and agreed to the published version of the manuscript.

Funding: This research was funded by Programme STAR 2017, financially supported by UniNA and Compagnia di San Paolo, grant number E62F16001250003 to M.M. and DAAD Mobility Program 2018–2020 to V.C.

Acknowledgments: A.E. is associated with "Istituto di Chimica Biomolecolare del CNR", Pozzuoli, Italy.

Conflicts of Interest: The authors declare no conflict of interest.

References

1. World Health Organization (WHO); Antimicrobial Resistance. No Time to Wait: Securing the Future from Drug-Resistant Infections. Report to the Secretary-General of the United Nations. Available online: https://www.who.int/antimicrobial-resistance/interagency-coordination-group/IACG_final_report_EN.pdf?ua=1 (accessed on 8 April 2020).
2. Ciofu, O.; Mandsberg, L.F.; Wang, H.; Høiby, N. Phenotypes selected during chronic lung infection in cystic fibrosis patients: Implications for the treatment of *Pseudomonas aeruginosa* biofilm infections. *FEMS Immunol. Med. Microbiol.* **2012**, *65*, 215–225. [CrossRef]
3. Cantone, E.; Negri, R.; Roscetto, E.; Grassia, R.; Catania, M.R.; Capasso, P.; Maffei, M.; Soriano, A.A.; Leone, C.A.; Iengo, M.; et al. In vivo biofilm formation, Gram-negative infections and TAS2R38 polymorphisms in CRSw NP patients. *Laryngoscope* **2018**, *128*, E339–E345. [CrossRef] [PubMed]

4. Gebreyohannes, G.; Nyerere, A.; Bii, C.; Sbhatu, D.B. Challenges of intervention, treatment, and antibiotic resistance of biofilm-forming microorganisms. *Heliyon* **2019**, *5*, e02192. [CrossRef] [PubMed]
5. Hall, C.W.; Mah, T.F. Molecular mechanisms of biofilm-based antibiotic resistance and tolerance in pathogenic bacteria. *FEMS Microbiol. Rev.* **2017**, *41*, 276–301. [CrossRef] [PubMed]
6. Zhang, Q.; Li, L. Photodynamic combinational therapy in cancer treatment. *J. Buon.* **2018**, *23*, 561–567.
7. Barra, F.; Roscetto, E.; Soriano, A.A.; Vollaro, A.; Postiglione, I.; Pierantoni, G.M.; Palumbo, G.; Catania, M.R. Photodynamic and antibiotic therapy in combination to fight biofilms and resistant surface bacterial infections. *Int. J. Mol. Sci.* **2015**, *16*, 20417–20430. [CrossRef]
8. Hu, X.; Huang, Y.Y.; Wang, Y.; Wang, X.; Hamblin, M.R. Antimicrobial photodynamic therapy to control clinically relevant biofilm infections. *Front. Microbiol.* **2018**, *9*, 1299. [CrossRef]
9. Leaper, D.; Wilson, P.; Assadian, O.; Edmiston, C.; Kiernan, M.; Miller, A.; Bond-Smith, G.; Yap, J. The role of antimicrobial sutures in preventing surgical site infection. *Ann. R. Coll. Surg. Engl.* **2017**, *99*, 439–443. [CrossRef] [PubMed]
10. Balato, G.; Roscetto, E.; Vollaro, A.; Galasso, O.; Gasparini, G.; Ascione, T.; Catania, M.R.; Mariconda, M. Bacterial biofilm formation is variably inhibited by different formulations of antibiotic-loaded bone cement in vitro. *Knee Surg. Sports Traumatol. Arthrosc.* **2019**, *27*, 1943–1952. [CrossRef] [PubMed]
11. Malek, A.E.; Raad, I.I. Preventing catheter-related infections in cancer patients: A review of current strategies. *Expert Rev. Anti. Infect. Ther.* **2020**. [CrossRef] [PubMed]
12. Artini, M.; Cicatiello, P.; Ricciardelli, A.; Papa, R.; Selan, L.; Dardano, P.; Tilotta, M.; Vrenna, G.; Tutino, M.L.; Giardina, P.; et al. Hydrophobin coating prevents *Staphylococcus epidermidis* biofilm formation on different surfaces. *Biofouling* **2017**, *33*, 601–611. [CrossRef] [PubMed]
13. Vila, J.; Moreno-Morales, J.; Ballesté-Delpierre, C. Current landscape in the discovery of novel antibacterial agents. *Clin. Microbiol. Infect.* **2019**, *26*, 596–603. [CrossRef]
14. Ricciardelli, A.; Casillo, A.; Papa, R.; Monti, D.M.; Imbimbo, P.; Vrenna, G.; Artini, M.; Selan, L.; Corsaro, M.M.; Tutino, M.L.; et al. Pentadecanal inspired molecules as new antibiofilm agents against *Staphylococcus epidermidis*. *Biofouling* **2018**, *34*, 1110–1120. [CrossRef] [PubMed]
15. Chung, P.Y.; Khanum, R. Antimicrobial peptides as potential anti-biofilm agents against multidrug-resistant bacteria. *J. Microbiol. Immunol. Infect.* **2017**, *50*, 405–410. [CrossRef] [PubMed]
16. Roscetto, E.; Contursi, P.; Vollaro, A.; Fusco, S.; Notomista, E.; Catania, M.R. Antifungal and anti-biofilm activity of the first cryptic antimicrobial peptide from an archaeal protein against *Candida* spp. clinical isolates. *Sci. Rep.* **2018**, *8*, 1–11. [CrossRef]
17. He, M.; Zhang, H.; Li, Y.; Wang, G.; Tang, B.; Zhao, J.; Huang, Y.; Zheng, J. Cathelicidin-derived antimicrobial peptides inhibit Zika virus through direct inactivation and interferon pathway. *Front. Immunol.* **2018**, *9*, 722. [CrossRef]
18. Gaglione, R.; Pirone, L.; Farina, B.; Fusco, S.; Smaldone, G.; Aulitto, M.; Dell'Olmo, E.; Roscetto, E.; Del Gatto, A.; Fattorusso, R.; et al. Insights into the anticancer properties of the first antimicrobial peptide from Archaea. *Biochim. Biophys. Acta Gen. Subj.* **2017**, *1861*, 2155–2164. [CrossRef]
19. Li, J.W.H.; Vederas, J.C. Drug discovery and natural products: End of an era or an endless frontier? *Science* **2009**, *325*, 161–165. [CrossRef]
20. Cragg, G.M.; Newman, D.J. Natural products: A continuing source of novel drug leads. *Biochim. Biochim. Biophys. Acta Gen. Subj.* **2013**, *1830*, 3670–3695. [CrossRef]
21. Schueffler, A.; Anke, T. Fungal natural products in research and development. *Nat. Prod. Rep.* **2014**, *31*, 1425–1448. [CrossRef]
22. Thomford, N.E.; Senthebane, D.A.; Rowe, A.; Munro, D.; Seele, P.; Maroyi, A.; Dzobo, K. Natural products for drug discovery in the 21st century: Innovations for novel drug discovery. *Int. J. Mol. Sci.* **2018**, *19*, 1578. [CrossRef]
23. Wright, G.D. Unlocking the potential of natural products in drug discovery. *Microb. Biotechnol.* **2019**, *12*, 55–57. [CrossRef] [PubMed]
24. Masi, M.; Maddau, L.; Linaldeddu, B.T.; Scanu, B.; Evidente, A.; Cimmino, A. Bioactive metabolites from pathogenic and endophytic fungi of forest trees. *Curr. Med. Chem.* **2018**, *25*, 208–252. [CrossRef] [PubMed]
25. Andolfi, A.; Maddau, L.; Basso, S.; Linaldeddu, B.T.; Cimmino, A.; Scanu, B.; Deidda, A.; Tuzi, A.; Evidente, A. Diplopimarane, a 20-nor-ent-pimarane produced by the oak pathogen *Diplodia quercivora*. *J. Nat. Prod.* **2014**, *77*, 2352–2360. [CrossRef] [PubMed]

26. Graniti, A.; Sparapano, L.; Evidente, A. Cyclopaldic acid, a major phytotoxic metabolite of *Seiridium cupressi*, the pathogen of a canker disease of cypress. *Plant Pathol.* **1992**, *41*, 563–568. [CrossRef]
27. Evidente, A.; Andolfi, A.; Maddau, L.; Franceschini, A.; Marras, F. Biscopyran, a phytotoxic hexasubstituted pyranopyran produced by *Biscogniauxia mediterranea*, a fungus pathogen of cork oak. *J. Nat. Prod.* **2005**, *68*, 568–571. [CrossRef]
28. Evidente, A.; Sparapano, L.; Fierro, O.; Bruno, G.; Giordano, F.; Motta, A. Sphaeropsidins B and C, phytotoxic pimarane diterpenes from *Sphaeropsis sapinea* f. sp. *cupressi* and *Diplodia mutila*. *Phytochemistry* **1997**, *45*, 705–713. [CrossRef]
29. Cimmino, A.; Maddau, L.; Masi, M.; Evidente, M.; Linaldeddu, B.T.; Evidente, A. Further secondary metabolites produced by *Diplodia corticola*, a fungal pathogen involved in cork oak decline. *Tetrahedron* **2016**, *72*, 6788–6793. [CrossRef]
30. Evidente, A.; Maddau, L.; Scanu, B.; Andolfi, A.; Masi, M.; Motta, A.; Tuzi, A. Sphaeropsidones, phytotoxic dimedone methyl ethers produced by *Diplodia cupressi*: A structure-activity relationship study. *J. Nat. Prod.* **2011**, *74*, 757–763. [CrossRef]
31. Masi, M.; Maddau, L.; Linaldeddu, B.T.; Cimmino, A.; D'Amico, W.; Scanu, B.; Evidente, M.; Tuzi, A.; Evidente, A. Bioactive secondary metabolites produced by the oak pathogen *Diplodia corticola*. *J. Agric. Food Chem.* **2016**, *64*, 217–225. [CrossRef] [PubMed]
32. Evidente, A.; Randazzo, G.; Ballio, A. Structure determination of seiridin and isoseiridin, phytotoxic butenolides from culture filtrate of *Seiridium cardinale*. *J. Nat. Prod.* **1986**, *49*, 593–601. [CrossRef]
33. Ballio, A.; Evidente, A.; Graniti, A.; Randazzo, G.; Sparapano, L. Seiricuprolide, a new phytotoxic macrolide from a strain of *Seiridium cupressi* infecting cypress. *Phytochemistry* **1988**, *27*, 3117–3121. [CrossRef]
34. Cimmino, A.; Maddau, L.; Masi, M.; Linaldeddu, B.T.; Evidente, A. Secondary metabolites produced by *Sardiniella urbana*, a new emerging pathogen on European hackberry. *Nat. Prod. Res.* **2019**, *33*, 1862–1869. [CrossRef]
35. Masi, M.; Di Lecce, R.; Tuzi, A.; Linaldeddu, B.T.; Montecchio, L.; Maddau, L.; Evidente, A. Hyfraxinic acid, a phytotoxic tetrasubstituted octanoic Acid, produced by the ash (*Fraxinus excelsior* L.) pathogen *Hymenoscyphus fraxineus* together with viridiol and some of its analogues. *J. Agric. Food Chem.* **2019**, *67*, 13617–13623. [CrossRef] [PubMed]
36. Evidente, A.; Maddau, L.; Spanu, E.; Franceschini, A.; Lazzaroni, S.; Motta, A. Diplopyrone, a new phytotoxic tetrahydropyranpyran-2-one produced by *Diplodia mutila*, a fungus pathogen of cork oak. *J. Nat. Prod.* **2003**, *66*, 313–315. [CrossRef] [PubMed]
37. Sparapano, L.; Bruno, G.; Fierro, O.; Evidente, A. Studies on structure–activity relationship of sphaeropsidins A–F, phytotoxins produced by *Sphaeropsis sapinea* f. sp. *cupressi*. *Phytochemistry* **2004**, *65*, 189–198. [CrossRef]
38. Reveglia, P.; Masi, M.; Evidente, A. Melleins—Intriguing natural compounds. *Biomolecules* **2020**, *10*, 772. [CrossRef] [PubMed]
39. Barilli, E.; Cimmino, A.; Masi, M.; Evidente, M.; Rubiales, D.; Evidente, A. Inhibition of spore germination and appressorium formation of rust species by plant and fungal metabolites. *Nat. Prod. Commun.* **2016**, *11*, 1934578X1601100940. [CrossRef]
40. Barilli, E.; Cimmino, A.; Masi, M.; Evidente, M.; Rubiales, D.; Evidente, A. Inhibition of early development stages of rust fungi by the two fungal metabolites cyclopaldic acid and *epi*-epoformin. *Pest Manag. Sci.* **2017**, *73*, 1161–1168. [CrossRef] [PubMed]
41. Cimmino, A.; Andolfi, A.; Avolio, F.; Ali, A.; Tabanca, N.; Khan, I.A.; Evidente, A. Cyclopaldic Acid, seiridin, and sphaeropsidin a as fungal phytotoxins, and larvicidal and biting deterrents against *Aedes aegypti* (Diptera: Culicidae): Structure-activity relationships. *Chem. Biodivers.* **2013**, *10*, 1239–1251. [CrossRef]
42. Fernández-Aparicio, M.; Masi, M.; Maddau, L.; Cimmino, A.; Evidente, M.; Rubiales, D.; Evidente, A. Induction of haustorium development by sphaeropsidones in radicles of the parasitic weeds *Striga* and *Orobanche*. A structure–activity relationship study. *J. Agric. Food Chem.* **2016**, *64*, 5188–5196. [CrossRef] [PubMed]
43. Evidente, A.; Venturi, V.; Masi, M.; Degrassi, G.; Cimmino, A.; Maddau, L.; Andolfi, A. In vitro antibacterial activity of sphaeropsidins and chemical derivatives toward *Xanthomonas oryzae* pv. *oryzae*, the causal agent of rice bacterial blight. *J. Nat. Prod.* **2011**, *74*, 2520–2525. [CrossRef] [PubMed]

44. Mathieu, V.; Chantôme, A.; Lefranc, F.; Cimmino, A.; Miklos, W.; Paulitschke, V.; Mohr, T.; Maddau, L.; Kornienko, A.; Berger, W.; et al. Sphaeropsidin A shows promising activity against drug-resistant cancer cells by targeting regulatory volume increase. *Cell. Mol. Life Sci.* **2015**, *72*, 3731–3746. [CrossRef] [PubMed]
45. Ingels, A.; Dinhof, C.; Garg, A.D.; Maddau, L.; Masi, M.; Evidente, A.; Berger, W.; Dejaegher, B.; Mathieu, V. Computed determination of the in vitro optimal chemocombinations of sphaeropsidin A with chemotherapeutic agents to combat melanomas. *Cancer Chemoth. Pharmacol.* **2017**, *79*, 971–983. [CrossRef]
46. Evidente, A.; Andolfi, A.; Cimmino, A. Relationships between the stereochemistry and biological activity of fungal phytotoxins. *Chirality* **2011**, *23*, 674–693. [CrossRef]
47. Evidente, A.; Cimmino, A.; Andolfi, A. The effect of stereochemistry on the biological activity of natural phytotoxins, fungicides, insecticides and herbicides. *Chirality* **2013**, *25*, 59–78. [CrossRef]
48. Masi, M.; Cimmino, A.; Maddau, L.; Kornienko, A.; Tuzi, A.; Evidente, A. Crystal structure and absolute configuration of sphaeropsidin A and its 6-o-*p*-bromobenzoate. *Tetrahedron Lett.* **2016**, *57*, 4592–4594. [CrossRef]
49. Mazzeo, G.; Cimmino, A.; Masi, M.; Longhi, G.; Maddau, L.; Memo, M.; Evidente, A.; Abbate, S. Importance and difficulties in the use of chiroptical methods to assign the absolute configuration of natural products: The case of phytotoxic pyrones and furanones produced by *Diplodia corticola*. *J. Nat. Prod.* **2017**, *80*, 2406–2415. [CrossRef]
50. Fusè, M.; Mazzeo, G.; Longhi, G.; Abbate, S.; Masi, M.; Evidente, A.; Puzzarini, C.; Barone, V. Unbiased determination of absolute configurations by vis-à-vis comparison of experimental and simulated spectra: The challenging case of diplopyrone. *J. Phys. Chem. B* **2019**, *123*, 9230–9237. [CrossRef]
51. Fazli, M.; Bjarnsholt, T.; Kirketerp-Møller, K.; Jørgensen, B.; Andersen, A.S.; Krogfelt, K.A.; Givskov, M.; Tolker-Nielsen, T. Nonrandom distribution of *Pseudomonas aeruginosa* and *Staphylococcus aureus* in chronic wounds. *J. Clin. Microbiol.* **2009**, *47*, 4084–4089. [CrossRef]
52. Martin, J.M.; Zenilman, J.M.; Lazarus, G.S. Molecular microbiology: New dimensions for cutaneous biology and wound healing. *J. Investig. Dermatol.* **2010**, *130*, 38–48. [CrossRef] [PubMed]
53. Lachiewicz, A.M.; Hauck, C.G.; Weber, D.J.; Cairns, B.A.; van Duin, D. Bacterial infections after burn injuries: Impact of multidrug resistance. *Clin. Infect. Dis.* **2017**, *65*, 2130–2136. [CrossRef] [PubMed]
54. Eisner, R.; Lippmann, N.; Josten, C.; Rodloff, A.C.; Behrendt, D. Development of the bacterial spectrum and antimicrobial resistance in surgical site infections of trauma patients. *Surg. Infect.* **2020**. [CrossRef] [PubMed]
55. Kaur, A.; Singh, S. Prevalence of extended spectrum betalactamase (ESBL) and metallobetalactamase (MBL) producing *Pseudomonas aeruginosa* and *Acinetobacter baumannii* isolated from various clinical samples. *J. Pathog.* **2018**, *2018*, 6845985. [CrossRef] [PubMed]
56. Royer, G.; Fourreau, F.; Boulanger, B.; Mercier-Darty, M.; Ducellier, D.; Cizeau, F.; Potron, A.; Podglajen, I.; Mongardon, N.; Decousser, J.W. Local outbreak of extended-spectrum β-lactamase SHV2a-producing *Pseudomonas aeruginosa* reveals the emergence of a new specific sub-lineage of the international ST235 high-risk clone. *J. Hosp. Infect.* **2020**, *104*, 33–39. [CrossRef] [PubMed]
57. Vestergaard, M.; Frees, D.; Ingmer, H. Antibiotic resistance and the MRSA problem. *Gram Posit. Pathog.* **2019**, *7*, 747–765.
58. Serra, R.; Grande, R.; Butrico, L.; Rossi, A.; Settimio, U.F.; Caroleo, B.; Amato, B.; Gallelli, L.; de Franciscis, S. Chronic wound infections: The role of *Pseudomonas aeruginosa* and *Staphylococcus aureus*. *Expert. Rev. Anti. Infect. Ther.* **2015**, *13*, 605–613. [CrossRef] [PubMed]
59. De Vor, L.; Rooijakkers, S.H.M.; van Strijp, J.A.G. Staphylococci evade the innate immune response by disarming neutrophils and forming biofilms. *FEBS Lett.* **2020**. [CrossRef]
60. Wolcott, R.D. Biofilms cause chronic infections. *J. Wound Care* **2017**, *26*, 423–425. [CrossRef]
61. Roy, S.; Santra, S.; Das, A.; Dixith, S.; Sinha, M.; Ghatak, S.; Ghosh, N.; Banerjee, P.; Khanna, S.; Mathew-Steiner, S.; et al. *Staphylococcus aureus* biofilm infection compromises wound healing by causing deficiencies in granulation tissue collagen. *Ann. Surg.* **2019**. [CrossRef]
62. Dewick, P.M. *Medicinal Natural Products: A Biosynthetic Approach*, 3rd ed.; John Wiley & Sons: Chichester, UK, 2009.
63. Le Calve, B.; Lallemand, B.; Perrone, C.; Lenglet, G.; Depauw, S.; Van Goietsenoven, G.; Bury, M.; Vurro, M.; Herphelin, F.; Andolfi, A.; et al. In vitro anticancer activity, toxicity and structure–activity relationships of phyllostictine A, a natural oxazatricycloalkenone produced by the fungus *Phyllosticta cirsii*. *Toxicol. Appl. Pharmacol.* **2011**, *254*, 8–17. [CrossRef] [PubMed]

64. Pillai, S.K.; Moellering, R.C.; Eliopoulos, G.M. Antimicrobial combinations. In *Antibiotics in Laboratory. Medicine*, 5th ed.; Lorian, V., Ed.; The Lippincott Williams & Wilkins Co.: Philadelphia, PA, USA, 2005; pp. 365–440.
65. Stepanović, S.; Vuković, D.; Hola, V.; di Bonaventura, G.; Djukić, S.; Cirković, I.; Ruzicka, F. Quantification of biofilm in microtiter plates: Overview of testing conditions and practical recommendations for assessment of biofilm production by Staphylococci. *Apmis* **2007**, *115*, 891–899. [CrossRef] [PubMed]

SCIENTIFIC REPORTS

OPEN

YB-1 recruitment to stress granules in zebrafish cells reveals a differential adaptive response to stress

Received: 27 September 2018
Accepted: 4 June 2019
Published online: 21 June 2019

Andrea Maria Guarino[1], Giuseppe Di Mauro[2,3], Gennaro Ruggiero[2], Nathalie Geyer[2], Antonella Delicato[1], Nicholas S. Foulkes[2], Daniela Vallone[2] & Viola Calabrò[1]

The survival of cells exposed to adverse environmental conditions entails various alterations in cellular function including major changes in the transcriptome as well as a radical reprogramming of protein translation. While in mammals this process has been extensively studied, stress responses in non-mammalian vertebrates remain poorly understood. One of the key cellular responses to many different types of stressors is the transient generation of structures called stress granules (SGs). These represent cytoplasmic foci where untranslated mRNAs are sorted or processed for re-initiation, degradation, or packaging into mRNPs. Here, using the evolutionarily conserved Y-box binding protein 1 (YB-1) and G3BP1 as markers, we have studied the formation of stress granules in zebrafish (*D. rerio*) in response to different environmental stressors. We show that following heat shock, zebrafish cells, like mammalian cells, form stress granules which contain both YB-1 and G3BP1 proteins. Moreover, zfYB-1 knockdown compromises cell viability, as well as recruitment of G3BP1 into SGs, under heat shock conditions highlighting the essential role played by YB-1 in SG assembly and cell survival. However, zebrafish PAC2 cells do not assemble YB-1-positive stress granules upon oxidative stress induced by arsenite, copper or hydrogen peroxide treatment. This contrasts with the situation in human cells where SG formation is robustly induced by exposure to oxidative stressors. Thus, our findings point to fundamental differences in the mechanisms whereby mammalian and zebrafish cells respond to oxidative stress.

Stress caused by environmental insults or disease can disrupt cellular, tissue and organ homeostasis. Proteostasis, ribostasis and the appropriate regulation of the transcriptome, are often compromised under stress conditions. Stress-induced damage may culminate in cell or even organismal death[1]. Eukaryotes respond to detrimental conditions by activating a set of conserved processes that aim to re-establish cellular homeostasis. This multifaceted response is critical for cell survival[1]. It is characterized by stress-dependent changes in the transcriptome and down-regulation of global translation[2]. At the same time, the production of molecular chaperones is enhanced to promote the refolding or degradation of damaged proteins[3,4].

After exposure to distinct environmental insults, such as oxidative stress, hypothermia or extreme heat, eukaryotic cells relocate proteins and messenger RNA into transient, dynamic structures known as Processing Bodies (PBs) and Stress Granules (SGs). PBs are associated with mRNA decay and contain decapping enzymes and scaffolding proteins[5]. Stress granules, instead, directly respond to the protein synthesis status of cells, and contain mRNAs, small ribosomal subunits and factors such as G3BP1 and YB-1 as their core components[6]. In SGs, messengers are sequestered and regulated following stressful conditions. They possess mRNA in a repressed state that may subsequently re-initiate translation in response to specific signals[7].

Stress granules were initially described in tomato cells exposed to heat shock but they are also observed in other plants, protozoa, yeast, *Caenorhabditis elegans*, *Drosophila*, and mammalian cells[8–10]. Thus, SG assembly appears to represent a highly conserved cellular strategy to minimize stress-related damage and promote cell

[1]University of Naples Federico II, Department of Biology, Monte Sant'Angelo Campus, Via Cinthia 4, Naples, 80126, Italy. [2]Institute of Toxicology and Genetics, Karlsruhe Institute of Technology, Hermann-von-Helmholtz-Platz 1, 76344, Eggenstein-Leopoldshafen, Germany. [3]University of Ferrara, Department of Life Sciences and Biotechnology, Via Borsari 46, 44121, Ferrara, Italy. Correspondence and requests for materials should be addressed to D.V. (email: daniela.vallone@kit.edu) or V.C. (email: vcalabro@unina.it)

survival. Beyond their fundamental role in the stress response, SGs have also been implicated in human pathology. Abnormalities in SG formation have been associated with cancer, neurodegeneration and viral infections[11]. In addition, SGs have been reported to promote oncogenesis by supporting cancer cell survival while defects in SG dynamics can accelerate neurodegeneration. Notably, proteins involved in the pathogenesis of Alzheimer's disease, amyotrophic lateral sclerosis (ALS), frontotemporal dementia (FTD), spinocerebellar ataxia (SCA) and Huntington's disease (FUS, hnRNPA1, SMN, TAU and TDP43) are also SG components[1].

In addition to saving anabolic energy by preventing the synthesis of housekeeping proteins, SGs promote cell survival by sequestering pro-apoptotic factors and promoting the translation of stress activated messengers such as BCL2 and ATF4[12–14]. Furthermore, SGs are extremely dynamic structures changing shape, dimensions and protein content depending on the signaling pathways which have been activated and the types of stress stimuli experienced[6]. However, all SGs share mRNAs and RNA-binding proteins[15]. Although the composition of SG protein aggregates is well studied, their precise function remains unclear and how RNAs are sorted and regulated in SGs is still unknown[15–17].

The YB-1 protein belongs to the highly conserved cold shock domain (CSD) protein family and plays a critical role in SG assembly[18]. CSDs are nucleic acid-binding modules with broad binding properties that are present in several prokaryotic and eukaryotic stress-inducible proteins. YB-1 has been implicated in several cellular processes including regulation of transcription and translation, pre-mRNA splicing, DNA repair and mRNA packaging[19]. Although YB-1 is mainly located in the cytoplasm, recent evidence has shown that YB-1 can shuttle between the cytoplasm and nucleus where it regulates gene expression and participates in DNA-damage repair[20]. Increasing evidence highlights the importance of YB-1 function in the oxidative stress response[18]. More specifically, in normal conditions YB-1 co-localizes with GW182 in Processing Bodies (PBs) while, during oxidative stress it interacts with G3BP1 and leads to SG formation as part of a pro-survival program[19]. YB-1 can also bind to tiRNAs (tRNA-derived stress-induced RNAs) and this interaction is required for packaging of tiRNA-repressed mRNAs into SGs.

Most of our current knowledge concerning the function and regulation of stress granules in vertebrates, as well as the contribution of regulatory factors such as YB-1, is based on studies of mammalian cells. However, very little is known about the regulation and function of stress granules formation in non-mammalian vertebrates. The zebrafish (*Danio rerio*) is a fresh-water fish of the cyprinid family, and it represents one of the most popular and versatile genetic models for environmental and human disease studies[21,22]. However, in zebrafish, only limited information concerning the presence and regulation of SG-like structures is available[23–25]. We have recently shown that the subcellular localization of YB-1 is regulated by the circadian clock in zebrafish[26]. Here, using zebrafish cells as a model system and YB-1 as a marker for SG assembly, we reveal that stress granule formation is encountered upon exposure to heat shock in a similar manner to mammalian cells. However, while oxidative stress readily induces SG formation in human cells, no SGs were detected in ROS treated zebrafish cells. These results are consistent with fundamental differences in the response of fish and mammalian cells to oxidative stress.

Results

YB-1 positive aggregates in PAC2 cells and fin tissue. Many reports have documented that upon exposure to cellular stressors, the hYB-1 protein undergoes dynamic structural modifications leading to changes in its subcellular localization and function[27]. In order to use YB-1 to explore cytoplasmic stress granule formation in zebrafish cells under stress conditions, we exploited the high homology between human and zebrafish YB-1[26,28] together with a set of antibodies that have been raised against specific portions of the human protein (Fig. S1). To assess which human YB-1 antibody was the more appropriate for visualizing cytoplasmic YB-1 protein, we performed immunofluorescence and western blot analysis of the zebrafish fibroblast-like PAC2 cell line using YB-1 antibodies raised against the C-terminal (C-ter YB-1) and N-terminal (N-ter YB-1) domains of the protein. As previously reported for mammalian cells[20], immunofluorescence staining of the PAC2 cell line using the C-ter YB-1 antibody, detected a predominantly cytoplasmic signal which was distributed in a fine, punctate pattern (Fig. 1a, left panel). By western blot analysis, the same antibody recognized bands of about 50 and 36 kDa, previously described as the full length and truncated forms of the YB-1 protein, respectively[20,26,29] which are localized in both nucleus and cytoplasm. It also recognized various high molecular weight, highly modified forms of YB-1[20,26,29] (Fig. 1b) which appear to be predominantly nuclear proteins. On the contrary, by immunofluorescence assays performed in PAC2 cells, the N-ter YB-1 antibody detected mainly a nuclear signal and in western blot analysis it clearly detected all the forms recognized by the C-ter antibody with the exception of the 50 kDa band that was only barely detectable (Fig. 1a, right side of the panels and Fig. 1b). Based on these results and given the exclusively cytoplasmic localization described for SGs[1], we chose to use the C-ter YB-1 antibody to visualize cytoplasmic YB-1-associated SG formation in response to different types of stress.

In mammalian cells, YB-1 has been reported to localize in SGs upon heat shock treatment[18]. Therefore, we subjected the zebrafish cells to a heat shock by transferring them abruptly from 26 °C to 37 °C, 42 °C or 45 °C and then examined the impact on mRNA expression and the distribution of the zfYB-1 protein. Incubation at the highest temperature did not result in a significant reduction in PAC2 cell viability over a 90′ period (Fig. 2a), however, consistent with a robust heat shock response, expression of the heat shock gene *zf hsp70* was strongly induced by incubation of the cells at all three elevated temperatures (Fig. 2b). Furthermore, in PAC2 cells during 45 °C heat shock, *zf yb-1* mRNA levels were also strongly increased for the entire duration of the experiment (6 hours) (Fig. 2c) compared with a shallow, transient induction observed during the first hour following heat shock in the human HaCaT cell line (Fig. 2d). This data suggests that *yb-1* mRNA up-regulation may represent a species-specific aspect of the heat shock response.

We next explored whether heat shock treatment induced changes in the subcellular localization of YB-1, including the formation of aggregates in zebrafish cells. We performed an immunofluorescence assay for YB-1 in PAC2 cells which had been heat shock treated at different temperatures (37 °C, 40 °C, 42 °C and 45 °C).

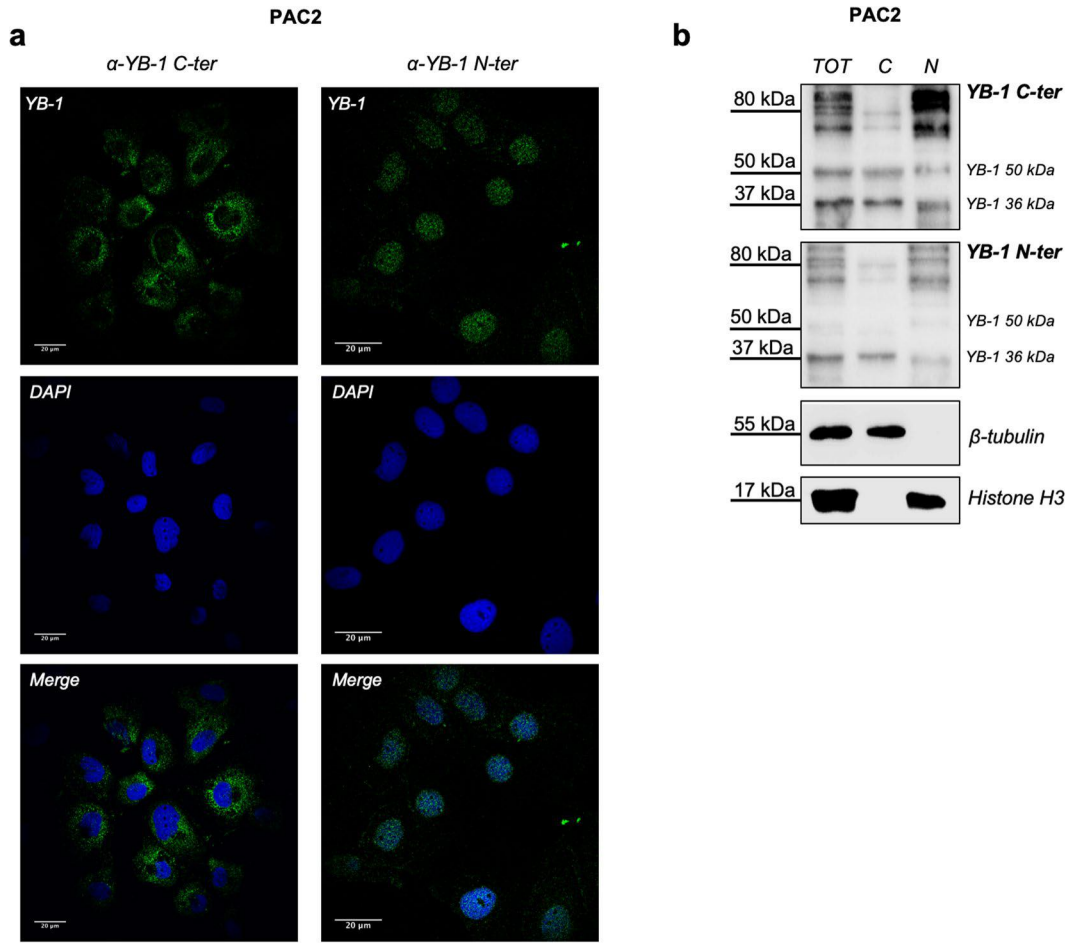

Figure 1. Immunoreactivity of human YB-1 antibodies against zebrafish YB-1. (**a**) confocal immunofluorescence analysis of PAC2 cells stained with human YB-1 antibodies (α-YB-1 C-ter and α-YB-1 N-ter), nuclei were stained with DAPI (blue); (**b**) western blot of PAC2 total (*TOT*), Cytoplasmic (**C**) and nuclear (N) protein extracts analysed with α-YB-1 N-ter and α-YB-1 C-ter antibodies; Histone H3 and ß-tubulin were used as loading controls for the nuclear and cytoplasmic extracts, respectively. Each panel is assembled from cropped western blotting images (see Supplementary Material file for the original images).

Interestingly, only zebrafish cells subjected to the treatment at 45 °C exhibited perinuclear aggregates similar to those observed in mammalian HaCaT cells, (Figs 3a and S2a,b). These YB-1 aggregates showed a significantly increased diameter compared with the diffuse punctate cytoplasmic YB-1 distribution in untreated cells (Fig. S2c). However, the YB-1 aggregates observed in PAC2 cells appeared smaller (67% +/− 1.5%) compared to those in HaCaT cells (Fig. 3b). The formation of similar perinuclear YB-1 aggregates was also observed in adult zebrafish caudal fins which had been first clipped from the animal, and immediately subjected to heat shock at 45 °C for 45 minutes prior to fixation of the tissue and the YB-1 immunofluorescence assay (Fig. 3c). To explore in more detail the heat shock-induced formation of YB-1 aggregates, we decided to examine the dynamics of aggregate formation. Thus, we exposed PAC2 cells to 45 °C for different periods of time from 30 to 90 minutes. Our immunofluorescence data showed that YB-1 positive aggregates already began to concentrate in the perinuclear compartment after 30 minutes of incubation and, after 45 minutes YB-1 aggregates were exclusively perinuclear (Fig. 4a,c). We then tested whether this YB-1 aggregate formation could be reversed by abruptly returning the cells to 26 °C after 45 minutes of heat shock treatment. We observed a significant decrease in the percentage of cells exhibiting YB-1 aggregates, as well as a reduction in aggregate size after only 15 minutes following return to the lower temperature. (Fig. 4b–d). Thus, comparing these observations with previous reports[30], the YB-1 aggregates formed in zebrafish cells after heat shock treatment at 45 °C appear to have similar properties to the classical SGs observed in mammalian cells.

Heat shock induced YB-1 aggregates represent *bona fide* SGs. To test whether the heat-shock induced YB-1 positive aggregates in PAC2 cells indeed represent SGs, we performed immunofluorescence co-localization experiments using antibodies against YB-1 and the stress granule assembly factor 1 (G3BP1). G3BP1 protein is a well know component of SGs in mammals and has been shown to initiate the assembly of SGs by forming a homo-multimeric and a hetero-multimeric complex with its close relative G3BP2[31].

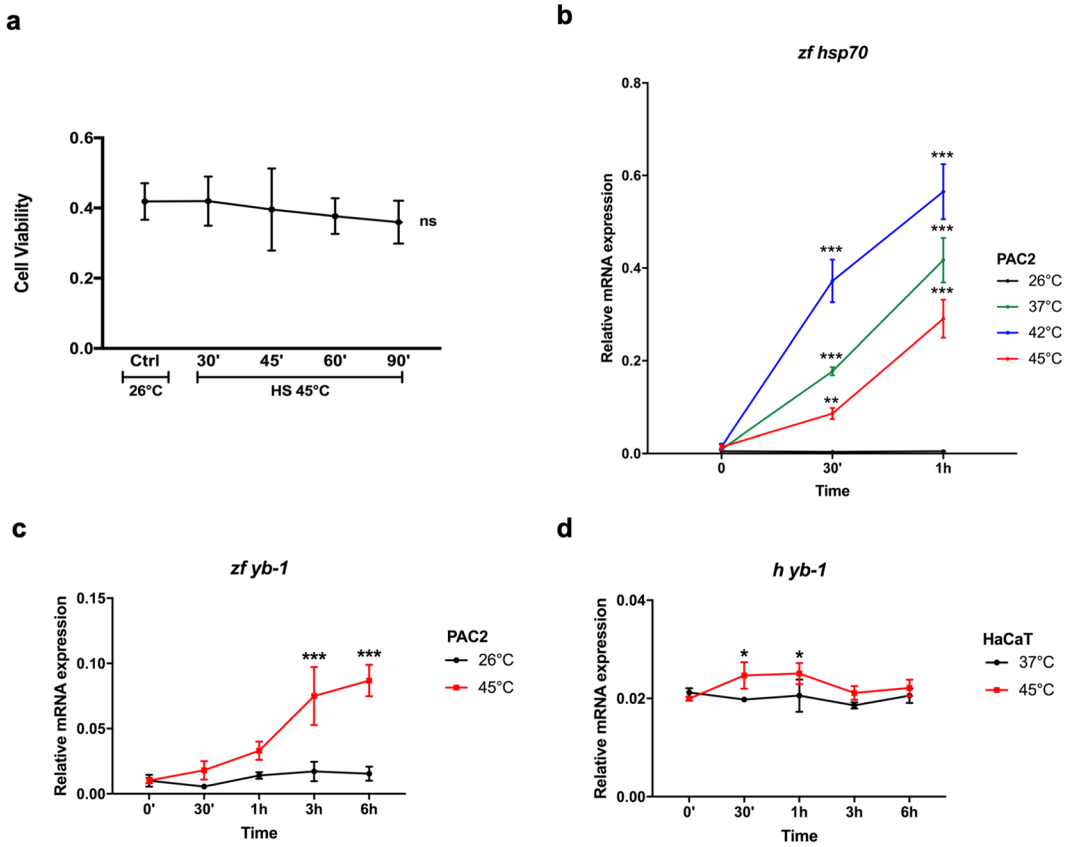

Figure 2. Heat shock induces *yb-1* transcript levels in zebrafish but not in mammalian cells. **(a)** cell viability of PAC2 cells after heat shock treatment at 45 °C. Cells were subjected to elevated temperatures for the times indicated on the x-axis and cell viability values (MTT) are plotted on the y-axis. Statistical analysis was performed using 1-way ANOVA followed by Dunnett's multiple comparisons test; *ns* indicates no statistical significance (see also Table S1); (**b–d**) RT-qPCR analysis of zebrafish *zf hsp70* (**b**), *zf yb-1* (**c**) in PAC2 cells and human *h yb-1* (**d**) in HaCaT cells. Samples were taken at different time points during and after 1 hour of heat shock treatment at the indicated temperatures (for precise experimental details, see materials and methods section). Mean mRNA relative expression ($n = 3$) ± SD is plotted on the y-axes, whereas time is plotted on the x-axes. Statistical analysis was performed using 2-way ANOVA and Sidak's multiple comparison test. Levels of significance between points of expression and time 0 are indicated (***$p < 0.001$, **$p < 0.01$, *$p < 0.05$) (see also Table S1 for statistical analysis).

We first verified cross-reactivity of human G3BP1 antibodies with the zebrafish ortholog by western blot and immunofluorescence assays in PAC2 cells (Fig. S3). In control zebrafish cells cultured at 26 °C, the signal from the anti G3BP1 antibody was almost uniformly distributed within the cytoplasmic compartment of the cells (Fig. 5a, upper panel and S3b). However, following the shift to 45 °C, we observed G3BP1 and YB-1 co-localization in perinuclear aggregates (Fig. 5a, lower panels). In mammalian cells, it has previously been demonstrated that cycloheximide prevents SG aggregation as a consequence of the blockade of protein synthesis[32,33]. Thus, to further confirm the SG identity of the YB-1 positive aggregates in zebrafish cells, we inhibited protein synthesis in PAC2 cells by treatment with cycloheximide prior to and during heat shock treatment. Consistent with the previous results in mammalian cells, in heat shock-treated zebrafish cells cycloheximide treatment significantly reduced ($p < 0.05$) the diameter of YB-1 positive aggregates (Fig. 5b,c), although YB-1 continued to show a diffuse perinuclear localization.

Previous studies in mammalian cells have highlighted a key role for YB-1 within the context of SGs for cell survival upon stress conditions[18]. We therefore assessed the consequence of reducing YB-1 protein expression by siRNA silencing on the survival of heat shock treated PAC2 cells. We transfected PAC2 cells with a siYB-1 already successfully used in our previous studies[26]. This resulted in a reduction of all the immunoreactive YB-1 forms in western blot analysis, as well as a reduced immunofluorescent YB-1 signal (Fig. S4a,b, respectively). Strikingly, upon 45 minutes of heat shock treatment at 45 °C we failed to detect the typical pattern of perinuclear G3BP1/YB-1- positive SG aggregates in cells with reduced YB-1 expression (Fig. 6a). Moreover, we encountered a reduced cell viability in siYB-1- transfected cells compared with control cells that were maintained at 26 °C (Fig. 6b). Together, our data confirm that in zebrafish cells YB-1 perinuclear aggregates which form after heat shock treatment are *bona fide* SGs and point to an essential functional role played by YB-1 in SG assembly and cell survival under thermal stress.

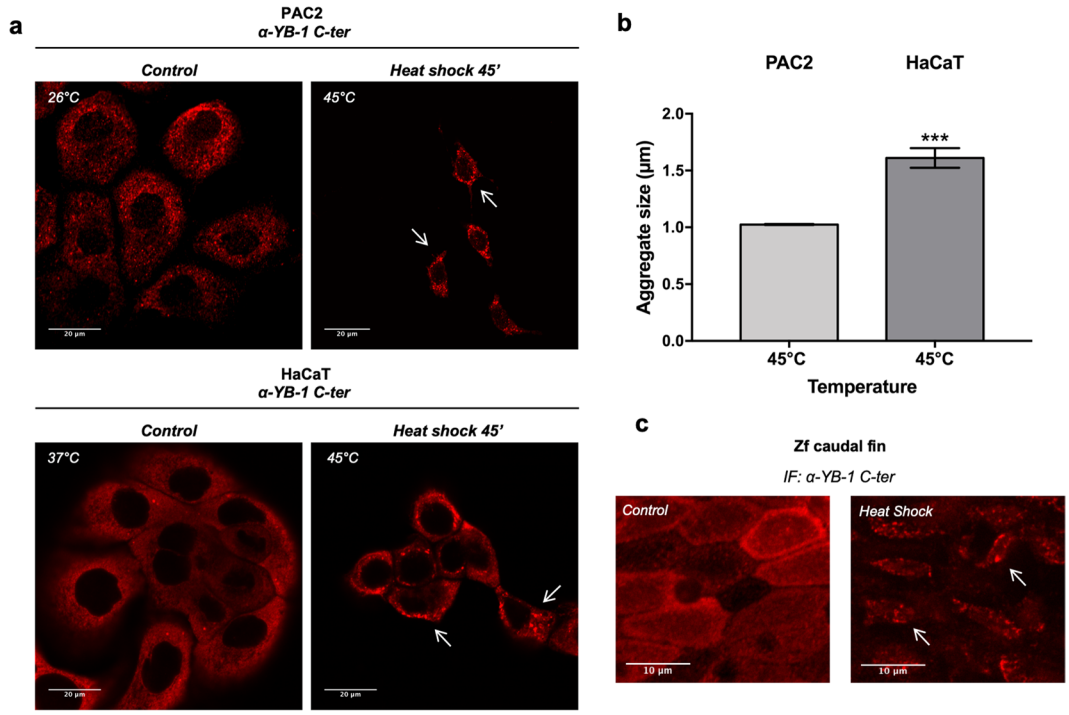

Figure 3. Heat shock promotes assembly of YB-1 positive aggregates in zebrafish and mammalian cells. **(a)** confocal immunofluorescence of PAC2 cells (*upper panels*) and HaCaT cells (*lower panels*) stained with human α-YB-1 C- ter antibody (red); some YB-1 aggregates are indicated by arrows; (**b**) quantification of YB-1 aggregate dimensions after heat shock at 45 °C for 45′ in PAC2 and HaCaT cells (unpaired t-test with Welch's correction *p = 0.007, see also Table S1); (**c**) confocal immunofluorescence of adult zebrafish caudal fins at 26 °C (control) and after heat shock at 45 °C, stained with human α-YB-1 C-ter antibody. YB-1 aggregates are indicated by arrows.

Differential response to ROS. Heat shock is not the only type of stress treatment that has been shown to induce the formation of stress granules in mammalian cells. Oxidative stress also represents one of the key environmental stressors triggering SG formation[1]. We have previously revealed major differences in the transcriptional response to ROS between mammalian and zebrafish cells[34,35]. We therefore questioned whether differences in the SG response to oxidative stress might also exist between mammalian and zebrafish cells. Thus, we incubated PAC2 cells for 30 minutes or 1 hour with three typical oxidative stressors at working concentrations according to those used in previous publications[18]: sodium arsenite (Na Ars, 250 µM), hydrogen peroxide (H_2O_2, 300 µM) and copper (Cu II, 500 µM). Interestingly, by immunofluorescence assay we failed to detect either significant changes in YB-1 cytoplasmic distribution or the formation of aggregate structures resembling SGs (Figs 7a,c and S5a). Conversely, similar treatments in mammalian HaCaT cells, efficiently induced YB-1 positive SGs (Fig. 7b,d). Furthermore, we did not observe a reduction of YB1-silenced PAC2 cells viability upon treatment with hydrogen peroxide, thus indicating that YB-1 does not play a pro-survival role under oxidative stress, at least under the experimental conditions tested (Fig. 7e).

To explore the possibility that SG-like aggregation in zebrafish cells may occur at higher doses of oxidative stressors, we exposed PAC2 cells to a broad range of concentrations of Na Ars, H_2O_2 and copper (from 600 µM to 1.5 mM). Although with higher concentrations we observed an enrichment of the perinuclear localization of YB-1and G3BP1, we failed to detect the formation of YB-1 positive SGs aggregates even at the highest concentrations of oxidative stressors (Fig. S6). Importantly, acute changes in the expression of genes which have previously been shown to be linked with the cellular response to oxidative stress (*jun-B*, *jun-D*, *c-fos*, *cry1a* and *cry5*)[34] were already observed in PAC2 cells treated with 300 µM H_2O_2 (Fig. S5b).

We next wished to exclude that this differential response to stressors observed in PAC2 cells compared with mammalian cells may be simply due to the different cell type origin of these two cell lines (fibroblast-like for PAC2 cells and keratinocyte for HaCaT cells). We performed an immunofluorescence assay for YB-1 in a human dermal fibroblast cell line (HDF) after heat shock at 45 °C, as well as upon Na Ars (250 µM), H_2O_2 (50 µM) and Cu II (500 µM) treatments. As for the HaCaT cell line, and consistent with previous reports for many other human cell lines[36–38], all the stressors used were able to induce SG formation in HDF cells (Fig. 8a). Interestingly, we also observed a reduction of cell viability in human fibroblasts after treatment with H_2O_2 whereas zebrafish PAC2 fibroblasts were almost unaffected by the same treatment (Fig. 8b), thus indicating a lower sensitivity of zebrafish cells to oxidative stress.

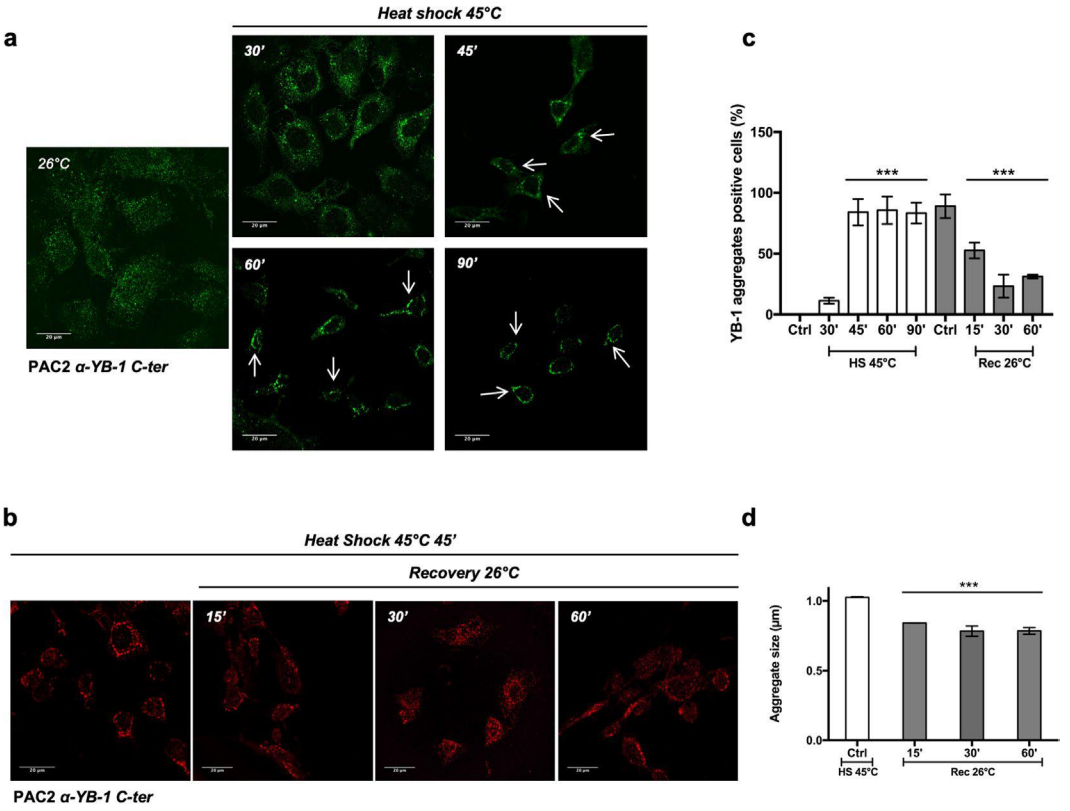

Figure 4. Kinetics of YB-1 aggregate formation. (**a**) confocal immunofluorescence of YB-1 (Green) in PAC2 cells at 26 °C (control) or after heat shock at 45 °C for the indicated times; (**b**) confocal immunofluorescence for YB-1(red) in PAC2 cells incubated at 45 °C for 45′ and then replaced at 26 °C for recovery from the heat shock at the indicated times; (**c**) percentage of cells forming YB-1 positive aggregates (plotted on the y-axes) incubated at 45 °C for the indicated times (white bars) and then allowed to recover for 15, 30 and 60 minutes at 26 °C (grey bars). Statistical analysis was performed using 1-way ANOVA and Dunnett's multiple comparisons. Levels of significance are indicated (***$p < 0.001$) (see also Table S1); (**d**) quantification of YB-1 positive aggregate dimensions in PAC2 cells incubated at 45 °C for 45 minutes (white bar) and then allowed to recover at 26 °C for the indicated times (grey bars). Statistical analysis was performed using 1-way ANOVA and Dunnett's multiple comparisons. Levels of significance are indicated (***$p < 0.001$) (see also Table S1).

Discussion

Stress granule formation has been observed in plants, protozoa, yeast, *C. elegans*, *Drosophila* and mammalian cells. Despite enormous interest in SGs due to their possible contribution to the pathogenesis of several human diseases, many aspects of SG function are poorly understood. In particular, little is known about how SG formation is tailored to the particular environmental challenges faced by different species. Here, we have revealed that in zebrafish fibroblast cells, heat shock induces the formation of SGs in a comparable manner to that described in mammalian cells. In contrast, while ROS treatment robustly induces SG formation in mammalian cells, there is no SG response in PAC2 zebrafish cells.

Our study has exploited YB-1 protein as a marker for stress granule formation in zebrafish. However, our understanding of the precise role played by YB-1 in SG assembly remains incomplete. Previous studies highlighted the role of YB-1 in formation of stress granules[18], whereas in other reports, YB-1 silencing apparently does not alter the formation of SGs[39,40]. In our study, consistent with Somasekharan, S. P. *et al.*[18], we reveal that knock down of YB-1 expression in zebrafish cells leads to impaired SG assembly and reduced cell viability following heat shock. In human cells, YB-1 protein was first reported to indirectly increase SG formation during oxidative stress by translationally activating G3BP1, a nucleator for SG assembly[18]. YB-1 was then shown to bind to tiRNA via its cold shock domain to package tiRNA-repressed mRNAs into SGs, a pathway that is independent of G3BP1[41]. Previous studies have revealed that YB-1 function is predominantly regulated by posttranslational modifications, protein cleavage and subcellular compartmentalization[26,27,42]. Indeed, YB-1 is abundant and constitutively expressed in multiple human tissues and its expression is further induced in tumor cells or following DNA damage by E box binding transcription factors such as c-Myc[43] and Twist[44]. Interestingly, we have revealed that YB-1 mRNA expression is induced upon heat shock in zebrafish but not in mammalian cells suggesting that in fish cells *de novo* YB-1 protein synthesis is an essential requirement for the pro-survival response to thermal stress. It is tempting to speculate that mammalian cells, being more sensitive to thermal stress, are more reliant on a pre-existing pool of YB-1 protein to allow an immediate response following heat shock.

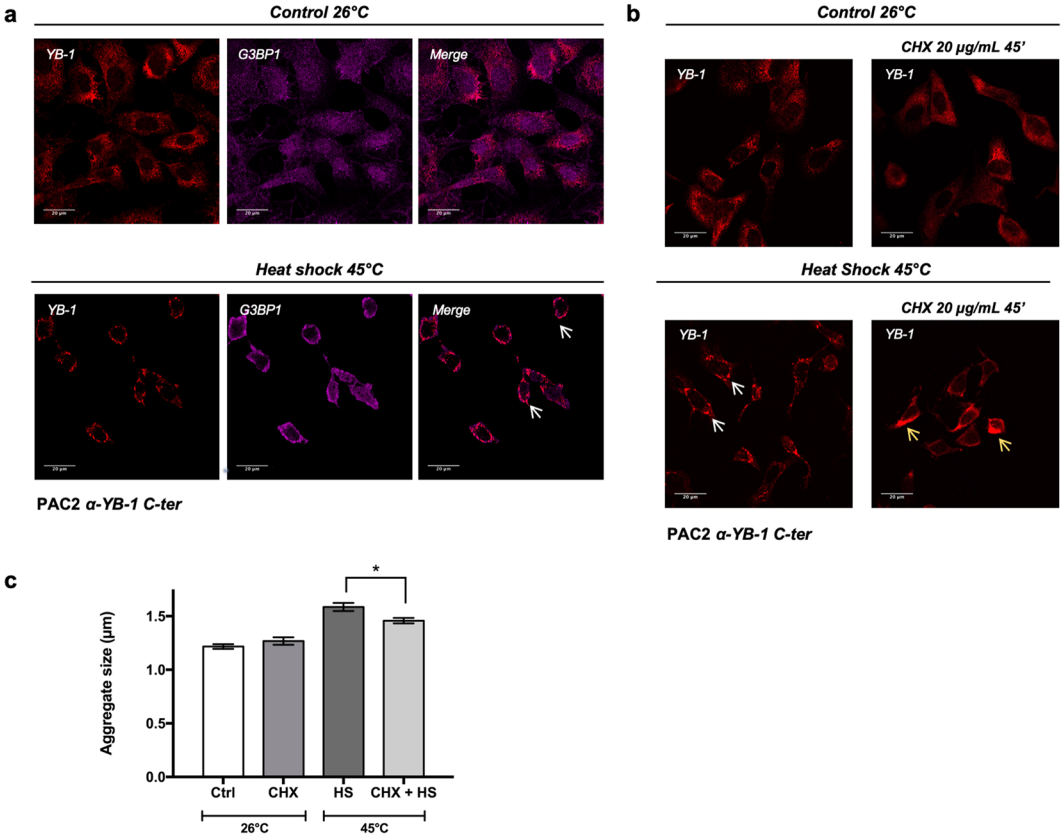

Figure 5. Heat shock induced YB-1 aggregates represent *bona fide* SGs. (**a**) Confocal immunofluorescence analysis of YB-1 (red) and G3BP1 (magenta) in PAC2 cells at 26 °C (control) or after heat shock at 45 °C for 45 minutes. Cellular colocalization is present in perinuclear aggregates indicated by white arrows; (**b**) confocal immunofluorescence of YB-1 in PAC2 cells treated with cycloheximide (20 µg/ml) at 26 °C (upper part of the panel) or after heat shock at 45 °C for 45 minutes (lower part of the panel). Controls are represented in the left part of the panel. White arrows indicate YB-1 positive aggregates (lower panel, left). Yellow arrows indicate the bulk of the protein not forming aggregates (lower panel, right); (**c**) quantification of YB-1 positive SG aggregate dimensions in PAC2 cells documented in the cycloheximide treatment analysis presented in panel b. Statistical analysis was performed using 1-way ANOVA followed by Tukey's multiple comparisons test. Levels of significance are indicated (*p = 0.05) (see also Table S1).

Conservation of Stress Granule formation in response to heat shock. Our results revealing that heat shock induces stress granule formation in both zebrafish and mammalian cells are consistent with this function representing a highly conserved facet of the cellular response to heat shock. In both cell types these granules are a site of colocalization of YB-1 and G3BP1 and exhibit a perinuclear distribution. Furthermore, similar kinetics was observed for the assembly of YB-1 positive SGs at 45 °C in mammalian and zebrafish cells. However, while in mammalian cells an increase of 8 °C (37 °C to 45 °C) is sufficient to trigger SGs formation, for zebrafish cells a temperature shift of 19 °C (26 °C to 45 °C) is required. Furthermore, after 45 minutes incubation at 45 °C, more than 90% of zebrafish cells were still viable and able to recover from stress upon return to 26 °C. This contrasts with the situation in mammalian cells where a moderate temperature elevation (37 °C to 45 °C) for a relatively short time (30–45 minutes) can reduce cell survival to 10%[45]. These data indicate that zebrafish cells are generally more resistant to temperature changes than mammalian cells, only mounting a SG response after a relatively large increase in temperature and also showing lower mortality under elevated temperatures. It is tempting to speculate that this reflects the fact that zebrafish is an ectothermic organism living in shallow, slow-flowing water, and so may have adapted to frequent changes in body temperature[46]. Indeed, zebrafish as ectotherms, show a greater tolerance of environment-induced changes in body temperature[47] compared with endothermic mammals.

Species- and stressor-specific differences in SG assembly. We have revealed significant differences in SG formation in response to heat shock and oxidative stress between zebrafish and mammalian cells. Our own data and that of previous reports fail to indicate any cell type-specificity in mammalian stress granule formation in response to stress. However, consistent with the general notion of an inherent plasticity in SG function, recent data have pointed to stress-specific differences in the composition and dynamics of SGs in mammalian cells[48]. For example, accumulation of heat shock proteins (HSPs) including HSP27 and HSP70 is the most prominent part of the complex cellular response to hyperthermic conditions in all type of organisms. HSP27 is only found in SGs induced by heat shock, but is absent in sodium arsenite induced SGs[49]. Furthermore, while mRNAs encoding

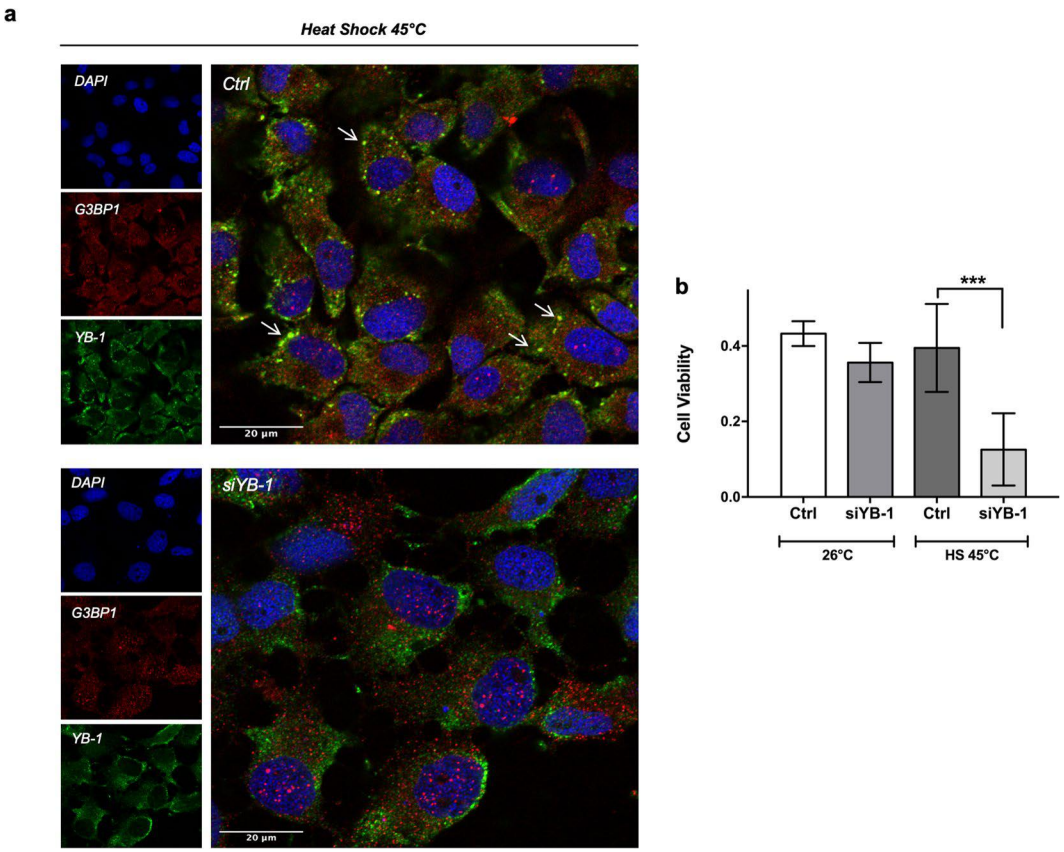

Figure 6. YB-1 is essential for SG formation and PAC2 cell viability upon thermal stress. (**a**) Confocal immunofluorescence analysis of G3BP1 (red) and YB-1 (green) in control (upper panel) and YB-1-silenced PAC2 cells (lower panel) after heat shock treatment (45 minutes at 45 °C). Nuclei were stained with DAPI (blue) and both single and merged images are presented. White arrows indicate SGs; (**b**) cell viability assay (MTT) in control or YB-1-silenced PAC2 cells at 26 °C or after heat shock (45 minutes at 45 °C). Statistical analysis was performed using 1-way ANOVA followed by Tukey's multiple comparisons test. Levels of significance are indicated (***p 0.001) (see also Table S1).

house-keeping proteins are recruited to heat-shock induced SGs, transcripts encoding HSP70 proteins are selectively excluded[50]. HSP90 mRNA transcripts, instead, are selectively excluded from oxidative-stress induced SGs[51]. Stress and species-specific differences have also been reported in the mechanisms regulating SG formation in mammalian cells. For example, mammalian cells use two key regulatory mechanisms to rapidly shut down general protein synthesis. The first involves eIF2α phosphorylation by stress-activated eIF2a kinases (eIF2αK)[52,53], while a second mechanism involves p-4E-BPs dephosphorylation that prevents the assembly of eIF4F and inhibits translation initiation[54]. eIF2α phosphorylation is required for SG assembly in mammalian cells, but not in *Drosophila*, *C. elegans* or yeast. Furthermore, in mammalian cells, certain types of stress, including oxidative stress, are strictly reliant on eIF2Fa phosphorylation for the promotion of SG formation while heat shock also induces SGs through 4E-BP activation[55]. A HAP1 human cell line expressing a non-phosphorylatable form of eIF2α (S51A) was shown to be unable to assemble stress granules in response to sodium arsenite and was hypersensitive to the toxic effects of low doses of sodium arsenite. However, after heat shock, this cell line demonstrated no difference in its ability to induce SGs thus suggesting that heat shock may also function through alternative p-eIF2a-independent pathways that rely on the activation of 4E-BPs[48].

We have shown that zebrafish fibroblasts exposed to oxidative stressors such as sodium arsenite, hydrogen peroxide and copper do not produce SGs, however, without any significant reduction of cell viability. Due to the limited repertoire of established, stable zebrafish cell lines available, we cannot exclude cell type-specificity in the stress response for this fish species. However, our data obtained from fibroblast cells points to the existence of alternative pathways, not involving SG assembly that may operate in zebrafish cells helping them to tolerate oxidative stress insults. In this regard, our previous data have already revealed significant differences in the transcriptional response to ROS between mammals and zebrafish cells. Indeed, while in mammalian cells, ROS-induced gene expression is mediated by various signaling proteins and transcription factors including NF-kB, PI3K, MAPK and p53, in zebrafish, the D-box enhancer appears to represent the principle oxidative stress responsive enhancer element[34]. This D-box mediated response to ROS in fish cells has been associated with the regulation of gene expression by direct exposure to visible light, a property which is absent in mammalian cells. Thus, together, our results point to fundamental changes in the mechanisms whereby vertebrate cells respond to oxidative stress during evolution.

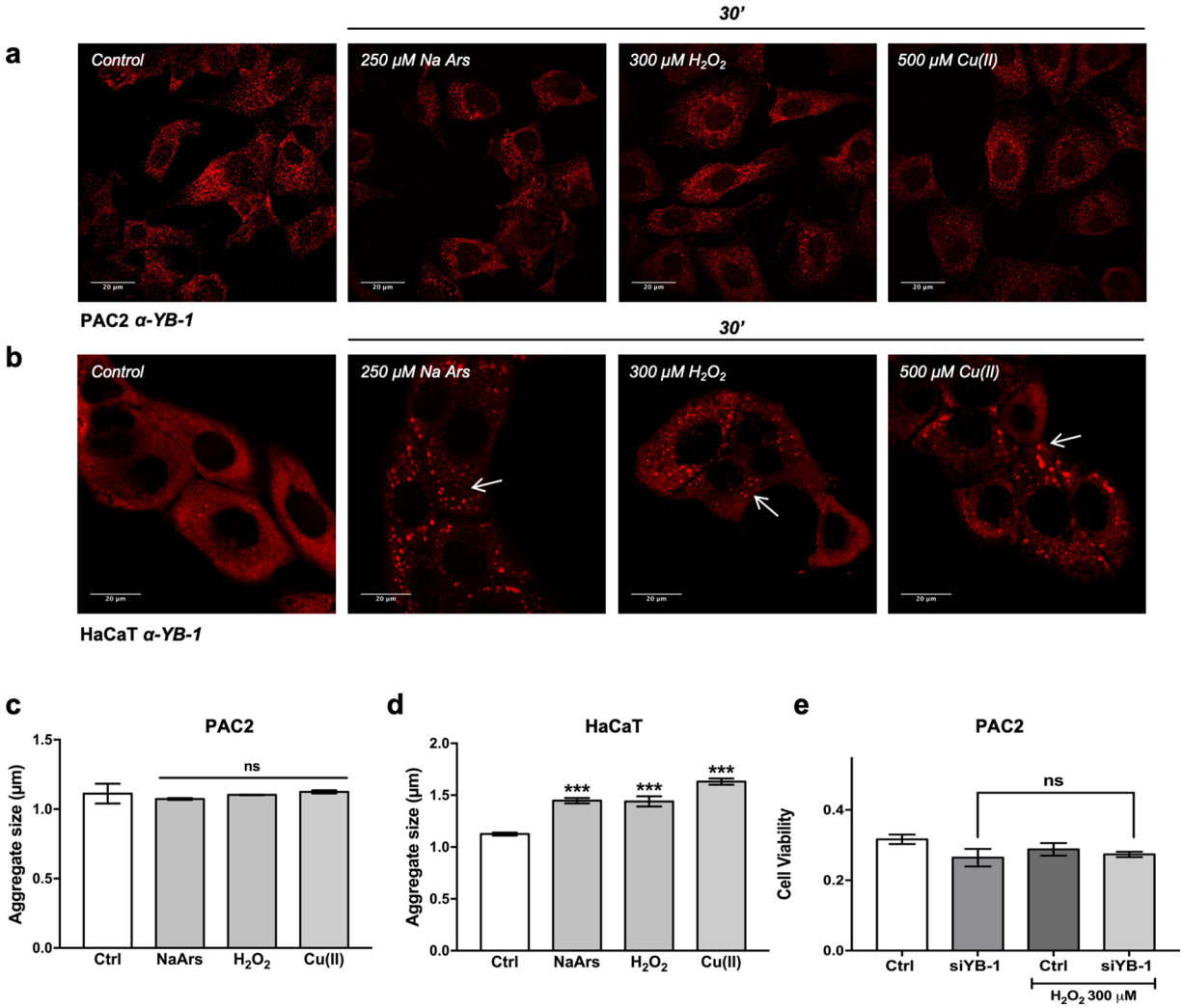

Figure 7. Oxidative stressors induce SGs in mammalian but not in zebrafish cells. (**a,b**) Representative confocal immunofluorescence for YB-1 (red) in (**a**) PAC2 cells and (**b**) HaCaT cells treated with 250 μM Na Ars, 300 μM H_2O_2 and 500 μM Cu(II) for 30 minutes. YB-1 positive SGs present in HaCaT cells are indicated by white arrows. (**c,d**) Quantification of aggregate size for the immunofluorescence analysis presented in panels a and b, respectively. (**e**) Cell viability assay (MTT) in control or YB-1-silenced PAC2 cells at 26 °C or after 300 μM H_2O_2 treatment for 45 minutes. Statistical analysis was performed using 1-way ANOVA followed by Tukey's multiple comparisons test (see also Table S1).

Methods

Fish care, treatment and ethical statements. All husbandry and experimental procedures were performed in accordance with European Legislation for the Protection of Animals used for Scientific Purposes (Directive 2010/63/EU), the German Animal Protection Law (May 18th, 2006 (BGBl. I S. 1206, 1313), last changed March 29th, 2017 (BGBl. I S. 626). Research was also approved by the Local Government of Baden-Württemberg, Karlsruhe, Germany (35-9185.81/G-131/16). General license for fish maintenance and breeding: Az.: 35-9185.64.

Zebrafish (*Dario rerio*, Tübingen strain) were maintained according to standard procedures[56] in a re-circulating water system at 26 °C and under 14:10 light: dark cycles. For our experiment 6–12 months old zebrafish males (n = 5) were used and chosen based on a health check. The caudal fins were amputated using razor blades following anesthesia with 0.02% w/v MS222 (3- aminobenzoate methanesulfonic acid, Sigma-Aldrich, St Louis, MO). Fish were left to recover in an isolated cage in the presence of 0.00005% methylene blue for 24 hours to avoid distress and for the health to be monitored.

Cell culture. The zebrafish PAC2[57] cell line was propagated at 26 °C in an atmospheric CO_2, non-humidified cell culture incubator; cells were cultured in L-15 (Leibovitz) medium (Gibco BRL) supplemented with 15% Fetal Bovine Serum (Sigma-Aldrich, St Louis, MO), 100 units/ml penicillin, 100 μg/ml streptomycin and 50 μg/ml gentamicin (Gibco BRL).

HaCaT (human spontaneously immortalized keratinocytes from adult skin) and HDF (human primary dermal fibroblast) were purchased from Cell Line Service (CLS, Germany) and cultured in a humidified incubator

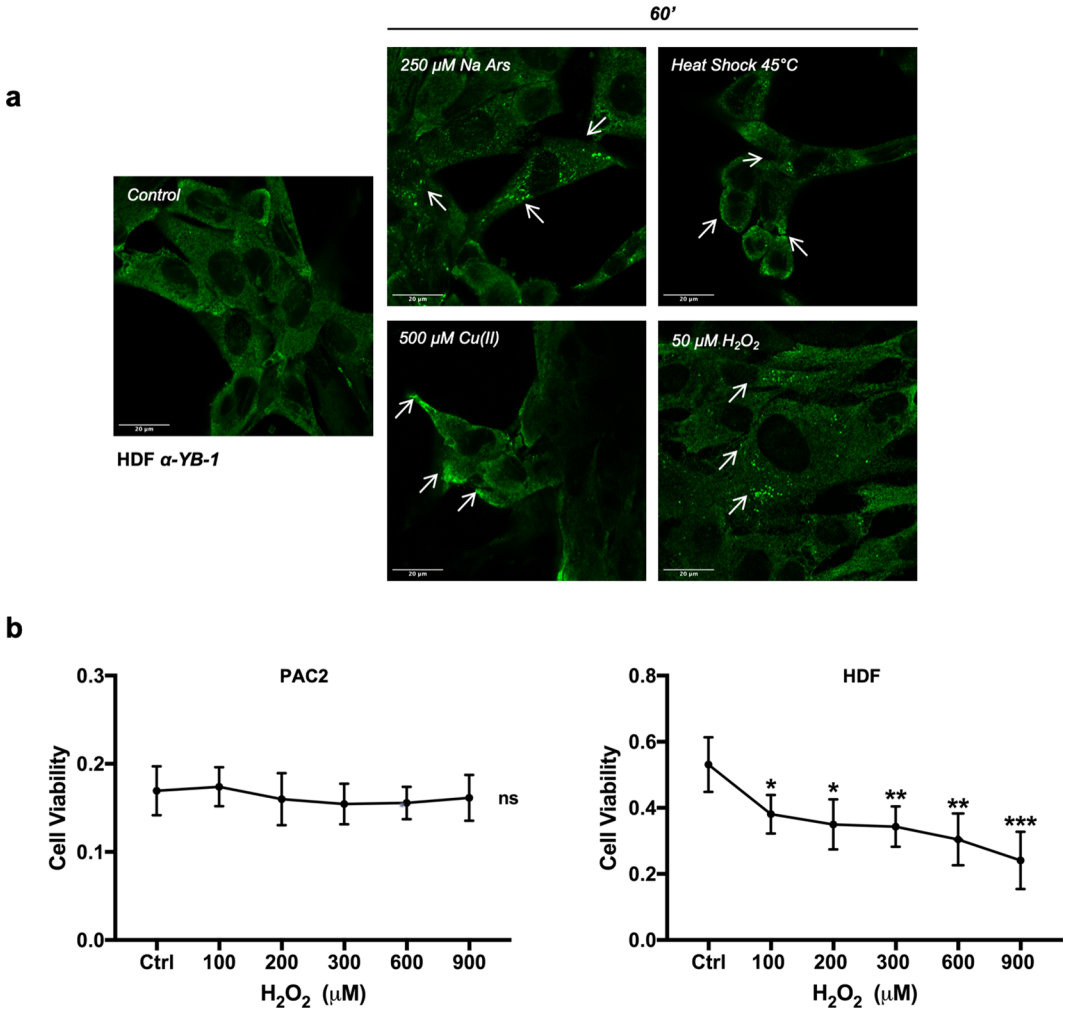

Figure 8. Heat shock, Arsenite, Copper and H_2O_2 treatment promotes assembly of YB-1 positive aggregates in human HDF fibroblast cells. (**a)** Representative confocal immunofluorescence images of HDF cells stained with human α-YB-1 C- ter antibody (green). Some YB-1 aggregates are indicated by arrows. (**b)** Cell viability assay (MTT) in PAC2 and HDF cells after 45 minutes treatment with different doses of H_2O_2. Statistical analysis was performed using 1-way ANOVA followed by Tukey's multiple comparisons test. Levels of significance are indicated (***p 0.001) (see also Table S1).

at 37 °C and 5% CO_2 in DMEM High Glucose (Gibco BRL) supplemented with 10% Fetal Bovine Serum (Gibco BRL), 1% L-Glutamine (Gibco BRL) and 1% Pen-Strep solution (Gibco BRL).

Cells were routinely checked for mycoplasma contamination, using a mycoplasma detection kit (abm, Canada).

Immunofluorescence microscopy of zebrafish cells and zebrafish adult caudal fins. PAC2 cells were seeded on coverslips (6.0×10^4 cells) and maintained in constant darkness for the subsequent 48 hours prior to treatment. HaCaT cells were seeded on coverslips (3.0×10^4 cells) and treated after 24 hours. Following treatment, both mammalian and zebrafish cells were gently rinsed with 1X PBS and then fixed in PFA 3.7% for 10 and 15′, respectively. After 3 washes with 1X PBS (10 minutes each), cells were washed twice with 0.01% Tween-PBS and blocked for 1 hour with a 1% BSA-0.01% Tween-PBS solution for PAC2 and with a 3% BSA solution for mammalian cells to avoid non-specific binding of antibodies. PAC2 cells were then incubated overnight at 4 °C with the primary antibodies. Primary antibody incubation for mammalian cells was performed for 1 hour in darkness at room temperature. After incubation with primary antibodies, cells were washed three times with 0.01% Tween-PBS (10 minutes each) and incubated with secondary antibodies for 45 minutes in darkness. Then, both PAC2 and HaCaT cells were incubated for 5 minutes in a DAPI solution (1:50000) (Sigma-Aldrich, St Louis, MO) followed by 3 washes in 0.01% Tween PBS. Coverslips were immersed in a Dako mounting medium (Agilent).

Immunofluorescence analysis of zebrafish caudal fins was performed as previously reported[58]. Specifically, after an overnight fixation of the fin-clips in Carnoy's solution (60% ethanol, 30% chloroform, 10% acetic acid) at 4 °C, fins were incubated overnight in 100% Methanol and then subjected to sequential rehydration steps of 10′ in 100%, 66% and 33% methanol in PBTX (1XPBS, 0,3% Triton X100). At this stage, fins were pre-incubated

in PBTX plus 1% BSA blocking solution for 3 hours. Then the primary antibody was added and the samples were incubated at 4 °C overnight. After several washes, samples were incubated at 4 °C with the secondary fluorescent antibody overnight. DAPI staining was used for visualization of nuclei. Then samples were mounted on glass slides. All images were acquired using a Leica SPE confocal microscope (63x oil immersion objective) or Carl Zeiss LSM 700 (63x oil immersion objective) microscope. The size of aggregate/stress granules in confocal immunofluorescence images was measured with Fiji (ImageJ) software to calculate the Feret's statistical diameter (Fig. S7). Feret's statistical diameter is the perpendicular distance between parallel tangents touching opposite sides of the profile of elliptical/circular shaped particles. This parameter is a reliable indicator of aggregate shape and dimensions[59,60]. Analysis were performed on threshold images. Particles with areas outside the range of 0.2–2.0 μm and with size circularity values outside 1.00 were ignored.

Cell viability assay. Cell viability was determined by the MTT 3-(4,5-dimethylthiazol-2-yl)-2,5-diphenyl tetrazolium bromide assay (Sigma-Aldrich, St Louis, MO). PAC2 cells were seeded in 96-well plates at 2.0×10^4 per well and the assay was performed accordingly to the manufacturer´s instructions. The optical absorbance was determined at 570 nm using an iMark microplate reader (Bio-Rad, USA).

siRNAs and transfections. PAC2 cells were transfected using Fugene HD (Promega) according to the manufacturer's recommendations. A 4:1 ratio (4 μl of Fugene HD reagent for each μg of siRNA) was used. Briefly, cells were seeded at 70–80% confluence (1.5×10^6) in 100-mm dishes; after 48 hours of incubation in darkness, cells were transiently transfected with siRNA (100 nM final concentration). 24 hours after siRNA transfection, cells were treated or left untreated. Negative Control siRNA, provided by Riboxx (Germany) as a pool of 3 different siRNAs, was used as a negative control. A predesigned siRNA for YB-1 was purchased from Riboxx (Germany):

zfYB-1 siRNA guide sequence (5′-3′): UUCUCCUUAUCCUCCUCUCCCCC zfYB-1 siRNA passenger sequence (5′-3′): GGGGGAGAGGAGGAUAAGGAGAA;

siRNA Negative Control-1 guide sequence (5′-3′): UUGUACUACACAAAAGUACCCCC siRNA Negative Control-1 passenger sequence (5′-3′): GGGGGUACUUUUGUGUAGUACAA

siRNA Negative Control-2 guide sequence (5′-3′): GAACGAAUUUAUAAGUGGCCCCC siRNA Negative Control-2 passenger sequence (5′-3′): GGGGGCCACUUAUAAAUUCGUUC

siRNA Negative Control-3 guide sequence (5′-3′): UUGUACUACACAAAAGUACCCCC siRNA Negative Control-3 passenger sequence (5′-3′): GGGGGUACUUUUGUGUAGUACAA.

Antibodies. Primary antibodies: anti-YB-1 raised against amino acids 1 to 100 of hYB-1 protein (Abcam 12148 N-ter); anti-YB-1 raised against amino acids 307–324 of hYB-1 (Sigma-Aldrich, St Louis, MO, Y0396 C-ter); anti-vinculin (Sigma-Aldrich, St Louis, MO, V9131); anti-β-tubulin (H-235 Santa Cruz Biotechnology); anti-Histone H3 (9715 Cell Signaling); anti-G3BP1 (611127 BD transduction Laboratories, BD Biosciences).

Secondary fluorescent antibodies: Alexa Fluor 488 anti-rabbit (Thermo-Fisher Scientific); Alexa Fluor 647 anti-goat (Thermo-Fisher Scientific); Cy3 anti-rabbit (Jackson ImmunoResearch); DAPI (Sigma-Aldrich, St Louis, MO, D9542).

Immunoblot analysis. For total protein extraction, 1.5×10^6 cells were seeded in individual 100-mm petri dishes. After 48 hours, cells were harvested in Lysis Buffer (50 mM Tris-HCl pH 7.5, 5 mM EDTA, 150 mM NaCl, 1% NP-40, 0.5% sodium deoxycholate) with the addition of 1 mM phenylmethylsulfonyl fluoride and protease inhibitor cocktail (Sigma-Aldrich, St Louis, MO). Cells were detatched with a scraper and left on ice for 30′. Then extracts were clarified by centrifugation at 13200 rpm for 30′ at 4 °C.

For nuclear-cytoplasmic fractionation, 1.5×10^6 cells were seeded in 100-mm dishes. 24 hours after seeding, cell lysates were fractionated to obtain cytoplasmic and nuclear fractions as previously reported[24]. The amount of protein in the samples was determined by the Bio-Rad protein assay (Bio-Rad, Milan, Italy).

After the addition of Laemmli buffer (Sigma-Aldrich, St Louis, MO) samples were boiled at 100 °C for 5 min and resolved by SDS- polyacrylamide gel electrophoresis (SDS-PAGE). About 10 μg of nuclear and 30 μg of cytoplasmic or total extracts (1:3 rate) were separated by SDS-PAGE.

Proteins were then transferred to a polyvinylidene difluoride membrane (PDVF, Millipore) using a Mini trans-blot apparatus (Bio-Rad, Milan, Italy) according to the manufacturer's instructions. The PVDF membrane was blocked in 5% w/v milk buffer (5% w/v non-fat dried milk, 50 mM Tris, 200 mM NaCl, 0.2% Tween 20) and incubated overnight at 4 °C with primary antibodies diluted in 5% w/v milk or bovine serum albumin (BSA) buffer according to the manufacturer's instructions. Following three washes with TTBS (Tris-buffered saline, 0.1% Tween), the blots were incubated for 1 hour at RT with HRP-conjugated secondary antibodies (Sigma-Aldrich, St Louis, MO). Proteins were visualized by an enhanced chemiluminescence method (ECL, Bio-Rad, Milan, Italy) and analyzed by Quantity One W software of ChemiDoc TM XRS system (Bio-Rad, Milan, Italy).

Heat Shock treatments in cells and adult zebrafish caudal fins. Cells cultured in petri dishes were abruptly placed on the surface of a pre-heated water bath at the indicated time points and temperatures by floating the Petri dishes on a water bath floater (Promega).

Following heat shock treatment, cells were processed for immunofluorescence analysis. For the heat shock recovery experiment, cells were returned to a 26 °C incubator for the designated time.

For the analysis of mRNA expression during heat shock treatment, cells were exposed for 1 hour to heat shock and then returned to a 26 °C incubator for the remainder of the time course in order to avoid mortality due to prolonged exposure to the higher temperature.

Fins were gently placed in 2 ml Eppendorf tubes filled with complete cell culture medium (Leibovitz's L-15, Gibco BRL) and placed in a pre-warmed water bath at 45 °C for the designated time or in a cell culture incubator at 26 °C as a control.

Quantitative RT-PCRs. Total RNA was extracted with Trizol Reagent (Gibco) according to the manufacturer's instructions. Reverse transcription was performed using Superscript III RT (Invitrogen). A StepOnePlus Real-Time qRT-PCR System (Applied Biosystems) and SYBR Green I fluorescent dye (Promega) were used. Expression levels were normalized using *zf β-actin* and *gapdh* mRNA expression for zebrafish PAC2 and human HaCaT cells, respectively. The relative levels of mRNA were calculated using the $2^{-\Delta\Delta CT}$ method. For each gene, primer sequences are presented in Supplementary Table S2.

Statistical analysis. Statistical analyses were performed using GraphPad Prism7 (GraphPad Software Inc). Statistical significance of difference in measured variables between control and treated groups was determined by t-test or analysis of variance (1-way or 2-way ANOVA) followed by Tukey's, Dunnett's, or Sidak's multiple comparisons post-test depending on the experiment as specified in the figure legends and Table S1. To report p-values the NEJM (New England Journal of Medicine) decimal format was used; differences were considered statistically significant at $*P < 0.033$, $**P < 0.002$ and $***P < 0.001$. Detailed statistical information is summarized in Table S1.

References

1. Mahboubi, H. & Stochaj, U. Cytoplasmic stress granules: Dynamic modulators of cell signaling and disease. *Biochim Biophys Acta* **1863**, 884–895, https://doi.org/10.1016/j.bbadis.2016.12.022 (2017).
2. Thomas, M. G., Loschi, M., Desbats, M. A. & Boccaccio, G. L. RNA granules: the good, the bad and the ugly. *Cell Signal* **23**, 324–334, https://doi.org/10.1016/j.cellsig.2010.08.011 (2011).
3. Morimoto, R. I. The heat shock response: systems biology of proteotoxic stress in aging and disease. *Cold Spring Harb Symp Quant Biol* **76**, 91–99, https://doi.org/10.1101/sqb.2012.76.010637 (2011).
4. Walters, R. W. & Parker, R. Coupling of Ribostasis and Proteostasis: Hsp70 Proteins in mRNA Metabolism. *Trends Biochem Sci* **40**, 552–559, https://doi.org/10.1016/j.tibs.2015.08.004 (2015).
5. Kedersha, N. & Anderson, P. Mammalian stress granules and processing bodies. *Methods Enzymol* **431**, 61–81, https://doi.org/10.1016/S0076-6879(07)31005-7 (2007).
6. Protter, D. S. W. & Parker, R. Principles and Properties of Stress Granules. *Trends Cell Biol* **26**, 668–679, https://doi.org/10.1016/j.tcb.2016.05.004 (2016).
7. Nagamori, I., Cruickshank, V. A. & Sassone-Corsi, P. Regulation of an RNA granule during spermatogenesis: acetylation of MVH in the chromatoid body of germ cells. *J Cell Sci* **124**, 4346–4355, https://doi.org/10.1242/jcs.096461 (2011).
8. Anderson, P. & Kedersha, N. RNA granules. *J Cell Biol* **172**, 803–808, https://doi.org/10.1083/jcb.200512082 (2006).
9. Gimenez-Barcons, M. & Diez, J. Yeast processing bodies and stress granules: self-assembly ribonucleoprotein particles. *Microb Cell Fact* **10**, 73, https://doi.org/10.1186/1475-2859-10-73 (2011).
10. Rieckher, M. & Tavernarakis, N. P-body and Stress Granule Quantification in Caenorhabditis elegans. *Bio Protoc* **7**, https://doi.org/10.21769/BioProtoc.2108 (2017).
11. Buchan, J. R. mRNP granules. Assembly, function, and connections with disease. *RNA Biol* **11**, 1019–1030, https://doi.org/10.4161/15476286.2014.972208 (2014).
12. Kim, W. J., Back, S. H., Kim, V., Ryu, I. & Jang, S. K. Sequestration of TRAF2 into stress granules interrupts tumor necrosis factor signaling under stress conditions. *Mol Cell Biol* **25**, 2450–2462, https://doi.org/10.1128/MCB.25.6.2450-2462.2005 (2005).
13. Arimoto, K., Fukuda, H., Imajoh-Ohmi, S., Saito, H. & Takekawa, M. Formation of stress granules inhibits apoptosis by suppressing stress-responsive MAPK pathways. *Nat Cell Biol* **10**, 1324–1332, https://doi.org/10.1038/ncb1791 (2008).
14. Takahara, T. & Maeda, T. Transient sequestration of TORC1 into stress granules during heat stress. *Mol Cell* **47**, 242–252, https://doi.org/10.1016/j.molcel.2012.05.019 (2012).
15. Buchan, J. R. & Parker, R. Eukaryotic stress granules: the ins and outs of translation. *Mol Cell* **36**, 932–941, https://doi.org/10.1016/j.molcel.2009.11.020 (2009).
16. Anderson, P. & Kedersha, N. Visibly stressed: the role of eIF2, TIA-1, and stress granules in protein translation. *Cell Stress Chaperones* **7**, 213–221 (2002).
17. Loschi, M., Leishman, C. C., Berardone, N. & Boccaccio, G. L. Dynein and kinesin regulate stress-granule and P-body dynamics. *J Cell Sci* **122**, 3973–3982, https://doi.org/10.1242/jcs.051383 (2009).
18. Somasekharan, S. P. *et al*. YB-1 regulates stress granule formation and tumor progression by translationally activating G3BP1. *J Cell Biol* **208**, 913–929, https://doi.org/10.1083/jcb.201411047 (2015).
19. Suresh, P. S., Tsutsumi, R. & Venkatesh, T. YBX1 at the crossroads of non-coding transcriptome, exosomal, and cytoplasmic granular signaling. *Eur J Cell Biol* **97**, 163–167, https://doi.org/10.1016/j.ejcb.2018.02.003 (2018).
20. Kim, E. R. *et al*. The proteolytic YB-1 fragment interacts with DNA repair machinery and enhances survival during DNA damaging stress. *Cell Cycle* **12**, 3791–3803, https://doi.org/10.4161/cc.26670 (2013).
21. Hollert, H. & Keiter, S. H. Danio rerio as a model in aquatic toxicology and sediment research. *Environ Sci Pollut Res Int* **22**, 16243–16246, https://doi.org/10.1007/s11356-015-5362-1 (2015).
22. Penberthy, W. T., Shafizadeh, E. & Lin, S. The zebrafish as a model for human disease. *Front Biosci* **7**, d1439–1453 (2002).
23. Bosco, D. A. *et al*. Mutant FUS proteins that cause amyotrophic lateral sclerosis incorporate into stress granules. *Hum Mol Genet* **19**, 4160–4175, https://doi.org/10.1093/hmg/ddq335 (2010).
24. Acosta, J. R. *et al*. Mutant human FUS Is ubiquitously mislocalized and generates persistent stress granules in primary cultured transgenic zebrafish cells. *PLoS One* **9**, e90572, https://doi.org/10.1371/journal.pone.0090572 (2014).
25. Zampedri, C. *et al*. Zebrafish P54 RNA helicases are cytoplasmic granule residents that are required for development and stress resilience. *Biol Open* **5**, 1473–1484, https://doi.org/10.1242/bio.015826 (2016).
26. Pagano, C. *et al*. The tumor-associated YB-1 protein: new player in the circadian control of cell proliferation. *Oncotarget* **8**, 6193–6205, https://doi.org/10.18632/oncotarget.14051 (2017).
27. Eliseeva, I. A., Kim, E. R., Guryanov, S. G., Ovchinnikov, L. P. & Lyabin, D. N. Y-box-binding protein 1 (YB-1) and its functions. *Biochemistry (Mosc)* **76**, 1402–1433, https://doi.org/10.1134/S0006297911130049 (2011).
28. Woolley, A. G. *et al*. Prognostic association of YB-1 expression in breast cancers: a matter of antibody. *PLoS One* **6**, e20603, https://doi.org/10.1371/journal.pone.0020603 (2011).
29. di Martino, O. *et al*. DeltaNp63alpha controls YB-1 protein stability: evidence on YB-1 as a new player in keratinocyte differentiation. *Genes Cells* **21**, 648–660, https://doi.org/10.1111/gtc.12373 (2016).
30. Moutaoufik, M. T. *et al*. UVC-induced stress granules in mammalian cells. *PLoS One* **9**, e112742, https://doi.org/10.1371/journal.pone.0112742 (2014).
31. Matsuki, H. *et al*. Both G3BP1 and G3BP2 contribute to stress granule formation. *Genes Cells* **18**, 135–146, https://doi.org/10.1111/gtc.12023 (2013).
32. Wilczynska, A., Aigueperse, C., Kress, M., Dautry, F. & Weil, D. The translational regulator CPEB1 provides a link between dcp1 bodies and stress granules. *J Cell Sci* **118**, 981–992, https://doi.org/10.1242/jcs.01692 (2005).

33. Kedersha, N. *et al.* Evidence that ternary complex (eIF2-GTP-tRNA(i)(Met))-deficient preinitiation complexes are core constituents of mammalian stress granules. *Mol Biol Cell* **13**, 195–210, https://doi.org/10.1091/mbc.01-05-0221 (2002).
34. Pagano, C. *et al.* Evolution shapes the responsiveness of the D-box enhancer element to light and reactive oxygen species in vertebrates. *Sci Rep* **8**, 13180, https://doi.org/10.1038/s41598-018-31570-8 (2018).
35. Zhao, H. *et al.* Modulation of DNA repair systems in blind cavefish during evolution in constant darkness. *Current Biology* **28**, 3229-3243, https://doi.org/10.1016/j.cub.2018.08.039 (2018).
36. Guarino, A. M. *et al.* Oxidative Stress Causes Enhanced Secretion of YB-1 Protein that Restrains Proliferation of Receiving Cells. *Genes (Basel)* **9**, https://doi.org/10.3390/genes9100513 (2018).
37. Souquere, S. *et al.* Unravelling the ultrastructure of stress granules and associated P-bodies in human cells. *J Cell Sci* **122**, 3619–3626, https://doi.org/10.1242/jcs.054437 (2009).
38. Albornoz, A., Carletti, T., Corazza, G. & Marcello, A. The stress granule component TIA-1 binds tick-borne encephalitis virus RNA and is recruited to perinuclear sites of viral replication to inhibit viral translation. *J Virol* **88**, 6611–6622, https://doi.org/10.1128/JVI.03736-13 (2014).
39. Bley, N. *et al.* Stress granules are dispensable for mRNA stabilization during cellular stress. *Nucleic Acids Res* **43**, e26, https://doi.org/10.1093/nar/gku1275 (2015).
40. Bounedjah, O. *et al.* Free mRNA in excess upon polysome dissociation is a scaffold for protein multimerization to form stress granules. *Nucleic Acids Res* **42**, 8678–8691, https://doi.org/10.1093/nar/gku582 (2014).
41. Lyons, S. M., Achorn, C., Kedersha, N. L., Anderson, P. J. & Ivanov, P. YB-1 regulates tiRNA-induced Stress Granule formation but not translational repression. *Nucleic Acids Res* **44**, 6949–6960, https://doi.org/10.1093/nar/gkw418 (2016).
42. Palicharla, V. R. & Maddika, S. HACE1 mediated K27 ubiquitin linkage leads to YB-1 protein secretion. *Cell Signal* **27**, 2355–2362, https://doi.org/10.1016/j.cellsig.2015.09.001 (2015).
43. Uramoto, H. *et al.* p73 Interacts with c-Myc to regulate Y-box-binding protein-1 expression. *J Biol Chem* **277**, 31694–31702, https://doi.org/10.1074/jbc.M200266200 (2002).
44. Shiota, M. *et al.* Twist and p53 reciprocally regulate target genes via direct interaction. *Oncogene* **27**, 5543–5553, https://doi.org/10.1038/onc.2008.176 (2008).
45. Kampinga, H. H. Thermotolerance in mammalian cells. Protein denaturation and aggregation, and stress proteins. *J Cell Sci* **104**(Pt 1), 11–17 (1993).
46. Arunachalam, M., Raja, M., Vijayakumar, C., Malaiammal, P. & Mayden, R. L. Natural history of zebrafish (Danio rerio) in India. *Zebrafish* **10**, 1–14, https://doi.org/10.1089/zeb.2012.0803 (2013).
47. Spence, R., Gerlach, G., Lawrence, C. & Smith, C. The behaviour and ecology of the zebrafish, Danio rerio. *Biol Rev Camb Philos Soc* **83**, 13–34, https://doi.org/10.1111/j.1469-185X.2007.00030.x (2008).
48. Aulas, A. *et al.* Stress-specific differences in assembly and composition of stress granules and related foci. *J Cell Sci* **130**, 927–937, https://doi.org/10.1242/jcs.199240 (2017).
49. Kedersha, N. L., Gupta, M., Li, W., Miller, I. & Anderson, P. RNA-binding proteins TIA-1 and TIAR link the phosphorylation of eIF-2 alpha to the assembly of mammalian stress granules. *J Cell Biol* **147**, 1431–1442 (1999).
50. Kedersha, N. & Anderson, P. Stress granules: sites of mRNA triage that regulate mRNA stability and translatability. *Biochem Soc Trans* **30**, 963–969, doi:10.1042/ (2002).
51. Stohr, N. *et al.* ZBP1 regulates mRNA stability during cellular stress. *J Cell Biol* **175**, 527–534, https://doi.org/10.1083/jcb.200608071 (2006).
52. Holcik, M. & Sonenberg, N. Translational control in stress and apoptosis. *Nat Rev Mol Cell Biol* **6**, 318–327, https://doi.org/10.1038/nrm1618 (2005).
53. Sonenberg, N. & Hinnebusch, A. G. Regulation of translation initiation in eukaryotes: mechanisms and biological targets. *Cell* **136**, 731–745, https://doi.org/10.1016/j.cell.2009.01.042 (2009).
54. Jackson, R. J., Hellen, C. U. & Pestova, T. V. The mechanism of eukaryotic translation initiation and principles of its regulation. *Nat Rev Mol Cell Biol* **11**, 113–127, https://doi.org/10.1038/nrm2838 (2010).
55. Sukarieh, R., Sonenberg, N. & Pelletier, J. The eIF4E-binding proteins are modifiers of cytoplasmic eIF4E relocalization during the heat shock response. *Am J Physiol Cell Physiol* **296**, C1207–1217, https://doi.org/10.1152/ajpcell.00511.2008 (2009).
56. Nüsslein-Volhard, C. & Dahm, R. *Zebrafish: a practical approach*. (Oxford University Press, 2002).
57. Lin, S. *et al.* Integration and germ-line transmission of a pseudotyped retroviral vector in zebrafish. *Science* **265**, 666–669 (1994).
58. Idda, M. L. *et al.* Circadian timing of injury-induced cell proliferation in zebrafish. *PLoS One* **7**, e34203, https://doi.org/10.1371/journal.pone.0034203 (2012).
59. Vogler, T. O. *et al.* TDP-43 and RNA form amyloid-like myo-granules in regenerating muscle. *Nature* **563**, 508–513, https://doi.org/10.1038/s41586-018-0665-2 (2018).
60. Walton, W. H. Feret's Statistical Diameter as a Measure of Particle Size. *Nature* **162**, 2 (1948).

Acknowledgements

We thank H. Zhao, R. Siauciunaite, A. Troiano and D. Antonini for support and discussion. The authors also thank the practical students from the European School Karlsruhe for technical help. This research was funded through the Helmholtz funding programme BIFTM for N. Geyer, D. Vallone and N.S. Foulkes; the German Israeli Foundation for Scientific research and Development for G. Ruggiero. A.M. Guarino is supported by 31st PhD program in Biotechnology 2016-2019-MIUR. V. Calabrò is supported by Ricerca Dipartimentale 2017-2018-MIUR. G. Di Mauro is supported by research grants from the University of Ferrara (FAR 2015-2017) and by IUSS 2017 for PhD mobility. Exchange between the N.S Foulkes and V. Calabro' laboratories is also supported by the MIUR-DAAD Joint Mobility Program 2018. We acknowledge support by the Deutsche Forschungsgemeinschaft and the open access publishing fund of Karlsruhe Institute of Technology.

Author Contributions

D. Vallone, V. Calabro', N.S. Foulkes and A.M. Guarino designed the research project and prepared the manuscript; A.M. Guarino, G. Di Mauro, G. Ruggiero, A. Delicato and N. Geyer performed the experiments; D. Vallone, V. Calabro', N.S. Foulkes and A.M. Guarino analyzed the data; A.M. Guarino prepared the figures.

Additional Information

Supplementary information accompanies this paper at https://doi.org/10.1038/s41598-019-45468-6.

Competing Interests: The authors declare no competing interests.

Publisher's note: Springer Nature remains neutral with regard to jurisdictional claims in published maps and institutional affiliations.

Biochimie 179 (2020) 205–216

Contents lists available at ScienceDirect

Biochimie

journal homepage: www.elsevier.com/locate/biochi

Y box binding protein 1 (YB-1) oncoprotein at the hub of DNA proliferation, damage and cancer progression

Felicia Sangermano[*, 1], Antonella Delicato [1], Viola Calabrò

Dipartimento di Biologia, Università di Napoli Federico II, Complesso Universitario Monte S. Angelo, Via Cintia 4, 80126, Napoli, Italy

ARTICLE INFO

Article history:
Received 22 May 2020
Received in revised form
6 October 2020
Accepted 7 October 2020
Available online 12 October 2020

Keywords:
Y-box binding protein 1
Proliferation
Cancer
Chemoresistance
DNA damage

ABSTRACT

The Y Box binding protein 1 (YB-1) belongs to the highly conserved Cold Shock Domain protein family and is a major component of messenger ribonucleoprotein particles (mRNPs) in various organisms and cells. Cold Shock proteins are multifunctional nucleic acids binding proteins involved in a variety of cellular functions. Biological activities of YB-1 range from the regulation of transcription, splicing and translation, to the orchestration of exosomal RNA content. The role of YB-1 in malignant cell transformation and fate transition is the subject of intensive investigation. Besides, emerging evidence indicates that YB-1 participates in several DNA damage repair pathways as a non-canonical DNA repair factor thus pointing out that the protein can allow cancer cells to evade conventional anticancer therapies and avoid cell death. Here, we will attempt to collect and summarize the current knowledge on this subject and provide the basis for further lines of inquiry.

Contents

1. The multitasking Y box binding protein 1

The Y Box Binding Protein 1, also known as YB-1, encoded by the YBX-1 gene, is one of the best-characterized members of the highly

* Corresponding author.
E-mail address: felicia.sangermano@unina.it (F. Sangermano).
[1] The authors have equally contributed to this manuscript.

https://doi.org/10.1016/j.biochi.2020.10.004
0300-9084/

conserved Cold Shock Protein (CSP) family. Initially identified in bacteria, when a sudden drop in temperature-induced the cold shock protein A (CspA), they were isolated from many other organisms including humans. In humans, five groups of human cold shock proteins (YB-1/Dbp, LIN28, CHSP1, PIPP'in, UNR/CSDE1) were identified and all of them contain at least one CSD [89]. Such a domain possesses nucleic acid binding properties and thus functions pleiotropically in a variety of processes such as transcription, translation, cell proliferation, differentiation, and cell fate transition [13]. However, the Cold Shock Domain (CSD) is highly conserved between all members of the Cold shock proteins therefore its function must be considered in the context of the protein it belongs to.

In humans, YB-1 represents the predominant form of CSP [89]. Based on NMR data, the protein maintains an unfolded structure except for the isolated CSD, which has a tertiary structure represented by a five-stranded β-barrel with consensus sequences RNP-1 (K/N-G-F/Y-G-F-I/V) and RNP-2 (V-F-V-H-F) on strands 2 and 3 [78]. The open structure of YB-1 gives the protein functional versatility and ability to associate with a multitude of molecular partners while the RNP consensus sequences mediate YB-1 specific and non-specific interactions with nucleic acids. In addition to the CSD, YB-1 consists of an alanine/proline-rich N-terminal domain (A/P domain) involved in protein/protein interactions and in stabilizing RNA binding and a large C-terminal domain (CTD) with alternating clusters of positively and negatively charged amino acid residues implicated both in nucleic acids binding and protein/protein interactions [12,91]. A cytoplasmic retention signal CRS (247–267) and three nuclear localization signals NLS1 (aa 149–156); NLS2 (aa 185–194) and NLS3 (aa 276–292) were identified [132]. A specific cleavage site for the 20S proteasome was identified between Glu219 and Gly220 (Fig. 1).

The subcellular localization of YB-1 is finely regulated. The cytoplasmic form is predominant in physiological conditions with an apparent molecular weight of 45–50 kDa. However, its cellular localization was found to be linked to progression through the cell cycle. Indeed, primarily perinuclear during G1 and S phases, YB-1 enters the nucleus at cells transition through late G2/M and exits at the end of mitosis [97]. A 36 kDa nuclear form of YB-1 was also described and believed to be generated by the 20S proteasome specific cleavage between glutamic acid 219 and glycine 220 in response to genotoxic stress [77,123]. However, some observations are inconsistent with the proteolysis model. Indeed, recent data show that full-length YB-1 is present in both nuclear and cytoplasmic compartments and that proteasomal cleavage of YB-1 does not occur in response to treatment with Doxorubicin or Paclitaxel [97].

For example, a strong induction of cleaved YB-1 in response to cisplatin was not accompanied by a concomitant decrease of full-length YB-1 [123] and in a separate study, neither paclitaxel nor cisplatin induced YB-1 cleavage under conditions in which nuclear translocation of YB-1 was occurring [38]. Moreover, Cohen et al., have provided evidence of genotoxic stress-induced nuclear localization of YB-1 in the absence of proteolytic processing [19].

The YB-1 protein interacts with different types of RNA such as messenger RNA (mRNA) and microRNA, managing their fate both under physiological and stress conditions [77]. Intracellular RNA distribution and YB-1 post-translation modifications are both relevant for controlling the subcellular localization of YB-1 [85].

Binding to DNA [140], YB-1 carries out its functions as a transcription factor controlling the expression of genes involved in cell cycle progression and stress response [27] or as non-canonical DNA-repair factor participating in different DNA repair mechanisms [27,28,44,56,87].

As RNA-binding protein [27,122], YB-1 mediates pre-mRNA splicing, participates in RNP granules assembly in the cytoplasm [11], and modulates mRNA translation [27,29]. At a low YB-1/RNA ratio, the protein binds to mRNA as a monomer thus allowing

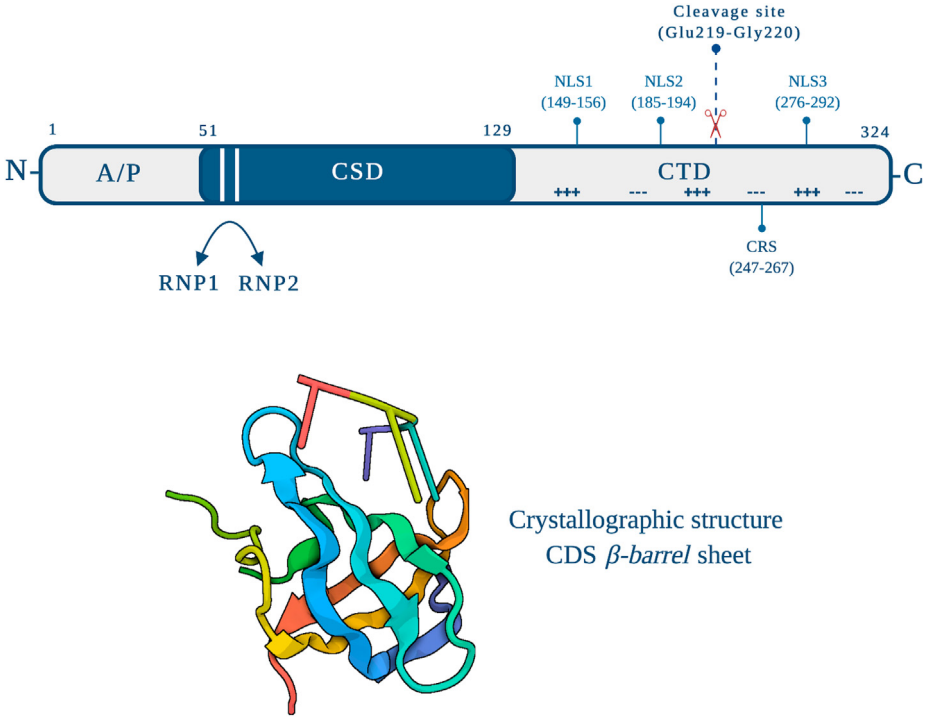

Fig. 1. Schematic representation and crystallographic structure of the Y box binding protein 1. The protein has three domains: A/P, CSD, CTD; the protein contains a cytoplasmic retention signal CRS (247–267) and three nuclear localization signals NLS1 (aa 149–156); NLS2 (aa 185–194) and NLS3 (aa 276–292). A specific cleavage site for the 20S proteasome (Glu219-Gly220) is also indicated. The CSD domain is the only one to maintain a three-dimensional structure consisting of five β-barrel strands.

RNA translation and turnover while at a high YB-1/RNA ratio, mRNAs remain inaccessible for translation initiation machinery and degradation by exonucleases [99]. Moreover, in the cytoplasm, YB-1 is a major component of mRNP complexes formed by human Argonautes (AGO), which are central to small RNA-mediated silencing [55,61]. YB-1 is linked to multiple noncoding RNAs and the pluripotency factor lin-28, a processor of the *let*-7 miRNA precursor thus suggesting that it may have a broad role in small RNA processing and metabolism [90,142].

Remarkably, there is also evidence that YB-1 interacts with viral RNA. YB-1 enhances the production of HIV-1 viral particles by stabilizing HIV RNAs and increasing viral protein expression [100]. Using quantitative PCR and an *in vivo* nuclear import assay with fluorescently labeled viral particles Weydert et al. have shown that YBX-1 gene knockdown leads to a block between reverse transcription and nuclear import of HIV-1 [139]. The YB-1 protein was also identified as an interacting partner of the Hepatitis C virus (HCV) genomic RNA. YB-1 stabilizes the viral NS5A protein [135] and NS3/4A serine-protease controlling the balance between viral RNA genome replication and production of infectious viral particles [16]. In cells infected by the influenza virus, YB-1 translocates to the nucleus and accumulates in PML nuclear bodies. The viral RNPs associate with YB-1 into the PML bodies and are exported to the cytoplasm where they are recruited to microtubules. It has been speculated that vRNP-YB-1 complexes, recruited on microtubules, may be disassembled and loaded onto Rab11a-positive recycling endosomes for efficient virus budding [74]. Notably, a functional relationship between YB-1 and microtubules dynamics was already documented [17].

One of the most intriguing aspects of YB-1 biology is the fact that, under certain conditions, YB-1 protein can be secreted. YB-1-derived polypeptides were found in the plasma of patients with sepsis and malignancies, independent of the origin of the tumor [126]. YB-1 was found to be secreted by monocytic and mesangial cells upon inflammation [37]. In 2018, we demonstrated that, under oxidative stress, YB-1 contributes to the formation of stress granules (SGs) with a parallel increase of YB-1 secretion in the cellular medium. SGs are cytoplasmic foci where untranslated messenger RNAs (mRNAs) are sorted or processed for reinitiation, degradation, or packaging into ribonucleoprotein particles (mRNPs) [121]. An enriched fraction of extracellular YB-1 (exYB-1) significantly inhibited proliferation of receiving cells thus indicating that acute oxidative stress causes the sustained release of YB-1 as a paracrine/autocrine signal that stimulates cell cycle arrest [49].

1.1. YB-1 in cell proliferation

An intracellular increase of YB-1 protein or the accumulation of YB-1 in the nuclear compartment was shown to influence the expression of genes responsible for cell division, differentiation, multiple drug resistance, and so on [27]. YBX-1 gene expression is elevated in proliferating normal cells. Moreover, YB-1 relocalizes from the cytoplasm to the nucleus at the G1/S phase transition and its nuclear accumulation was found to be associated with increased cyclin A and B1 expression [72] as well as the up-regulation of Topoisomerase IIa [116] and DNA polymerase α [28], possibly promoting DNA replication. More recent data indicate that YB-1 regulates not only the G1 phase but also the G2/M phases by controlling cell cycle-related genes [75,84]. Recently, Mehta et al. have demonstrated that YB-1 cellular localization is variable in the cell cycle and that YB-1 dephosphorylation is required for a nuclear entry during the G2 phase [97].

After growth stimuli, YB-1 is phosphorylated by the RSK, AKT or ERK1/2 kinases and translocates to the nucleus where it can transcriptionally induce growth-promoting genes containing Y/CCAAT box sequence in their promoter or enhancer such as EGFR [125], HER2 [117] and the PgP/MDR1 gene conferring multidrug resistance [6,130]. Besides, YB-1 was shown to control the expression of phosphatase PTP1B [41], matrix metalloproteinases (MMP-2 and MMP-12) [95,96,113], collagen α 1(I) [106], and collagen α 2(I) [26,60], all of which are involved in cell adhesion and motility. Genes that are transcriptionally repressed by YB-1 include collagenα1, MHC class II and granulocyte-macrophage colony-stimulating factor (GM-CSF) [79,86]. The regulation of gene expression by nuclear YB-1 was interpreted as evidence for YB-1 involvement in transcription regulation in the vast majority of manuscripts although this is not unequivocally established given the possibility of YB-1 to control mRNA localization and stability (Fig. 2).

1.2. YB-1 in DNA damage

The emerging role of YB-1 as an important player and coordinator in the maintenance of genome integrity deserves closer inspection [105]. Cells could proliferate while harboring DNA lesions, which significantly increases the chance of genetic mutation or chromosomal rearrangements inducing cancer progression, antineoplastic resistance and metastases. Involvement in DNA repair is not unusual for an RNA-binding protein (RBPs) since RBPs coat nascent transcripts and prevents transcription-associated DNA damage [21,54]. Certain RBPs and RNA species are recruited at DNA damage sites induced by various stressors such as UV, reactive oxygen species and ionizing radiation [54]. RBPs facilitate DNA damage responses by interacting with DNA repair proteins. YB-1 exhibits a strong affinity for damaged DNA and RNA [64] as well as for Poly (ADP-ribose) whose dynamic within the cell is essential for DNA repair [42].

Genotoxic stress was found to induce a relocation of full-length YB-1 from the cytoplasm to the nucleus [8,19,38,108] following a specific phosphorylation event at Ser102. This aspect, however, is controversial as others have demonstrated that stress-induced phosphorylation of YB-1 occurs into the nucleus and it depends on p90Ribosomal S6 Kinase (RSK) nuclear trafficking [128].

In multiple myeloma, YB-1 nuclear localization and interaction with the splicing factor U2AF65 promote mRNA processing and the stabilization of transcripts involved in homologous recombination in response to DNA damage [93].

The DNA damage response (DDR) consists of a plethora of signaling and repair mechanisms that together constitute important tool cells utilize to preserve genome stability. Low levels of DNA damage can cause cell cycle arrest, down-regulation of gene expression and promote repair of DNA lesions [2] whereas severe DNA damage leads to apoptosis or permanent cell cycle arrest (senescence) to avoid neoplastic transformation.

Distinct repair mechanisms are used to correct different types of DNA lesions. DSB (double-stranded break) is the most severe form of genomic lesions which can be induced by environmental exposure such as chemicals, ultraviolet (UV) or ionizing radiation (IR), as well as endogenous agents like reactive oxygen species generated by tissue inflammation and cell metabolism [14]. Depending on the type of lesions, different axes of the DNA damage response (DDR) are activated. For example, double-strand breaks (DSBs) recruit the ATM and DNA-PK kinases, while single-stranded breaks (SSBs) recruit the ATR kinase. Following their activation, the ATM/ATR kinases activate other kinases, including CHK1 and CHK2 [14]. DNA mismatch repair and base-excision repair (BER) act on simple lesions, while nucleotide excision repair (NER), non-homologous end joining (NHEJ) and homologous recombination (HR) deal with more complex lesions. Successful HR is generally error-free while NHEJ and other alternative forms of DNA repair are more likely to introduce DNA lesions.

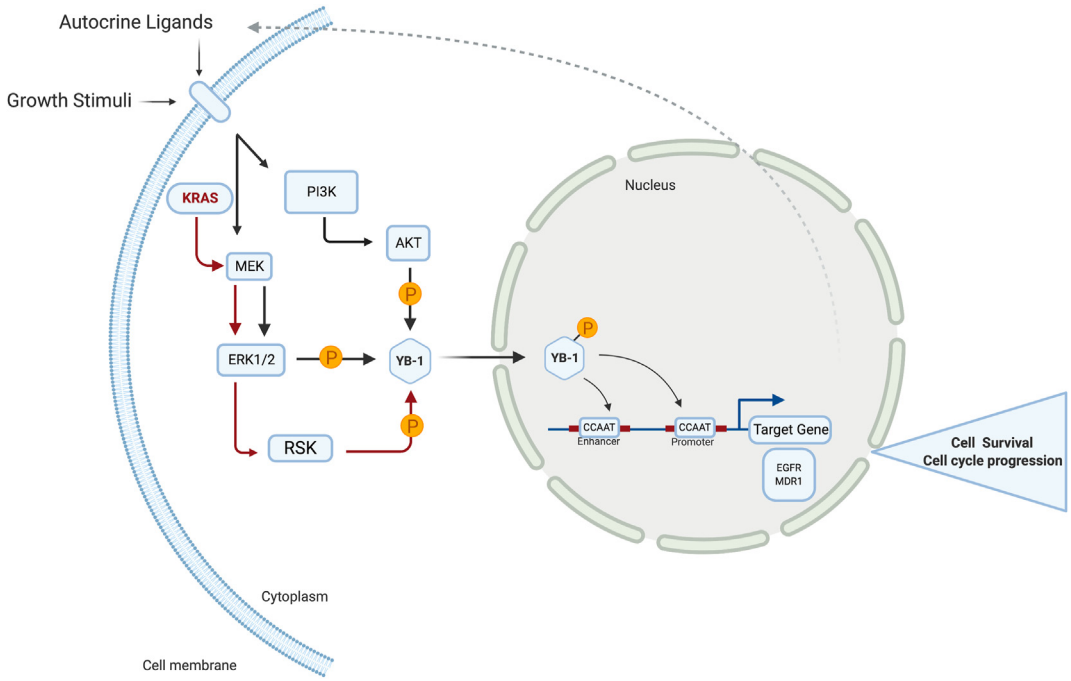

Fig. 2. Mitogenic stimuli induce YB-1-driven transcription. In figure are represented different ways of phosphorylation and activation of the YB-1 protein and its involvement in the regulation of cell cycle progression and proliferation.

Genomic lesions can be recognized and labeled by the recruitment of sensor proteins, which activate the complex DDR network and mobilizes DNA repair machinery [69]. YB-1 is just emerging as an important sensor of the cellular DDR and a critical factor in the response to different stressors such as chemicals, IR and UV irradiation. According to that, YB-1 null fibroblasts isolated from mice embryos and adult tissues have shown a reduction in the response to oxidative, oncogene and genotoxic stresses [153].

YB-1 participation in DNA repair was first hypothesized as far back as 1991 when YB-1 was shown to have increased affinity for DNA with apurinic sites [56]. This suggestion was supported by evidence for elevated DNA binding activity of YB-1 in nuclear extracts of cells exposed to UV radiation or anticancer agents [80,98,129].

YB-1 regulates the separation of DNA strands in case of mismatch repairs or mutation caused by drugs [29,60,104] and efficiently melt duplexes with unpaired bases. Moreover, YB-1 exhibits a slight 3′–5′ exonuclease and endonuclease activity on single- and double-stranded DNAs that might be strongly dependent on the DNA sequence and structure [44,50,65].

YB-1 regulates both base-excision repair and mismatch repair pathways by conducting multiple associations with DNA repair proteins: base excision repair enzymes NEIL2 [22], APE1 [114], DNA polymerase β [22], DNA polymerase δ [44], PCNA [64], DNA-ligase IIIα [22], NEIL1, PARP1, and PARP2 [1], mismatch repair enzymes (MSH2 [44]), and DNA double-stranded breaks repair enzymes Ku80 [44]. YB-1 is required for the recognition of bulky lesions by NER factor XPC-HR23b [35] and modulates the activity of key and regulatory BER enzymes [1,22,35,94] such as glycosylase NEIL 1, NEIL2, DNA ligase IIIa, DNA polymerase b and d, MSH2, Ku80, APE1, WRN and endonuclease III [57,63,110]. For istance, YB-1 enhances the enzymatic activity of DNA glycosylases NEIL-2 and hNth1, which initiates base excision repair of pyrimidines modified by reactive oxygen species, ionizing, and ultraviolet radiation [22,50,94]. In 2012 Pestryakov P. and co-workers found that YB-1 inhibited AP site cleavage by NEIL-1 when the AP site was in single-stranded DNA.

In other studies, YB-1 has been suggested to be involved in the Nucleotide Excision Repair (NER) mechanism where YB-1 binds to DNA containing a bulky of clustered lesions forming a complex with the NER factor XPC-HR23B [35]. Moreover, it was also found to be associated with Rad50 and MRE11 under IR stimuli [34].

The physical interaction of YB-1 with key BER factors such as PARP1, PARP2, APE1, NEIL1 and pol β has been characterized by Alemasova E.E. et al. in 2016. Data on functional interactions revealed strong stimulation of PARP1 self poly (ADP-ribosyl)ation and inhibition of poly (ADP-ribose) degradation by PARG in the presence of YB-1. YB-1, itself, was shown to be poly-ADP-ribosylated in the presence of RNA [1], it acted as a potent poly (ADP-ribose) polymerase 1 (PARP1) cofactor that can reduce the efficiency of PARP1 inhibitors. The C-terminal domain of YB-1 proved to be indispensable for PARP1 stimulation and the functional interactions of YB-1 and PARP1 were shown to be mediated and regulated by poly (ADP-ribose) [3].

Remarkably, YB-1 directly interacts with the p53 oncosuppressor protein which is physically involved in DNA repair by interacting with damaged DNA [7,67] and nucleotide excision repair factors such as XPB and XPD [137,152] have shown that genotoxic stresses induce nuclear localization of YB-1 only in cells with wild-type p53 [152]. Moreover, they demonstrated that tumor-associated p53 mutants are attenuated for YB-1 nuclear localization and that YB-1 inhibits p53-induced cell death and its ability to trans-activate promoters of genes involved in cell death signaling. These data indicate that some forms of mutant p53 can cause YB-1 accumulation in the nucleus, which in turn inhibits p53 activity providing further insights into the role of YB-1 into the mechanisms that allow the tumor cells to escape from death.

Intriguingly, YB-1 was also found to be localized to mitochondria in human cells, and significantly contribute to the mismatch-binding and mismatch-repair activity detected in mitochondrial extracts, Moreover, YB-1 depletion in cells was shown to increase mitochondrial DNA mutagenesis [25].

All these observations suggest that YB-1 participates in the recognition of damaged DNA with multiple mechanisms (Fig. 3) and acts as a scaffold in forming a repair complex at the damaged site thus highlighting the high relevance of this protein for the response of tumor cells to chemotherapy. It would be interesting to further investigate this aspect by using an appropriate cellular model such as the AsiSI system. This system is based on the use of SfaAI (AsiSI) restriction enzyme to generate unambiguously positioned sequence-specific DSBs [4,103].

1.3. YB-1 a versatile hub in cancer

YB-1 is highly expressed in several types of tumors such as breast, prostate, osteosarcoma, lung, colorectal, glioblastoma, ovarian, gastric, head-neck cancer, and melanoma, and therefore its overexpression is regarded as a hallmark of cancer [32,46,48,82,83,107,116,125,143,146]. However, the involvement of YB-1 in multiple mechanisms regulating cell homeostasis makes it difficult to define how this protein contributes to cancer pathogenesis and progression. Table 1 summarises the proposed roles of YB-1 in cancer.

In all the studies done so far, YB-1 overexpression in cancer is associated with poor prognosis and unfavorable outcome [68,116], in most of them, the worst prognosis is associated with the nuclear accumulation of YB-1, especially of the phosphorylated form [9,107,115,120,146]. However, some studies have disputed the fact that only nuclear accumulation is associated with poor outcomes as it was reported in nasopharyngeal [127] and breast cancer [66]. In others, cytoplasmic YB-1 that does not exhibit phosphorylation at Ser102 stimulates tumorigenesis and invasiveness of cancer cells by influencing the epithelial-mesenchymal transition [31,83]. Indeed, under normal conditions, YB-1 has a predominantly cytoplasmic localization where it inhibits PI3K/Akt-induced oncogenic transformation by blocking the translation of growth-related mRNA species [30]. However, when phosphorylated at serine 102, by Akt or p90 ribosomal S6 kinases RSK1/2 [5,30,124], YB-1 moves from the cytosol to the nucleus where it is required for transcriptional activation of growth-enhancing and chemoresistance genes notably the human epidermal growth factor receptor HER2/neu, the epidermal growth factor receptor EGFR, the proliferating cell nuclear antigen PCNA, c-MET, the cyclins A and B, the matrix metalloproteinase-2 (MMP-2) and the multi-drug resistance 1 (P-gp/MDR1) gene [33,73,80,109,125,129,141].

Below are some examples of how YB-1 is involved in different types of tumors and the postulated mechanisms by which it is believed to perform its oncogenic functions. We have mainly focused on the most frequent cancer types for which data from patients rather than cell lines alone were available. A summary of references reporting the YB-1 subcellular localization associated to the different type of tumors is shown in Table 2.

1.3.1. Breast cancer

The association of YB-1 with breast cancer is very frequent but its etiological significance is still unclear. In 2005, Bergman and coworkers found that one of the earliest and most remarkable changes observed in human mammary epithelial cells following YB-1 induction was the strikingly high incidence of multinucleated cells. At 48 h following YB-1 induction, a significant proportion of cells were binucleate thus indicating mitotic failure and centrosome amplification. They postulated that overexpression of YB-1 may be an initiating event for the early development of breast cancer [10].

In 2011, YB-1 was shown to localize to the centrosome in a phosphorylation-dependent manner where it was associated in a complex with pericentrin and γ-tubulin [23]. This was found to be essential in maintaining the structural integrity and microtubule nucleation capacity of the organelle. Prolonged exposure to YB-1 led to rampant acceleration toward tumourigenesis with most of

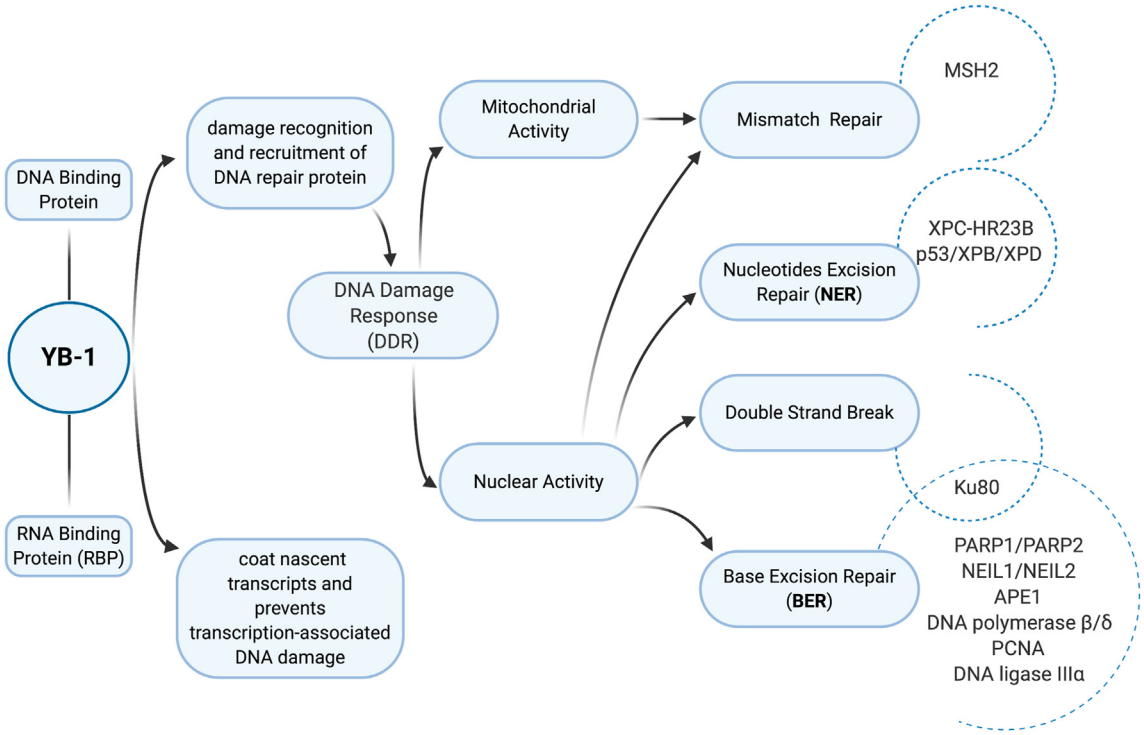

Fig. 3. YB-1 protein activity in recognition and repair of DNA damage. The figure shows that YB-1 is involved in different mechanisms of DNA repair (NER, BER, Mismatch Repair, Double Strand Break) by interacting with several factors.

Table 1
Proposed roles of YB-1 in cancer.

TYPE OF TUMOR	PROPOSED YB-1 ONCOGENIC FUNCTION	REFERENCES
EPIDERMOID CARCINOMA	Reduced sensitivity to cisplatin, mitomycin C, and UV radiation.	[108]
OSTEOSARCOMA	P-gp/MDR1 overexpression.	[107]
GLIOBLASTOMA	EGFR upregulation. Increased cell proliferation and invasion. Reduced sensitivity to temozolomide. miRNAs expression deregulation.	[32] [43] [119]
NEUROBLASTOMA	Increased cell proliferation, migration and invasion. Cisplatin-resistance.	[133]
BLADDER CANCER	Promotion of aerobic glycolysis by Myc and HIF1 upregulation.	[114]
PROSTATE AND RENAL CANCER	AR overexpression. Castration-resistant growth. Drug resistance.	*Heumann A.* et al., *2017.* [151]
COLORECTAL CANCER	Cell invasion and lymph-node metastasis. Reduced sensitivity to radio and chemotherapy.	*Kim A.* et al., *2019.* [92]
LUNG CANCER AND MESOTHELIOMA	EGFR, BRAF and ALK upregulation. Lymph-node metastasis.	[70]
BREAST CANCER	Chromosomal abnormalities. Her2/neu and EGFR overexpression. Lymph-node metastasis.	[40] [8]

cells acquiring numerical and structural chromosomal abnormalities. Slippage through the G_1/S checkpoint due to YB-1-driven cyclin E overexpression promoted continued proliferation of these genomically compromised cells. Cytokinesis failure can lead to both centrosome amplification and production of tetraploid cells, which could set the stage for the development of breast cancer cells [39]. The described phenotype was contingent upon YB-1 Ser102 phosphorylation as transient expression of phosphor-mimetic mutant YB-1^{S102D} could recapitulate the phenotype whereas YB-1^{S102A} could not. In YB-1 knock-down cells, instead, lobulated nuclei were assembled at the G1 phase due to a defective reassembly of nuclear envelope caused by sporadic non-centrosomal microtubule formation at the end of mitosis [39].

Increased expression of YB-1 in breast cancer was associated with a poorer prognosis in terms of decreased patient survival and increased recurrence rates [101]. Using meta-analysis on a wide number of published studies, Wang X. et al., found that YB-1 overexpression in breast cancer did not correlate with the lymph node status, high histological type or grade, or p53 status. However, a higher level of YB-1 protein was associated with other unfavorable factors such as ER negativity, HER2/neu positivity and high tumor T stage [136].

In a more recent study, performed by immunohistochemistry, on histopathology specimens of 74 patients with breast carcinoma, YB-1 expression was quantified in terms of "immunoreactive score" and correlated with clinical parameters, hormone receptor status, and Her2neu overexpression. In this study, YB-1 showed cytoplasmic positivity in all the cases, whereas nuclear expression of YB-1 was found to be positive in 48.6% cases and had a significant association with Her2 positivity and ER and PR negativity. Taking as positive only YB-1 nuclear expression no association was found with tumor grade and stage whereas lymph node metastasis had a significant positive correlation with YB-1 expression. Triple-negative breast carcinoma constituted 25.6% of the total cases, out of which 73.6% were YB-1 positive. However, no association was found with tumor grade, stage, histological subtype, presence of *in situ* component, or other clinical parameters such as age or menopausal status [8].

Receptor tyrosine kinase HER2 and EGFR are frequently over-expressed in human breast cancer [62]. The overexpression of the epidermal growth factor receptor (EGFR) and HER-2 underpin the growth of aggressive breast cancer. Importantly, the co-expression of Her2 and Her3 activates the downstream PI3k/Akt pathway which is considered a carcinogenic function of overexpressed Her2.

Table 2
Summary of references reporting the YB-1 subcellular localization associated to the different type of tumors.

TYPE OF TUMOR	SUBCELLULAR LOCALIZATION		
	Nuclear	***Cytoplasmic***	***Nuclear/Cytoplasmic***
BREAST CANCER	[20] [141] [112] [88] [18] [15] *Fang Yang* et al., *2019*	[101] Anbok L. et al., *2016*	[8]
COLORECTAL CANCER	[120] [116] [102]		[92]
EPIDERMOID CARCINOMA	[108]		
OSTEOSARCOMA	[107] [40]		
NEUROBLASTOMA			[133]
GLIOBLASTOMA MULTIFORME	[43]	[119]	[32]
BLADDER CANCER	[114]		
LUNG CANCER AND MESOTHELIOMA	[70] [51]		[115] [71]
PROSTATE AND RENAL CANCER	[118] *Heumann A.* et al., *2017*		

In turn, the PI3K/Akt signaling leads to YB-1 phosphorylation on Ser102, inducing its nuclear translocation. In this case, YB-1 can bind directly and activate the Her2 and EGFR gene promoters. Mutating YB-1 at Ser102, which resides in the DNA-binding domain, prevented growth induction. Based on chromatin immunoprecipitation, the mutant YB-1 protein was unable to optimally bind to the EGFR and HER-2 promoters. Furthermore, knocking down YB-1 with small interfering RNA suppressed the expression of EGFR and HER-2 and this was coupled with a decrease in tumor cell growth. In conclusion, YB-1Ser102 was considered a point of molecular vulnerability for maintaining the expression of EGFR and HER-2 [141] and the YB-1-Her2 axis is now considered important for personalized therapies using targeted drugs in breast cancer, particularly in tumors that overexpress Her2 [8]. Remarkably, the nuclear expression of YB-1 in breast cancer was also thought to be associated with intrinsic P-glycoprotein (MDR1) and multidrug resistance which is a common clinical problem in breast cancer treatment [112]. In recent studies, it has been demonstrated that YB-1 promotes breast cancer metastases and invasion by regulating MMP1 and β−catenin [89] or the EZH2/amphiregulin signaling induced by LPA [18].

Interleukin 6 (IL-6) has emerged as a key inflammation-associated cytokine significantly produced by breast cancer cells and adipocytes with the potential of inducing proliferation, epithelial-mesenchymal transition, angiogenesis and therapeutic resistance [52]. In breast cancer, IL-6 was found to increase the phosphorylation level of YB-1 on Ser-102 and promote its translocation in the nucleus with the consequent activation of YB-1 target genes. YB-1, in turn, was shown to bind and stabilize IL-6 mRNA, so creating a positive feed-forward loop between each other [15].

In 2019, the YBX-1 gene was successfully knocked out in MCF-7 breast cancer stem cells using the CRISPR/Cas9 system. By this approach, YB-1 was shown to maintain the stemness of breast cancer stem cells by promoting the expression of stemness-related genes (FZD-1, p21, GLP-1, GINS1, and Notch2). Therefore, YB-1 plays a key role in the activation and reversion of the totipotency/pluripotency of differentiated cancer cells [148].

1.3.2. Colorectal cancer

Colorectal cancer (CRC) is still one of the most lethal sex-independent cancers in the world [111,112]. YB-1 overexpression was associated with colorectal cancer invasion, lymph node metastasis and resistance to radio and chemotherapy [146]. YB-1 expression was analyzed by immunohistochemistry in CRC tissues of 124 patients who underwent curative resection. High-grade nuclear YB-1 expression was detected in 80 out of 124 samples and found to be a useful predictor of poorer overall survival and relapse-free survival. Moreover, it was found to correlate with EGFR status in CRC patients [121]. According to the Shiraiwa's work, Nagasu found that YB-1 knockdown reduces the expression of EGFR in human colon carcinoma cell lines with concomitant induction of apoptosis-related genes [103].

Remarkably, colorectal cancers characterized by KRAS mutation are resistant to treatment with cetuximab, an EGFR monoclonal antibody. The ability of oncogenic mutated KRAS to overcome cetuximab treatment in CRC cells was investigated in 2019 [93]. It was shown that mutated KRAS stimulated YB-1 phosphorylation via RSK and this was associated with cetuximab resistance. Besides, inhibition of YB-1 phosphorylation by targeting RSK stimulated the PI3K/Akt prosurvival signaling thus interfering with the anti-proliferative effects of RSK inhibition. In this scenario, PI3K/Akt activation induces YB-1 translocation so that YB-1 can participate in the control of gene expression and DNA repair. Thus, dual targeting of RSK and PI3K/Akt in combination with chemotherapy has been proposed as a promising therapeutic strategy to efficiently inhibit cell proliferation and sensitize colon cancer cells to 5-FU-induced apoptosis [93]. Recently, the PI3K inhibitor BEZ235 (dactolisib) was shown to repress YB-1 expression and enhance the cytotoxicity of radiation [76].

1.3.3. Epidermoid carcinoma

In 1996, the team of Takefumi Ohga at Kyushu University School of Medicine reported the first evidence of an association between YB-1 and drug sensitivity in epidermoid carcinoma. They found enhanced expression of YB-1 in cisplatinum resistant KB cell lines and demonstrated that YB-1 depletion was responsible for increased cell sensitivity to cisplatin, mitomycin C, and UV radiation but not to vincristine, doxorubicin, camptothecin, or etoposide. Remarkably, they observed that the cellular sensitivity to chemotherapy was inversely proportional to the expression of YB-1 protein. They postulated, for the first time, that YB-1 may recognize damaged DNA that contains cross-links induced by UV-radiation and drugs and participate in DNA repair processes [109].

1.3.4. Osteosarcoma

High expression of YB-1 protein was observed in osteosarcoma [108]. Oda and collaborators evaluated the expression level of YB-1 protein by immunohistochemistry in 69 untreated biopsy specimens of conventional osteosarcomas and compared it with the expression of the P-glycoprotein (P-gp/MDR-1) which functions as an ATP-dependent efflux pump and reduces drug buildup in resistant cells. A significant correlation was observed between the nuclear expression of YB-1 and the level of membrane P-gp/MDR1 glycoprotein [108]. In chondroblastic osteosarcoma, YB-1 was located in the nucleus more frequently than in other types of osteosarcoma. This evidence suggested that nuclear YB-1 could be a prognostic marker for multi-drug resistance in osteosarcoma however, the molecular mechanism driving nuclear translocation of YB-1 in osteosarcoma is still awaiting clarification. In 2013, Fujiwara-Okada and coworkers investigated the effect of YB-1 silencing in osteosarcoma cells. They found a significant inhibition of cell proliferation with a reduction of cyclin A and D1 expression however the specific function of YB-1 in this type of tumor remains largely undefined [40].

1.3.5. Neuroblastoma

Neuroblastoma is an embryonal tumor arising from neuroblast cells of the autonomic nervous system[131,132]. Since most neuroblastomas express high levels of YB-1, this protein was expected to play an important role in the pathogenesis of this tumor [134]. In 2010, a tissue macro array with 37 neuroblastoma samples was analyzed by immunohistochemistry for YB-1 expression. Enhanced expression of YB-1 was detected in 35 out 37 (94.6%) of neuroblastoma cases examined. Nevertheless, no correlation of YB-1 expression level with survival, risk factors, or disease stage was found [134].

To investigate the functional role of YB-1 in neuroblastoma, Wang H. and collaborators, in 2017, silenced YB-1 using RNA interference (shRNA) in neuroblastoma SH-SY5Y cells. They found that YBX-1 gene silencing decreased the proliferation, migration, and invasion of SH-SY5Y cells. At the molecular level, inhibition of YB-1 decreased the expression level of PCNA as well as MMP-2 and sensitized SH-SY5Y cells to cisplatin. Moreover, down-regulation of multidrug resistance (MDR) 1 protein via NF-κB signaling pathway promoted apoptosis in SH-SY5Y cells treated with cisplatin. Based on these data YB-1 targeting was indicated as a promising therapeutic strategy for neuroblastoma and for overcoming its cisplatin resistance [135].

1.3.6. Glioblastoma multiforme

YB-1 was found to be overexpressed in pediatric (pGMBs) but not adult glioblastomas (aGMB) [32]. pGMB is a rare but devastating tumor [24]. Besides, in pGMBs associated with Ras/Akt activation YB-1 was mainly nuclear and associated with increased expression of EGFR and transcripts encoding stress- and growth-related proteins. It was postulated that Akt-mediated YB-1 phosphorylation contributes to gliomagenesis in pGBM by relieving the translational repression of YB-1 on numerous pro-mRNAs, increasing EGFR levels and interfering with p53 function [32].

In aGBM, the most common and aggressive type of human brain tumor in adults less than 3% of newly diagnosed cases in the patients will survive more than 5 years. YB-1 inhibition reduced tumor cell invasion and growth *in vitro* and delayed tumor onset in mice. The most potent antitumor agent against adult and pediatric glioblastomas thus far is temozolomide, a DNA alkylating agent. YB-1 protein is highly expressed in primary GBM but not in normal brain tissues based on the evaluation of primary tumors. It has been questioned whether GBM depends on YB-1 for growth and/or response to temozolomide. Notably, inhibiting YB-1, enhanced temozolomide sensitivity was observed in models of adult and pediatric GBM thereby reinforcing the idea that inhibiting YB-1 sensitizes brain tumor cells to chemotherapy [43].

Glioblastoma is associated with aberrant expression of miRNAs (in particular the miR29 family, consisting of miR-29a, miR-29b and miR-29c which is known to critically influence cancer progression by functioning as a tumor suppressor [150,151]. For instance, miR-29b is an epi-miRNA that targets DNA methyltransferases (DNMT) and/or regulates members of the DNA demethylation pathway, leading to the downregulation of global DNA methylation in malignant cells [148]. In 2015, Shuai-Lai Wu and colleagues demonstrated the involvement of YB-1 regulation in miRNA expression. Genome-wide analyses revealed YB-1 binding to the ring regions of miRNAs. It has been shown that YB-1 interacts with the ring regions of the R-29b-2 miRNA and remodel the pre-miRNA in a structure not suitable for the Drosha and Dicer complexes. Moreover, it can block the loading of the microprocessor or Dicer group on the primary or precursor of miR-29b-2 through static impediments. In GBM, YB-1 is, therefore, able to reduce the post-transcriptional expression of miR29b and the biogenesis of miR29b2, thus promoting proliferation, tumor development and metastasis [120].

1.3.7. Bladder cancer

A novel oncogenic function of YB-1 was proposed in bladder cancer by Xu L. and coworkers in 2017. They found that YB-1 promoted glycolysis in bladder cancer cells by modulating the expression of Myc and HIF1 [145]. cMYC and HIF facilitate the expression of glycolytic enzymes [149]. Cancer cells convert glucose into lactate instead of oxidative phosphorylation, even in the presence of oxygen. This mechanism is also known as aerobic glycolysis or the Warburg effect. Since it is highly associated with malignant cell phenotypes, aerobic glycolysis is considered a metabolic feature for invasive cancer. Therapeutic targeting of glycolysis in cancer patients has been proposed as a potential therapeutic strategy in bladder cancer. Therefore, considering that YB-1 protein is involved in the regulatory mechanisms of glycolysis, YB-1 knock-down was indicated as a promising therapeutic target in bladder cancer [144,145].

1.3.8. Lung cancer and mesothelioma

Lung cancers and malignant pleural mesothelioma (MPM) have some of the worst 5-year survival rates of all cancer types, primarily due to a lack of effective treatment options for most patients [72]. The Cancer Genome Atlas data shows that elevated YB-1 mRNA expression was highly prognostic in a cohort of 1926 patients with non-small cell lung carcinoma (NSCLC), including adenocarcinoma (ADC) and squamous cell carcinoma (SCC) and 83 mesothelioma patients [47,53]. In the SCC data set only PIK3CA and SOX2 were significantly co-expressed. Notably, this analysis did not show YB-1 alteration to be significantly associated with the current targetable oncogenes ALK, BRAF and EGFR in ADC suggesting that YB-1 deregulation may represent a unique subpopulation of patients that may not have a targetable mutation. A recent meta-analysis of data from 692 NSCLC patients shows that high YB-1 protein expression significantly correlates with poorer overall survival and clinicopathological features [71]. Unfortunately, TCGA data is currently not available for SCLC. Therefore, a prognostic study on YB-1 expression in SCLC is still not available so far [72].

YB-1 intracellular localization was assessed in a sample of 196 patients with non-small cell lung carcinoma (NSCLC) by immunohistochemistry [116]. YB-1 was found in the nucleus and cytoplasm. However, nuclear YB-1 expression significantly correlated with lymph node metastasis and malignant stages. Nuclear YB-1 expression in squamous cell carcinoma meant a significantly unfavorable prognosis compared with cytoplasmic YB-1 expression. However, there was no significant correlation between nuclear YB-1 expression and prognosis in patients with adenocarcinoma. Thus, the nuclear localization of YB-1 might occur during the process of the tumor progression especially in squamous cell carcinomas, the result being an unfavorable prognosis. Determination of the intracellular localization of YB-1 may prove useful to predict malignancy or disease progression in NSCLC [116].

One recent study has shown that YB-1 enforces lung cancer metastatic cancer stem cell-like properties *in vitro* and *in vivo* through transcriptional upregulation of *NANOG*, a marker of stemness required for the invasion and sphere formation of adenocarcinoma cells *in vitro* [51].

1.3.9. Renal and prostate cancer

Early studies suggested that the androgen receptor (AR) might play important roles to promote renal [36] and prostate carcinoma progression [58,138]. Previous studies on renal carcinoma RCC have shown that the elevated nuclear Y-box binding protein 1 (YB-1) expression is closely related to the tumor growth and aggressive cancer phenotype, leading to poor prognosis of RCC patients. YB-1 induces AR expression at the transcriptional level; overexpression of AR, as well as YB-1, conferred castration-resistant growth in prostate cancer cells [59,119].

The complement component 1, q subcomponent binding protein (C1QBP) is a ubiquitously expressed and multi-compartmental cellular protein involved in various biological processes [45]. In human RCC clinical tissues, it was demonstrated the higher YB-1 expression with lower C1QBP expression, and the intensity of C1QBP was negatively correlated with the YB-1 nuclear expression. C1QBP was shown to inhibit YB-1 to suppress the AR-enhanced RCC cell invasion. Therefore, the newly identified C1QBP/YB-1/AR/MMP9 signal pathway was indicated as a new potential therapeutic target to better suppress RCC metastasis [152]. Moreover, a differential gene expression analysis by microarrays on YB-1-knocked-down stable renal carcinoma cells showed that the YBX1 gene knockdown influenced cell adhesion molecules (CAMs). Four genes (*CLDN4, NRXN3, ITGB8,* and *VCAN*) related to CAMs were confirmed by real-time PCR. Functional assays have finally demonstrated that YB-1 could regulate TGF-β activity, supporting that YB-1 functions through ITGB8/TGF-β signaling and eventually contributes to RCC cell adhesion [139].

2. Concluding remarks

YB-1 abnormal expression appears to be a central driver of cancer development and is commonly associated with increased proliferation and chemoradiation resistance. Thanks to its structural flexibility and ability to move from one cellular district to another, YB-1 can control a plethora of different biological processes. As we have described, the YB-1 protein is overexpressed in a large variety of cancers, sometimes aggressive or for which there is no effective cure. Aggressive forms of cancers often display enhanced YB-1 level in the nucleus which correlates with chemoradiation resistance and worse prognosis. Strikingly, YB-1 is increasingly emerging as a key multifaceted player in the detection and repair of DNA lesions and maintenance of genome integrity. Exactly when the cell is under stress conditions, YB-1 plays its pro-survival role by first participating in stress granules where it temporarily controls protein synthesis and then taking part in DNA damage repair when significant genotoxic damage has occurred. In this way, it can contribute to preserving cancer cells from chemotherapy-induced death [153].

YB-1 oncogenic functions are generally activated by phosphorylation. However, because the protein is a downstream target of multiple kinases, a combination therapy against RSK, ERKs and PI3K/Akt kinases may be necessary to achieve therapeutical significant results. Therefore, we believe that strategies aimed to counteract YB-1 activities in DNA shelter may significantly increase the success of anticancer therapies.

Author contribution

All the authors contributed to the design of the study, the data collection, writing of the manuscript and figures construction.

All authors have approved the manuscript and agree with its submission to the Biochimie.

Funding

This research received no specific grant from any funding agency in the public, commercial or not-for-profit sectors. Felicia Sangermano and Antonella Delicato are supported by 33rd and 35rd PhD program in Biotechnology-MIUR, respectively. Viola Calabrò is supported by Ricerca Dipartimentale 2018-2019-MIUR.

Acknowledgment

The authors thank Prof. Girolama La Mantia of Department of Biology University of Naples Federico II, for her critical reading and advice in writing this review.

References

[1] E.E. Alemasova, N.A. Moor, K.N. Naumenko, M.M. Kutuzov, M.V. Sukhanova, P.E. Pestryakov, O.I. Lavrik, Y-box-binding protein 1 as a non-canonical factor of base excision repair, Biochim. Biophys. Acta Protein Proteonomics 1864 (12) (2016) 1631–1640.
[2] E.E. Alemasova, K.N. Naumenko, N.A. Moor, O.I. Lavrik, Y-box-binding protein 1 stimulates abasic site cleavage, Biochemistry (Mosc.) 82 (12) (2017) 1521–1528.
[3] E.E. Alemasova, K.N. Naumenko, T.A. Kurgina, R.O. Anarbaev, O.I. Lavrik, The multifunctional protein YB-1 potentiates PARP1 activity and decreases the efficiency of PARP1 inhibitors, Oncotarget 9 (34) (2018) 23349.
[4] S. Ambrosio, S. Amente, G. Napolitano, G. Di Palo, L. Lania, B. Majello, Myc impairs resolution of site-specific DNA double-strand breaks repair, Mutat. Res. 774 (2015) 6–13.
[5] A.G. Bader, P.K. Vogt, Phosphorylation by Akt disables the anti-oncogenic activity of YB-1, Oncogene 27 (8) (2008) 1179–1182.
[6] K. Asakuno, K. Kohno, T. Uchiumi, T. Kubo, S. Sato, M. Isono, M. Kuwano, Involvement of a DNA binding protein, MDR-NF1/YB-1, in human MDR1 gene expression by actinomycin D, Biochem. Biophys. Res. Commun. 199 (3) (1994) 1428–1435.
[7] G. Bakalkin, T. Yakovleva, G. Selivanova, K.P. Magnusson, L. Szekely, E. Kiseleva, K.G. Wiman, p53 binds single-stranded DNA ends and catalyzes DNA renaturation and strand transfer, Proc. Natl. Acad. Sci. Unit. States Am. 91 (1) (1994) 413–417.
[8] T. Bansal, N. Tanveer, U.R. Singh, S. Sharma, N. Kaur, Y-Box binding protein 1 expression in breast cancer and its correlation with hormone receptors and other prognostic markers, J. Lab. Phys. 10 (4) (2018) 420.
[9] R.C. Bargou, K. Jürchott, C. Wagener, S. Bergmann, S. Metzner, K. Bommert, H.D. Royer, Nuclear localization and increased levels of transcription factor YB-1 in primary human breast cancers are associated with intrinsic MDR1 gene expression, Nat. Med. 3 (4) (1997) 447–450.
[10] A.M. Bergman, P.P. Eijk, V.W.R. van Haperen, K. Smid, G. Veerman, I. Hubeek, G.J. Peters, In vivo induction of resistance to gemcitabine results in increased expression of ribonucleotide reductase subunit M1 as the major determinant, Canc. Res. 65 (20) (2005) 9510–9516.
[11] G. Blobel, Protein tightly bound to globin mRNA, Biochem. Biophys. Res. Commun. 47 (1) (1972) 88–95.
[12] K.S. Bommert, M. Effenberger, E. Leich, M. Küspert, D. Murphy, C. Langer, A. Rosenwald, The feed-forward loop between YB-1 and MYC is essential for multiple myeloma cell survival, Leukemia 27 (2) (2013) 441–450.
[13] K.S. Budkina, N.E. Zlobin, S.V. Kononova, L.P. Ovchinnikov, A.V. Babakov, Cold shock domain proteins: structure and interaction with nucleic acids, Biochemistry (Mosc.) 85 (Suppl 1) (2020) S1–S19.
[14] W.J. Cannan, D.S. Pederson, Mechanisms and consequences of double-strand DNA break formation in chromatin, J. Cell. Physiol. 231 (1) (2016) 3–14.
[15] B. Castellana, T. Aasen, G. Moreno-Bueno, S.E. Dunn, S.R. y Cajal, Interplay between YB-1 and IL-6 promotes the metastatic phenotype in breast cancer cells, Oncotarget 6 (35) (2015) 38239.
[16] L. Chatel-Chaix, M.A. Germain, M. Götte, D. Lamarre, Direct-acting and host-targeting HCV inhibitors: current and future directions, Current opinion in virology 2 (5) (2012) 588–598.
[17] K.G. Chernov, P.A. Curmi, L. Hamon, A. Mechulam, L.P. Ovchinnikov, D. Pastré, Atomic force microscopy reveals binding of mRNA to microtubules mediated by two major mRNP proteins YB-1 and PABP, FEBS Lett. 582 (19) (2008) 2875–2881.
[18] K.H. Cho, B.Y. Jeong, C.G. Park, H.Y. Lee, The YB-1/EZH2/amphiregulin signaling axis mediates LPA-induced breast cancer cell invasion, Arch Pharm. Res. (Seoul) 42 (6) (2019) 519–530.
[19] S.B. Cohen, W. Ma, V.A. Valova, M. Algie, R. Harfoot, A.G. Woolley, A.W. Braithwaite, Genotoxic stress-induced nuclear localization of oncoprotein YB-1 in the absence of proteolytic processing, Oncogene 29 (3) (2010) 403–410.
[20] E. Dahl, A. En-Nia, F. Wiesmann, R. Krings, S. Djudjaj, E. Breuer, P.R. Mertens, Nuclear detection of Y-boxprotein-1 (YB-1) closely associates with progesterone receptor negativity and is a strong adverse survival factor in human breast cancer, BMC Canc. 9 (1) (2009) 410.
[21] G. D'Alessandro, F.D.A. di Fagagna, Transcription and DNA damage: holding hands or crossing swords? J. Mol. Biol. 429 (21) (2017) 3215–3229.
[22] S. Das, R. Chattopadhyay, K.K. Bhakat, I. Boldogh, K. Kohno, R. Prasad, T.K. Hazra, Stimulation of NEIL2-mediated oxidized base excision repair via YB-1 interaction during oxidative stress, J. Biol. Chem. 282 (39) (2007) 28474–28484.
[23] A.H. Davies, I. Barrett, M.R. Pambid, K. Hu, A.L. Stratford, S. Freeman, S.E. Dunn, YB-1 evokes susceptibility to cancer through cytokinesis failure, mitotic dysfunction and HER2 amplification, Oncogene 30 (34) (2011) 3649–3660.
[24] M.E. Davies, Glioblastoma: overview of disease and treatment, Clin. J. Oncol. Nurs. 20 (5) (2016) S2–S8.
[25] N.C. De Souza-Pinto, P.A. Mason, K. Hashiguchi, L. Weissman, J. Tian, D. Guay, V.A. Bohr, Novel DNA mismatch-repair activity involving YB-1 in human mitochondria, DNA Repair 8 (6) (2009) 704–719.
[26] S. Dooley, H.M. Said, A.M. Gresner, J. Floege, A. En-Nia, P.R. Mertens, Y-box protein-1 is the crucial mediator of antifibrotic interferon-gamma effects, J. Biol. Chem. 281 (3) (2006) 1784–1795.
[27] I.A. Eliseeva, E.R. Kim, S.G. Guryanov, L.P. Ovchinnikov, D.N. Lyabin, Y-box-binding protein 1 (YB-1) and its functions, Biochemistry (Mosc.) 76 (13) (2011) 1402–1433.
[28] A. En-Nia, E. Yilmaz, U. Klinge, D.H. Lovett, I. Stefanidis, P.R. Mertens, Transcription factor YB-1 mediates DNA polymerase α gene expression, J. Biol. Chem. 280 (9) (2005) 7702–7711.
[29] V.M. Evdokimova, E.A. Kovrigina, D.V. Nashchekin, E.K. Davydova, J.W. Hershey, L.P. Ovchinnikov, The major core protein of messenger ribonucleoprotein particles (p50) promotes initiation of protein biosynthesis in vitro, J. Biol. Chem. 273 (6) (1998) 3574–3581.
[30] V. Evdokimova, P. Ruzanov, M.S. Anglesio, A.V. Sorokin, L.P. Ovchinnikov, J. Buckley, P.H. Sorensen, Akt-mediated YB-1 phosphorylation activates translation of silent mRNA species, Mol. Cell. Biol. 26 (1) (2006) 277–292.
[31] V. Evdokimova, C. Tognon, T. Ng, P. Ruzanov, N. Melnyk, D. Fink, P.H. Sorensen, Translational activation of snail1 and other developmentally regulated transcription factors by YB-1 promotes an epithelial-mesenchymal transition, Canc. Cell 15 (5) (2009) 402–415.
[32] D. Faury, A. Nantel, S.E. Dunn, M.C. Guiot, T. Haque, P. Hauser, E. Lopez-Aguilar, Molecular profiling identifies prognostic subgroups of pediatric glioblastoma and shows increased YB-1 expression in tumors, J. Clin. Oncol. 25 (10) (2007) 1196–1208.
[33] M.R. Finkbeiner, A. Astanehe, K. To, A. Fotovati, A.H. Davies, Y. Zhao,

P. Comoglio, Profiling YB-1 target genes uncovers a new mechanism for MET receptor regulation in normal and malignant human mammary cells, Oncogene 28 (11) (2009) 1421–1431.
[34] E.E. Fomina, P.E. Pestryakov, D.A. Kretov, D.O. Zharkov, L.P. Ovchinnikov, P.A. Curmi, O.I. Lavrik, Inhibition of abasic site cleavage in bubble DNA by multifunctional protein YB-1, J. Mol. Recogn. 28 (2) (2015) 117–123.
[35] E.E. Fomina, P.E. Pestryakov, E.A. Maltseva, I.O. Petruseva, D.A. Kretov, L.P. Ovchinnikov, O.I. Lavrik, Y-box binding protein 1 (YB-1) promotes detection of DNA bulky lesions by XPC-HR23B factor, Biochemistry (Mosc.) 80 (2) (2015) 219–227.
[36] S. Foersch, M. Schindeldecker, M. Keith, K.E. Tagscherer, A. Fernandez, P.J. Stenzel, S. Mache-Goeppinger, Prognostic relevance of androgen receptor expression in renal carcinoma, Oncotarget 8 (45) (2017) 78545–78555.
[37] B.C. Frye, S. Halfter, S. Djudjaj, P. Muehlenberg, S. Weber, U. Raffetseder, J. Bernhagen, Y-box protein-1 is actively secreted through a non-classical pathway and acts as an extracellular mitogen, EMBO Rep. 10 (7) (2009) 783–789.
[38] T. Fujita, K.I. Ito, H. Izumi, M. Kimura, M. Sano, H. Nakagomi, K. Kohno, Increased nuclear localization of transcription factor Y-box binding protein 1 accompanied by up-regulation of P-glycoprotein in breast cancer pretreated with paclitaxel, Clin. Canc. Res. 11 (24) (2005) 8837–8844.
[39] T. Fujiwara, M. Bandi, M. Nitta, E.V. Ivanova, R.T. Bronson, D. Pellman, Cytokinesis failure generating tetraploids promotes tumorigenesis in p53-null cells, Nature 437 (7061) (2005) 1043–1047.
[40] Y. Fujiwara-Okada, Y. Matsumoto, J. Fukushi, N. Setsu, S. Matsuura, S. Kamura, H. Yamada, Y-box binding protein-1 regulates cell proliferation and is associated with clinical outcomes of osteosarcoma, Br. J. Canc. 108 (4) (2013) 836–847.
[41] T. Fukada, N.K. Tonks, Identification of YB-1 as a regulator of PTP1B expression: implications for regulation of insulin and cytokine signaling, EMBO J. 22 (3) (2003) 479–493.
[42] J.P. Gagne, M. Isabelle, K.S. Lo, S. Bourassa, M.J. Hendzel, V.L. Dawson, G.G. Poirier, Proteome-wide identification of poly (ADP-ribose) binding proteins and poly (ADP-ribose)-associated protein complexes, Nucleic Acids Res. 36 (22) (2008) 6959–6976.
[43] Y. Gao, A. Fotovati, C. Lee, M. Wang, G. Cote, E. Guns, S.E. Dunn, Inhibition of Y-box binding protein-1 slows the growth of glioblastoma multiforme and sensitizes to temozolomide independent O6-methylguanine-DNA methyltransferase, Mol. Canc. Therapeut. 8 (12) (2009) 3276–3284.
[44] I. Gaudreault, D. Guay, M. Lebel, YB-1 promotes strand separation in vitro of duplex DNA containing either mispaired bases or cisplatin modifications, exhibits endonucleolytic activities and binds several DNA repair proteins, Nucleic Acids Res. 32 (1) (2004) 316–327.
[45] B. Ghebrehiwet, E.I. Peerschke, cC1q-R (calreticulin) and gC1q-R/p33: ubiquitously expressed multi-ligand binding cellular proteins involved in inflammation and infection, Mol. Immunol. 41 (2–3) (2004) 173–183.
[46] P. Giménez-Bonafé, M.N. Fedoruk, T.G. Whitmore, M. Akbari, J.L. Ralph, S. Ettinger, C.C. Nelson, YB-1 is upregulated during prostate cancer tumor progression and increases P-glycoprotein activity, Prostate 59 (3) (2004) 337–349.
[47] B. Győrffy, Pawel Surowiak, Budczies Jan, András Lánczky, Online survival analysis software to assess the prognostic value of biomarkers using transcriptomic data in non-small-cell lung cancer, PloS One 18 (12) (2013), e82241, 8.
[48] C. Gu, T. Oyama, T. Osaki, K. Kohno, K. Yasumoto, Expression of Y box-binding protein-1 correlates with DNA topoisomerase IIalpha and proliferating cell nuclear antigen expression in lung cancer, Anticanc. Res. 21 (4A) (2001) 2357–2362.
[49] A.M. Guarino, A. Troiano, E. Pizzo, A. Bosso, M. Vivo, G. Pinto, V. Calabrò, Oxidative stress causes enhanced secretion of YB-1 protein that restrains proliferation of receiving cells, Genes 9 (10) (2018) 513.
[50] D. Guay, A.A. Evoy, E. Paquet, C. Garand, M. Bachvarova, D. Bachvarov, M. Lebel, The strand separation and nuclease activities associated with YB-1 are dispensable for cisplatin resistance but overexpression of YB-1 in MCF7 and MDA-MB-231 breast tumor cells generates several chemoresistance signatures, Int. J. Biochem. Cell Biol. 40 (11) (2008) 2492–2507.
[51] T. Guo, S. Zhao, P. Wang, X. Xue, Y. Zhang, M. Yang, L. Zhao, YB-1 regulates tumor growth by promoting MACC1/c-Met pathway in human lung adenocarcinoma, Oncotarget 8 (29) (2017) 48110.
[52] J. Gyamfi, M. Eom, J.S. Koo, J. Choi, Multifaceted roles of interleukin-6 in adipocyte–breast cancer cell interaction, Trans. Oncol. 11 (2) (2018) 275–285.
[53] B. Győrffy, P. Surowiak, J. Budczies, A. Lánczky, Online survival analysis software to assess the prognostic value of biomarkers using transcriptomic data in non-small-cell lung cancer, PloS One 8 (12) (2013).
[54] B. Haley, T. Paunesku, M. Protić, G.E. Woloschak, Response of heterogeneous ribonuclear proteins (hnRNP) to ionising radiation and their involvement in DNA damage repair, Int. J. Radiat. Biol. 85 (8) (2009) 643–655.
[55] S.M. Hammond, S. Boettcher, A.A. Caudy, R. Kobayashi, G.J. Hannon, Argonaute2, a link between genetic and biochemical analyses of RNAi, Science 293 (5532) (2001) 1146–1150.
[56] S.L. Hasegawa, P.W. Doetsch, K.K. Hamilton, A.M. Martin, S.A. Okenquist, J. Lenz, J.M. Boss, DNA binding properties of YB-1 and dbpA: binding to doublestranded, single-stranded, and abasic site containing DNAs, Nucleic Acids Res. 19 (18) (1991) 4915–4920.
[57] M.L. Hegde, S. Banerjee, P.M. Hegde, L.J. Bellot, T.K. Hazra, I. Boldogh, S. Mitra, Enhancement of NEIL1 protein-initiated oxidized DNA base excision repair by heterogeneous nuclear ribonucleoprotein U (hnRNP-U) via direct interaction, J. Biol. Chem. 287 (41) (2012) 34202–34211.
[58] C.A. Heinlein, C. Chang, Androgen receptor in prostate cancer, Endocr. Rev. 25 (2) (2004) 276–308.
[59] A. Heuman, O. Kaya, C. Hube-Magg, M. Kluth, S.L. Dagmar, S. Ronald, Upregulation and nuclear translocation of Y-box binding protein 1 (YB-1) are linked to poor prognosis in ERG-negative prostate cancer, Sci. Rep. 7 (2017), 2056.
[60] K. Higashi, Y. Inagaki, N. Suzuki, S. Mitsui, A. Mauviel, H. Kaneko, I. Nakatsuka, Y-box-binding protein YB-1 mediates transcriptional repression of human α2 (I) collagen gene expression by interferon-γ, J. Biol. Chem. 278 (7) (2003) 5156–5162.
[61] J. Höck, L. Weinmann, C. Ender, S. Rüdel, E. Kremmer, M. Raabe, G. Meister, Proteomic and functional analysis of Argonaute-containing mRNA–protein complexes in human cells, EMBO Rep. 8 (11) (2007) 1052–1060.
[62] J.L. Hsu, M.C. Hung, The role of HER2, EGFR, and other receptor tyrosine kinases in breast cancer, Canc. Metastasis Rev. 35 (4) (2016) 575–588.
[63] T. Hung, Y. Wang, M.F. Lin, A.K. Koegel, Y. Kotake, G.D. Grant, Y. Wang, Extensive and coordinated transcription of noncoding RNAs within cell-cycle promoters, Nat. Genet. 43 (7) (2011) 621.
[64] T. Ise, G. Nagatani, T. Imamura, K. Kato, H. Takano, M. Nomoto, T. Uchiumi, Transcription factor Y-box binding protein 1 binds preferentially to cisplatin-modified DNA and interacts with proliferating cell nuclear antigen, Canc. Res. 59 (2) (1999) 342–346.
[65] H. Izumi, T. Imamura, G. Nagatani, T. Ise, T. Murakami, H. Uramoto, T. Okamoto, Y box-binding protein-1 binds preferentially to single-stranded nucleic acids and exhibits 3′→ 5′ exonuclease activity, Nucleic Acids Res. 29 (5) (2001) 1200–1207.
[66] A. Lee, J. Woo, H. Park, S.H. Sung, J.Y. Seoh, W. Lim, et al., The value of cytoplasmic Y box binding protein 1 as a prognostic marker for breast cancer in Korean, Breast Cancer 23 (5) (2016) 685–691.
[67] S. Lee, B. Elenbaas, A. Levine, J. Griffith, p53 and its 14 kDa C-terminal domain recognize primary DNA damage in the form of insertion/deletion mismatches, Cell 81 (7) (1995) 1013–1020.
[68] M. Janz, N. Harbeck, P. Dettmar, U. Berger, A. Schmidt, K. Jürchott, H.D. Royer, Y-box factor YB-1 predicts drug resistance and patient outcome in breast cancer independent of clinically relevant tumor biologic factors HER2, uPA and PAI-1, Int. J. Canc. 97 (3) (2002) 278–282.
[69] G. Jiang, A. Sancar, Recruitment of DNA damage checkpoint proteins to damage in transcribed and non-transcribed sequences, Mol. Cell. Biol. 26 (1) (2006) 39–49.
[70] L. Jiang, G.L. Yuan, Q.L. Liang, H.J. Zhang, J. Huang, S.A. Cheng, X.X. Peng, Positive expression of Y-box binding protein 1 and prognosis in non-small cell lung cancer: a meta-analysis, Oncotarget 8 (33) (2017) 55613.
[71] T.G. Johnson, K. Schelch, S. Mehta, A. Burgess, G. Reid, Why be one protein when you can affect many? The multiple roles of YB-1 in lung cancer and mesothelioma, Front. Cell Develop. Biol. 7 (2019) 221.
[72] K. Jürchott, S. Bergmann, U. Stein, W. Walther, M. Janz, I. Manni, H.D. Royer, YB-1 as a cell cycle-regulated transcription factor facilitating cyclin A and cyclin B1 gene expression, J. Biol. Chem. 278 (30) (2003) 27988–27996.
[73] M. Kashihara, K. Azuma, A. Kawahara, Y. Basaki, S. Hattori, T. Yanagawa, K. Nakano, Nuclear Y-box binding protein-1, a predictive marker of prognosis, is correlated with the expression of HER2/ErbB2 and HER3/ErbB3 in non-small cell lung cancer, J. Thorac. Oncol. 4 (9) (2009) 1066–1074.
[74] A. Kawaguchi, K. Matsumoto, K. Nagata, YB-1 functions as a porter to lead influenza virus ribonucleoprotein complexes to microtubules, J. Virol. 86 (20) (2012) 11086–11095.
[75] P. Khandelwal, M.K. Padala, J. Cox, R.V. Guntaka, The N-terminal domain of y-box binding protein-1 induces cell cycle arrest in g2/m phase by binding to cyclin d1, Int. J. Cell Biol. 2009 (2009) 243532.
[76] A. Kim, S. Shim, Y.H. Kim, M.J. Kim, S. Park, J.K. Myung, Inhibition of Y box binding protein 1 suppresses cell growth and motility in colorectal cancer, Mol. Canc. Therapeut. 19 (2) (2020) 479–489.
[77] E.R. Kim, A.A. Selyutina, I.A. Buldakov, V. Evdokimova, L.P. Ovchinnikov, A.V. Sorokin, The proteolytic YB-1 fragment interacts with DNA repair machinery and enhances survival during DNA damaging stress, Cell Cycle 12 (24) (2013) 3791–3803.
[78] C.P. Kloks, C.A. Spronk, E. Lasonder, A. Hoffmann, G.W. Vuister, S. Grzesiek, C.W. Hilbers, The solution structure and DNA-binding properties of the cold-shock domain of the human Y-box protein YB-1, J. Mol. Biol. 316 (2) (2002) 317–326.
[79] K. Kohno, H. Izumi, T. Uchiumi, M. Ashizuka, M. Kuwano, The pleiotropic functions of the Y-box-binding protein, YB-1. *Bioessays* 25 (7) (2003) 691–698.
[80] K. Kohno, M. Kuwano, Is human multidrug resistance 1 a stress-induced SOS gene?, in: Excerpta Medica International Congress Series, vol. 1026 Elsevier, 1993, 21-21.
[82] A. Kolk, N. Jubitz, K. Mengele, K. Mantwill, O. Bissinger, M. Schmitt, P.S. Holm, Expression of Y-box-binding protein YB-1 allows stratification into long-and short-term survivors of head and neck cancer patients, Br. J. Canc. 105 (12) (2011) 1864–1873.
[83] C. Kosnopfel, T. Sinnberg, B. Sauer, C. Busch, H. Niessner, A. Schmitt, S.E. Dunn, YB-1 expression and phosphorylation regulate tumorigenicity and invasiveness in melanoma by influencing EMT, Mol. Canc. Res. 16 (7) (2018)

1149–1160.
[84] Y. Kotake, N. Arikawa, K. Tahara, H. Maru, M. Naemura, Y-box binding protein 1 is involved in regulating the G 2/, M Phase of the Cell Cycle 37 (4) (2017) 1603–1608.
[85] D.A. Kretov, M.J. Clément, G. Lambert, D. Durand, D.N. Lyabin, G. Bollot, L. Hamon, YB-1, an abundant core mRNA-binding protein, has the capacity to form an RNA nucleoprotein filament: a structural analysis, Nucleic Acids Res. 47 (6) (2019) 3127–3141.
[86] M. Ladomery, J. Sommerville, A role for Y-box proteins in cell proliferation, Bioessays 17 (1) (1995) 9–11.
[87] A. Lasham, S. Moloney, T. Hale, C. Homer, Y.F. Zhang, J.G. Murison, J. Watson, The Y-box-binding protein, YB1, is a potential negative regulator of the p53 tumor suppressor, J. Biol. Chem. 278 (37) (2003) 35516–35523.
[88] J.P. Lim, S. Nair, S. Shyamasundar, P.J. Chua, U. Muniasamy, K. Matsumoto, B.H. Bay, Silencing Y-box binding protein-1 inhibits triple-negative breast cancer cell invasiveness via regulation of MMP1 and beta-catenin expression, Canc. Lett. 452 (2019) 119–131.
[89] J.A. Lindquist, P.R. Mertens, Cold shock proteins: from cellular mechanisms to pathophysiology and disease, Cell Commun. Signal. 16 (1) (2018) 63.
[90] T.T. Liu, G. Arango-Argoty, Z. Li, Y. Lin, S.W. Kim, A. Dueck, B. John, Noncoding RNAs that associate with YB-1 alter proliferation in prostate cancer cells, Rna 21 (6) (2015) 1159–1172.
[91] D.N. Lyabin, I.A. Eliseeva, L.P. Ovchinnikov, YB-1 protein: functions and regulation, Wiley Interdisciplinary Reviews: RNA 5 (1) (2014) 95–110.
[92] E. Maier, F. Attenberger, A. Tiwari, K. Lettau, S. Rebholz, B. Fehrenbacher, M. Toulany, Dual targeting of Y-box binding protein-1 and Akt inhibits proliferation and enhances the chemosensitivity of colorectal cancer cells, Cancers 11 (4) (2019) 562.
[93] M. Marchesini, Y. Ogoti, E. Fiorini, A.A. Samur, L. Nezi, M. D'Anca, N. Mistry, ILF2 is a regulator of RNA splicing and DNA damage response in 1q21-amplified multiple myeloma, Canc. Cell 32 (1) (2017) 88–100.
[94] D.R. Marenstein, M.T. Ocampo, M.K. Chan, A. Altamirano, A.K. Basu, R.J. Boorstein, G.W. Teebor, Stimulation of human endonuclease III by Y box-binding protein 1 (DNA-binding protein B) interaction between A base excision repair enzyme and A transcription factor, J. Biol. Chem. 276 (24) (2001) 21242–21249.
[95] P.R. Mertens, S. Harendza, A.S. Pollock, D.H. Lovett, Glomerular mesangial cell-specific transactivation of matrix metalloproteinase 2 transcription is mediated by YB-1, J. Biol. Chem. 272 (36) (1997) 22905–22912.
[96] P.R. Mertens, K. Steinmann, M.A. Alfonso-Jaume, A. En-Nia, Y. Sun, D.H. Lovett, Combinatorial interactions of p53, activating protein-2, and YB-1 with a single enhancer element regulate gelatinase A expression in neoplastic cells, J. Biol. Chem. 277 (28) (2002) 24875–24882.
[97] S. Metha, C. McKinney, M. Algie, C.S. Berma, S. Cannan, R. Hartfoot, et al., Dephosphorylation of YB-1 is required for nuclear localisation during G(2) phase of the cell cycle Cancers (Basel) 12 (2) (2020) 315, 2020 Feb.
[98] M. Miyazaki, K. Kohno, T. Uchiumi, H. Tanimura, K.I. Matsuo, M. Nasu, M. Kuwano, Activation of human multidrug resistance-1 gene promoter in response to heat shock stress, Biochem. Biophys. Res. Commun. 187 (2) (1992) 677–684.
[99] D. Mordovkina, D.N. Lyabin, E.A. Smolin, E.M. Sogorina, L.P. Ovchinnikov, I. Eliseeva, Y-box binding proteins in mRNP assembly, translation, and stability control, Biomolecules 10 (4) (2020) 591.
[100] X. Mu, W. Li, X. Wang, G. Gao, YB-1 stabilizes HIV-1 genomic RNA and enhances viral production, Protein & cell 4 (8) (2013) 591–597.
[101] E. Mylona, S. Melissaris, I. Giannopoulou, I. Theohari, C. Papadimitriou, A. Keramopoulos, L. Nakopoulou, Y-box-binding protein 1 (YB1) in breast carcinomas: relation to aggressive tumor phenotype and identification of patients at high risk for relapse, Eur. J. Surg. Oncol. 40 (3) (2014) 289–296.
[102] S. Nagasu, T. Sudo, T. Kinugasa, T. Yomoda, K. Fujiyoshi, T. Shigaki, Y. Akagi, Y-box-binding protein 1 inhibits apoptosis and upregulates EGFR in colon cancer, Oncol. Rep. 41 (5) (2019) 2889–2896.
[103] G. Napolitano, S. Amente, M. Lubrano, G. Di Palo, S. Ambrosio, L. Lania, et al., Sequence-specific double stranded breaks trigger P-TEFb-dependent Rpb1-CTD hyperphosphorylation, Mutat. Res. 749 (2013) 21–27.
[104] M.P. Nekrasov, M.P. Ivshina, K.G. Chernov, E.A. Kovrigina, V.M. Evdokimova, A.A. Thomas, L.P. Ovchinnikov, The mRNA-binding protein YB-1 (p50) prevents association of the eukaryotic initiation factor eIF4G with mRNA and inhibits protein synthesis at the initiation stage, J. Biol. Chem. 278 (16) (2003) 13936–13943.
[105] K. Nishida, Y. Kuwano, T. Nishikawa, K. Masuda, K. Rokutan, RNA binding proteins and genome integrity, Int. J. Mol. Sci. 18 (7) (2017) 1341.
[106] J.T. Norman, G.E. Lindahl, K. Shakib, A. En-Nia, E. Yilmaz, P.R. Mertens, The Y-box binding protein YB-1 suppresses collagen α1 (I) gene transcription via an evolutionarily conserved regulatory element in the proximal promoter, J. Biol. Chem. 276 (32) (2001) 29880–29890.
[107] Y. Oda, A. Sakamoto, N. Shinohara, T. Ohga, T. Uchiumi, K. Kohno, Y. Iwamoto, Nuclear expression of YB-1 protein correlates with P-glycoprotein expression in human osteosarcoma, Clin. Canc. Res. 4 (9) (1998) 2273–2277.
[108] T. Ohga, K. Koike, M. Ono, Y. Makino, Y. Itagaki, M. Tanimoto, K. Kohno, Role of the human Y box-binding protein YB-1 in cellular sensitivity to the DNA-damaging agents cisplatin, mitomycin C, and ultraviolet light, Canc. Res. 56 (18) (1996) 4224–4228.
[109] T. Ohga, T. Uchiumi, Y. Makino, K. Koike, M. Wada, M. Kuwano, K. Kohno, Direct involvement of the Y-box binding protein YB-1 in genotoxic stress-induced activation of the human multidrug resistance 1 gene, J. Biol. Chem. 273 (11) (1998) 5997–6000.
[110] S.J. Petesch, J.T. Lis, Overcoming the nucleosome barrier during transcript elongation, Trends Genet. 28 (6) (2012) 285–294.
[111] P. Rawla, T. Sunkara, A. Barsouk, Epidemiology of colorectal cancer: incidence, mortality, survival, and risk factors, Przeglad Gastroenterol. 14 (2) (2019) 89–103.
[112] H. Saji, M. Toi, S. Saji, M. Koike, K. Kohno, M. Kuwano, Nuclear expression of YB-1 protein correlates with P-glycoprotein expression in human breast carcinoma, Canc. Lett. 190 (2) (2003) 191–197.
[113] S. Samuel, J.C. Twizere, L.R. Bernstein, YB-1 represses AP1-dependent gene transactivation and interacts with an AP-1 DNA sequence, Biochem. J. 388 (3) (2005) 921–928.
[114] S. Sengupta, A.K. Mantha, S. Mitra, K.K. Bhakat, Human AP endonuclease (APE1/Ref-1) and its acetylation regulate YB-1-p300 recruitment and RNA polymerase II loading in the drug-induced activation of multidrug resistance gene MDR1, Oncogene 30 (4) (2011) 482–493.
[115] K. Shibahara, K. Sugio, T. Osaki, T. Uchiumi, Y. Maehara, K. Kohno, M. Kuwano, Nuclear expression of the Y-box binding protein, YB-1, as a novel marker of disease progression in non-small cell lung cancer, Clin. Canc. Res. 7 (10) (2001) 3151–3155.
[116] K. Shibao, H. Takano, Y. Nakayama, K. Okazaki, N. Nagata, H. Izumi, H. Itoh, Enhanced coexpression of YB-1 and DNA topoisomerase II α genes in human colorectal carcinomas, Int. J. Canc. 83 (6) (1999) 732–737.
[117] T. Shibata, H. Kan, Y. Murakami, H. Ureshino, K. Watari, A. Kawahara, M. Kuwano, Y-box binding protein-1 contributes to both HER2/ErbB2 expression and lapatinib sensitivity in human gastric cancer cells, Mol. Canc. Therapeut. 12 (5) (2013) 737–746.
[118] M. Shiota, A. Takeuchi, Y. Song, A. Yokomizo, E. Kashiwagi, T. Uchiumi, S. Naito, Y-box binding protein-1 promotes castration-resistant prostate cancer growth via androgen receptor expression, Endocr. Relat. Canc. 18 (4) (2011) 505.
[119] Shuai-Lai Wu, X. Fu, J. Huang, T.T. Jia, F.Y. Zong, S.R. Mu, H. Zhu, et al., Genome-wide analysis of YB-1 RNA interactions reveals a novel role of YB-1 in miRNA processing in glioblastoma multiforme, Nucleic Acids Res. 43 (17) (2015) 8516–8528.
[120] S. Shiraiwa, T. Kinugasa, A. Kawahara, T. Mizobe, T. Ohchi, K. Yuge, et al., Nuclear Y-box −binding protein-1expression PredictsPoor clinical outcome in stage III colorectal cancer, Anticancer Res. 36 (7) (2016), 3781:8.
[121] S.P. Somasekharan, A. El-Naggar, G. Leprivier, H. Cheng, S. Hajee, T.G. Grunewald, Y. Wang, YB-1 regulates stress granule formation and tumor progression by translationally activating G3BP1, JCB (J. Cell Biol.) 208 (7) (2015) 913–929.
[122] T. Soop, D. Nashchekin, J. Zhao, X. Sun, A.T. Alzhanova-Ericsson, B. Björkroth, B. Daneholt, A p50-like Y-box protein with a putative translational role becomes associated with pre-mRNA concomitant with transcription, J. Cell Sci. 116 (8) (2003) 1493–1503.
[123] A.V. Sorokin, A.A. Selyutina, M.A. Skabkin, S.G. Guryanov, I.V. Nazimov, C. Richard, V. Evdokimova, Proteasome-mediated cleavage of the Y-box-binding protein 1 is linked to DNA-damage stress response, EMBO J. 24 (20) (2005) 3602–3612.
[124] A.L. Stratford, C.J. Fry, C. Desilets, A.H. Davies, Y.Y. Cho, Y. Li, S.E. Dunn, Y-box binding protein-1 serine 102 is a downstream target of p90 ribosomal S6 kinase in basal-like breast cancer cells, Breast Canc. Res. 10 (6) (2008) R99.
[125] A.L. Stratford, G. Habibi, A. Astanehe, H. Jiang, K. Hu, E. Park, M. Marra, Epidermal growth factor receptor (EGFR) is transcriptionally induced by the Y-box binding protein-1 (YB-1) and can be inhibited with Iressa in basal-like breast cancer, providing a potential target for therapy, Breast Canc. Res. 9 (5) (2007) R61.
[126] F. Tacke, O. Galm, N. Kanig, E. Yagmur, S. Brandt, J.A. Lindquist, P.R. Mertens, High prevalence of Y-box protein-1/p18 fragment in plasma of patients with malignancies of different origin, BMC Canc. 14 (1) (2014) 33.
[127] W.L. Tay, G.W.C. Yip, P.H. Tan, K. Matsumoto, R. Yeo, T.P. Ng, B.H. Bay, Y-Box-binding protein-1 is a promising predictive marker of radioresistance and chemoradioresistance in nasopharyngeal cancer, Mod. Pathol. 22 (2) (2009) 282–290.
[128] A. Tiwari, S. Rebholz, E. Maier, M.D. Harati, D. Zips, C. Sers, H.P. Rodeman, M. Toulany, Stress-induced phosphorylation of nuclear YB-1 depends on nuclear trafficking of p90 ribosomal S6 kinase, Int. J. Mol. Sci. 19 (2018) 2441–2453.
[129] T. Uchiumi, K. Kohno, H. Tanimura, K.I. Matsuo, S. Sato, Y. Uchida, M. Kuwano, Enhanced expression of the human multidrug resistance 1 gene in response to UV light irradiation, Cell Growth Differ. 4 (1993), 147-147.
[130] A.V. Vaiman, T.P. Stromskaya, E.Y. Rybalkina, A.V. Sorokin, S.G. Guryanov, T.N. Zabotina, A.A. Stavrovskaya, Intracellular localization and content of YB-1 protein in multidrug-resistant tumor cells, Biochemistry (Mosc.) 71 (2) (2006) 146–154.
[131] K.J. Van Arendok, D.H. Chung, Neuroblastoma: tumor Biology and its implications for staging and treatment, Children 6 (1) (2019) 12.
[132] C.R. van Roeyen, F.G. Scurt, S. Brandt, V.A. Kuhl, S. Martinkus, S. Djudjaj, S. Dooley, Cold shock Y-box protein-1 proteolysis autoregulates its transcriptional activities, Cell Commun. Signal. 11 (1) (2013) 63.
[133] R. Wachowiak, S. Thieltges, T. Rawnaq, J.T. Kaifi, H. Fiegel, R. Metzger, J.R. Izbicki, Y-box-binding protein-1 is a potential novel tumor marker for neuroblastoma, Anticanc. Res. 30 (4) (2010) 1239–1242.

[134] H. Wang, R. Sun, Z. Chi, S. Li, L. Hao, Silencing of Y-box binding protein-1 by RNA interference inhibits proliferation, invasion, and metastasis, and enhances sensitivity to cisplatin through NF-κB signaling pathway in human neuroblastoma SH-SY5Y cells, Mol. Cell. Biochem. 433 (1–2) (2017) 1–12.
[135] W.T. Wang, T.Y. Tsai, C.H. Chao, B.Y. Lai, Y.H.W. Lee, Y-box binding protein 1 stabilizes hepatitis C virus NS5A via phosphorylation-mediated interaction with NS5A to regulate viral propagation, J. Virol. 89 (22) (2015) 11584–11602.
[136] X. Wang, X.B. Guo, X.C. Shen, H. Zhou, D.W. Wan, X.F. Xue, Q.M. Zhi, Prognostic role of YB-1 expression in breast cancer: a meta-analysis, Int. J. Clin. Exp. Med. 8 (2) (2015) 1780.
[137] X.W. Wang, H. Yeh, L. Schaeffer, R. Roy, V. Moncollin, J.M. Egly, V.A. Bohr, p53 Modulation of TFIIH–associated nucleotide excision repair activity, Nat. Genet. 10 (2) (1995) 188–195.
[138] Y. Wang, J. Su, D. Fu, Y. Wang, Y. Chen, R. Chen, D. Yue, The role of YB1 in renal cell carcinoma cell adhesion, Int. J. Med. Sci. 15 (12) (2018) 1304.
[139] C. Weydert, B. van Heertum, L. Dirix, S. De Houwer, F. De Wit, J. Mast, J. De Rijck, Y-box-binding protein 1 supports the early and late steps of HIV replication, PloS One 13 (7) (2018).
[140] A.P. Wolffe, Structural and functional properties of the evolutionarily ancient Y-box family of nucleic acid binding proteins, Bioessays 16 (4) (1994) 245–251.
[141] J. Wu, C. Lee, D. Yokom, H. Jiang, M.C. Cheang, E. Yorida, C.B. Gilks, Disruption of the Y-box binding protein-1 results in suppression of the epidermal growth factor receptor and HER-2, Canc. Res. 66 (9) (2006) 4872–4879.
[142] S.L. Wu, X. Fu, J. Huang, T.T. Jia, F.Y. Zong, S.R. Mu, W. Yan, Genome-wide analysis of YB-1-RNA interactions reveals a novel role of YB-1 in miRNA processing in glioblastoma multiforme, Nucleic Acids Res. 43 (17) (2015) 8516–8528.
[143] Y. Wu, K.Y. Wang, Z. Li, Y.P. Liu, H. Izumi, H. Uramoto, K. Kohno, Y-box binding protein 1 enhances DNA topoisomerase 1 activity and sensitivity to camptothecin via direct interaction, J. Exp. Clin. Canc. Res. 33 (1) (2014) 112.
[144] L. Xu, H. Li, L. Wu, S. Huang, YBX1 promotes tumor growth by elevating glycolysis in human bladder cancer, Oncotarget 8 (39) (2017) 65946.
[145] Y. Xuebing, L. Yan, J. Zhou, S. Liu, Z. Shan, C. Jiang, et al., High Expression of Y-box-binding protein 1 is associated with local recurrence and predicts poor outcome in patients with colorectal cancer, Int. J. Clin. Exp. Pathol. 1 (12) (2014) 8715–8723, 7.
[146] H. Yahata, Kobayashi h, Kamura T, Amada S, Hirakawa T, Kohno K, Kuwano M and Nakano H: increased nuclear localization of transcription factor YB-1 in acquired cisplatin resistant ovarian cancer, J. Canc. Res. Clin. Oncol. 128 (11) (2002) 621–626.
[148] F. Yang, P. Cui, Y. Lu, X. Zhang, Requirement of the transcription factor YB-1 for maintaining the stemness of cancer stem cells and reverting differentiated cancer cells into cancer stem cells, Stem Cell Res. Ther. 10 (1) (2019) 233.
[149] S.J. Yeung, J. Pan, M.H. Lee, Roles of p53, MYC and HIF-1 in regulating glycolysis—the seventh hallmark of cancer, Cell. Mol. Life Sci. 65 (24) (2008) 3981.
[150] W. Yu, S. Liang, C. Zhang, Aberrant miRNAs regulates the biological hallmarks of glioblastoma, NeuroMolecular Med. 20 (4) (2018) 452–474.
[151] D. Yue, Y. Wang, Y. Sun, Y. Niu, C. Chang, C1QBP regulates YBX1 to suppress the androgen receptor (AR)-enhanced RCC cell invasion, Neoplasia 19 (2) (2017) 135–144.
[152] Y.F. Zhang, C. Homer, S.J. Edwards, L. Hananeia, A. Lasham, J. Royds, A.W. Braithwaite, Nuclear localization of Y-box factor YB1 requires wild-type p53, Oncogene 22 (18) (2003) 2782–2794.
[153] H.L. Zhi, Books J., & Ley T.J. YB-1 is important for late-stage embryonic development, optimal cellular stress response and the prevention of mature senescence, Mol. Cell Biol. 25 (11) (2005) 4625–4637.

genes

MDPI

Brief Report

YB-1 Oncoprotein Controls PI3K/Akt Pathway by Reducing Pten Protein Level

Antonella Delicato, Eleonora Montuori, Tiziana Angrisano, Alessandra Pollice * and Viola Calabrò *

Department of Biology, University of Naples Federico II, MSA-Via Cinthia, 26-80126 Naples, Italy; antonella.delicato@unina.it (A.D.); el.montuori@studenti.unina.it (E.M.); tangrisa@unina.it (T.A.)
* Correspondence: apollice@unina.it (A.P.); vcalabro@unina.it (V.C.)

Abstract: YB-1 is a multifunctional protein overexpressed in many types of cancer. It is a crucial oncoprotein that regulates cancer cell progression and proliferation. Ubiquitously expressed in human cells, YB-1 protein functions are strictly dependent on its subcellular localization. In the cytoplasm, where YB-1 is primarily localized, it regulates mRNA translation and stability. However, in response to stress stimuli and activation of PI3K and RSK signaling, YB-1 moves to the nucleus acting as a prosurvival factor. YB-1 is reported to regulate many cellular signaling pathways in different types of malignancies. Furthermore, several observations also suggest that YB-1 is a sensor of oxidative stress and DNA damage. Here we show that YB-1 reduces PTEN intracellular levels thus leading to PI3K/Akt pathway activation. Remarkably, PTEN reduction mediated by YB-1 overexpression can be observed in human immortalized keratinocytes and HEK293T cells and cannot be reversed by proteasome inhibition. Real-time PCR data indicate that YB-1 silencing up-regulates the PTEN mRNA level. Collectively, these observations indicate that YB-1 negatively controls PTEN at the transcript level and its overexpression could confer survival and proliferative advantage to PTEN proficient cancer cells.

Keywords: YB-1; PTEN; cold-shock proteins; proteasome; PI3K/Akt pathway

Citation: Delicato, A.; Montuori, E.; Angrisano, T.; Pollice, A.; Calabrò, V. YB-1 Oncoprotein Controls PI3K/Akt Pathway by Reducing Pten Protein Level. *Genes* **2021**, *12*, 1551. https://doi.org/10.3390/genes12101551

Academic Editor: Peixin Dong

Received: 21 August 2021
Accepted: 28 September 2021
Published: 29 September 2021

1. Introduction

YB-1 is a DNA- and RNA-binding protein and transcription factor with an evolutionarily ancient and conserved cold shock domain [1]. In healthy tissues, YB-1 is primarily cytoplasmic, where it plays an important role in regulating various aspects of RNA biology [2]. YB-1 is a major component of translationally inactive messenger ribonucleoprotein particles (mRNPs) and is mainly responsible for the storage of mRNAs in a silent state [3].

Since its initial discovery, the Y-box binding protein 1 (YB-1) was linked to oncogenic functions and chemotherapy resistance. YB-1 is upregulated in tumors and its nuclear localization is associated with a more aggressive phenotype indicating a poor prognosis [4–7]. In response to genotoxic stress, YB-1 translocates from the cytoplasm to the nucleus [8], where it acts as a transcriptional regulator to overcome DNA damage-dependent cell cycle arrest and promote cell survival [9].

YB-1 is a direct target of the serine/threonine kinase Akt. Akt is activated by phosphorylation at Ser473. Overstimulated Akt activity in cancer cells [10] induces YB-1 phosphorylation at Ser102 and nuclear accumulation without changing the total amount of the protein. This results in reduced DNA repair in cancer cells after irradiation [3].

The nuclear accumulation of YB-1 in response to DNA damage or transcription inhibition requires a decrease in the cytoplasmic mRNA level [11]. Indeed, like Akt, YB-1 is associated with inactive mRNPs and, activated Akt relieves translational repression of the YB-1-bound mRNAs thereby facilitating translational activation of silenced mRNA species [3,12].

The main negative regulator of the PI3K-Akt pathway remains the PTEN phosphatase. Phosphatase and tensin homolog deleted on chromosome 10 (PTEN) is recognized as a tu-

mor suppressor due to its negative regulation of the phosphatidylinositol-4, 5-bisphosphate 3-kinase (PI3K)/protein kinase B (Akt) signaling pathway [13], see Figure 1. The major target of PTEN is phosphatidylinositol (3, 4, 5)-triphosphate (PIP3), which is generated by PI3K and acts as a bridge to recruit 3-phosphoinositide-dependent protein kinase 1 (PDK1) and AKT to the plasma membrane, further activating AKT by phosphorylation at its T308 site [13,14]. PTEN converts PIP3 into PIP2, interrupting the interaction between PDK1 and AKT, and thus negatively mediating the activation of AKT. Apart from its membrane-bound form, nuclear PTEN has multiple functions, including the induction of cell cycle arrest by inhibiting cyclin D1 expression [15], maintenance of chromosomal stability, and DNA double-strand break repair [16].

Loss of PTEN activity has been identified in a wide spectrum of primary and metastatic neoplasms, including breast cancer [17]. This condition, which results in low or null expression of the protein, is believed to be an early oncogenic event in several tumor types [18,19]. Given the ability of Akt to physically interact and activate YB-1 oncogenic functions [3] we hypothesize that YB-1 was, in turn, able to regulate Akt by a positive control that could mirror what happens in vivo when YB-1 overexpression sustains the proliferative and survival potential of cancer cells. Very little information about YB-1 and PTEN functional crosstalk is now available. However, a significant association of YB-1 nuclear accumulation with PTEN deletion in advanced prostate tumor stages was reported by Heumann and collaborators in 2017 thus suggesting a possible reciprocal regulation between the two proteins of the PI3K/Akt pathway [20]. Here we provide compelling evidence that YB-1 can sustain Akt activation by controlling PTEN.

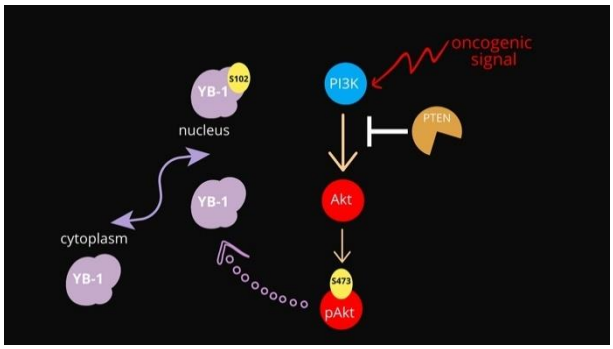

Figure 1. Schematic representation of the PI3K/Akt pathway overseeing YB-1 activation.

2. Materials and Methods

2.1. Plasmids and Reagents

The expression plasmid 3XFlag-YB-1 wt was used for the transfection and provided by Dr. Arezoo Astanehe (Abbotsford, BC, Canada). The pcDNA-GFP plasmid, used as a control, was purchased by Thermo-Fisher Scientific (Waltham, MA, USA). Sodium (meta)arsenite ($NaAsO_2$, S7400, Sigma-Aldrich, St. Louis, MO, USA) and copper (II) sulfate (C1297, Sigma-Aldrich) were used to treat cell culture at 300 µM and 10 µM final concentrations, respectively. MG-132 (M8699, Sigma-Aldrich) was used as a proteasome inhibitor at 10 µM final concentration, for 4h.

2.2. Cell Cultures

Human embryonic kidney cells (HEK293T) and HaCaT (human spontaneously immortalized keratinocytes from adult skin) were purchased from Cell Line Service (CLS, Germany) and cultured in a humidified incubator at 37 °C and 5% CO2 in DMEM High glucose (Gibco BRL, Grand Island, NY, USA) supplemented with 10% Fetal Bovine Serum (Gibco BRL), 1% L-glutamine (Gibco BRL) and 1% Pen-Strep solution (Gibco BRL). Cells were routinely checked for mycoplasma contamination, using a mycoplasma detection kit (Abcam, Quebec, QC, Canada).

To increase HEK293T adhesion to glass/plastic surfaces, plates were treated with poly-D-lysine (0.1 mg/mL, P7405, Sigma-Aldrich) before seeding cells.

2.3. Immunoblotting Analysis

For total protein extraction 2.5×10^5 cells were seeded in 6-well. After 48 h, cells were harvested in lysis buffer (50 mM Tris-HCl pH 7.5, 5 mM EDTA, 150 mM NaCl, 1% NP-40, 0.5% sodium deoxycholate) with the addition of 1 mM phenylmethylsulfonyl fluoride and protease and phosphatase inhibitor cocktail (Sigma-Aldrich). Cells were detached with a scraper and left on ice for 30′. Then extracts were clarified by centrifugation at 13,200 rpm for 30′ at 4 °C. The amount of protein in the samples was determined by the Bio-Rad protein assay (Bio-Rad, Milan, Italy).

After the addition of Laemmli buffer (Sigma-Aldrich) samples were boiled at 100 °C for 5 min and resolved by SDS- polyacrylamide gel electrophoresis (SDS-PAGE). About 20 μg of total extracts were separated by SDS-PAGE.

Proteins were then transferred to a polyvinylidene difluoride membrane (PVDF, Millipore) using a Mini trans-blot apparatus (Bio-Rad) according to the manufacturer's instructions. The PVDF membrane was blocked in 5% *w/v* milk buffer (5% *w/v* non-fat dried milk, 50 mM Tris, 200 mM NaCl, 0.2% Tween 20) and incubated overnight at 4 °C with primary antibodies diluted in 5% *w/v* milk or bovine serum albumin (BSA) buffer according to the manufacturer's instructions. Following three washes with TBST (Tris-buffered saline, 0.1% Tween), the blots were incubated for 1 hour at RT with HRP-conjugated secondary antibodies (Sigma-Aldrich). Proteins were visualized by enhanced chemiluminescence (ECL, Bio-Rad) and analyzed by Quantity One W software of ChemiDoc TM XRS system (Bio-Rad).

Band intensities were quantified by ImageJ Software (http://imageJ.nih.gov/ij/, accessed on 21 August 2021, free software, downloaded from the NIH, Bethesda, MD, USA), normalized respect loading control and reported as fold enrichment to the control sample.

2.4. Antibodies

The primary antibodies used are: anti-YB-1 raised against the region 1 to 100 of YB-1 protein (12148 Abcam, Cambridge, UK); anti-Actin (8432 Santa Cruz, Dallas, TX, USA); anti-PTEN (Cell Signaling, Danvers, MA, USA, 9559S); anti-Phospho-Akt (Ser473) (193H12) (Cell Signaling, 4058S); anti-Akt (Cell Signaling, 2920S).

2.5. Transfections and RNA Interference

Cells were transfected using Lipofectamine 2000 (Life Technologies, Carlsbad, CA, USA) according to the manufacturer's recommendations. Briefly, cells were seeded at 70–80% confluence (2.5×10^5) in 6-well and transiently transfected with plasmids at a concentration of 300 ng for 48h. MG-132 was added to the cells at the concentration of 10 μM 4 h before the end of transfection.

YB-1 transient silencing was carried out with IBONI YB-1 small interfering (siRNA) pool (RIBOXX GmbH, Radebeul, Germany) as a pool of 3 different siRNAs and RNAiMAX reagent (Life Technologies), according to the manufacturer's recommendations. Cells were seeded at 70–80% confluence (2.5×10^5) in 6-well and transiently silenced with IBONI YB1-siRNA at 150 nM final concentration.

Negative Control siRNA, provided by RIBOXX (Germany) was used as a negative control.

YB-1 guide and passenger sequences:
h YBX-1 guide (5′-3′):
UUUAUCUUCUUCAUUGCCGCCCCC
UUAUUCUUCUUUAUGGCAGCCCCC
UAUUUGAUGACCACACCAGCCCCC
h YBX-1 passenger (5′-3′):

GGGGGCGGCAAUGAAGAAGAUAAA
GGGGGCUGCCAUAAAGAAGAAUAA
GGGGGCUGGUGUGGUCAUCAAAUA

2.6. Co-Immunoprecipitation

For co-immunoprecipitations (Co-IP) 2×10^6 HEK293T cells were seeded in poly-D-lysine pre-treated 100-mm dishes; the day after Dynabeads Protein A (Invitrogen) were incubated with antibodies against YB-1, 3 µg for 1.5 mg of protein extract for 10′ at room temperature in rotation after protein extract was incubated with the Dynabeads-Ab complex overnight at 4 °C. Immunoglobulin G (IgG) 3 µg for 1.5 mg of protein extract was used as a negative control. Immunocomplexes were resolved with SDS-PAGE; immunoblot was performed with anti-PTEN antibody and anti-YB1 antibody.

2.7. Quantitative Real Time-PCR

Total RNA was extracted with Trizol reagent (Gibco) according to the manufacturer's instructions. Reverse transcription was performed using All-In-One 5X RT MasterMix (Abcam). AriaMx Real-Time PCR System (Agilent Technologies, Santa Clara, CA, USA) and Brilliant HRM Ultrafast Starter Pack were used. Quantitative relative expression was calculated according to the $2^{-\Delta\Delta CT}$ method (Delta CT method) normalizing to *rpl0* mRNA expression. Sequences of primers used:

PTEN *For:* CTCAGCCGTTACCTGTGTGT
PTEN *Rev*: AGGTTTCCTCTGGTCCTGGT
YB-1 *For*: CGACCAGACTCTCATCCTGC
YB-1 *Rev:* TTTGATGACCACACCAGGCA
RPL0 *For*: GACGGATTACACCTTCCCACTT
RPL0 *Rev:* GGCAGATGGATCAGCCAAGA

2.8. Statistical Analysis

Statistical analyses were performed using GraphPad Prism (version 8.1.2, GraphPad Software Inc., San Diego, CA, USA). Data were presented as the mean ± standard deviation and analyzed for statistical significance using one-way or two-way analysis of variance (ANOVA) and multiple comparisons. For all tests, $p < 0.05$ was considered to indicate a statistically significant difference. To report *p*-values, the *New England Journal of Medicine* (NEJM) decimal format was used; differences were considered statistically significant at * $p < 0.033$, ** $p < 0.002$ and *** $p < 0.001$.

3. Results

Firstly, we wondered whether there was a direct functional relationship between YB-1 and PTEN. We hypothesized that YB-1 could control PTEN protein level. To address this point, we decided to analyze the effect of YB-1 downregulation on PTEN protein intracellular level.

To this aim, we used PTEN proficient immortalized HaCaT and HEK293T cells, showing robust expression of endogenous YB-1 resembling actively proliferating pre-malignant cells. YB-1 expression was depleted by RNAi and PTEN levels were checked by immunoblot. Control (siRNA NC) and YB-1 depleted cells (siPool YB-1) were collected 48h after transfection and analysed by immunoblot. As shown in Figure 2A we observed a clear increase of PTEN levels in YB-1 depleted HaCaT cells compared to the control with a concomitant reduction of $pAkt^{S743}$ (Figure 2B) in line with a potential role of YB-1 in enhancing Akt phosphorylation at S743 by directly impinging on PTEN/PI3K pathway. An even more evident increase of PTEN protein levels was observed in HEK293T cells upon YB-1 depletion (Figure 2B). Interestingly, an increase of PTEN protein level was also observed in total extracts from HaCaT and HEK293T cells whose level of YB-1 was reduced by oxidative stress stimuli such as that with NaArs and Cu++ treatments (Figure 2C), as we have previously shown [21].

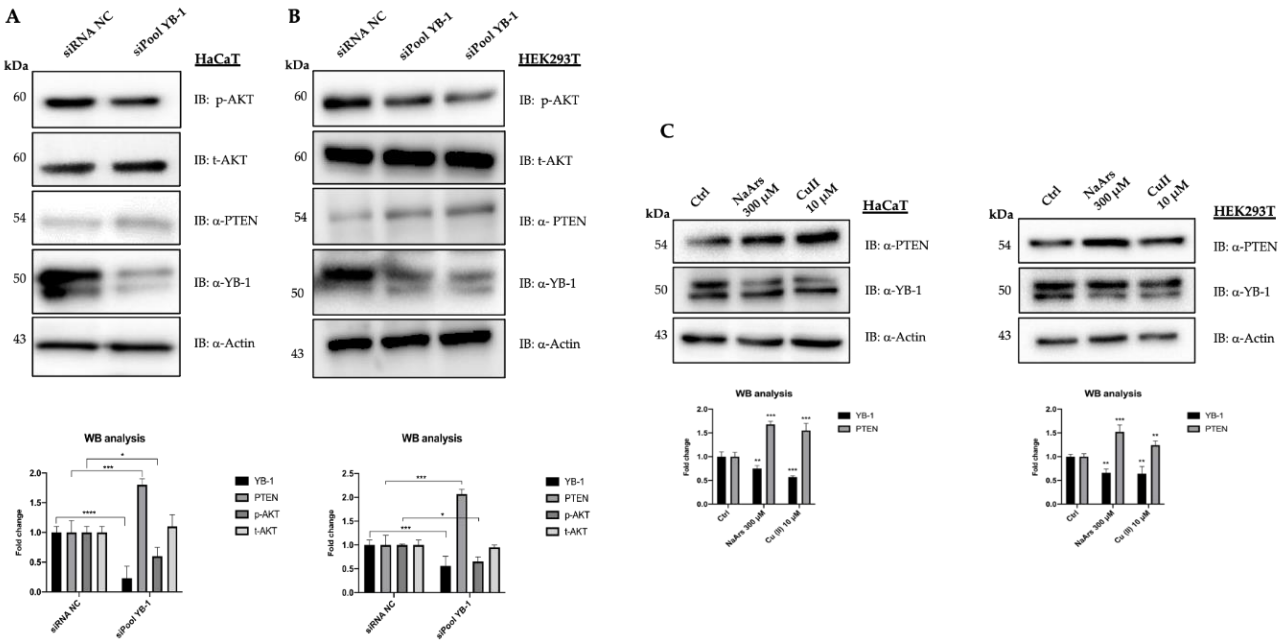

Figure 2. YB-1 controls PTEN levels in HaCaT and HEK293T cells. (**A**) HaCaT cells were transfected with 10 nM final siRNA-poolYB-1 or siRNA-Negative Control (NC). The effect on PTEN intracellular levels was evaluated 48 h post-transfection by western blot on whole protein lysates probed with anti-PTEN antibodies. Immunoblots were also probed with antibodies against YB-1, pAkt^{S743}, tAKT and actin as a loading control. (**B**) HEK293T cells were transfected with 10 nM final siRNA-NC or siRNA-poolYB-1 (duplicated). Whole protein lysates were collected and analysed 48 h after transfection as described in (**A**); (**C**) HaCaT and HEK293T cells were treated with NaArs and Cu (II) for 2 h to induce oxidative stress. Cell lysates were analyzed by immunoblot with antibodies against PTEN, YB1 and actin used as a loading control. For comparison, siRNA-transfected extracts were used. Statistical analyses were performed using 2-way ANOVA and Sidak's multiple comparison or Dunnett's multiple comparisons test. Levels of significance between points of expression are indicated (*** $p < 0.001$, ** $p < 0.01$, * $p < 0.05$).

We then decided to look next at the effect of YB-1 overexpression on PTEN protein levels. To this aim, we transfected YB1 expression vector in HEK293T or HaCat cells treated or not with the proteasome inhibitor MG132. At 48 h after transfection, cells were collected, and the extracts were analysed by immunoblot. As shown in Figure 3A we observed a moderate but significant reduction of PTEN protein level, compared to the control, that was not rescued by MG132 treatment thus suggesting that it does not occur through a proteasome-dependent mechanism. We also tested for a possible interaction between YB-1 and PTEN proteins by co-immunoprecipitation. However, as shown in Figure 3B, YB-1 antibodies were unable to immunoprecipitate endogenous PTEN.

Given the importance of YB-1 function in the control of RNA metabolism, we wished to explore whether YB-1 depletion was able to alter the level of PTEN mRNA. Therefore, we depleted HaCaT and HEK293T cells of YB-1 using the siRNA pool against YB-1 (siPoolYB-1) [21]. Total RNA was extracted and subjected to RT-qPCR. As shown in Figure 4, compared to the control sample the mRNA level of YB-1 was reduced to 0.25 in HaCaT and 0.40 in HEK293T cells while PTEN mRNA was increased to 1.75 in HaCaT and 1.5 in HEK293T cells.

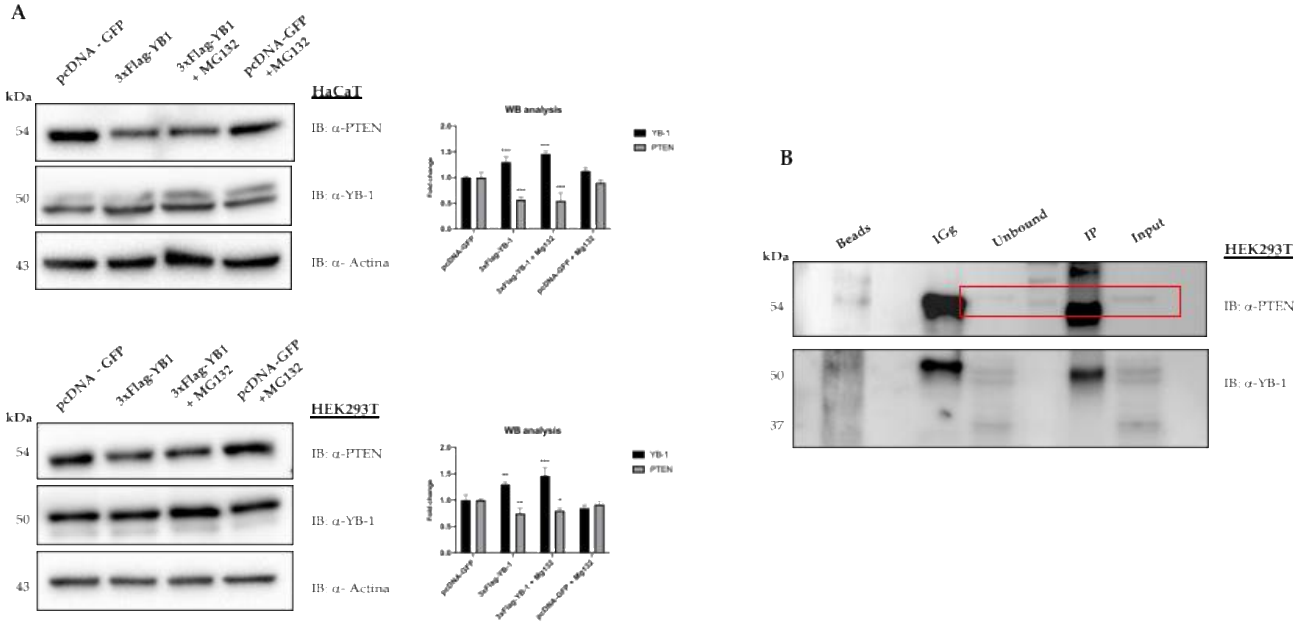

Figure 3. YB-1 mediated reduction of PTEN levels requires neither the proteasomal activity nor the physical interaction between the two proteins. (**A**) HaCaT cells (top panel) and HEK293T cells (lower panel) were transfected with 3XFlag-YB-1 plasmid or pcDNA-GFP as a control. Effect on PTEN intracellular levels was evaluated 48 h post-transfection by western blot on whole protein lysates probed with anti-YB-1, anti-PTEN, and anti-actin as a loading control. 10 μM MG132 for 4 h before the end of transfection was used to inhibit proteasome activity. (**B**) HEK293T protein extracts were immunoprecipitated with anti-YB-1 antibodies. Immunocomplexes were subjected to western blot and revealed using antibodies against PTEN. PTEN signal in unbound and input are highlighted in the rectangle box. Statistical analysis was performed using 2-way ANOVA and Sidak's multiple comparison test. Levels of significance between points of expression are indicated (*** $p < 0.001$, ** $p < 0.01$, * $p < 0.05$).

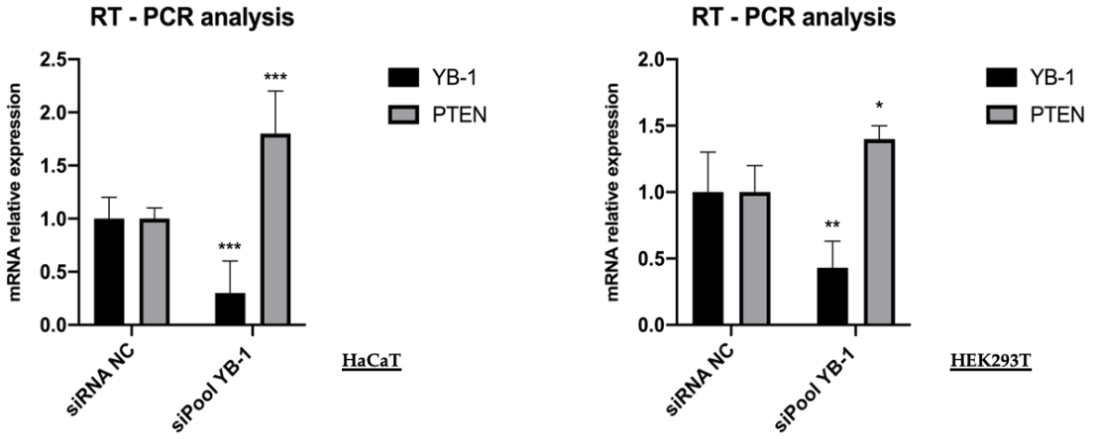

Figure 4. YB-1 depletion increases the level of PTEN transcript. HaCaT and HEK293T cells were transfected with 10 nM final siRNA-poolYB-1 or siNC; the effect on PTEN mRNA level was evaluated 48h post-transfection by qRT-PCR analysis. Relative mRNA levels were plotted on the y-axis and siRNA employed are indicated on the x-axis. RPL0 ribosomal protein mRNA was used for normalization. Statistical analyses were performed using 2-way ANOVA and Sidak's multiple comparison test. Levels of significance between points of expression are indicated (*** $p < 0.001$, ** $p < 0.01$, * $p < 0.05$).

This result showed that the effect of YB-1 on PTEN was primarily at mRNA level. It is important to remind that PTEN functions in a dosage-dependent manner during tumor development and that moderate PTEN reduction, without complete loss, has been reported to activate the PI3K/Akt pathway and to be associated with chemoresistance and cancer progression [22,23].

4. Conclusions

The data presented here show evidence that YB-1 controls PTEN protein levels by acting at the transcript level. Our data are in line with what is already known regarding the function of both proteins, although a direct functional link between PTEN and YB-1 has never been assessed. At the functional level increased expression of YB-1 can restrain PTEN expression thus enforcing Akt activation in premalignant cells (Figure 5). Akt, in turn, increases the pro-proliferative and pro-survival activities of YB-1 by inducing YB1 phosphorylation at S102 thereby promoting its nuclear translocation.

The PTEN level appears to be tightly controlled both transcriptionally and post-transcriptionally [24]. Some oncogenic microRNA and ncRNAs have been found to target PTEN mRNA and regulate malignant progression [25], ncRNAs including lncRNAs and miRNAs act alone or interact with each other to regulate PTEN expression and it has recently been proposed that some of the oncogenic effects of YB-1 in breast cancer may be mediated through its interactions with sncRNAs [26].

Although the precise mechanism through which YB-1 controls PTEN mRNA level remains to be determined, our data suggest the existence of a positive feedback loop between YB-1 and Akt, reinforcing each other, probably occurring at an early step in cancer progression and conferring a selective advantage to premalignant cells. Elucidation of the details about how YB-1 downregulates PTEN expression may provide novel insights into the regulation network of PTEN, which could suggest possible anticancer strategies focusing on targeting both YB-1 and the PI3K/Akt pathway.

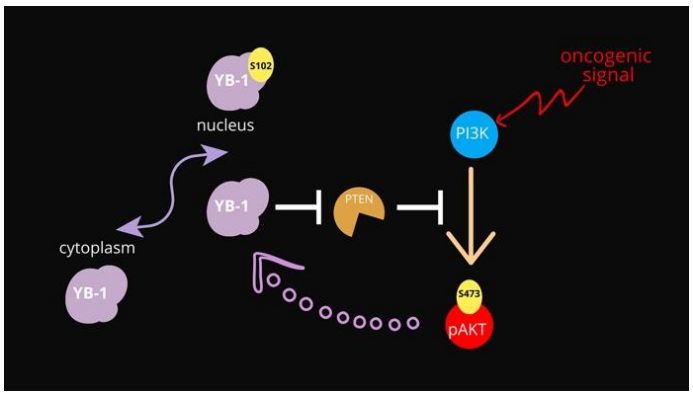

Figure 5. Schematic representation of the proposed functional relationships among YB-1, PTEN and Akt. In normal conditions, YB-1 is mainly cytoplasmic. The Akt-dependent phosphorylation of YB-1 at S102 promotes its translocation to the nuclear compartment promoting cell survival.

Author Contributions: Conceptualization: V.C.; Methodology and investigation: A.D. and E.M.; data curation: A.D.; writing of the original draft preparation: V.C.; supervision, A.P., T.A. and V.C.; project administration and funding acquisition: A.P., V.C., T.A. All authors have read and agreed to the published version of the manuscript.

Funding: This research received funds from University Federico II of Naples, "Ricerca Dipartimentale 000020-PRD2020".

Institutional Review Board Statement: Not applicable.

Informed Consent Statement: Not applicable.

Conflicts of Interest: The authors declare no conflict of interest. The funders had no role in the design of the study; in the collection, analyses, or interpretation of data; in the writing of the manuscript, or in the decision to publish the results.

References

1. Lindquist, J.A.; Mertens, P.R. Cold shock proteins: From cellular mechanisms to pathophysiology and disease. *Cell Commun. Signal.* **2018**, *16*, 11–14. [CrossRef]
2. Metha, S.; McKinney, C.; Algie, M.; Verma, C.S.; Kannan, S.; Harfoot, R.; Bartolec, T.K.; Bhatia, P.; Fisher, A.J.; Gould, M.L.; et al. Dephosphorylation of yb-1 is required for nuclear localisation during G2 phase of the cell cycle. *Cancers* **2020**, *12*, 2–315.
3. Evdokimova, V.; Ruzanov, P.; Anglesio, M.S.; Sorokin, A.S.; Ovchinnikov, L.P.; Buckley, J.; Triche, T.J.; Sonenberg, N.; Sorensen, P.H.B. Akt-mediated YB-1 phosphorylation activates translation of silent mRNA species. *Mol. Cell. Biol.* **2006**, *26*, 277–292. [CrossRef]
4. Fujii, T.; Yokoyama, G.; Takahashi, H.; Namoto, R.; Nakagawa, S.; Toh, U.; Kage, M.; Shirouzu, K.; Kuwano, M. Preclinical studies of molecular-targeting diagnostic and therapeutic strategies against breast cancer. *Breast Cancer* **2008**, *15*, 73–78. [CrossRef] [PubMed]
5. Kuwano, M.; Oda, Y.; Izumi, H.; Yang, S.J.; Uchiumi, T.; Iwamoto, Y.; Toi, M.; Fujii, T.; Yamana, H.; Kinoshita, H.; et al. The role of nuclear Y-box binding protein 1 as a global marker in drug resistance. *Mol. Cancer Ther.* **2004**, *3*, 1485–1492. [PubMed]
6. Kashihara, M.; Azuma, K.; Kawahara, A.; Basaki, Y.; Hattori, S.; Yanagawa, T.; Terazaki, Y.; Takamori, S.; Shirouzu, K.; Aizawa, H.; et al. Nuclear Y-box binding protein-1, a predictive marker of prognosis, is correlated with expression of HER2/ErbB2 and HER3/ErbB3 in non-small cell lung cancer. *J. Thorac. Oncol.* **2009**, *4*, 1066–1074. [CrossRef] [PubMed]
7. Hohlfeld, R.; Brandt, S.; Bernhardt, A.; Gorny, X.; Schindele, D.; Jandrig, B.; Schostak, M.; Isermann, B.; Lindquist, J.A.; Mertens, P.R. Crosstalk between Akt signaling and cold shock proteins in mediating invasive cell phenotypes. *Oncotarget* **2018**, *9*, 19039. [CrossRef] [PubMed]
8. Cohen, S.B.; Ma, W.; Valova, V.A.; Algie, M.; Harfoot, R.; Woolley, A.G.; Robinson, P.J.; Braithwaite, A.W. Genotoxic stress-induced nuclear localization of oncoprotein YB-1 in the absence of proteolytic processing. *Oncogene* **2010**, *29*, 403–410. [CrossRef]
9. Eliseeva, I.A.; Kim, E.R.; Guryanov, S.G.; Ovchinnikov, L.P.; Lyabin, D.N. Y-box-binding protein 1 (YB-1) and its functions. *Biochemistry* **2011**, *76*, 1402–1433. [CrossRef]
10. Lettau, K.; Zips, D.; Toulany, M. Simultaneous targeting of rsk and akt efficiently inhibits yb-1-mediated repair of ionizing radiation-induced DNA double-strand breaks in breast cancer cells. *Int. J. Radiat. Oncol. Biol. Phys.* **2021**, *109*, 567–580. [CrossRef]
11. Kretov, D.A.; Mordovkina, D.A.; Eliseeva, I.A.; Lyabin, D.N.; Polyakov, D.N.; Joshi, V.; Desforges, B.; Hamon, L.; Lavrik, O.I.; Pastré, D.; et al. Inhibition of transcription induces phosphorylation of YB-1 at Ser102 and its accumulation in the nucleus. *Cells* **2020**, *9*, 104. [CrossRef]
12. Kuwano, M.; Shibata, T.; Watari, K.; Ono, M. Oncogenic Y-box binding protein-1 as an effective therapeutic target in drug-resistant cancer. *Cancer Sci.* **2019**, *110*, 1536–1543. [CrossRef] [PubMed]
13. Maehama, T.; Dixon, J.E. The tumor suppressor, PTEN/MMAC1, dephosphorylates the lipid second messenger, phosphatidylinositol 3, 4, 5-trisphosphate. *J. Biol. Chem.* **1998**, *273*, 13375–13378. [CrossRef] [PubMed]
14. Richman, S. Deficient mismatch repair: Read all about it. *Int. J. Oncol.* **2015**, *47*, 1189–1202. [CrossRef] [PubMed]
15. Radu, A.; Neubauer, V.; Akagi, T.; Hanafusa, H.; Georgescu, M.M. PTEN induces cell cycle arrest by decreasing the level and nuclear localization of cyclin D1. *Mol. Cell. Biol.* **2003**, *23*, 6139–6149. [CrossRef] [PubMed]
16. Ming, M.; He, Y.Y. PTEN in DNA damage repair. *Cancer Lett.* **2012**, *319*, 125–129. [CrossRef]
17. Carbognin, L.; Miglietta, F.; Paris, I.; Dieci, M.V. Prognostic and predictive implications of PTEN in breast cancer: Unfulfilled promises but intriguing perspectives. *Cancers* **2019**, *11*, 1401. [CrossRef] [PubMed]
18. Milella, M.; Falcone, I.; Conciatori, F.; Cesta Incani, U.; Del Curatolo, A.; Inzerilli, N.; Nuzzo, C.M.; Vaccaro, V.; Vari, S.; Cognetti, F.; et al. PTEN: Multiple functions in human malignant tumors. *Front. Oncol.* **2015**, *5*, 24. [CrossRef]
19. Lee, Y.R.; Chen, M.; Pandolfi, P.P. The functions and regulation of the PTEN tumour suppressor: New modes and prospects. *Nat. Rev. Mol. Cell Biol.* **2018**, *19*, 547–562. [CrossRef]
20. Heumann, A.; Kaya, Ö.; Burdelski, C.; Hube-Magg, C.; Kluth, M.; Lang, D.S.; Simon, R.; Beyer, B.; Thederan, I.; Sauter, G.; et al. Up regulation and nuclear translocation of Y-box binding protein 1 (YB-1) is linked to poor prognosis in ERG-negative prostate cancer. *Sci. Rep.* **2017**, *17*, 2056. [CrossRef]
21. Guarino, A.M.; Troiano, A.; Pizzo, E.; Bosso, A.; Vivo, M.; Pinto, G.; Amoresano, A.; Pollice, A.; La Mantia, G.; Calabrò, V. Oxidative stress causes enhanced secretion of YB-1 protein that restrains proliferation of receiving cells. *Genes* **2018**, *9*, 513. [CrossRef]
22. Alimonti, A.; Carracedo, A.; Clohessy, J.G.; Trotman, L.C.; Nardella, C.; Egia, A.; Salmena, L.; Sampieri, K.; Haveman, W.J.; Brogi, E.; et al. Subtle variations in Pten dose determine cancer susceptibility. *Nat. Genet.* **2010**, *42*, 454–458. [CrossRef]
23. Rich, J.N. Cancer stem cells in radiation resistance. *Cancer Res.* **2007**, *67*, 8980–8984. [CrossRef]
24. Leslie, N.R.; Foti, M. Non-genomic loss of PTEN function in cancer: Not in my genes. *Trends Pharmacol. Sci.* **2011**, *32*, 131–140. [CrossRef]
25. Mouw, J.K.; Yui, Y.; Damiano, L.; Bainer, R.O.; Lakins, J.N.; Acerbi, I.; Ou, G.; Wijekoon, A.C.; Levental, K.R.; Gilbert, P.M.; et al. Tissue mechanics modulate microRNA-dependent PTEN expression to regulate malignant progression. *Nat. Med.* **2014**, *20*, 360–367. [CrossRef] [PubMed]
26. Blenkiron, C.; Hurley, D.G.; Fitzgerald, S.; Print, C.G.; Lasham, A. Links between the oncoprotein YB-1 and small non-coding RNAs in breast cancer. *PLoS ONE* **2013**, *8*, e80171. [CrossRef] [PubMed]

Concluding remarks

Natural products have long been the main source of new drugs against infectious diseases, cancer, and neurodegenerative diseases. In parallel with the search for new metabolites with interesting biological activities, the goal of modern biotechnology is to continue to investigate, develop and optimize the application performance of already described molecules.
The term natural products include any substance produced by living organisms and can be extracted from the tissues of terrestrial plants, fungi, marine organisms, or fermentation by microorganisms. A single or a mixture of compounds from natural sources can exert beneficial effects as food supplements or cosmetics.
Nowadays, the interest in using natural products has increased significantly and the reason for this trend is the idea of using safe compounds compared to synthetic ones, availability, biocompatibility, low toxicity, and environmental responsibility.
During my PhD training, I learned how to isolate and functionally characterize extremely heterogeneous metabolites from plants grown and harvested in an extreme environment, such as a desert. Plants living in a desert have evolved to produce secondary metabolites, capable of guaranteeing their survival in extreme environment conditions.

From the first species *Crinum biflorum*, an Amaryllidaceae plant used in African traditional medicine, collected in Senegal, I have isolated and characterized four different homoisoflavanoids and one alkylamide. Flavonoids showed promising anticancer properties being cytotoxic at low micromolar concentrations towards HeLa and A431 human cancer cell lines. The N-p- coumaroyltyramine, instead, was selectively toxic to A431 and HeLa cancer cells, while it protected immortalized HaCaT cells against oxidative stress induced by hydrogen peroxide. Flavonoids also inhibited acetylcholinesterase activity. The anti-amylase and the strong anti-glucosidase activity of N-p-coumaroyltyramine were confirmed. The obtained data extends the chemical library of compounds that can be a potential candidates for the treatment of cancer, viral infections, diabetes and Alzheimer's disease.

The second species, *Cistanche phelypaea*, belonging to the Orobancaceae family of plants, was also collected in a desert

environment and is widely used in traditional Chinese medicine for its innumerable beneficial properties. From this plant, I was able to isolate and characterize mainly two classes of compounds: phenyl-ethanoid glycosides and iridoid glycosides. Phenolics are the most common group of natural products in the plant kingdom. Phenolic compounds occupy a privileged position in the life of humans due to their widespread applications and are potent antioxidants due to their higher chelation efficiency. Phenolic compounds from plants are reported as potential sources of new natural medicines, antibiotics, insecticides, and herbicides. This study aims to characterize the antioxidant activity of *C. phelypaea* metabolites, in the light of their application in nutraceutical and cosmeceutical industries; and the effect of acetoside, the most abundant metabolite in *C. phelypaea* extract, on human keratinocyte and pluripotent stem cell proliferation and differentiation. Besides its strong antioxidant potential, acetoside appears to preserve the proliferative potential of human basal keratinocyte and mesenchymal progenitors which is necessary for tissue morphogenesis and renewal. The use of stem cells in tissue engineering demands their controlled differentiation; hMSCs have great therapeutic potential, however, their usefulness is limited by cellular senescence occurring secondary to increased levels of reactive oxygen species during their propagation in culture. In this respect, acetoside can be of practical relevance for the clinical application of human stem cell cultures for regenerative medicine.

Part of my PhD project was dedicated to the revaluation of waste from the agri-food industry of our area, using the waste from pomace. Food waste such as peels and seeds derived from fruit and vegetable processing can also be an important source of bioactive compounds, A large variety of compounds from different natural sources (e.g., phenolic compounds, dietary fibers, polysaccharides, vitamins, carotenoids, pigments, and oils) can have a variety of beneficial activities. One way to improve foods, food supplements or cosmetics is to add natural metabolites with antioxidant and anti-aging properties.

Nutraceuticals provide an excellent option to assimilate natural substances with numerous benefits for human health. They are also a boon for some patients who are reluctant to undergo conventional chemical therapy and have gained much attention in the cancer research field. Nutraceuticals are known to be effective against age-related and chronic diseases. Many of these nutraceuticals are rich sources of antioxidants and would target signaling pathways related to redox-mediated transcription factors. They are also known to moderate the endocrine system, the immunological cascade, and inflammation-

related enzymes. DNA repair and cleavage processes are also influenced by such compounds. It has been found that many nutraceuticals such as green tea, curcumin, isoflavones, polyphenols, lycopene, resveratrol, etc. reverse, prevent, or delay the carcinogenic process. The chemopreventive components present in fruits and vegetables also have potential anticarcinogenic and antimutagenic activities. The demand for nutraceuticals is associated with the prevalence of several chronic diseases such as cancer, diabetes, and cardiovascular disease.

During my PhD training I optimized the extraction process from pomace waste in terms of sustainability. Moreover, I characterized the extracts from their phenols composition which depends on the nutritional characteristics of the soil and the atmospheric agents of the place where the grape is grown. Catechin and its epimer epicatechin have been found among the most abundant polyphenols, in this pomace extract. These complex blends of polyphenols have been encapsulated in edible formulations based on pectin, also derived from the same waste-maximizing recycling, and bivalent ions such as calcium and iron ions, to support the demand for these essential micronutrients. The calcium ion-based formulation was found to be promising for the transport of these powerful antioxidants along the gastrointestinal tract and intestinal absorption.

In conclusion, natural metabolites remain a promising pool for the nutraceutical and cosmeceutical industry that can be directly used or derivatized to obtain new interesting health-promoting products.

References

A. Assifaoui, O. Chambin, P. Cayot, Carbohydr. Drug release from calcium and zinc pectinate beads: Impact of dissolution medium composition. *Carbohydrate polymers*, 2011, 85.2: 388-393.

Abd El Hafiz, M.A.; Ramadan, M.A.; Jung, M.L.; Beck, J.P.; Anton, R. Cytotoxic activity of Amaryllidaceae alkaloids from *Crinum augustum* and *Crinum bulbispermum. Planta Med*. 1991, 57, 437–439.

Abd El-Hafiz, M.A. Aliphatic hydroxyketones from *Crinum augustum*. *Phytochemistry* 1991, 30, 3127–3129.

Abdel-Halim, O.B.; Marzouk, A.M.; Mothana, R.; Awadh, N. A new tyrosinase inhibitor from *Crinum yemense* as potential treatment for hyperpigmentation. *Die Pharm. Int. J. Pharm*. Sci. 2008, 63, 405–407.

activity. *Phytochemistry* 2020, 175, 112390.

Acun, S.; Gül, H. Effects of grape pomace and grape seed flours on cookie quality. *Qual. Assur. Saf. Crop. Food* 2014, *6*, 81–88.

Ahn, J. H., Jo, Y. H., Kim, S. B., Turk, A., Oh, K. E., Hwang, B. Y., ... & Lee, M. K. Identification of antioxidant constituents of the aerial part of Plantago asiatica using LC–MS/MS coupled DPPH assay. *Phytochemistry Letters*, 2018, 26: 20-24.

Amoresano, A., Di Costanzo, A., Leo, G., Di Cunto, F., La Mantia, G., Guerrini, L., & Calabro, V. Identification of ΔNp63α protein interactions by mass spectrometry. *Journal of Proteome Research*, 2010, 9.4: 2042-2048.

Averilla, J.N.; Oh, J.; Kim, H.J.; Kim, J.S.; Kim, J.S. Potential health benefits of phenolic compounds in grape processing by-products. *Food Sci. Biotechnol.* 2019, *28*, 1607–1615.

Balbinoti, T.C.V.; Stafussa, A.P.; Haminiuk, C.W.I.; Maciel, G.M.; Sassaki, G.L.; Jorge, L.M.D.M.; Jorge, R.M.M. Addition of grape pomace in the hydration step of parboiling increases the antioxidant properties of rice. *Int. J. Food Sci. Technol.* 2020, *55*, 2370–2380.

Beladjila K. A., Berrehal D., De Tommasi N., Granchi C., Bononi G., Braca A., De Leo M. New phenylethanoid glycosides from *Cistanche* phelypaea and their activity as inhibitors of monoacylglycerol lipase (MAGL). Planta Medica, 2018, 84.09/10: 710-715.

Bender, A.B.; Speroni, C.S.; Salvador, P.R.; Loureiro, B.B.; Lovatto, N.M.; Goulart, F.R.; Lovatto, M.T.; Miranda, M.Z.; Silva, L.P.; Penna, N.G. Grape pomace skins and the effects of its inclusion in the technological properties of muffins. *J. Culin. Sci. Technol.* 2017, *15*, 143–157.

Bender, A.B.B.; Speroni, C.S.; Moro, K.I.B.; Morisso, F.D.P.; dos Santos, D.R.; da Silva, L.P.; Penna, N.G. Effects of micronization on dietary fiber composition, physicochemical properties, phenolic compounds, and antioxidant capacity of grape pomace and its dietary fiber concentrate. *LWT* 2020, *117*, 108652.

Bennato, F.; Di Luca, A.; Martino, C.; Ianni, A.; Marone, E.; Grotta, L.; Ramazzotti, S.; Cichelli, A.; Martino, G. Influence of Grape Pomace Intake on Nutritional Value, Lipid Oxidation and Volatile Profile of Poultry Meat. *Foods* 2020, *9*, 508.

Beres, C.; Costa, G.N.; Cabezudo, I.; da Silva-James, N.K.; Teles, A.S.; Cruz, A.P.; Mellinger-Silva, C.; Tonon, R.V.; Cabral, L.M.; Freitas, S.P. Towards integral utilization of grape pomace from winemaking process: A review. *Waste Manag.* 2017, *68*, 581–594.

Bernfeld, P. Amylases, α and β. 1955.

Bougandoura, A., D'Abrosca, B., Ameddah, S., Scognamiglio, M., Mekkiou, R., Fiorentino, A., … Benayache, F. Chemical constituents and *in vitro* anti-inflammatory activity of *Cistanche* violacea Desf.(Orobanchaceae) extract. *Fitoterapia*, 2016, 109: 248-253.

Brabson, J. P., Leesang, T., Mohammad, S., & Cimmino, L. Epigenetic regulation of genomic stability by vitamin C. *Frontiers in Genetics*, 2021, 12: 675780.

Burkill, H.M. The Useful Plants of West Tropical Africa; *Royal Botanic Gardens: London*, UK, 1985; Volume 1, p. 163.

Bustamante, M.A.; Moral, R.; Paredes, C.; Pérez-Espinosa, A.; Moreno-Caselles, J.; Pérez-Murcia, M.D. Agrochemical characterisation of the solid by-products and residues from the winery and distillery industry. *Waste Manag.* 2008, *28*, 372–380.

C.K. Yeung, R.E. Glahn, R.M. Welch, D.D. Miller. Prebiotics and iron bioavailability—is there a connection?. *Journal of food science*, 2005, 70.5: R88-R92.

Christenhusz, M.J.; Byng, J.W. The number of known plants species in the world and its annual increase. *Phytotaxa* 2016, 26, 201–217.

Cimmino, L., Neel, B. G., & Aifantis, I. Vitamin C in stem cell reprogramming and cancer. *Trends in cell biology*, 2018, 28.9: 698-708.

Collins, P. L., Purman, C., Porter, S. I., Nganga, V., Saini, A., Hayer, K. E., ... & Oltz, E. M. DNA double-strand breaks induce H2Ax phosphorylation domains in a contact-dependent manner. *Nature communications*, 2020, 11.1: 1-9.

Coviello, T., Matricardi, P., Marianecci, C., & Alhaique, F. Polysaccharide hydrogels for modified release formulations. *Journal of controlled release*, 2007, 119.1: 5-24.

Dekens, M. P., Santoriello, C., Vallone, D., Grassi, G., Whitmore, D., & Foulkes, N. S. Light regulates the cell cycle in zebrafish. *Current Biology*, 2003, 13.23: 2051-2057.

Delalande, O., Gao, K., Fan, B. T., Zakrzewska, K., El Fassi, N., Jia, Z. J., ... & Doucet, J. P. Docking study of cistanoside C to telomeric DNA fragment. *SAR and QSAR in Environmental Research*, 2002, 13.7-8: 675-688.

Deng, Q.; Penner, M.H.; Zhao, Y. Chemical composition of dietary fiber and polyphenols of five different varieties of wine grape pomace skins. *Food Res. Int.* 2011, *44*, 2712–2720.

Dewick, P.M. *Medicinal Natural Products:* A Biosynthetic Approach; John Wiley & Sons: Chichester, UK, 2009.

Deyama, T., Yahikozawa, K., Al-Easa, H. S., & Rizk, A. M. Constituents of plants growing in Qatar: part xxviii. Constituents Of *cistanche* phelypaea. 1995.

di Martino, O., Troiano, A., Guarino, A. M., Pollice, A., Vivo, M., La Mantia, G., & Calabrò, V. ΔNp63α controls YB-1 protein stability: evidence on YB-1 as a new player in keratinocyte differentiation. *Genes to Cells*, 2016, 21.6: 648-660.

Dickey, J.S.; Redon, C.E.; Nakamura, A.J.; Baird, B.J.; Sedelnikova, O.A.; Bonner, W.M. H2AX: Functional roles and potential applications. *Chromosoma* 2009, 118, 683–692.

Divekar, P. A., Narayana, S., Divekar, B. A., Kumar, R., Gadratagi, B. G., Ray, A., ... & Behera, T. K. Plant secondary metabolites as defense tools against herbivores for sustainable crop protection. *International journal of molecular sciences*, 2022, 23.5: 2690.

Dwyer, K.; Hosseinian, F.; Rod, M.R. The market potential of grape waste alternatives. *J. Food Res.* 2014, *3*, 91.

Eleonora, N.; Dobrei, A.; Alina, D.; Bampidis, V.; Valeria, C. Grape pomace in sheep and dairy cows feeding. *J. Hortic. For. Biotechnol.* 2014, *18*, 146–150.

Ellman, G. L., Courtney, K. D., Andres Jr, V., & Featherstone, R. M. A new and rapid colorimetric determination of acetylcholinesterase activity. *Biochemical pharmacology*, 1961, 7.2: 88-95.

Evidente, A., Iasiello, I., & Randazzo, G. An improved method for the large-scale preparation of lycorine. *CHEMISTRY & INDUSTRY*, 1984, 9: 348-349.

F. Ghibaudo, E. Gerbino, V. Campodall' Orto, A. Gómez-Zavaglia. Pectin-iron capsules: Novel system to stabilise and deliver lactic acid bacteria. *Journal of Functional Foods*, 2017, 39: 299-305.

FAOSTAT. Food and Agriculture Organization of the United Nations, 2018. Available online: (accessed on 31 July 2020).

Fu, G., Pang, H., & Wong, Y. H. Naturally occurring phenylethanoid glycosides: potential leads for new therapeutics. *Current Medicinal Chemistry*, 2008, 15.25: 2592-2613.

García-Lomillo, J.; González-SanJosé, M.L. Applications of wine pomace in the food industry: Approaches and functions. *Compr. Rev. Food Sci. Food Saf.* 2017, *16*, 3–22.

Garrido, M.D.; Auqui, M.; Martí, N.; Linares, M.B. Effect of two different red grape pomace extracts obtained under different extraction systems on meat quality of pork burgers. *Lwt-Food Sci. Technol.* 2011, *44*, 2238–2243.

Ghosal, S.; Saini, K.S.; Razdan, *S. Crinum* alkaloids: Their chemistry and biology. *Phytochemistry* 1985, 24, 2141–2156.

Gong, L., Feng, D., Wang, T., Ren, Y., Liu, Y., & Wang, J. Inhibitors of α-amylase and α-glucosidase: Potential linkage for whole cereal foods on prevention of hyperglycemia. *Food science & nutrition*, 2020, 8.12: 6320-6337.

Gu, C., Yang, X., & Huang, L. *Cistanche*s Herba: a neuropharmacology review. *Frontiers in Pharmacology*, 2016, 7: 289.

Hajiaghaee, R., & Akhondzadeh, S. Herbal medicine in the treatment of Alzheimer's disease. *Journal of Medicinal plants*, 2012, 11.41: 1-7.

Hoshino, O. The amaryllidaceae alkaloids. *Alkaloids* 1998, 51, 323–376.

Hove, M., van Hille, R. P., & Lewis, A. E. Iron solids formed from oxidation precipitation of ferrous sulfate solutions. *AIChE journal*, 2007, 53.10: 2569-2577.

Howes, M. J. R., Perry, N. S., & Houghton, P. J. Plants with traditional uses and activities, relevant to the management of Alzheimer's disease and other cognitive disorders. *Phytotherapy Research:*

An International Journal Devoted to Pharmacological and Toxicological Evaluation of Natural Product Derivatives, 2003, 17.1: 1-18.

Ianni, A.; Di Maio, G.; Pittia, P.; Grotta, L.; Perpetuini, G.; Tofalo, R.; Cichelli, A.; Martino, G. Chemical–nutritional quality and oxidative stability of milk and dairy products obtained from Friesian cows fed with a dietary supplementation of dried grape pomace. *J. Sci. Food Agric.* 2019, *99*, 3635–3643.

Ibrakav, A.S.; Akinfewa, A.O.; Hussein, A.A. A comprehensive review on non-alkaloids chemical constituents from Amaryllidaceae. *South Afr. J. Bot*. 2020. In press.

Idda, M. L., Kage, E., Lopez-Olmeda, J. F., Mracek, P., Foulkes, N. S., & Vallone, D. Circadian timing of injury-induced cell proliferation in zebrafish. *PloS one*, 2012, 7.3: e34203.

Jiang, Y., Mao, S., Huang, W., Lu, B., Cai, Z., Zhou, F., ... & Zhao, Y. Phenylethanoid glycoside profiles and antioxidant activities of Osmanthus fragrans Lour. flowers by UPLC/PDA/MS and simulated digestion model. *Journal of agricultural and food chemistry*, 2016, 64.12: 2459-2466.

Jin, A.; Li, X.; Zhu, Y.Y.; Yu, H.Y.; Pi, H.F.; Zhang, P.; Ruan, H.L. Four new compounds from the bulbs of Lycoris aurea with neuroprotective effects against CoCl2 and H_2O_2-induced SH-SY5Y cell injuries. *Arch. Pharm. Res*. 2014, 37, 315–323.

Jin, Z.; Yao, G. Amaryllidaceae and Sceletium alkaloids. *Nat. Prod. Rep*. 2019, 36, 1462–1488.

Ka, S., Merindol, N., Sow, A. A., Singh, A., Landelouci, K., Plourde, M. B., ... & Desgagné-Penix, I. Amaryllidaceae alkaloid cherylline inhibits the replication of dengue and Zika viruses. *Antimicrobial agents and chemotherapy*, 2021, 65.9: e00398-21.

Ka, S.; Masi, M.; Merindol, N.; Di Lecce, R.; Plourde, M.B.; Seck, M.; Marcin, G.; Pescitelli, G.; Desgagne-Penix, I.; Evidente, A. Gigantelline, gigantellinine and gigancrinine, cherylline-and crinine-type alkaloids isolated from *Crinum jagus* with antiacetylcholinesterase

Kammerer, D.; Claus, A.; Carle, R.; Schieber, A. Polyphenol screening of pomace from red and white grape varieties (Vitis vinifera L.) by HPLC-DAD-MS/MS. *J. Agric. Food Chem.* 2004, *52*, 4360–4367.

Khoi, N.M.; Dat, N.T.; Na, M.K.; Thuong, P.T.; Min, B.S.; Bae, K.H. Cytotoxic activity of parthenin, a sesquiterpene isolated from a *Crinum ensifolium. Nat. Prod. Sci.* 2011, 17, 100–103.

Kianfé, B.Y.; Teponno, R.B.; Kühlborn, J.; Tchuenguem, R.T.; Ponou, B.K.; Helaly, S.E.; Dzoyemd, J.P.; Opatz, T.; Tapondjou, L.A. Flavans and other chemical constituents of *Crinum biflorum* (Amaryllidaceae). *Biochem. Syst. Ecol*. 2019, 87, 103953.

Kornienko, A.; Evidente, A. Chemistry, biology, and medicinal potential of narciclasine and its congeners. *Chem. Rev.* 2008, 108, 1982–2014.

L. Liu, M.L. Fishman, K.B. J. Kost, Hicks. Pectin-based systems for colon-specific drug delivery via oral route. *Biomaterials*, 2003, 24.19: 3333-3343.

Lakhdari, W., Dehliz, A., Acheuk, F., Mlik, R., Hammi, H., Doumandji-Mitiche, B., & Chergui, S. Ethnobotanical study of some plants used in traditional medicine in the region of Oued Righ (Algerian Sahara). 2016.

Lee, M. K., Kang, S. J., Poncz, M., Song, K. J., & Park, K. S. Resveratrol protects SH-SY5Y neuroblastoma cells from apoptosis induced by dopamine. *Experimental & molecular medicine*, 2007, 39.3: 376-384.

Li, H., Jiang, H., & Liu, J. Traditional Chinese medical therapy for erectile dysfunction. *Translational andrology and urology*, 2017, 6.2: 192.

Li, X., Xie, Y., Li, K., Wu, A., Xie, H., Guo, Q., … Chen, D. Antioxidation and cytoprotection of acteoside and its derivatives: comparison and mechanistic chemistry. *Molecules*, 2018, 23.2: 498.

Likhitwitayawuid, K.; Ruangrungsi, N.; Cordell, G.A. Amabiloside, a new glycoside from Crinum amabile. *Nat. Prod. Lett*. 1993, 3, 1–4.

Masi, M.; Mubaiwa, B.; Cimmino, A.; Van Otterlo,W.A.L.; Green, I.R.; Evidente, A. First isolation of acetovanillone and piceol from *Crinum buphanoides and Crinum graminicola* (I. Verd.) Amaryllidaceae. *South Afric. J. Bot*. 2018, 114, 37–39.

Mckie, Andrew T., et al. An iron-regulated ferric reductase associated with the absorption of dietary iron. *Science*, 2001, 291.5509: 1755-1759.

Meerloo, J. V., Kaspers, G. J., & Cloos, J. Cell sensitivity assays: the MTT assay. In: *Cancer cell culture*. Humana Press, 2011. p. 237-245.

Melek, F. R., El-Shabrawy, O. A., El-Gindy, M., & Miyase, T. Pharmacological activity and composition of ethyl acetate extract of *Cistanche* phelypaea. *FITOTERAPIA-MILANO-*, 1993, 64: 11-11.

Mildner-Szkudlarz, S.; Bajerska, J.; Zawirska-Wojtasiak, R.; Górecka, D. White grape pomace as a source of dietary fibre and polyphenols and its effect on physical and nutraceutical characteristics of wheat biscuits. *J. Sci. Food Agric.* 2013, *93*, 389–395.

Mimeault, M., Hauke, R., & Batra, S. K. Stem cells: a revolution in therapeutics—recent advances in stem cell biology and their therapeutic applications in regenerative medicine and cancer therapies. *Clinical Pharmacology & Therapeutics*, 2007, 82.3: 252-264.

Morikawa, T., Xie, H., Pan, Y., Ninomiya, K., Yuan, D., Jia, X., …Muraoka, O. A review of biologically active natural products from a desert plant *Cistanche* tubulosa. *Chemical and Pharmaceutical Bulletin*, 2019, 67.7: 675-689.

Mracek, P., Santoriello, C., Idda, M. L., Pagano, C., Ben-Moshe, Z., Gothilf, Y., ... & Foulkes, N. S. Regulation of per and cry genes reveals a central role for the D-box enhancer in light-dependent gene expression. *PLoS One*, 2012, 7.12: e51278.

Nagarajaiah, S.B.; Prakash, J. Chemical composition and bioactivity of pomace from selected fruits. *Int. J. Fruit Sci.* 2016, *16*, 423–443.

Nair, J.J.; Bastida, J.; Codina, C.; Viladomat, F.; van Staden, J. Alkaloids of the South African Amaryllidaceae: A review. *Nat. Prod. Commun*. 2013, 8, 1335–1350.

Nakamura A.J. Sedelnikova OA Solier S. Pommier Y. γH2AX and cancer. *Nat. Rev. Cancer*, 2008, 8: 957-967.

Nam, N.H.; Jae, Y.Y. NF- B Inhibitory activities of the methanol extracts and some constituents therein of some Vietnamese medicinal plants. *Sci. Pharm*. 2009, 77, 389–400.

Nkanwen, E.R.S.; Gatsing, D.; Ngamga, D.; Fodouop, S.P.C.; Tane, P. Antibacterial agents from the leaves of *Crinum purpurascens* herb (Amaryllidaceae*). Afric. Health Sci.* 2009, 9, 264–269.

O. Munjeri, J.H. Collett, J.T. Fell. Hydrogel beads based on amidated pectins for colon-specific drug delivery: the role of chitosan in modifying drug release. *Journal of Controlled Release*, 1997, 46.3: 273-278.

Okita, K., & Yamanaka, S. Induced pluripotent stem cells: opportunities and challenges. *Philosophical Transactions of the Royal Society B: Biological Sciences*, 2011, 366.1575: 2198-2207.

Ornstrup, M. J., Harsløf, T., Sørensen, L., Stenkjær, L., Langdahl, B. L., & Pedersen, S. B. Resveratrol increases osteoblast

differentiation *in vitro* independently of inflammation. *Calcified tissue international*, 2016, 99.2: 155-163.

Osbourn, A.E.; Lanzotti, V. Plant-Derived Natural Products Dordrecht; Springer: Berlin, Germany, 2009; pp. 361–384.

Ozcan, T., Akpinar-Bayizit, A., Yilmaz-Ersan, L., & Delikanli, B. Phenolics in human health. *International Journal of chemical engineering and applications*, 2014, 5.5: 393.

Pateiro, M., Gómez, B., Munekata, P. E., Barba, F. J., Putnik, P., Kovačević, D. B., & Lorenzo, J. M. Nanoencapsulation of promising bioactive compounds to improve their absorption, stability, functionality and the appearance of the final food products. *Molecules*, 2021, 26.6: 1547.

Patrick, L. Lead toxicity part II: the role of free radical damage and the use of antioxidants in the pathology and treatment of lead toxicity. *Alternative medicine review*, 2006, 11.2.

Qiao, Z., Tang, J., Wu, W., Tang, J., & Liu, M. Acteoside inhibits inflammatory response via JAK/STAT signaling pathway in osteoarthritic rats. *BMC complementary and alternative medicine*, 2019, 19.1: 1-8.

Rehecho, S., Uriarte-Pueyo, I., Calvo, J., Vivas, L. A., & Calvo, M. I. Ethnopharmacological survey of medicinal plants in Nor-Yauyos, a part of the Landscape Reserve Nor-Yauyos-Cochas, Peru. *Journal of ethnopharmacology*, 2011, 133.1: 75-85.

Rogakou, E. P., Boon, C., Redon, C., & Bonner, W. M. Megabase chromatin domains involved in DNA double-strand breaks in vivo. *The Journal of cell biology*, 1999, 146.5: 905-916.

Rogakou, E.P.; Pilch, D.R.; Orr, A.H.; Ivanova, V.S.; Bonner, W.M. DNA doublestranded breaks induce histone H2AX phosphorylation on serine 139. *J. Biol. Chem.* 1998, 273, 5858–5868.

S. Das, K. Ng. Colon-specific delivery of resveratrol: Optimization of multi-particulate calcium-pectinate carrier. *International journal of pharmaceutics*, 2010, 385.1-2: 20-28.

Sangermano, F.; Masi, M.; Vivo, M.; Ravindra, P.; Cimmino, A.; Pollice, A.; Evidente, A.; Calabrò, V. Higginsianins A and B, two fungal diterpenoid -pyrones with cytotoxic activity against human cancer cells. *Toxicol. In Vitro* 2019, 61, 104614.

Sedelnikova, O. A., Pilch, D. R., Redon, C., & Bonner, W. M. Histone H2AX in DNA damage and repair. *Cancer Biology and Therapy*, 2003, 2.3: 233-235.

Shahidi, F., & Yeo, J. Bioactivities of phenolics by focusing on suppression of chronic diseases: A review. *International journal of molecular sciences*, 2018, 19.6: 1573.

Shi, Y., Wang, W., Shi, Y., Jia, Z., Yao, S., Lin, W., ... & Zheng, R. Fast repair of dAMP hydroxyl radical adduct by verbascoside via electron transfer. *Science in China Series C: Life Sciences*, 1999, 42.6: 621-627.

Smith, T. A., Kirkpatrick, D. R., Smith, S., Smith, T. K., Pearson, T., Kailasam, A., ... & Agrawal, D. K. Radioprotective agents to prevent cellular damage due to ionizing radiation. *Journal of translational medicine*, 2017, 15.1: 1-18.

Soldani, C., Lazzè, M. C., Bottone, M. G., Tognon, G., Biggiogera, M., Pellicciari, C. E., & Scovassi, A. I. Poly (ADP-ribose) polymerase cleavage during apoptosis: when and where?. *Experimental cell research*, 2001, 269.2: 193-201.

Song, Y., Zeng, K., Jiang, Y., & Tu, P. *Cistanche*s Herba, from an endangered species to a big brand of Chinese medicine. *Medicinal Research Reviews*, 2021, 41.3: 1539-1577.

Sousa, E.C.; Uchôa-Thomaz, A.M.A.; Carioca, J.O.B.; Morais, S.M.D.; Lima, A.D.; Martins, C.G.; Alexandrino, C.D.; Ferreira, P.A.T.; Rodrigues, A.L.M.; Rodrigues, S.P.; et al. Chemical composition and bioactive compounds of grape pomace (Vitis vinifera L.), Benitaka variety, grown in the semiarid region of Northeast Brazil. *Food Sci. Technol.* 2014, *34*, 135–142.

Strober, W. Trypan blue exclusion test of cell viability. *Current protocols in immunology*, 2015, 111.1: A3. B. 1-A3. B. 3.

Sun, Q.; Zhang, W.D.; Shen, Y.H.; Zhang, C.; Li, H.L. A new phenolic compound from *Crinum asiaticum L. Chin. Chem. Lett*. 2008, 19, 447–449.

Syad, A. N., & Devi, K. P. Botanics: a potential source of new therapies for Alzheimer's disease. *Botanics*, 2014, 4: 11-16.

T. Coviello, P. Matricardi, C. Marianecci, F. Alhaique. Polysaccharide hydrogels for modified release formulations. *Journal of controlled release*, 2007, 119.1: 5-24.

Thorogood, C. J., Leon, C. J., Lei, D., Adughayman, M., Huan, L.-F., & Hawkins, J. A. Desert hyacinths: An obscure solution to a global problem?. *Plants, People, Planet*, 2021, 3.4: 302-307.

Trampetti, F., Pereira, C., Rodrigues, M. J., Celaj, O., D'Abrosca, B., Zengin, G., … Cust odio, L. Exploring the halophyte *Cistanche* phelypaea (L.) Cout as a source of health promoting products: *In vitro* antioxidant and enzyme inhibitory properties, metabolomic profile and computational studies. *Journal of Pharmaceutical and Biomedical Analysis*, 2019, 165: 119-128.

Truong, V. L., Jun, M., & Jeong, W. S. Role of resveratrol in regulation of cellular defense systems against oxidative stress. *Biofactors*, 2018, 44.1: 36-49.

Vallone, D., Gondi, S. B., Whitmore, D., & Foulkes, N. S. E-box function in a period gene repressed by light. *Proceedings of the National Academy of Sciences*, 2004, 101.12: 4106-4111.

Vatine, G., Vallone, D., Appelbaum, L., Mracek, P., Ben-Moshe, Z., Lahiri, K., ... & Foulkes, N. S. Light directs zebrafish period2 expression via conserved D and E boxes. PLoS biology, 2009, 7.10: e1000223.

V.R. Sinha, R. Kumria. Polysaccharides in colon-specific drug delivery. *International journal of pharmaceutics*, 2001, 224.1-2: 19-38.

Vivo, M., Fontana, R., Ranieri, M., Capasso, G., Angrisano, T., Pollice, A., Calabrò V. & La Mantia, G. p14ARF interacts with the focal adhesion kinase and protects cells from anoikis. *Oncogene*, 2017, 36.34: 4913-4928.

Volpato, G., Saleh, S. M. L., & Di Nardo, A. Ethnoveterinary of Sahrawi pastoralists of Western Sahara: camel diseases and remedies. *Journal of ethnobiology and ethnomedicine*, 2015, 11.1: 1-22.

Wang, C., Gong, X., Bo, A., Zhang, L., Zhang, M., Zang, E., ... & Li, M. Iridoids: research advances in their phytochemistry, biological activities, and pharmacokinetics. *Molecules*, 2020, 25.2: 287.

Wang, H., & Joseph, J. A. Quantifying cellular oxidative stress by dichlorofluorescein assay using microplate reader. *Free radical biology and medicine*, 1999, 27.5-6: 612-616.

Wang, Y. E., Zhang, L. I., Du, Z., Pei, J., & Huang, L. Chemical diversity and prediction of potential cultivation areas of *Cistanche* herbs. *Scientific reports*, 2019, 9.1: 1-13.

Watt, J.M.; Breyer-Brandwijk, M.G. The medicinal and poisonous plants of Southern and Eastern Africa. *Kew Bull*. 1964, 17, 463.

Wu, L., Georgiev, M. I., Cao, H., Nahar, L., El-Seedi, H. R., Sarker, S. D., ... & Lu, B. Therapeutic potential of phenylethanoid glycosides: A systematic review. *Medicinal Research Reviews*, 2020, 40.6: 2605-2649.

Xu, R., Chen, J., Chen, S. L., Liu, T. N., Zhu, W. C., & Xu, J. *Cistanche* deserticola Ma cultivated as a new crop in China. *Genetic resources and crop evolution*, 2009, 56.1: 137-142.

Xue, J., Wang, Y., Jia, X., Du, C., & Tang, W. Classification and research progress on phenylethanoid glycosides. *J Pharma Res*, 2018, 37.5: 282-289.

Xue, Z., & Yang, B. Phenylethanoid glycosides: Research advances in their phytochemistry, pharmacological activity and pharmacokinetics. *Molecules*, 2016, 21.8: 991.

Yang, L., Zhang, B., Liu, J., Dong, Y., Li, Y., Li, N., … Ma, X. Protective effect of acteoside on ovariectomy-induced bone loss in mice. *International Journal of Molecular Sciences*, 2019, 20.12: 2974.

Zhang, C. Z., Wang, S. X., Zhang, Y., Chen, J. P., & Liang, X. M. *In vitro* estrogenic activities of Chinese medicinal plants traditionally used for the management of menopausal symptoms. *Journal of ethnopharmacology*, 2005, 98.3: 295-300.

Zhang, J., Zhao, S., Yin, P., Yan, L., Han, J., Shi, L., ... & Ma, C. α-Glucosidase inhibitory activity of polyphenols from the burs of Castanea mollissima Blume. *Molecules*, 2014, 19.6: 8373-8386.

Zhao, H., Di Mauro, G., Lungu-Mitea, S., Negrini, P., Guarino, A. M., Frigato, E., ... & Foulkes, N. S. Modulation of DNA repair systems in blind cavefish during evolution in constant darkness. *Current Biology*, 2018, 28.20: 3229-3243. e4.

APPENDIX I

Matherials and methods

General Experimental Procedures

A JASCO P-1010 digital polarimeter (Jasco, Tokyo, Japan) was used to measure the
optical rotations in CH_3OH. Electronic circular dichroism (ECD) spectra were recorded on a JASCO J-815 spectrometer (Jasco, Tokyo, Japan) in CH_3OH. 400 Anova Advance (Bruker, Karlsruhe, Germany) and Inova 500 MHz (Varian, Palo Alto, CA, USA) instruments were used to record ^{1}H and ^{13}C NMR spectra in $CDCl_3$ or CD_3OD at 400/100 or 500/125 MHz, respectively. The same solvents were used as internal standards. Correlation spectroscopy with a 45° mixing pulse (COSY-45), Nuclear Overhauser effect spectroscopy (NOESY), heteronuclear single quantum correlation (HSQC) and heteronuclear multiple bond correlation (HMBC) experiments were performed using Bruker or Varian microprograms. Electrospray ionization (ESI) mass spectra and liquid chromatography/mass spectrometry (LC/MS) analyses were carried out using the LC/MS time-of-flight (TOF) system Agilent 6230B, high-performance liquid chromatography (HPLC) 1260 Infinity. A Phenomenex LUNA [C18 (2) 5 um 150 Å~ 4.6 mm column] was utilized to perform the HPLC separations. Analytical and preparative thin-layer chromatography (TLC) were performed on silica gel (Kieselgel 60, F254, 0.25 and 0.5 mm, respectively, Merck) plates. The spots were visualized
by exposure to ultraviolet (UV) radiation (254) or iodine vapors. Column chromatography (CC) was performed using silica gel (Kieselgel 60, 0.063–0.200 mm, Merck). Sigma-AldrichCo. (St. Louis, MO, USA) supplied all the reagents and the solvents.

Plant Material

C. biflorum
Bulbs of *C. biflorum* were collected in Senegal, in the Kaffrine department, in December 2018. A senior scientist from the Herbarium of IFAN of University Cheikh Anta Diop of
Dakar taxonomically identified the plant materials. Fresh bulbs of *C. biflorum* were dried at room temperature and then finely powdered. The resultant powder (545 g) was extracted with ethanol by Soxhlet obtaining a semisolid brown extract (450 mg). The latter was

fractionated by CC eluted with CHCl3/EtOAc/CH3OH (3:1.5:0.5 v/v/v), affording eight groups of homogeneous fractions (F1-F8). The residue (102.8 mg) of fraction F1 was further purified by CC eluted with CHCl3/isoPrOH (97:3 v/v) yielding ten groups of homogeneous fractions (F1.1-F1.10). The residue (15.8 mg) of F1.3 was purified by preparative TLC eluting with CH2Cl2/MeOH (97:3 v/v) yielding compound 4 (3.04 mg). The residue (14.3 mg) of F1.5 was purified by preparative TLC eluting with n-hexane/EtOAc (6:4 v/v) yielding compound 1 (1.42 mg) and compound 3 (3.52 mg). Compound 1 was crystallized from a CHCl3-isoPrOH 9:1 v/v solution. The residue (6.7 mg) of F1.6 was purified by TLC eluted with CHCl3/isoPrOH (9:1 v/v) yielding compound 2 (1.61 mg). The residue (15.2 mg) of F4 was further purified by preparative TLC eluting with CHCl3/isoPrOH (95:5 v/v) yielding compound 5 (1.19 mg).

C. phelypaea

400 g of *C. phelypaea*'s dried bulbs was milled with a blender and extracted with a Soxhlet apparatus using EtOH (1 × 500 ml, 12 h) obtaining 9.3 g of organic extract as an oily residue. This residue was dissolved in distilled H2O (200 ml) and extracted with EtOAc (3 × 200 ml) obtaining 4.4 g of organic extract that was further fractionated by column chromatography on silica gel eluted with CHCl3/isoPrOH (9:1, v/v) yielding 11 homogeneous fractions (F1-F11). The residue (695.7 mg) of F5 was further purified by CC on silica gel, eluting with EtOAc/MeOH/H2O (85:10:5, v/v/v), yielding nine homogeneous fractions (F5.1-F5.9). The residue of F5.3 (62.9 mg) was further purified by preparative TLC eluting with EtOAc/MeOH/H2O (85:10:5, v/v/v) affording 20-O-acetylacetoside (2, 20.9 mg) as an amorphous solid. The residue (172.1 mg) of F5.4 was purified by CC on reverse phase eluted with MeCN/H2O (3.5:6.5, v/v) affording acetoside (1, 30.1 mg) and tubuloside B (3, 5.5 mg). The residue (18.3 mg) of F5.8 was further purified by TLC on reverse phase eluting with MeCN/ H2O (3.5:6.5, v/v) yielding bartioside (4, 14.9 mg). The residue (336.5 mg) of F7 was purified by CC on reverse phase eluting with MeCN/ H2O (3.5:6.5, v/v) affording five fractions (F7.1-F7.5)
yielding 6-deoxycatalpol (5, 7.48 mg) and glucuroside (6, 1.50 mg). The purification process has been repeated five times to accumulate the pure compounds for chemical and biological characterization.

Grape pomace

1 kg of pomace was first subjected to freeze-drying, to eliminate the water fraction. Subsequently the solid phase was extracted by

maceration in pure ethanol (2 L), at room temperature and for 12 hours. Following the maceration process, the solid phase was separated from liquid phase and the solvent was removed using Rotar vapor. The organic extract obtained was further fractionated by column chromatography on silica gel eluted with CHCl3/isoPrOH (9:1, v/v) to isolate the most abundant metabolites among the flavonoids and characterizing the type of pomace. Two metabolites were identified (by comparing their ^{1}H-NMR spectra and specific optical power with data reported in the literature) and purified through by TLC on reverse phase eluting with MeCN/ H2O as (+)-catechin (yield 24 mg/kg) and (-)-epicatechin (56 mg/kg).

Cell Culture and Reagents

HaCaT, spontaneously immortalized keratinocytes from adult skin, were purchased from Service Cell Line (GmBH, Eppelheim, CLS, Germany) and cultured as described
(Amoresano et al., 2010). HeLa cervical cancer cells (CCL-2) and A431 (ATCC-CRL1555) human epidermoid carcinoma cells were from American Type Culture Collection (ATCC, Manassas, VA, USA). According to the p53 compendium database (http://p53.fr/tp53-database/the-tp53- cell-line-compendium, 05/05/2021), HaCaT cells contain mutant p53 (H179Y/R282W), HeLa have p53 impaired function by viral infection while A431 cells contain only one p53 mutated allele (R273H). All mentioned cell lines were cultured in Dulbecco's Modified Eagle's Medium (DMEM, Sigma Chemical Co, St. Louis, MO, USA) supplemented with 10% fetal bovine serum (FBS, Hyclone Laboratories, Inc. Logan, UT, USA) at 37 °C in a humified atmosphere of 5% CO2. hTERT-immortalized adipose-derived mesenchymal stem cells (hMSCs) were purchased from American Type Culture Collection (ATCC SCRC-4000; Virginia, USA). Cells (3–4 passages) were cultured in DMEM high glucose supplemented with 10% South American Fetal Bovine Serum (FBS), 2 mM glutamine, 100 units/ml Penicillin/Streptomycin (Gibco), and maintained in a humidified atmosphere of 5% CO^2 at 37 °C. Media, serum, and antibiotics for cell culture were from Thermo Fisher Scientific (Waltham, MA, USA). All cell lines were routinely tested for mycoplasma contamination and were not infected.

MTT Assay

Cell viability was evaluated by measuring the reduction of 3-(4,5-dimethylthiazol-2) 2,5- diphenyltetrazolium bromide (MTT) to formazan by the mitochondrial enzyme succinate dehydrogenase (Van Meerloo, Kaspers, & Cloos, 2011). Briefly, cells were seeded at $10^5/cm^2$ in 96-well plates and exposed to different concentrations of total extract or purified metabolites at indicate concentrations for 48 and 72 h. MTT/PBS solution (0.5 mg/ml) was then added to the wells and incubated for 3 h at 37 °C in a humidified atmosphere. The reaction was stopped by removal of the supernatant followed by dissolving the formazan product in acidic isopropanol and the optical density was measured with Sinergy H4 microplate reader Gen5 2.07 (Thermofisher, Waltham MA, USA) using a 570 nm filter. Under these experimental conditions, no undissolved formazan crystals were observed. Cell viability was assessed by comparing the optical density of the treated samples compared to the controls. Values shown in the plot are mean ± SD of sixfold determinations. Mean and the standard deviation was calculated on biological triplicates using GraphPad Prism8 software (GraphPad, San Diego, CA).

Trypan blue assay

1 part of 0.4% trypan blue and 1 part of cell suspension were mixed. The mixture was allowed to incubate for 3' at room temperature. The mixture was loaded into a Bürker chamber and the dead cells and the total number of cells were counted to evaluate the percentage of viable cells (Strober W., 2015).

Cell proliferation analysis

A total of 6×10^4 HaCaT and A431 cells were seeded in a 12-well plate; cells were serum-starved for 24 h; after starvation, total extract or acetoside of *C. phelypaea* were added at different concentrations. Every 24 h cells were gently rinsed with 1×PBS, trypsinized, and counted. The count was confirmed by Scepter 2.0 analysis (Millipore, Burlington, MI, USA).

Differentiation protocol

For HaCaT differentiation, cells were seeded in an RMPI medium. The day after seeding, the medium wad changed in RMPI without FBS, and

cells were treated with Ca^{2+} at 2 mM until the cells reach confluence. For osteogenic differentiation, the previously stored cells were plated at 8×10^3 cells/cm^2 on 0.2 µg/cm^2 human collagen I coating (Corning) in a growth medium for 3 days at 37 °C, 5% CO^2 in a humidified incubator, changing the medium after 2 days, before replacing the growth medium with osteogenic media (StemPro Osteogenesis Differentiation Kits_ThermoFisher Scientific) and maintaining for up to 18 days, with media changes every 2–3 days.

Detection of DNA Damage

Cells were seeded in 35 mm dishes on micro cover glasses (BDH) and treated with the metabolites of *C. biflorum* at a concentration of 10 µM. At 48 h after treatment, cells were washed with cold phosphate-buffered saline (PBS) and fixed with 4% paraformaldehyde Sigma- Aldrich (Merck Life Science, Milan, Italy) for 15 min at RT. Cells were permeabilized with ice-cold 0.5% Triton X-100 for 5 min and then washed with PBS. Cells were then incubated with phospho-histone H2A.X (Ser139) antibody (from Cell Signaling Technologies 9542, Boston, MA, USA) for 1 h, followed by DAPI (Sigma-Aldrich) for 3 min and washed with PBS/0.05% Tween. Coverslip was mounted with Ibidi mounting medium (Ibidi GmbH, Martinsried, Germany). Images were taken with a Zeiss confocal laser-scanning microscope Axio Observer (Zeiss, Ostfilden, Germany) (scale bar, 20 µm). A 40Å~ objective was used and image analysis was performed using Fiji ImageJ open source software project (https://imagej.net/imaging/). All the images were taken with the same setting (Vivo M. et al., 2017).

Western Blot Analysis

Western blot was performed as previously reported (di Martino et al., 2016). Briefly, 30 µg of whole cell extracts were separated by sodium dodecyl sulfate polyacrylamide gel electrophoresis (SDS-PAGE), subjected to Western blot and incubated overnight at 4 °C with antibodies. Antibodies against p21WAF, Poly [ADP-ribose] polymerase 1 (PARP1) and actin were from Cell Signaling Technologies 9542, Boston, MA, USA; antibodies against Cytokeratin (VIK-10) and Cytokeratin (K1207) were from CellSignaling Technologies (Boston, MA, USA), and ΔNp63α from Abcam (Cambridge, UK). Each experiment was run in triplicate. Signal intensities of Western blot bands were quantified by Quantity One analysis software (Version Number 2,

Biorad Laboratories, London, UK) and analyzed by GraphPad Prism 8.0.2 software (GraphPad, San Diego, CA).

DCFDA Assay

Antioxidant activity was measured for the following metabolites or extracts: N-p-coumaroyltyramine of *C. biflorum*), metabolites 1–6 of *C. phelypaea*, total organic extract of grape pomace or the same released extract from beads, at indicate concentrations. It was measured using 2′−7′dichlorofluorescein diacetate (DCFDA), a non-fluorescent compound permeable to the cell membrane, which can be oxidized by reactive oxygen species (ROS) giving a fluorescent compound. Cells were seeded at 2.5 Å~ 104 in 96 well and pre-treated with N-pcoumaroyltyramine or 1-6 *C. phelypaea* metabolites at 50 or 100 µM as indicated. The medium was removed after 4 h and 1 mM (3%) H_2O_2 was added for 45 min, 1.5 and 2.0 h. Cells were washed with PBS and a fresh medium with DCFDA (30 µM) was added for 45 min, then DCFDA was removed by washing in PBS and the cells were harvested. The measurement of ROS was obtained using the Sinergy H4 microplate reader (Gen5 2.07, Thermofisher, Waltham MA, USA. The fluorescence emitted from the cells treated with DCFDA was compared to the untreated cells. Trolox was used as a positive control in all assays. Values shown in the plot are mean ± SD of sixfold determinations. The mean and the standard deviation were calculated on biological triplicates using GraphPad Prism 8.0.2 software (GraphPad, San Diego, CA).

Pseudotyped HIV-1GFP Infectivity Assay

The anti-HIV-1 activity of compounds 1–5 of *C. biflorum* was evaluated using VSV-G pseudotyped NL43GFP infection of human monocytic THP-1 cells. THP-1 and NL4–3GFP were generously provided by Lionel Berthoux and Amita Singh and are described in Ka et al. (Ka S. et al., 2021). THP-1 cells were seeded at 2.0 x 10^4 cells per well in 96 well-plates. The next day, cells were treated with 4 concentrations of each compound (12.5, 25, 50 and 100 mM) and then infected with HIVGFP at a MOI of 1. After 72 h, cells were stained with propidium iodide (PI, 0.5 mg/mL) and both PI+ and HIV-1GFP+ infected cells frequencies were assessed on a FC500 MPL cytometer (Beckman Coulter, Inc., Mississauga, ON, Canada) and analyzed using FlowJo software (FlowJo LLC, BD Biosciences, Ashland, OR, USA). Matched

concentrations of dimethyl sulfoxide (DMSO) were used as negative controls. All infection assays were performed in triplicate.

α-Glucosidase and α-Amylase Inhibitor Assay

α-glucosidase and α-amylase inhibitor screening kits (colorimetric) were purchased from Biovision (Milpitas, CA, USA). In total, 10 mM of stock solution of all the tested compounds were dissolved in DMSO and serially diluted in the assay buffer of each kit. Experiments were performed according to the manufacturer's protocol. Briefly, for the α-glucosidase assay, 10 µL of serially diluted compounds of *C. biflorum* at the corresponding concentration (10 nm—1 mM) were added into designated wells of clear 96 well-plates. Subsequently, 10 µL of the α-glycosidase enzyme was added to each well and volume was adjusted to 80 µL and plates were incubated for 15-min at room temperature in dark condition. Then, 20 µL of α-glycosidase substrate mixture was added in all wells and kinetic of reaction was measured at OD: 410 nm for 60 min at 2 min intervals by using a multiplate reader, Biotek instrument, Inc., Canada. Enzyme control (no inhibitor), background control (no enzyme), solvent control (DMSO) and inhibitor control (acarbose) were included in the plates. For the α-amylase assay, 50 µL of serially diluted compounds (3.25 µM to 500 µM) were added into a clear 96-well plate with 50 µL of assay buffer and 50 µL of α-amylase enzymes. The plate was incubated at room temperature in the dark for 10 min. Then 50 µL of the α-amylase substrate was added in all wells. The kinetic of reaction was measured at OD:410 nm for 26 min at intervals of 2 min by using a multiplate reader. Control α-amylase inhibitor was provided by the manufacturer, enzyme control, background control and solvent control were all included. Enzyme inhibition was calculated according to Zhang et al. (Zhang, J. et al., 2014). In summary, ODs were plotted according to the time for each sample. Areas under the curve (AUC) were calculated, and enzyme inhibition was measured as 100−(AUCcompound/AUCenzyme) Å~ 100 for each dilution of each compound.

Anti-Acetylcholinesterase Assays

In vitro acetylcholinesterase (AChE) activity was assessed exactly as in Ka et al. (2020)
following Ellman's colorimetric protocol (Ellman, G. L., et al., 1961) with the Acetylcholinesterase Assay Kit (Abcam Inc., Boston, MA, USA). Briefly, 50 µL serial dilutions (3.9–500 µM) of *C. biflorum* compounds

1–5 were prepared in Tris-HCl pH = 7.9 buffer into designated wells of a clear 96 wellplate. A total of 5 µL of DTNB was added in each well, then 50 µL of diluted acetycholinesterase was added. The plate was incubated for 10 min in the dark. Matched concentrations of DMSO were used as a negative control. Kinetic of reaction was measured in a multiple plate reader at 410 nm in kinetic mode for 40 min at room temperature. The percentage of anti-AChE inhibition was calculated according to the following formula: 100 − [((E − S)/E) Å~ 100], where E is the activity of the enzyme with matched concentrations of DMSO and S is the activity of the enzyme with the test sample.

RNA extraction, cDNA preparation, and qRT-PCR

Total RNA was extracted using TRIzol reagent (Invitrogen) and cDNA was synthesized using iScript cDNA Synthesis kit according to the manufacturer's instructions (Bio-Rad, Hercules, CA, USA). 1 µg of total RNA was used for each cDNA synthesis. Primer 3 software (http://primer3.ut.ee/) was used to design the oligo primers setting the annealing temperature to 59–61 °C for all primer pairs. Oligo sequences are reported in Table. For gene expression analyses, 25 ng of cDNA was used for each PCR reaction with each primer pair (forward/reverse primers mix: 0.2 µM, in a final volume of 25 µl). Real time-qPCR analysis was performed using the iTaq™ Universal SYBR® Green Supermix (Bio-Rad, Hercules, CA, USA) in a 7500 Real-Time PCR System (Applied Biosystems, Foster City, CA, USA) under the following conditions: 2 min at 50 °C, 10 min at 95 °C, followed by 40 cycles of 15 s at 95 °C, and 1 min at 60 °C. The GAPDH probe served as a control to normalize the data. The gene expression experiments were performed in triplicate on three independent experiments and a melting analysis was performed at the end of the PCR run. To calculate the relative expression level, we used the 2 DDCT method.

Gene name	Forward primer 5′–3′	Reverse primer 5′–3′
ENG	AGCCCCACAAGTCTTGCAG	GCTAGTGGTATATGTCACCTCGC
COL1A1	CCCCTGGAAAGAATGGAGATG	TCCAAACCACTGAAACCTCTG
OCN	GGCGCTACCTGTATCAATGG	TCAGCCAACTCGTCACAGTC
ALPL	ACGTACAACACCAATGCCC	GGTCACAATGCCCACAGATT
RUNX2	CTGTGGTTACTGTCATGGCG	AGGTAGCTACTTGGGGAGGA
GAPDH	GGTATCGTGGAAGGACTCATGAC	ATGCCAGTGAGCTTCCCGTTCAG

Structural analysis of pectin-based particles

Thermogravimetrical analysis were performed using a thermogravimetric analyzer TGA/DTG Perkin-Elmer PyrisDiamond, equipped with gas station. A 3–4 mg sample was placed in an open ceramic crucible and heated from 25 °C to 600 °C at a speed rate of 10 °C/min, under nitrogen at 30 mL/min.

The UV-vis spectra of the unentrapped fraction of grape pomace,in order to evaluate loading efficiency, were recorded using a spectrophotometer V−570 Jasco, double beam system with a single monochromator, Easton, Van Nuys, LA, USA. Calibration curve was calculated at five different concentration (0.5-2.5mg/ml) reading absorbance at 560nm.

Morphological analysis were performed by scanning electron microscope (SEM) (Quanta 200 FEG, 338 FEI, Eindhoven, The Netherlands). Surfaces were coated with a homogeneous layer (18 ± 0.2 nm) of Au and Pd alloy by means of a sputtering device (MED 020, Bal-Tec AG, Tucson, AZ, USA). The micrographs were performed at room temperature, in high vacuum mode. By means of energy dispersive X-ray spectroscopy (EDS), it was possible to perform the chemical analysis of selected microscopic regions. EDS was performed in the SEM by means of an Oxford Inca Energy 250 System equipped with an INCAx-act LN2-free detector, using an accelerating voltage of 20.0 kV.

Statistical analysis

Statistical analyses were carried out using the GraphPad Prism version 8.1.2 (https://www.graphpad.com/scientific-software/prism/). Data were represented as the mean standard deviation and analyzed for statistical significance using ordinary one-way analysis of variance (ANOVA) and multiple comparisons. For all tests, $p < 0.05$ was considered to indicate a statistically significant difference.

APPENDIX II

Scientific publication

- Guarino, A. M., Di Mauro, G., Ruggiero, G., Geyer, N., **Delicato, A**., Foulkes, N. S., ... & Calabrò, V. (2019). YB-1 recruitment to stress granules in *zebrafish* cells reveals a differential adaptive response to stress. *Scientific reports*, *9*(1), 1-14.

- Roscetto, E., Masi, M., Esposito, M., Di Lecce, R., **Delicato, A.**, Maddau, L., ... & Catania, M. R. (2020). Anti-Biofilm Activity of the Fungal Phytotoxin Sphaeropsidin A against Clinical Isolates of Antibiotic-Resistant Bacteria. *Toxins*, *12*(7), 444.

- Sangermano, F., **Delicato, A**., & Calabrò, V. (2020). Y box binding protein 1 (YB-1) oncoprotein at the hub of DNA proliferation, damage and cancer progression. *Biochimie*.

- Masi, M., Koirala, M., **Delicato, A.**, Di Lecce, R., Merindol, N., Ka, S., ... & Evidente, A. (2021). Isolation and Biological Characterization of Homoisoflavanoids and the Alkylamide Np-Coumaroyltyramine from *Crinum biflorum* Rottb., an Amaryllidaceae Species Collected in Senegal. *Biomolecules*, *11*(9), 1298.

- **Delicato, A.**, Montuori, E., Angrisano, T., Pollice, A., & Calabrò, V. (2021). YB-1 Oncoprotein Controls PI3K/Akt Pathway by Reducing Pten Protein Level. *Genes*, *12*(10), 1551.

- Tirri R., Ciccia F., Mauro D., Calabrò V., **Delicato A**., Ciancio A. (2022). Vexas sindrome challenges and opportunities. Reumatismo

- **Delicato A.,** Masi M., de Lara F., Rubiales D., Paolillo I., Lucci V., Falco G., Calabrò V. & Evidente A.. (2022). *In vitro* characterization of iridoid and phenylethanoid glycosides from *Cistanche* phelypaea for nutraceutical and pharmacological applications. *Phytotherapy Research,* 1-12.

Congresses and activities

- **XV FISV Congress** September 18-21, 2018. Sapienza University of Rome, Italy. Andrea Maria Guarino, Giuseppe Di Mauro, Gennaro Ruggiero, Concetta Sozio, **Antonella Delicato**, Nicholas Simon Foulkes, Daniela Vallone and Viola Calabrò. YB-1 recruitment to stress granules in *zebrafish* reveals a differential adaptive response.

- **Cold Shock Protein Symposium,** 2019. University of Magdeburg, Germany. Antonella Delicato, Andrea Maria Guarino, Felicia Sangermano, Rima Siauciunaite, Elio Pizzo, Andrea Bosso, Nicholas S. Foulkes, Daniela Vallone, Calabrò Viola. YB-1: a bridge between the circadian clock and cell cycle control.

- **AGI-SIMA Cogress,** Semptember 2019. Cortona, Italy. **Antonella Delicato**, Andrea Maria Guarino, Nicholas S. Foulkes, Daniela Vallone, Girolama La Mantia and Viola Calabrò. YB-1: a bridge between the circadian clock and cell cycle control.

- **Salk cell cycle meeting,** 22-25 June 2021. **Antonella Delicato,** Eleonora Montuori, Viola Calabrò. Y box binding protein 1 (YB-1) a multifunctional protein orchestrating cell proliferation, DNA damage, and cancer progression.

- **AGI-SIMA Congress**, 22-24 September 2021. **Antonella Delicato,** Eleonora Montuori, Tiziana Angrisano, Alessandra Pollice, Viola Calabrò. YB-1 Oncoprotein Controls PI3K/Akt Pathway by Reducing Pten Protein Level.

- **58° Congresso nazionale Società Italiana di Reumatologia**, 24-27 November 2021. Daniele Mauro, **Antonella Delicato**, Antonio Ciancio, Viola Calabrò, Francesco Ciccia, Rossella Tirri. Sindrome Vexas: sfide e opportunità.

- **XVI FISV Congress 2022**. *3R: Research, Resilience, Reprise*. 14-16 September 2022. Reggia di Portici (Naples), Italy. **Antonella Delicato,** Ida Paolillo, Antonio Pezone, Giuliana Napolitano, Viola Calabrò. Involvement of Y-box binding protein 1 (YB-1) in DNA damage and repair mechanisms.

- **PLS (Progetto Lauree Scientifiche)**. *Polymorphisms and DNA detection*. University of Naples Federico II. 11 February 2019, theoretical lesson; 14,16, 17, 24 February2019, laboratory experience (3h each).

- **XXXV Futuro Remoto**. *Transizioni*. 23 November to 3 December 2021, Naples.

APPENDIX III

Experience in foreign laboratory

P.I. Dr. Nicholas S. Foulkes,
nicholas.foulkes@kit.edu

Institute of Biological and Chemical Systems – Biological Information Processing (IBCS-BIP), Hermann-von-Helmholtz-Platz 1, 76344 Eggenstein-Leopoldshafen, Germany.

- From 4 October 2021 to 4 April 2022.

During my period abroad I've got the **FELASA** Federation of European Laboratory Animal Science Associations certificate following the International Zebrafish and Medaka Course (IZMC).